Modelling and Performance Assessment of OFDM and Fast-OFDM Wireless Communication Systems

Dimitrios Karampatsis

A thesis submitted for the degree of Doctor of Philosophy

August 2004

Department of Electronic and Electrical Engineering
University College London

ProQuest LLC
789 East Eisenhower Parkway
P.O. Box 1346
Ann Arbor, MI 48106-1346

Abstract

This thesis is mainly concerned with the design, modelling and performance assessment of modulation techniques for use in wireless communication systems. The work is divided, broadly in three areas; a multimode system proposal, an assessment of a new modulation scheme and a system optimisation technique. A multimode system architecture employing GSM and EDGE systems and an Orthogonal Frequency Division Multiplexing (OFDM) system is proposed. The OFDM system is designed to have similar frame structure, channel allocation and spectrum shape to those of the GSM and EDGE systems. The multimode system is evaluated under typical multipath fading environments specified for GSM/EDGE and adjacent-channel and co-channel interference. The results indicated that the proposed OFDM system can be perfectly integrated within the GSM/EDGE network core. Furthermore, a novel modulation technique is investigated. Fast-OFDM (FOFDM) is a variation of OFDM, which offers twice the bandwidth efficiency when compared to OFDM. However, the bandwidth efficiency only applies to one dimensional modulation schemes (BPSK or M-ASK). The suitability of FOFDM for wireless communications is assessed by studying its performance under receiver front-end distortions and multipath fading environments. The performance of the FOFDM system is compared with the performance of a similar OFDM system. The results indicated that under small distortion conditions, the performance of FOFDM and OFDM is comparable. Finally, the effect of interpolation filtering on OFDM systems in noise limited and interference limited environments is investigated. The aim of this study is to highlight that interference should be taken into consideration when designing systems for wireless communications. In addition, this study can be utilised in software defined radio schemes, offering optimised performance. Overall, this thesis presents work over a range of research areas, providing system proposals, modulation comparisons and system optimisation techniques that can be used by developers of future mobile systems.

Acknowledgements

I would like to thank sincerely and express my gratitude to my supervisor Dr. Izzat Darwazeh for his invaluable assistance, guidance and encouragement throughout the duration of this project and for commenting on the thesis. I would like to thank Izzat for being an excellent supervisor and a friend.

I would like also to express my gratitude to Nokia Networks UK for sponsoring and financially supporting this project and especially to my industrial supervisor from Nokia Networks UK, Mr. Kevin Lamacraft and to Dr. Gilles Charbit for their help and support in this project and for providing information and system specifications used in Chapter 4.

I would like to acknowledge Dr. Miguel Rodrigues for research collaboration and for his help. Finally, thanks to my colleagues in the Telecommunications Research Group at UCL, my colleagues at UMIST, where this work started, and my friends for making my life during the duration of the research enjoyable.

Last but not least, I would like to thank my parents for supporting me throughout the duration of my education.

Table of Contents

List of Figures

List of Tables

List of Abbreviations

1D	One Dimensional
1G	First Generation System
2.5G	Second Generation Plus
2D	Two Dimensional
2G	Second Generation System
3G	Third Generation System
3GPP	Third Generation Partnership Project
4G	Fourth Generation System
8PSK	8 point Phase Shift Keying
ACI	Adjacent Channel Interference
ADS	Advanced Design System
AMPS	Advanced Mobile Phone Service
ANSI	American National Standards Institute
ARIB	Association of Radio Industries and Businesses
ATM	Asynchronous Transfer Mode
AWGN	Additive White Gaussian Noise
BER	Bit Error Rate
BPSK	Binary Phase Shift Keying
BS	Base Station
BT	Bandwidth Bit/Symbol Duration Product
CCI	Co-Channel Interference
CDMA	Code Division Multiple Access
COFDM	Coded Orthogonal Frequency Division Multiplexing
DAB	Digital Audio Broadcasting
DCS	Data Communication System
DFT	Discrete Fourier Transform
DQPSK	Differential Quadrature Phase Shift Keying
DSP	Digital Signal Processing
DS-SS	Direct Sequence Spread Spectrum
DVB	Digital Video Broadcasting
DVB-C	Digital Video Broadcasting – Cable
DVB-S	Digital Video Broadcasting – Satellite
DVB-T	Digital Video Broadcasting – Terrestrial
ECSD	Enhanced Circuit Switched Data
EDGE	Enhanced Data Rates for GSM Evolution
EGPRS	Enhanced General Packet Radio Service
EMC	Electro-Magnetic Compatibility

ESPRIT	European Strategic Programme for Research and Development in Information Technology
ETSI	European Telecommunications Standards Institute
EVM	Error Vector Magnitude
FACCH	Fast Associative Control Channel
FDD	Frequency Division Duplex
FDM	Frequency Division Multiplex
FFH	Fast Frequency Hopping
FFT	Fast Fourier Transform
FHMA	Frequency Hopped Multiple Access
FH-SS	Frequency Hopped Spread Spectrum
FM	Frequency Modulation
FOFDM	Fast Orthogonal Frequency Division Multiplexing
FSK	Frequency Shift Keying
GMSK	Gaussian Minimum Shift Keying
GPRS	General Packet Radio Service
GSM	Global System for Mobile Communications
HAPS	High Altitude Platform Stations
HF	High Frequency
HSCSD	High Speed Circuit Switched Data
HSDPA	High Speed Downlink Packet Data Access
HT	Hilly Terrain
I/Q	Inphase/Quadrature
IC	Integrated Circuit
ICI	Intercarrier Interference
IDFT	Inverse Discrete Fourier Transform
IEC	International Electrotechnical Commission
IEEE	Institute of Electrical and Electronic Engineers
IF	Intermediate Frequency
IFFT	Inverse Fast Fourier Transform
IP	Internet Protocol
IPv4	Internet Protocol version 4
IPv6	Internet Protocol version 6
IR	Infra-Red
ISI	Intersymbol Interference
ISO	International Organisation for Standardisation
LAN	Local Area Network
LO	Local Oscillator
LOS	Line of Sight
LS	Least Squares
M-ASK	M-ary Amplitude Shift Keying
M-OQAM	M-ary Offset Quadrature Amplitude Modulation
MC-CDMA	Multicarrier CDMA
MC-DS-CDMA	Multicarrier Direct Sequence CDMA
MMSE	Minimum Mean Square Error

MPEG 2	Moving Pictures Experts Group – version 2
MS	Mobile Station
MSC	Mobile Switching Centre
MSK	Minimum Shift Keying
MT-CDMA	Multitone CDMA
NRZ	Non-Return to Zero
OFDM	Orthogonal Frequency Division Multiplexing
OFDMA	Orthogonal Frequency Division Multiple Access
OQAM	Offset Quadrature Amplitude Modulation
OVSF	Orthogonal Variable Spreading Factor
PAL	Phase Alternative Line
PAR	Peak-to-Average Power Ratio (also PAPR)
PCS	Personal Communication System
PMA	Personal Mobile Assistant
PMR	Peak-to-Minimum Average Power Ratio
PRBS	Pseudo Random Binary Sequence
PSAM	Pilot Symbol Assisted Modulation
QAM	Quadrature Amplitude Modulation
QoS	Quality of Service
QPSK	Quadrature Phase Shift Keying
RA	Rural Area
RAN	Radio Access Network
RF	Radio Frequency
RLC	Radio Link Protocol
rms	root mean square
RNC	Radio Network Controller
RoF	Radio-over-Fibre
RPE-LTP	Regular Pulse Excited Long-Term Prediction
RS	Reed Solomon Codes
RTT	Radio Transmission Technology
SECAM	System Electronique Couleur Avec Memoire
SF	Stealing Flag
SFH	Slow Frequency Hopping
SFN	Single Frequency Network
SMS	Short Message Service
SNR	Signal-to-Noise Ratio
TB	Tail Bits
TCH	Traffic Channel
TCH/F	Full Rate Traffic Channel
TCH/H	Half Rate Traffic Channel
TD/CDMA	Time Division CDMA
TD/SCDMA	Time Division Synchronous CDMA
TDD	Time Division Duplex
TDMA	Time Division Multiple Access
TIC	Technologies of Informations and Communications

TTA	Telecommunications Technology Association
TU	Typical Urban
UHF	Ultra High Frequency
UMTS	Universal Mobile Telecommunications System
UTRA	UMTS Terrestrial Radio Access
VLSI	Very Large Scale Integration
WCDMA	Wideband CDMA
WLAN	Wireless Local Area Network
W-OFDM	Wideband OFDM

Chapter 1

Introduction

The use of wireless communications has made an enormous impact on the living standards of many people. Such interest in this type of communication started in the late 80s by the introduction of the cellular Global System for Mobile Communications (GSM) in Europe. The GSM system offered many advantages compared to earlier technologies such as digital modulation, handover techniques and roaming, which lead many countries to adopt it. The popularity of GSM drove the mobile industry to develop improved systems to handle the increased demands of users and the addition of new services and applications. The GPRS (General Packet Radio Service), HSCSD (High Speed Circuit Switched Data) and EDGE (Enhanced Data Rates for GSM Evolution) were released in order to cope temporarily with such demand. At the same time, the mobile industry developed the next generation cellular system UMTS (Universal Mobile Telecommunications System), termed as 3G (3^{rd} Generation). UMTS introduces new services and applications and allows higher data rates. It is expected to handle the demands of users for the next decade. Furthermore, the mobile industry is already planning the 4^{th} Generation system (4G) offering even more services and higher data rates.

The popularity of cellular systems resulted in a broad interest in wireless systems in general. WLAN (Wireless Local Area Network) and Hiperlan/2 are examples of this trend. Such systems give wireless connectivity between computers and/or laptops in indoor environments. The popularity of wireless communications has resulted in the adoption of complex communication schemes such as OFDM (Orthogonal Frequency Division Multiplexing). OFDM offers many advantages for wireless communications, due to its excellent handling of frequency selective fading,

simple equalisation requirements and ease of generation and recovery using DSP techniques. OFDM is already adopted by IEEE WLAN 802.11a and ETSI Hiperlan/2, as well as, for other wireless applications such as Digital Audio Broadcast (DAB) and Digital Video Broadcast (DVB). Furthermore, a variation of OFDM has been developed, Fast-OFDM (FOFDM), which offers twice the bandwidth efficiency of OFDM.

This thesis covers a number of topics. Firstly, the design and modelling of an OFDM system to co-exist with GSM and EDGE systems is studied. Secondly, Fast-OFDM which is a variation of OFDM, is investigated by comparing its performance against OFDM in wireless channels. Finally, the effect of interpolation filters on the performance of wireless OFDM systems, in noise limited and interference limited environments is evaluated. The research reported in this thesis is modelling and simulation based. On occasions industrially provided, measurement based models, are used in our studies. The main tools that have been used for this purpose are Agilent Advanced Design System (ADS) and Matlab. The details of the thesis structure and contributions are given in the following sections.

1.1 Thesis structure

Following this introductory chapter, an overview of wireless communication systems and their evolution is carried out in Chapter 2. This chapter starts by giving a brief review on the evolution of the cellular network from the 1st Generation systems (1G) to 3G. Furthermore, the modulation and air interface of GSM and EDGE systems are explained. Subsequently, the new capabilities of 3G systems are outlined followed by a review of the considerations of 4G systems. The market and traffic forecast, service requirements, network architecture, modulation and signal transmission considered for 4G systems are described in this section. Section 2.7 includes a description of the basic principles of OFDM and its variants. This section starts by explaining the implementation of OFDM in continuous-time (oscillator based) and discrete-time (FFT based) configurations. Then, the importance of the guard interval is explained. The chapter continues by outlining the limitations of OFDM. Subsequently, the various configurations of multicarrier CDMA are described. The chapter ends by describing wireless applications that use OFDM. These are the WLAN and DVB systems.

In Chapter 3, further detailed design considerations of OFDM wireless systems are described. This chapter aims to guide designers on how to choose parameters of newly developed OFDM systems. The first section describes the design considerations of an OFDM transmitter. More specifically, the interaction between modulation, pilot symbols, guard interval and FFT size is analysed. Subsequently, the next section describes the two most important factors that define the wireless channel; noise and fading. The final section describes the design considerations for an OFDM receiver. This section starts by describing the effect on OFDM of carrier and symbol synchronisation errors. Methods to alleviate such effects are given in the next section that describes synchronisation methods. Finally, channel estimation methods for OFDM to overcome the fading effects of the channel are presented in the last section.

Chapters 4, 5 and 6 outline the modelling and design work carried out by the author. In Chapter 4, the design, implementation and performance assessment of a new multimode system suitable for transmission and reception of GSM, EDGE and OFDM signals are presented[1]. The chapter starts by summarising the research reported in this area. The next section discusses the design of the proposed OFDM system, in terms of the choice of; data rate, modulation, FFT size, pilot symbol and guard interval insertion, synchronisation and channel estimation methods. Subsequently, model development and verification of the designed system using the ADS simulation platform is described. This section verifies the appropriateness of the proposed OFDM. The multimode system will be evaluated under noise, fading, Adjacent Channel Interference (ACI) and Co-Channel Interference (CCI) conditions. Therefore, the simulation test benches used for such evaluation are described in the next section. The results of the simulations performed are displayed and discussed in the subsequent section. This is followed by a summary and discussion section.

In Chapter 5, Fast-OFDM (FOFDM) is described. The first section describes the basic principles of this modulation. The continuous-time and discrete-time implementations of FOFDM are presented. Subsequently, the limitations of FOFDM are described. The next section describes the design and modelling of OFDM and FOFDM systems in ADS. These models will be used for performance comparison between the two schemes, in terms of; receiver front-end non-idealities (I/Q imbalance, frequency offset, timing offset, phase noise) and multipath fading environments. The

[1] Some system parameters were provided by the industrial sponsor, Nokia Networks UK

simulation results obtained are depicted and then summarised in the subsequent sections.

In Chapter 6, the effect of interpolation filters on the performance of OFDM systems in wireless communications is analysed. The first section of this chapter describes the necessity of interpolation filters in digital communication systems. Subsequently, a review on interpolation filters for OFDM is carried out. The next section discusses the design of the models used to evaluate the effect of these filters on OFDM. The system will be tested in noise limited and interference limited (ACI limited) environments. The simulation results are displayed and discussed in the subsequent section. A summary of the results obtained is carried out in the final section.

Chapter 7 concludes this thesis, summarising the main contributions and suggesting areas for future work.

Finally, in the appendices, schematics of the simulation models designed in the simulation platform ADS are enclosed. Appendix A describes the modelling of the proposed OFDM system as well as GSM, EDGE and simulation environments that are discussed in Chapter 4. In Appendix B, schematics are given of Fast-OFDM simulation models, discussed in Chapter 5. Finally, in Appendix C, the modelling of the work carried out in Chapter 6 is described.

1.2 Contributions

The work reported in this thesis contains several novel elements and contributions of the author to the field of wireless communications. A summary of the main contributions in each chapter are listed below:

Chapter 4

- Development of a new system using OFDM. The proposed system is integrated within a multimode transceiver system using GSM and EDGE.
- Performance assessment of proposed OFDM system in GSM typical fading environments and comparison with GSM/EDGE.
- Performance assessment of multimode system under adjacent-channel and co-channel interference. The simulation results indicated that the interference from OFDM to GSM/EDGE systems causes similar levels of distortion as would a

GSM/EDGE interferer. Furthermore, simulation results showed that GSM and EDGE interferers cause the same levels of distortion to OFDM. On the other hand, OFDM interference to OFDM results in fewer bit errors.

Chapter 5

- Derivation of analytical expressions to determine the effect of I/Q imbalance, frequency offsets and timing offsets, on the received FOFDM demodulated symbols.
- Evaluation of FOFDM and OFDM modulations under receiver front-end non-idealities (I/Q imbalance, frequency offset, timing offset, phase noise). The simulation results indicate the high susceptibility of FOFDM to such distortions. Furthermore, the simulation results indicated that for small distortion factors the performance between the two modulations is comparable. As the distortion factors increase the performance of the FOFDM system deteriorates much faster than that of OFDM.
- Evaluation of FOFDM and OFDM modulations in fading channels. The modulations are tested in GSM Typical Urban, Rural Area and Hilly Terrain environments. The results indicated a comparable performance under such environments.

Chapter 6

- Study of the effect of interpolation filters on OFDM system performance and choice of optimum filters for operation in noise limited and interference limited environments.

The research reported here has resulted in seven publications including an invited paper, to date. These are listed below in chronological order:

1. Dimitrios Karampatsis, João Lima Pinto and Izzat Darwazeh, "Transmitter Modelling and EVM Estimation for the GSM Evolution - EDGE,", Proc. of the International Conference on Telecommunications (ICT 2001), vo. 3, pp. 511-515, Bucharest, Romania, June 2001

2. Dimitrios Karampatsis and Izzat Darwazeh, "OFDM: A Possible Technology for 4th Generation Mobile Systems?,", International Symposium on Telecommunications IST, pp. 650-653, Sept. 2001, Tehran, IRAN
3. João Lima Pinto, Dimitrios Karampatsis and Izzat Darwazeh, "GSM Evolution towards 3rd Generation – 2.5 Generation,", International Symposium on Telecommunications, pp. 239-243, Sept 2001, Tehran, Iran
4. Dimitrios Karampatsis and Izzat Darwazeh, "Modelling and Performance Assessment of OFDM Systems by Simulation,", Proc. of the International Conference on Telecommunications (ICT 2002), vol. 2, pp.420-424, Beijing, China, June 2002
5. D. Karampatsis, M.R.D. Rodrigues and I. Darwazeh, "Implications of Linear Phase Dispersion on OFDM and Fast-OFDM Systems,", Proc. of the London Communications Symposium-UCL, pp. 117-120, London, UK, Sept. 2002
6. D. Karampatsis, M.R.D. Rodrigues and I. Darwazeh, "Performance Comparison of OFDM and FOFDM Communication Systems: Effects of Frequency Selective Fading, Frequency and Timing Offsets and I/Q QAM Modulator/Demodulator Imbalance,", 7th World Multiconference on Systemics, Cybernetics and Informatics (SCI 2003), pp. 396-400, Orlando, USA, July 2003 (invited paper)
7. D. Karampatsis and I. Darwazeh, "Performance Comparison of OFDM and FOFDM Communication Systems in Typical GSM Multipath Environments,", Proc. of the London Communication Symposium-UCL, pp. 369-372, London, UK, Sept. 2003

Chapter 2

Mobile communication systems

2.1 Introduction

In this chapter an overview of mobile communication systems and their modulation schemes is carried out. Details of the physical layer and modulation schemes of the GSM and EDGE systems are provided. In addition, future technologies for mobile communication systems are described with 4G potential technologies outlined. In addition, one of the modulation schemes considered for the 4G system is described in detail. This modulation is Orthogonal Frequency Division Multiplexing (OFDM) and its basic principles are summarised. Finally, a basic description of systems already implementing OFDM is carried out.

2.2 Mobile communication systems overview

The first cellular system was released in Japan in 1979 and in the United States by AT&T Bell Laboratories in 1982. The Advanced Mobile Phone Service or AMPS mobile system operated in the 800 MHz band and used a 40 MHz system bandwidth (30 kHz per channel). Europe followed shortly with the European Total Access Communication System or ETACS which operated in the 900 MHz band and used a bandwidth of 45 MHz. Both systems were analogue in nature, using FM modulation, and were termed as 1st generation systems.

In the early 90s a new revolutionary system was introduced in Europe by Group Speciale Mobile or GSM. This later came to be termed as the Global System for

Mobile Communications (GSM again!). This system was developed in order to overcome limitations of the first cellular systems in Europe, such as incompatibilities between different European systems, small number of simultaneously active users and poor performance in fading environments. GSM is the world first cellular system to implement digital modulation and network level architectures and services. It operates in the 900 MHz and 1800 MHz (PCS1800) bands (and 1900 MHz in the US). Its success in Europe has led non-European countries to adopt it. It is now the world most popular standard.

However, GSM was not able to cope with the increased demand for new users and services. In order to respond to market demand three systems were proposed, namely the HSCSD (High Speed Circuit Switched Data), GPRS (General Packet Radio Service) and EDGE (Enhanced Data Services for GSM Evolution) offering new services and higher data rates. The new systems were termed as 2.5 generation or 2.5G since they act as a bridge between the 2nd and 3rd generation systems [1].

The 2.5-generation systems were developed as an intermediate solution to the increased demands. The Universal Mobile Telecommunications System (UMTS) proposed by the 3GPP (3rd Generation Partnership Project), is one of the 3G systems. This system can provide at best 2 Mbps for stationary or indoor environments and at least 144 kbps for vehicular (moving) environments [2]. It is expected to cope with the demand of high data rates and multimedia services for at least a decade. The UMTS system is based on the CDMA (Code Division Multiple Access) concept.

2.3 GSM overview

2.3.1 Introduction

The modulation used in GSM is Gaussian Minimum Shift Keying (GMSK) a variation of Frequency Shift Keying (FSK). It can provide data rates of up to 270.833 ksps per channel or 14.4 kbps per user.

The next sections describe the basic principles of GMSK modulation and the air interface of the GSM system.

2.3.2 GMSK modulation

2.3.2.1 MSK principle

GMSK is actually Minimum Shift Keying (MSK) modulation through a Gaussian filter of bandwidth duration product of 0.3. MSK is a variation of FSK. In FSK modulation, the binary bits are distinguished from each other by transmitting two sinusoidal waves at two different frequencies [3]. This effectively is FM modulation of the binary bit streams. Therefore the modulation index k_f of an FSK signal is similar to that of FM modulation and expressed as:

$$k_f = \frac{2\Delta f}{R_b} \qquad \text{eq. (2.1)}$$

where, Δf is the peak frequency deviation and R_b is the bit rate.

The difference between MSK and FSK is that the carrier frequencies in MSK have a fixed frequency relation. More specifically, the peak frequency deviation of an MSK signal is equal to 1/4 the bit rate. In other words MSK is a continuous phase FSK with a modulation index of 0.5 [4]. In FM the peak frequency deviation is defined as the difference of the centre frequency from its main sidelobes. Therefore, the two frequencies of MSK will be separated by 1/2 the bit rate while still retaining their orthogonality. Thus, in MSK, the *minimum* frequency separation that allows orthogonal detection is achieved. The main properties of MSK are its constant envelope, relatively narrow bandwidth, phase continuity in the RF carrier at the bit transition instants (the absolute phase difference every bit transition is always 90 degrees) and coherent detection capabilities [4],[5]. However, MSK does not satisfy the severe requirements in respect of out-of-band radiation for mobile radio [6].

2.3.2.2 Gaussian filtering with time-bandwidth product (BT) of 0.3

Gaussian pulse-shaping is a non-Nyquist filtering technique because it does not satisfy the Nyquist criterion for ISI cancellation. Therefore, such filters improve the spectral efficiency of the modulation with the tradeoff in increased ISI. Nyquist filters have zero-crossings at adjacent symbol peaks and a truncated transfer function, whereas

the Gaussian filter has a smooth transfer function with no zero-crossings. This is highly desirable since the linearity requirements of RF power components are relaxed.

A pre-modulation filter is needed to be applied to MSK in order to satisfy the requirements of out-of-band radiation in mobile radio. Therefore, such filter should have the following properties; narrow bandwidth and sharp cut-off, lower overshoot impulse response and preservation of the filter output pulse area which corresponds to a phase shift of 90°. The first condition is needed to suppress high frequency components, the second to protect against instantaneous frequency deviations and the third to maintain the coherent detection of MSK [6]. The Gaussian filter achieves the first two conditions by smoothing the phase trajectory of the MSK signal and hence stabilising the instantaneous frequency variation over time. This has the effect of considerably reducing the sidelobe levels in the transmitted spectrum [4]. Generally, the introduction of pre-modulation filters violates the minimum frequency spacing constraint and the fixed-phase constraint of MSK. However, the above two constraints are not intrinsic requirements for effective coherent binary FM with modulation index 0.5. The GMSK signal can be detected coherently because its pattern-averaged phase-transition trajectory does not deviate from that of simple MSK [6].

The GMSK pulse-shaping filter has an impulse response given by [4]:

$$h_G(t)=\frac{\sqrt{\pi}}{\alpha}e^{-\frac{\pi^2}{\alpha^2}t^2} \qquad \text{eq. (2.2)}$$

where, $T_s=(1+a)/2B$, B the 3 dB bandwidth and T_s the symbol period [4]

The transfer function is given by:

$$H_G(f)=e^{-\alpha^2 f^2} \qquad \text{eq. (2.3)}$$

The parameter α is related to the 3 dB bandwidth of the filter by:

$$\alpha=\frac{\sqrt{\ln 2}}{2B^2}=\frac{0.5887}{B} \qquad \text{eq. (2.4)}$$

The GMSK filter is usually described by its BT product (3 dB bandwidth B and the baseband symbol duration T).

Figure 2.1, shows the spectrum of the GMSK signal for various values of BT. As the value of the BT product decreases the sidelobe levels of the GMSK spectrum reduce. However, the ISI levels increase which, in turn, deteriorate the BER performance of the system. It was decided for GSM to use a Gaussian filter with a BT product of 0.3 which gives good overall performance in error rate and satisfy the spectral efficiency requirements.

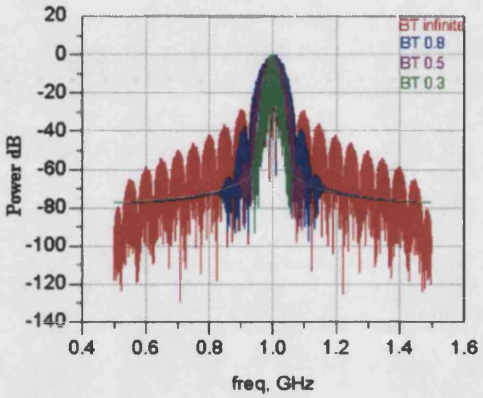

Figure 2.1 – GMSK frequency spectrum

2.3.3 GSM air interface

GSM uses Frequency Division Multiplex (FDM) to separate the frequencies into 124 carriers each of 200 kHz spacing. A combination of Time Division Multiplex (TDM) and Frequency Hopped Multiple Access (FHMA) techniques are then used to create 8 slots forming a burst frame, in the slow-frequency hopped carriers [7].

The GSM specifications specify a variety of GSM standards each with different range of frequencies. The standard GSM (GSM-900) uses two frequency bands each having a width of 25 MHz. The uplink (MS to BS) uses frequencies 890 to 915 MHz. The downlink (BS to MS) uses frequencies 935 to 960 MHz. Their spacing is 45 MHz, which is the same as for the analogue first generation system operated in the UK (ETACS). The development of GSM and the availability of new frequencies have introduced the DCS-1800 and PCS-1900 standards, where the uplink-downlink carrier separation is 85 MHz and 80 MHz, respectively. The full list of the standards used for GSM is shown in Table 2.1.

Table 2.1 – GSM frequency bands [8]

	Uplink (MHz)	Downlink (MHz)
GSM-450	450.3 – 457.6	460.4 – 467.6
GSM-480	478.8 – 486	488.8 – 496
GSM-850	824 – 849	869 – 894
Standard GSM-900	890 – 915	935 – 960
Extended GSM-900	880 – 915	925 – 960
Railways GSM-900	876 – 915	921 – 960
DCS-1800	1710 – 1785	1805 – 1880
PCS-1900	1850 – 1910	1930 – 1990

The radio interface of GSM uses slow frequency hopping for two main reasons. Firstly, its frequency diversity alleviates the effects of multipath fading and secondly, its interference diversity, a property associated with spectral spreading in order to spread the interference in many cells [9]. Frequency hopping is based on changing the frequency used by a channel at regular intervals. When the frequency changes quicker than the symbol rate it is termed as Fast Frequency Hopping (FFH), whereas, when the transmission frequency remains the same during the transmission of a whole symbol, it is termed as Slow Frequency Hopping (SFH). GSM uses the SFH scheme. For a set of n frequencies, GSM allows $64 \times n$ different hopping sequences to be produced.

2.3.4 Traffic channel

The Traffic Channel (TCH) allows the user to have a portion of the radio interface which is going to be used throughout the duration of the call. The TCH is subcategorised into two formats. Firstly, the full rate traffic channel (TCH/F), which allows the transmission of 13 kbps speech or data at a rate of 12, 6 or 3.6 kbps. Secondly, the half rate traffic data (TCH/H) which allows the transmission of 7 kbps speech or data at a rate of 6 or 3.6 kbps. The block diagram of the TCH/F channel is shown in Figure 2.2.

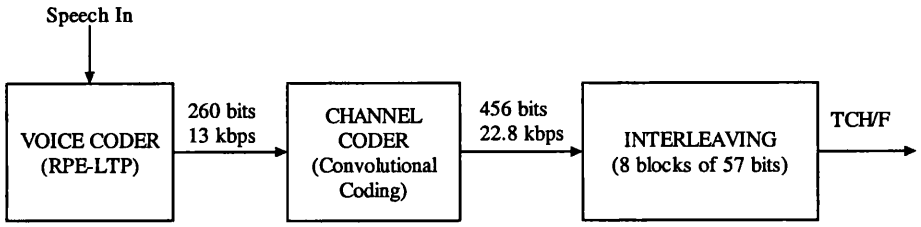

Figure 2.2 – Full rate traffic channel

The speech coder used in GSM uses the Regular Pulse Excited Long-Term Prediction (RPE-LTP) codec [10]. The net bit rate of the codec is 13 kbps. In effect it is a block coder which analyses speech samples in blocks of duration 20 ms. The resulting output block size is 260 bits.

Due to the lower samples of the coder, its performance is sensitive to errors. From the 260 bits per block, 182 (class 1 bits) are more sensitive to errors than the remaining 78 bits (the class 2 bits). The class 1 bits are further subdivided into two subclass of 1a (50 bits) [more sensitive] and 1b (132 bits). A half rate cyclic redundancy code is applied to the class 1 bits. To the class 1a bits a parity check is also added. The polynomial representing the detection code for category 1a bits is X^3+X+1. The convolutional code consists in adding 4 bits (set to "0") to the initial 185 bit sequence (182 + 3 parity bits) and applying two convolutions whose polynomials are respectively D^4+D^3+1 and D^4+D^3+D+1. No coding is applied to the remaining bits. With this method the number of bits per block is increased from 260 to 456, increasing the rate to 22.8 kbps [7],[9],[10].

The bits out of the channel coder are additionally protected by using interleaving. Although channel coding is very efficient, especially when bit errors are evenly distributed within the transmitted bit stream, it is not very efficient when fading errors exist, where errors occur in bursts. The bit interleaving process is a form of error protection used to solve the above problem. The sequence of 456 bits is re-ordered and then divided into 8 blocks of 57 bits. Each block is transmitted in a normal burst on the TCH. This is known as an interleaving depth of 8. Each individual bit in a block is allocated to the eight bursts. Each burst will contain bits from two separate speech samples because each normal burst has 114 data bits. The speech blocks are necessary to be available before a normal burst can be formed. This requires an interval of 40 ms

and hence the delay in coding for GSM is in the order of 40 ms. The de-interleaving process is simply the reverse of the interleaving process [7],[9],[10].

2.3.5 The normal burst

The burst is the transmission method for GSM. Its transmission takes place during a burst period of duration (15/26) μs or 0.577 μs. 8 burst periods (timeslots) form a TDMA frame. In GSM there are four types of bursts that can occupy a timeslot. The Frequency correction and Synchronising bursts are used for initial synchronisation between the mobile and the base station. The Access Burst is used to access a cell for the first time in case of call set-up or handover. Finally, the Normal Burst is used in all other cases.

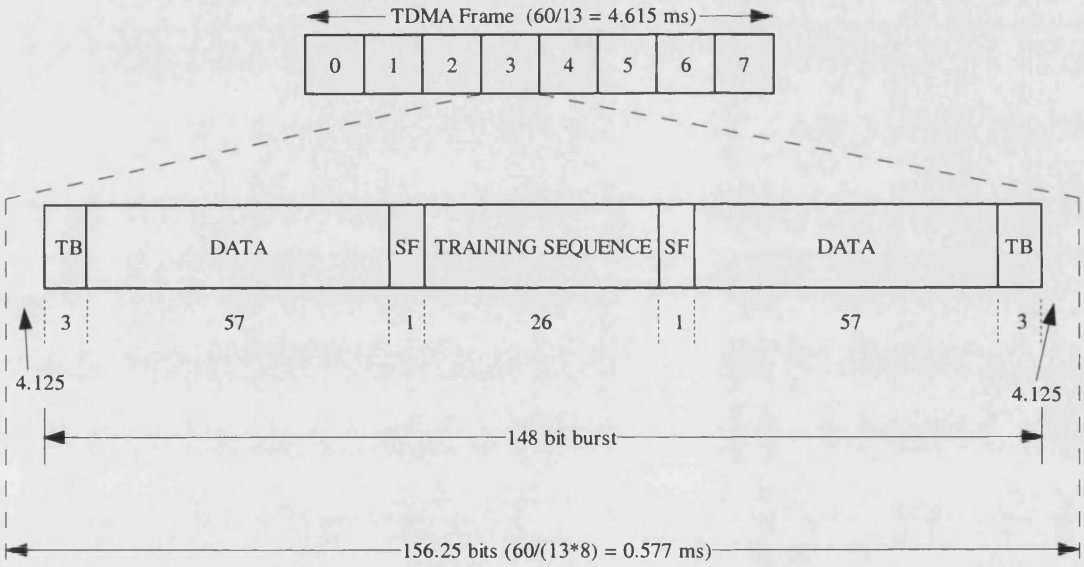

Figure 2.3 – The normal burst [7]

The data structure within a normal burst is shown in Figure 2.3. It consists of 148 bits (in 156.25 bit slots) transmitted at a rate of 270.833 kbps. Of these bits 114 bits are available for data transmission. These are the bits coming from the TCH. The remaining bits are used to assist reception and detection. A training sequence of 26 bits in the middle of the burst is used by the receiver to synchronise and estimate the propagation characteristics. This allows the setting up of an equaliser to compensate for time dispersion produced by multipath propagation (up to 16 μs time dispersion). Tail bits (TB) (3 bits) transmitted at either end of the burst enable the data bits near the edges

of each burst to be equalised as well as those in the middle. Two stealing flags (SF) (one at each end of the training sequence) are used to indicate that a burst which had initially been assigned to a traffic channel has been stolen for "signalling" purposes. The burst modulates one carrier of those assigned to a particular cell using Gaussian Minimum Shift Keying. (GMSK) [7].

The basic block diagram of a GSM system is shown in Figure 2.4.

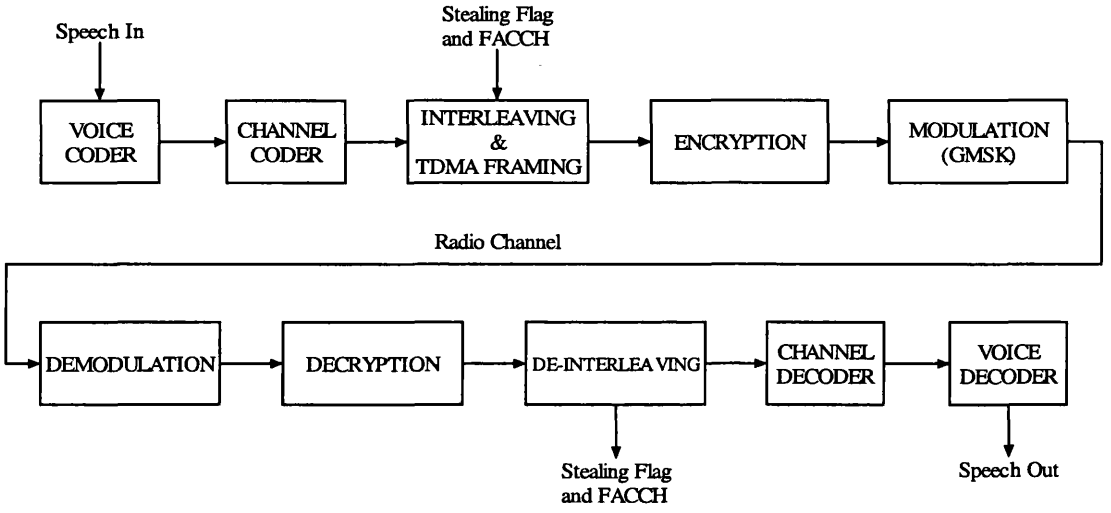

Figure 2.4 – Block diagram of GSM system

2.4 EDGE overview

2.4.1 Introduction

EDGE was one of the proposals to upgrade the GSM system using the same TDMA (Time Division Multiple Access) structure, logic channels and 200 kHz carrier bandwidth as in GSM networks [1]. In order to support higher transfer rates a new modulation scheme is introduced based on the 8 Phase Shift Keying (8PSK) modulation. In such scheme, three bits are assigned for each symbol. Thus in EDGE the data rate that can be achieved is up to three times the data rate of GSM. In addition, a special linearised Gaussian pre-modulation filter is used, in order to maintain the spectral specifications of the GSM system.

There are two configurations, one supporting the circuit switched principle (ECSD) and one supporting the packet principle (EGPRS). For ECSD, new channel coding schemes have been introduced allowing data rates of up to 43.5 kbps per timeslot. The maximum theoretical data rate when using all 8 timeslots of the TDMA

frame is 348 kbps. EGPRS is based on the GPRS system and its radio architecture [11]. It requires an improved radio link control (RLC) protocol to support higher data rates. In several channel coding schemes the use of link adaptation have been added to adapt the data protection to the channel quality [11]. The data rates range from 8.8 to 59.2 kbps, according to the coding scheme adapted. The maximum theoretical data rate that can be achieved when using all 8 multislots of the TDMA frame is 473.6 kbps.

2.4.2 Linearised Gaussian 3π/8 rotated 8PSK

In Binary Phase Shift Keying (BPSK) the phase of a constant amplitude signal is varied between two values according to the two binary signals. Normally, a binary 1 will have the following equation [3]:

$$S_{BPSK,1}(t)=\sqrt{\frac{2E_s}{T_s}}\cos(2\pi f_c t+\varphi) \qquad \text{eq. (2.5)}$$

and a binary 0 will have 180° phase shift:

$$S_{BPSK,0}(t)=\sqrt{\frac{2E_s}{T_s}}\cos(2\pi f_c t+\pi+\varphi)=-\sqrt{\frac{2E_s}{T_s}}\cos(2\pi f_c t+\varphi) \qquad \text{eq. (2.6)}$$

where, E_s is the energy per symbol and T_s the symbol period

8PSK involves the mapping of three bits at a time. A phase is assigned for each possible combination of the incoming 3-bit sequence. More specifically, the phase of each sequence is obtained by the following equation [12]:

$$\theta_i=\frac{2(i-1)\pi}{8}, \qquad i=1,2,...,8 \qquad \text{eq. (2.7)}$$

Consequently, the modulated waveform of an 8PSK signal is given by:

$$S_{8-PSK}(t)=\sqrt{\frac{2E_s}{T_s}}\cos(2\pi f_c t+\theta_i) \qquad \text{eq. (2.8)}$$

where, E_s is the energy per symbol and T_s the symbol period.

The 8PSK modulation scheme for EDGE signals is defined from ETSI in [13]. It consists of 8PSK mapping with Gray coding, $3\pi/8$ rotation and Gaussian filtering, as illustrated in the following figure.

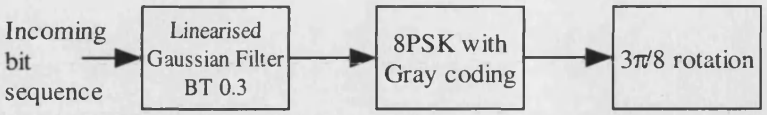

Figure 2.5 – EDGE 8PSK signal generation block diagram

The constellation diagram of an 8PSK signal with Gray coding is shown in Figure 2.6.

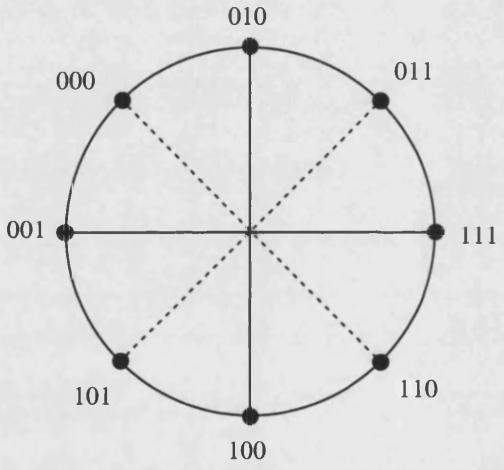

Figure 2.6 – 8PSK signal with Gray coding

The mapped symbols are now rotated by a phase shift of 3π/8 radians according to the following equation:

$$\hat{S}_i = S_i \cdot e^{ji\frac{3\pi}{8}} \qquad \text{eq. (2.9)}$$

where, i equals the number of the incoming 8PSK complex symbols and S_i is the 8PSK symbol.

Therefore, each consecutive incoming symbol is rotated by an increasing phase multiple of 3π/8 rad. This is illustrated in Figure 2.7. If the first bit sequence is 010 it will be rotated by 3π/8. Assuming that the second bit sequence is 101, it will be rotated

by twice that phase shift. Similarly if the third bit sequence is 011, the constellation point will be rotated by $3\times\frac{3\pi}{8}$ rad.

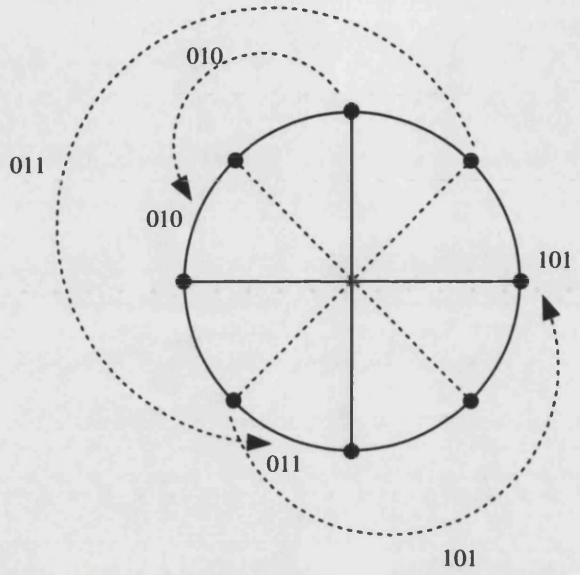

Figure 2.7 – 3π/8 rotation of 8PSK constellation

Due to such rotation the constellation points increase to 16 since the phase difference between two successive constellation points is halved [12]. Figure 2.8, shows the comparison of two 8PSK trajectory diagrams. The first one has no rotation whereas the second one has rotation of 3π/8 rad.

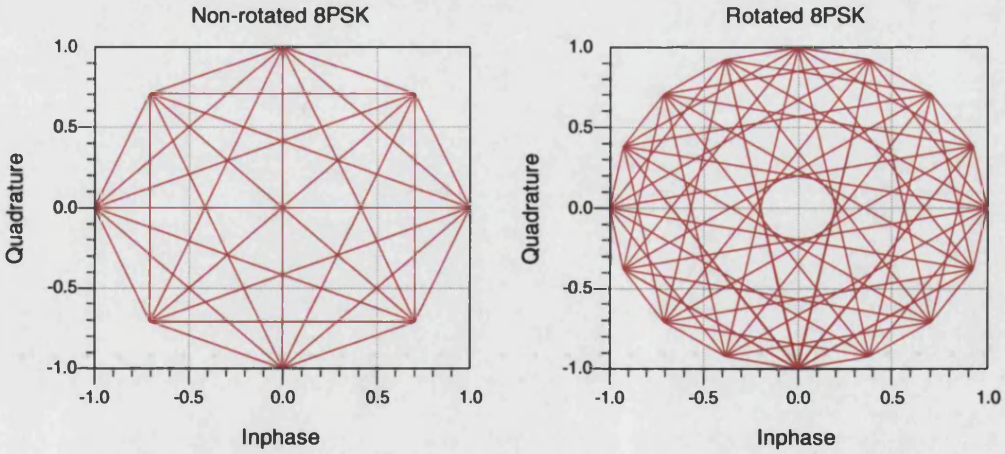

Figure 2.8 – Trajectory diagrams for non-rotated and 3π/8 rotated 8PSK

The important advantage of rotating the 8PSK symbols is that zero-crossings during symbol transitions are avoided. By avoiding such zero crossings the peak-to-average power ratio (PAR) and peak-to-minimum power ratio (PMR) produced in each transition remains relatively constant, which make feasible the use of non-highly linear RF components, similar to the GMSK modulation of GSM.

The final step in the 8PSK modulation for EDGE employs a linearised Gaussian filter of BT 0.3 to limit the spectrum of the 8PSK signal to the GSM spectrum mask. The filter which is specified by ETSI, is the main component in a Laurent decomposition of the GMSK modulation, with impulse response $c_0(t)$, given by the following equations [13]:

$$c_0(t) = \left\{ \begin{array}{l} \prod_{i=0}^{3} S(t + iT_s), \text{for } 0 \le t \le 5T_s \\ 0, \text{ else} \end{array} \right\} \qquad \text{eq. (2.10)}$$

where,

$$S(t) = \left\{ \begin{array}{l} \sin(\pi \int_0^t g(t')dt'), \text{for } 0 \le t \le 4T_s \\ \sin(\frac{\pi}{2} - \pi \int_0^{t-4T_s} g(t')dt'), \text{for } 4T_s < t \le 8T_s \\ 0, \text{else} \end{array} \right\} \qquad \text{eq. (2.11)}$$

$$g(t) = \frac{1}{2T_s}\left(Q(2\pi \cdot BT \frac{t - 5T_s/2}{T_s\sqrt{\log_e(2)}}) - Q(2\pi \cdot BT \frac{t - 3T_s/2}{T_s\sqrt{\log_e(2)}}) \right) \qquad \text{eq. (2.12)}$$

$$Q(t) = \frac{1}{\sqrt{2\pi}} \int_t^{\infty} e^{-\frac{\tau^2}{2}} d\tau \qquad \text{eq. (2.13)}$$

The bandwidth duration product (BT) is 0.3 and T_s is the symbol period.

The filter impulse response lasts for 5 symbol periods. Therefore, during one symbol period, a linearised Gaussian 8PSK signal will contain information of five consecutive symbols, resulting in ISI. Due to such filtering the transitions between consecutive symbol transitions is much smoother, as illustrated in Figure 2.9, where the trajectory diagram of an EDGE 8PSK signal is shown.

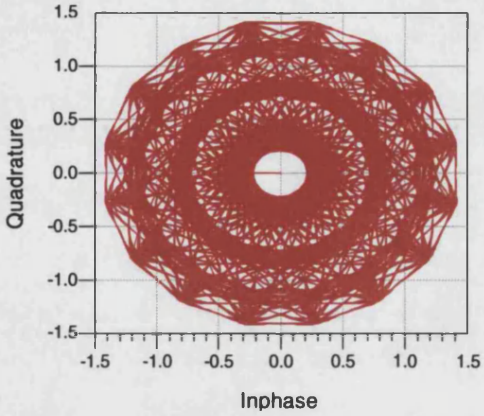

Figure 2.9 – EDGE 8PSK trajectory diagram

Figure 2.10, shows that the RF spectrum of an EDGE signal is within the GSM spectrum mask.

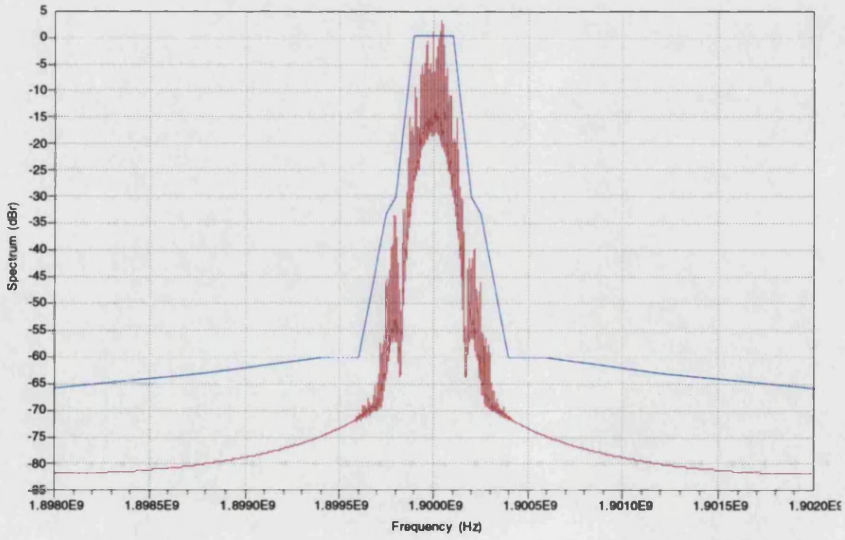

Figure 2.10 – EDGE RF spectrum in GSM spectrum mask

2.4.3 Framing and frequency allocation

The EDGE system was designed to extend the HSCSD and GPRS systems in order to provide further increases in data rates. It was designed to be introduced in the GSM network core with minimal effort and cost. It re-uses the existent protocols, frequency plans and frame structures. For example, the Normal Burst frame of an EDGE signal is identical to the burst frame of GSM, shown in Figure 2.3 with the only difference that the 114 data bits of the GSM burst frame are 114 8PSK symbols or 342 bits in the EDGE burst frame. Hence, more information is transmitted in one EDGE frame than in GSM. The training sequence bits of the EDGE signal remain the same.

2.5 The new capabilities of 3G systems

The first proposal for a 3rd generation system was carried out by ETSI (European Telecommunications Standards Institute). In December 98 the 3GPP group was formed (3rd Generation Partnership Project) following an agreement between six standard setting bodies around the world including ETSI, ARIB and TIC of Japan, ANSI USA and TTA of Korea. This group is responsible for setting the standards, approving and maintaining the technical specifications and reports for a 3G mobile system based on evolved GSM core networks and FDD and TDD radio access technologies [14].

The proposed standard for 3G mobile networks is based on CDMA radio access technology and supports three optional modes of operation, shown in Table 2.2.

It was agreed that for European 3G systems, two radio interface methods will be used. These are:

(i) WCDMA (FDD) operation in paired frequency bands

(ii) TD/CDMA (TDD) operation in unpaired frequency band

Table 2.2 – UMTS modes of operation

Mode	Title	Origin	Supporters
1	Direct Sequence FDD (Frequency Division Duplex)	Based on the first operational mode of ETSI's UTRA (UMTS Terrestrial Radio Access) RTT proposal	Japan's ARIB and GSM operators and vendors
2	Multi-Carrier FDD (Frequency Division Duplex)	Based on the cdma2000 RTT proposal from the US telecommunication industry	Cdmaone operators and members of the CDMA Development Group (CDG)
3	Time Division Duplex (TDD)	The second operational mode of ETSI's UTRA RTT (UMTS Terrestrial Radio Access) proposal. An unpaired band solution to better facilitate indoor cordless communications.	Harmonised with China's TD-SCDMA RTT proposal

The WCDMA (FDD) scheme is designed to operate in either of the following paired bands, shown in Table 2.3.

Table 2.3 – WCDMA frequency allocations

Region 1		Region 2	
Uplink	**Downlink**	**Uplink**	**Downlink**
1920 – 1980 MHz	2110 – 2170 MHz	1850 – 1910 MHz	1930 – 1990 MHz

Table 2.4 – TD/CDMA frequency allocations

Region 1		Region 2		
Uplink – Downlink (MHz)	**Uplink – Downlink (MHz)**	**Uplink – Downlink (MHz)**	**Uplink – Downlink (MHz)**	**Uplink – Downlink (MHz)**
1900 – 1920	2010 – 2025	1850 – 1910	1910 – 1930	1930 – 1990

The minimum transmit-receive frequency separation is 134.8 MHz and the maximum is 245.2 MHz. The default frequency separation when operating in the first paired band is 190 MHz, whereas in the second it is 80 MHz. For the TD/CDMA, one band is used for uplink-downlink using Time Division Duplex (TDD). The frequency allocation for this scheme is shown in Table 2.4 [15].

The main characteristics of the WCDMA format are shown in the table below.

Table 2.5 – WCDMA specifications [15]

Channel B/W	5 MHz
Duplex Mode	FDD and TDD
Downlink RF Channel Structure	Direct Spread
Chip Rate	3.84 Mc/s
Frame Length	10 ms
Spreading Modulation	Balanced QPSK (downlink) Dual-channel QPSK (uplink) Complex spreading circuit
Data Modulation	QPSK (downlink) BPSK (uplink)
Channel Coding	Convolution and Turbo codes
Coherent Detection	User dedicated time multiplexed pilot (downlink and uplink), common pilot in the downlink
Channel multiplexing in downlink	Data and Control channels time multiplexed
Channel multiplexing in uplink	Control and Pilot Channels time multiplexed I & Q multiplexing for data and control channel
Multirate	Variable spreading and multicode
Spreading factors	4-256 (uplink), 4-512 (downlink)
Power control	Open and fast closed loop (1.6 kHz)
Spreading (downlink)	OVSF sequences for channel separation Gold sequences 2^{18}-1 for cell and user separation (truncated cycle10 ms)
Spreading (uplink)	OVSF sequences, Gold sequences 2^{41} for user separation (different time shifts in I and Q channel, truncated cycle 10 ms)
Handover	Soft handover Interfrequency handover

2.6 Considerations for the 4G system

Currently, there is a growth in mobile use, with an estimated global-user base to exceed two billion by 2005 [16],[17]. Short message service is booming, especially with the younger generation averaging 100 messages per month. The 3rd generation or 3G system is expected to provide coverage for the current needs of the users for approximately 10 years time. 3G systems can support multimedia-internet type services at relatively high speeds and quality. The WCDMA radio air interface has been designed to provide improved high capacity coverage for medium bit rates (384 kbps) with limited coverage up to 2 Mbps. The efficiency of packet-mode transmission is also improved by statistical multiplexing on the air, allocating bandwidth dynamically, allowing more channels to be connected and making most efficient use of the allocated space. However, the 3G system have limitations. Firstly, due to excessive interference between services in CDMA, it is difficult to increase the data rates. Secondly, it is difficult to provide a full range of multirate services, all with different QoS (Quality of Service) and performance requirements. This is due to the constraints imposed on the core network by the air interference standard. Finally, the bandwidth available in the 2 GHz band allocated for 3G will soon become saturated and there are constraints on the combination of frequency and TDD modes of delivery imposed by regulators in order to serve different environments efficiently [16]. The roll off of the 3G system was scheduled to start by 2001 [18]. Unfortunately, the economic downturn in the telecommunications industry delayed the initial deployment of UMTS in the UK until 2003. However, even at the height of the economic downturn, it was expected that 3G technologies will have the potential to lead to substantial market opportunities with a predicted value of up to $320 billion in 2010, $233 billion of which to be generated by new services [18]. For these reasons, the mobile industry is already discussing the question of what comes after the 3rd generation. Different systems and structures are being discussed as well as a variety of modulation techniques. This section will focus on considerations for the 4th generation system. The forecast, targets, requirements and modulation techniques considered will be outlined.

2.6.1 Market and traffic forecast

There has been a step change in mobile communications systems every decade. The first generation mobile system was introduced in 1980s. The 2G system was introduced in 1990s. Both systems have been used mainly for voice applications and supporting circuit switched type services [19]. The 3G UMTS system is already deployed. Following the same progress pattern, the 4G system should be deployed around 2010.

In Japan, one of the most advanced countries in cellular communications, the number of mobile subscribers by the year 2010 is expected to be around 81 million [20]. It is also presumed that this number will be saturated by the year 2006. Although the number of mobile users will be saturated, it is expected that traffic will increase, since the number of Internet users is growing exponentially. One of the requirements of 4G systems is the integration of Internet and mobile communications aspects. Thus, in the future the amount of data to be transmitted will be proportional to the memory size of a PC and/or the number of pixels in a display. Knowing the vast advancement in computer technology it is obvious that by 2010 memory storage capacity will be considerably increased. Therefore, mobile users can transmit more complex graphics and/or videos. Moreover, the number of terminals will increase, since by 2010 it is predicted that there will be a variety of mobile communication devices ranging from wallets to Personal Digital Assistants (PDA). The relationship between number of subscribers and the increase in traffic is shown in the following figure.

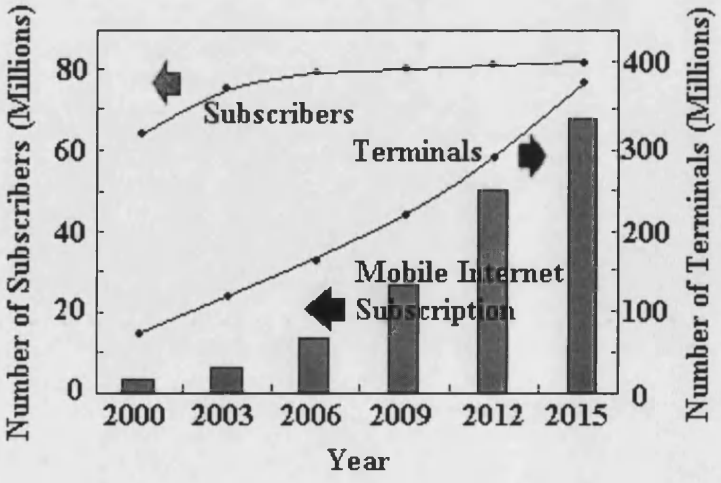

Figure 2.11 – Number of terminals and subscribers in Japan [20]

2.6.2 Service requirements

The conclusion from the previous section is that the traffic will be continuously increasing despite the saturation of mobile subscribers. Therefore, the first requirement of a 4G system will concern transmission rate. Data rate is one of the most fundamental parameters in the radio access network. Comparing 2G and 3G systems, the bit rate of the 3G system is around 10 times higher than that of a 2G. Therefore, the bit rate of the 4G system is expected to be 10 times higher than that of the 3G system. However, recently an evolutionary approach to the 3G system has been taken into consideration. It involves a phase called WCDMA/HSDPA (High Speed Downlink Packet Access) [21]. This system promises data rates of up to 10 Mbps and higher spectrum efficiency. It is often termed as 3.5G system, following the same pattern with the evolution of GSM through HSCSD, GPRS and EDGE which are termed as 2.5G systems. Having this in mind, the next generation technology should support data rates of at least 80 Mbps in low mobility and at least 20 Mbps in high mobility situations [22],[23]. The use of intelligent transport system is also required to enable high transfer speeds in high mobility situations [24].

The capacity of the 3G system, (the maximum possible information transfer rate that the system can tolerate), will not be sufficient to handle the explosively growing multimedia traffic in the 2010's. The capacity per unit area must be increased relatively to the increase in data rate. The cell radius of a cellular radio network is inversely proportional to its capacity. Therefore, in order to increase the capacity the cell radius must decrease. However, for high mobility situations wide area coverage is necessary. A possible solution is given in [24], where High Altitude Platform Station (HAPS) systems are used. This system uses large airships in communication platforms in a stratospheric layer 20 km above the ground.

The reduction of the size of the cell also introduces power and EMC problems, which must be taken into consideration. The increase in transfer rates means also that mobile users can access more information faster. The bit cost therefore should be dramatically cut so that people can use it without worrying about charges.

One important aspect of the 4G system, will be the support of next generation Internet, mainly, IPv6 multicast and Mobile IP. IPv6 offers a number of enhanced features in comparison with the current internet format IPv4 in order to cope with feature needs and demands [25]. The support of next generation Internet will enable

access to the network using means other than a mobile device. Internet services have also the potential to lower service cost (for example Voice over IP). However, wireless systems use limited radio resources (frequency bandwidth and transmitting power) and suffer from congestion. A wireless QoS resource control is necessary to maintain service quality and support various applications and service classes [24],[26]. In addition seamless connection between fixed and mobile systems is considered, since fixed systems have advantages in transfer speed, transmission quality and cost, but are applicable only to prescribed locations.

Another important issue is that of the "killer application". With every electronic system a "killer application" is associated, for example, Internet applications in computer systems. This is used mainly for marketing purposes in order to increase sales. In mobile phone systems, SMS in 2G systems and live videoconference in 3G systems are the killer applications. In 4G it is likely to be the personal mobile assistant (PMA), a combination of a mobile phone and a palmtop PC [16].

The choice of frequency spectrum allocation is also being considered. The sub 3 GHz band has been assigned to 2G and 3G systems. The 5 GHz, 40 GHz and 60 GHz bands have been assigned in Japan USA and Europe, for research and experiments on future systems [27].

2.6.3 Network architecture

The requirements of the 4G system to be high speed, have high capacity with low per-bit cost and support of new applications, require a different Radio Access Network (RAN) from current RANs. The 4G system will be based moreover in a micro-cellular environment. Current RANs are not optimised to high-speed micro-cellular networks. The structure of today's RAN has a vertical tree shape connected to a Radio Network Controller (RNC), as shown in Figure 2.12. When a mobile station (MS) is handed over between adjacent BSs, all signals including layer 1 received at each BS are transmitted to the RNC and combined for diversity handover. If three BSs are used for each handover, signal traffic on the entrance links between the BSs and RNC is tripled. The reduced cell size in the 4G system will result in more frequency handover operations. In such situations, heavy load will result in the entrance links and the RNC signal processing equipment. Such problems can be resolved by using advanced signal processing equipment. On the other hand, the complexity of such

equipment will result in considerably increasing the overall cost. In addition, when employing radio entrance links, a higher frequency band needs to be used to transmit broadband signals. Higher frequency bands suffer from rain and oxygen attenuation which means that the signal transmission range is limited to few kilometres. Therefore, radio repeaters are necessary for distant BS that will further increase the total cost.

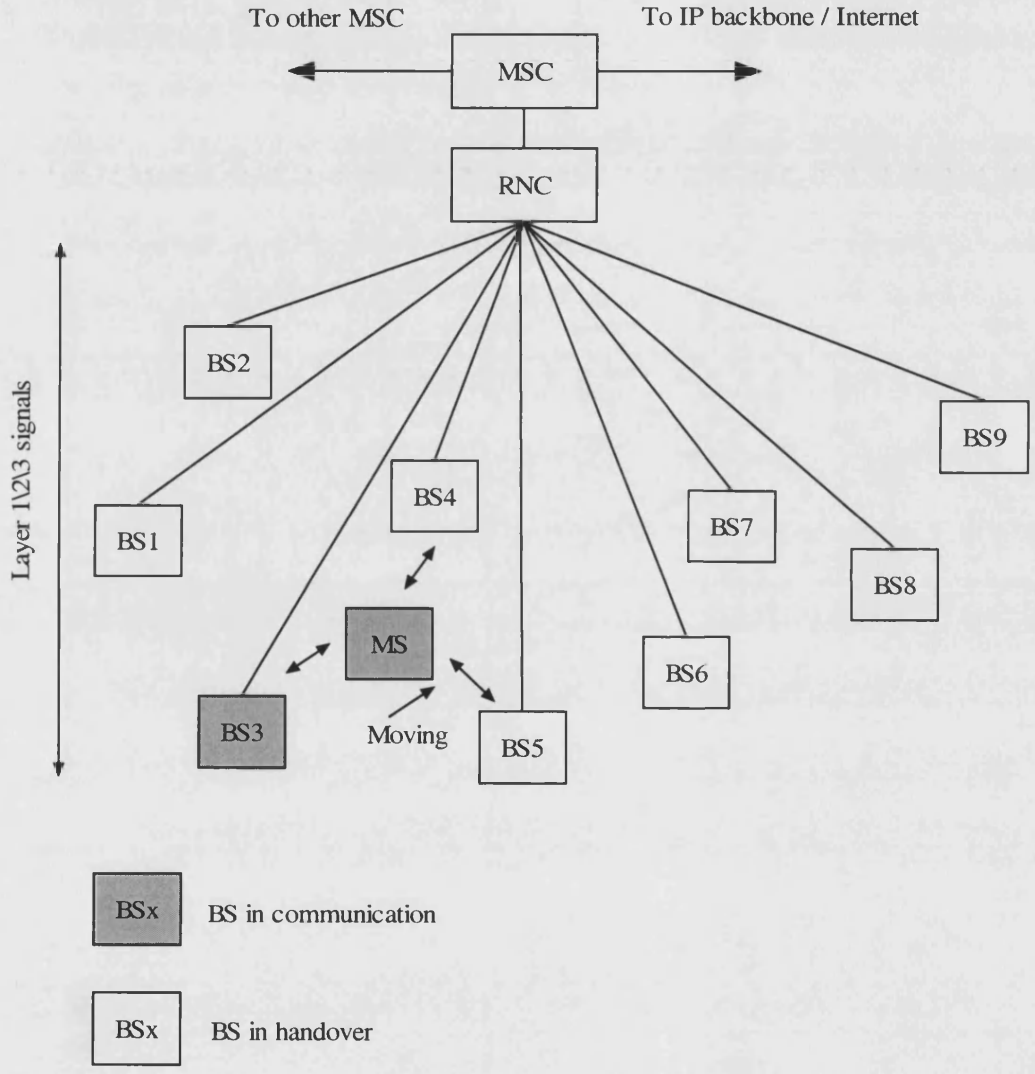

Figure 2.12 – Current radio access network architecture [26]

The new RAN structure must be designed in such way so as to minimise infrastructure cost. It should be able to have localised handover processing and Local Area Network (LAN) structure. One proposed RAN for the 4G system [26], is shown in Figure 2.13.

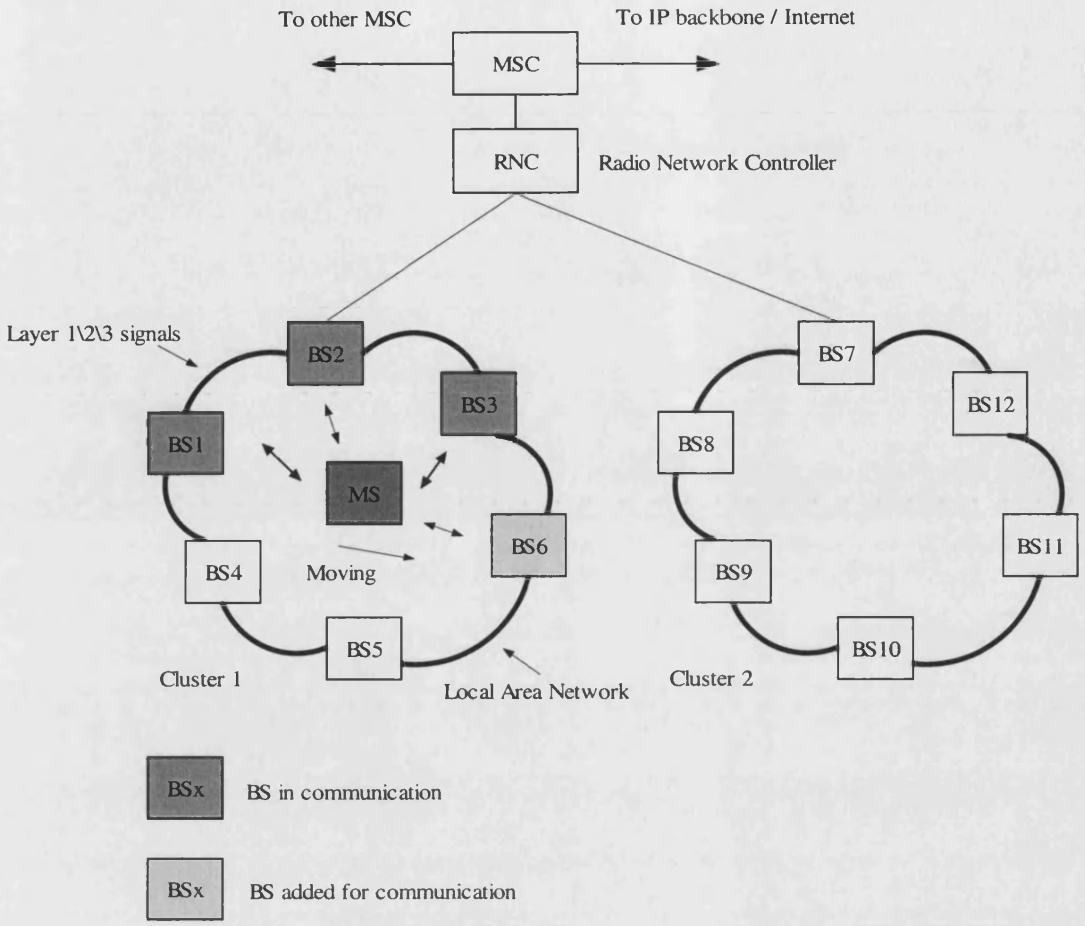

Figure 2.13 – Proposed RAN architecture (cluster RAN) [26]

Compared to the current RAN, shown in Figure 2.12, the BSs in the new RAN are grouped in a cluster with one BS, named cluster-head BS, connected to the RNC. This resembles a Local Area Network topology, where all the diversity handover between the BSs is processed in the cluster and not by the RNC as performed in current RANs. The RNC treats each cluster as a virtual BS. In this way, most of the layer 1 signal processing is performed inside the cluster, reducing the traffic load in the entrance links and the RNC processing equipment. Consequently, it is possible to employ more sophisticated and high-gain diversity schemes such as soft-decision combining, which reduce the required E/N_0 value and increase the cell radius and system capacity. The localised handover principle can also be incorporated for downlink adaptive transmission, where the BS can decide whether or not it is suitable to send a packet signal, reducing the probability of unnecessary or excessive power transmission [26].

One of the biggest problems in future RANs is output power. It is difficult to overcome this issue without increasing cost and fulfilling EMC restrictions. The most probable solution is smart antennas, especially adaptive array antennas [28]. Such antennas have high gain that counter the increased propagation loss, due to the use of higher frequency bands. In, addition adaptive array antennas have the capability to reduce co-channel interference, which has the effect of increasing capacity. Other technologies considered in order to improve the radio network are, software radio [29], which enables the coexistence of several telecommunication services and Radio-over-Fibre (RoF) [30]. RoF technology can reduce the infrastructure cost, when the length of a link is short, by using an optical fibre instead of a microwave link.

Another possibility is through the use of adhoc networks replacing the traditional ATM core network into heterogeneous distributed all-IP network architecture [22].

2.6.4 Multiple access schemes considered

For the 4G system there are three candidates, which are Code Division Multiple Access (CDMA), Time Division Multiple Access (TDMA) and Orthogonal Frequency Division Multiple Access (OFDMA) techniques. Each access scheme has its own advantages and disadvantages.

CDMA is a popular format mainly in the United States, where it is used in the US version of the 2G system, IS-95. CDMA is also implemented in the 3G system. The advantage of the CDMA technique is that it allows simultaneous use of all the allocated bandwidth. In addition, due to the spreading of the transmitted data (transmission of long symbols), the time span of the transmitted symbol is longer than the time spread of the channel resulting in the signal to be robust in fading channels and thus Intersymbol Interference (ISI) problems. Problems associated with CDMA are the highly complex rake receiver equalisers needed and the need for strict power control, resulting from the "near-far" effect. This effect is present when a CDMA interfering transmitter, having a spreading code "B", is much closer to the receiver than the intended transmitter, both having spreading code "A". Although the cross-correlation of code "A" and code "B" is low, the autocorrelation of the received signal from the interfering transmitter can exceed the autocorrelation of the received signal from the

intended transmitter. As a result data detection is not possible. Some systems using the CDMA scheme are given in [31]-[36].

TDMA is especially considered in Japan. It has advantages in allowing asymmetrical communications and flexibility in the frequency assignment. However, frame synchronisation among base stations remains a difficult issue.

The OFDM scheme is the most probable format that will be adopted for the 4G system [1],[37],[38]. An OFDM system simultaneously transmits a large number of narrow-band carriers (subcarriers), each modulated at a low data rate. The simultaneous transmission of those subcarriers increases the symbol duration, which combats multipath delay spread over wireless channels and results in high data rates. Problems associated with OFDM are Intercarrier Interference (ICI) and system limitations associated with the linearity and efficiency of amplifiers. OFDM has been chosen as the transmission method for the terrestrial and satellite European radio with Eureka 147 Digital Audio Broadcast (DAB) system [39],[40], the terrestrial Digital Video Broadcast (DVB-T) system [41] and wireless LAN systems such as ETSI Hiperlan/2 [42] and IEEE 802.11 standards [43]. There are also proposals for systems using OFDM modulation given in [44]-[47]. The basics of OFDM are described in the following section.

2.7 Variants of OFDM

OFDM stands for Orthogonal Frequency Division Multiplexing. The basic principle of OFDM is the division of the available spectrum into overlapping orthogonal subcarriers, where each is modulated by a low rate data stream. Its roots trace back to the 1950s where it was used for military applications. More specifically, it was used in military HF communication systems such as the KINEPLEX system [48]-[49] from Collins Radio Co. (USA), the ANDEFT/SC-320 system [50] from General Dynamics Corp. (USA) and the AN/GSC-10 KATHRYN system [51],[52] from General Atronics Corp. (USA). It has been then subject of important work in the mid-1960s at Bell Laboratories [53]-[56]. R.W. Chang was the first person to mention the term OFDM, for this orthogonal modulation [53]-[54].

The disadvantage of the proposed schemes was their complexity in terms of the many oscillators needed to form the OFDM signal. In such a case mutual interference existed between the subcarriers which distorted the signal. A novel solution to this

problem was presented in [57], where it was shown that an OFDM system can be implemented efficiently by an inverse discrete Fourier transform. At the receiver a forward discrete Fourier transform is used to recover the transmitted data bits. With the advancement of DSP and VLSI technology, it soon became possible to construct ICs of Fourier Transform and OFDM was starting to be reconsidered for use in modern communications systems. In [58], the performance of OFDM in digital mobile channels with multipath propagation and co-channel interference is evaluated. The results showed improvement in BER over flat Rayleigh fading environments. OFDM is now used in many communication systems and is considered as one of the modulation schemes to be used in the fourth generation mobile system, as we have discussed in the previous section.

The next sub-section will describe the basic principle of an oscillator-based (continuous-time) and FFT-based (discrete-time) OFDM system. Subsequently, modulation methods using the OFDM principle such as MC-CDMA and systems implementing OFDM (DVB, WLAN) will be presented. OFDM is discussed in more detail in Chapter 3, where its design issues in a wireless channel are studied.

2.7.1 Continuous-time (oscillator-based) OFDM

An OFDM signal is implemented by modulating a low rate data stream with duration T, with a number of orthogonal overlapping subcarriers each separated by a frequency of $1/T$ Hz. A frequency separation of $1/T$ Hz, is the minimum separation to achieve orthogonality. Consequently, the correlation between adjacent subcarriers is zero at the sampling instants, due to their orthogonality. Hence, the subcarriers may overlap with no loss of information. The OFDM signal is generated by adding up all the individual modulated subcarriers. The resulting data rate is N/T bits/s, where N is the total number of the subcarriers used. In other words, the total data rate to be sent on the channel is divided between the subcarriers.

The complex envelope representation of an OFDM signal is given by:

$$s_{tx}(t) = \sum_{k=-\infty}^{\infty} \sum_{n=0}^{N-1} a_{n,k}\, g_n(t - kT) \qquad \text{eq. (2.14)}$$

$$g_n(t)=\begin{cases}\frac{1}{\sqrt{T}}e^{j\frac{2\pi nt}{T}}, t\in[0,T]\\ 0, \quad t\notin[0,T]\end{cases} \qquad \text{eq. (2.15)}$$

where, T is the duration of the signalling interval, $a_{n,k}$ is the complex symbol transmitted on the n^{th} subcarrier at the k^{th} signalling interval, N is the number of OFDM subcarriers, $g_n(t-kT)$ represents the complex subcarrier used to convey the complex data in the same time slot and subchannel.

The spectrum of an OFDM signal is given by:

$$\begin{aligned}S_{tx}(f)&=\int s_{tx}(t)e^{-j2\pi ft}dt=\int\sum_{n=0}^{N-1}a_{n,k}e^{j\frac{2\pi nt}{T}}\cdot e^{-j2\pi ft}dt\\&=\int\sum_{n=0}^{N-1}a_{n,k}e^{-j2\pi\left(f-\frac{n}{T}\right)t}dt=\sum_{n=0}^{N-1}a_{n,k}\text{sinc}\left(\pi\left(f-\frac{n}{T}\right)T\right)e^{-j\pi\left(f-\frac{n}{T}\right)T}dt\end{aligned} \qquad \text{eq. (2.16)}$$

where,

$$\text{sinc}(x)=\frac{\sin(x)}{x} \qquad \text{eq. (2.17)}$$

The above equations indicate that the spectrum of an OFDM signal is comprised of a number of overlapping sinc functions as shown in Figure 2.14. There is no mutual interference since the zero-crossings meet at the maximum (sampling) point of each sinc function.

Two important facts can be obtained from this type of modulation. Firstly, by overlapping the subcarriers, a more efficient use of the spectrum is obtained, as it is depicted in Figure 2.14. Secondly, since an OFDM signal is an addition of low rate subcarriers, the timespan of the OFDM signal can be designed to be longer than the time spread of a frequency selective channel. This is an important advantage since a high data rate OFDM signal, implemented by low rate modulated subcarriers, has better performance over frequency selective channels than a high data rate single carrier system, occupying the same bandwidth.

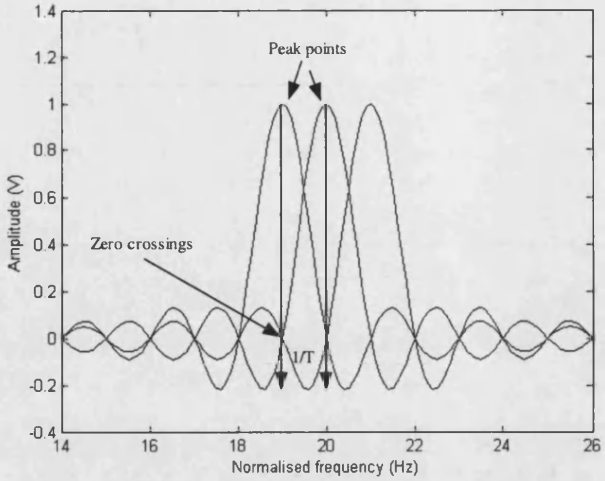

Figure 2.14 – Spectrum of an OFDM signal

The OFDM signal is demodulated making use of the orthogonality between the subcarriers. The n^{th} modulation symbol at the k^{th} signalling interval is demodulated by multiplying the received OFDM signal with the n^{th} complex conjugate subcarrier and by integrating over the signalling interval T. Therefore, the correlation of the received signal with one of the mirror complex subcarriers will give zero at all frequencies except from the frequency of the mirror subcarrier. In other words, this sort of demodulation resembles a matched filter receiver. The n^{th} received complex modulation symbol, at the k^{th} signalling interval, is given by:

$$y_{n,k} = \int_{kT}^{(k+1)T} S_{tx,OFDM}(t) \cdot g_n^*(t - kT)dt \qquad \text{eq. (2.18)}$$

The block diagram of an oscillator-based OFDM system is shown in Figure 2.15.

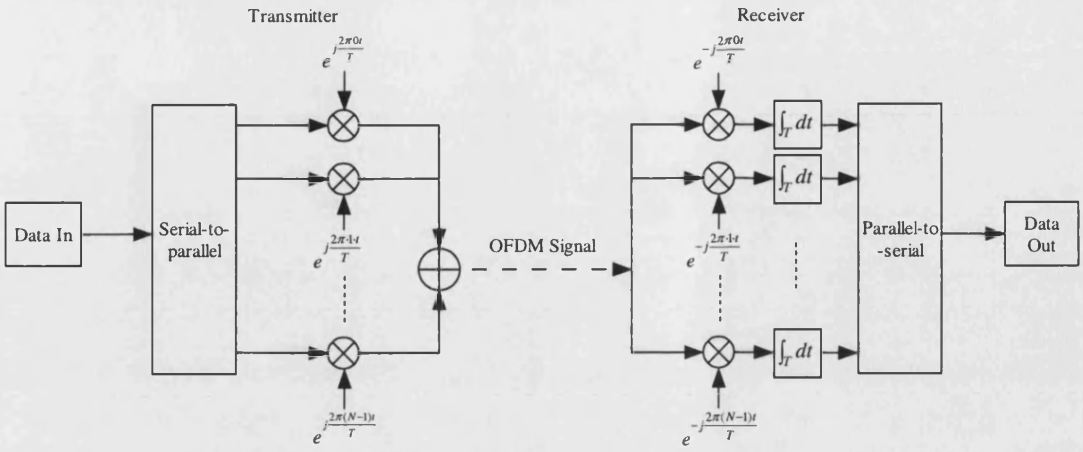

Figure 2.15 – Oscillator-based implementation of an OFDM system

2.7.2 Discrete-time (FFT-based) OFDM

In [57], the authors demonstrated that an OFDM signal can be realised by using an inverse discrete Fourier transform. The OFDM signal can then be demodulated by using a forward discrete Fourier transform. The IDFT correlates the input data with its orthogonal functions, which are sinusoids at pre-specified frequencies. In particular, the IDFT converts frequency-domain data to time-domain data. In practice, OFDM systems are implemented using a combination of Inverse Fast Fourier Transforms (IFFT) and Forward Fourier Transforms (FFT), which are mathematically equivalent versions of IDFT and DFT respectively, but more efficient to implement using modern DSP and VLSI technology.

The scaled samples $x_k = \sqrt{T/N}\,x(kT/\ N)$, where k is 0 to N-1, of an OFDM symbol can be generated by taking the IFFT of the complex modulation symbols, as shown in the following equation:

$$x_k = \frac{1}{N}\sum_{n=0}^{N-1} X_n e^{j\frac{2\pi kn}{N}}, k = 0,\ldots,N-1 \qquad \text{eq. (2.19)}$$

where, X_n are the modulated data symbols, N is the number of the FFT samples, n=0,…,N-1, are the position of the subcarriers (input IFFT samples) and k=0,…,N-1 are the output FFT samples.

At the receiver a forward FFT is used to demodulate the OFDM signal, thus:

$$X_n = \sum_{k=0}^{N-1} x_k e^{-j\frac{2\pi kn}{N}}, n = 0,..., N-1 \qquad \text{eq. (2.20)}$$

Some difference can be observed between the oscillator-based and FFT-based implementation of OFDM. In the latter case, each output OFDM sample is a summation of all the *N* input complex data to the IFFT, whereas in the oscillator-based implementation, each output OFDM sample corresponds to one complex symbol modulated by one subcarrier. However, the principle is still the same since in both cases a low rate data is modulated by orthogonal subcarriers.

The block diagram of an FFT-based OFDM system is shown in Figure 2.16.

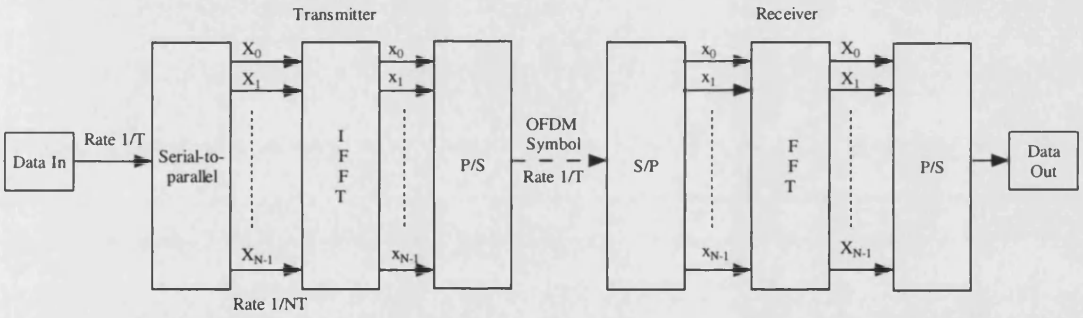

Figure 2.16 – FFT-based implementation of an OFDM system

2.7.3 Guard interval (cyclic prefix for OFDM)

We have stated that OFDM has an advantage over single carrier modulations in frequency selective channels because the timespan of the OFDM subcarriers is usually larger than the timespan of the channel. If we look at this in frequency terms, the bandwidth of each of the OFDM subcarriers is less than the coherence bandwidth of the channel. In a multipath channel, multiple delayed versions of the same signal arrive at the receiver due to reflections from obstacles. In this case, the OFDM frame is distorted by previous OFDM frames, as shown in Figure 2.17. This is also known as Intersymbol Interference or ISI. In addition, interference can appear amongst the OFDM symbol own subcarriers. In such a case, Intercarrier Interference (ICI) occurs. This is illustrated in Figure 2.18.

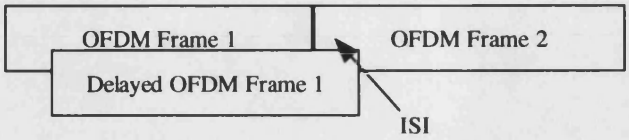

Figure 2.17 – Intersymbol interference in OFDM

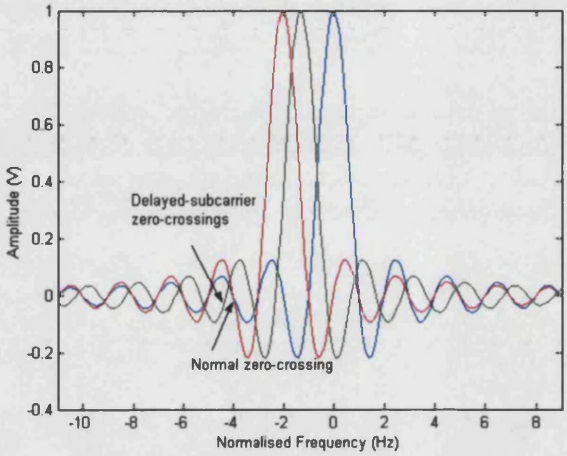

Figure 2.18 – Intercarrier interference in OFDM

Assuming that a direct and a delayed by t_0 OFDM signal arrives at the receiver, the channel impulse and corresponding frequency response (by taking the Fourier transform) of the signal are shown in Figure 2.19.

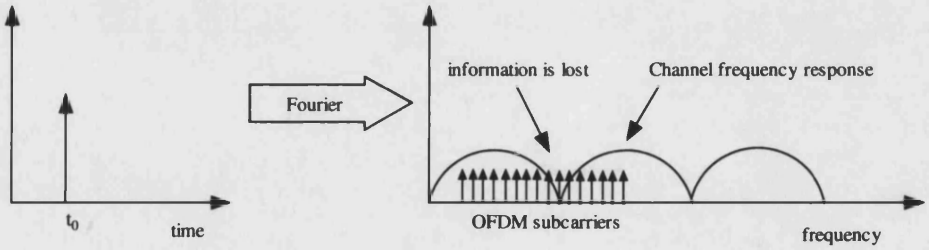

Figure 2.19 – Frequency response of a frequency selective channel

As observed from the above figure, only a portion of the subcarriers of an OFDM signal will be lost in a frequency selective channel, whereas the information on a single carrier system under the same environment would be degraded or even completely lost.

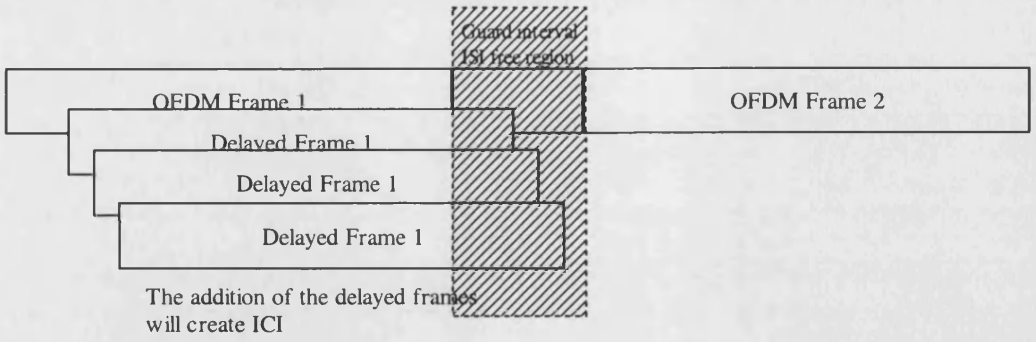

Figure 2.20 – Effects of guard interval (insert zeros) on OFDM signal

The OFDM system can be made though to be completely immune from multipath channels and thus ISI and ICI with the addition of a guard interval. In effect, the guard interval extends the duration of the OFDM signal by inserting zeros at the end of each frame. Although, this type of guard interval may alleviate the effects of ISI, as Figure 2.20 shows, it will not alleviate the effects of ICI. In a real channel the OFDM symbol is linearly convolved with the channel impulse response. However, the FFT only preserves the orthogonality of the subcarriers when the convolution in time is cyclic rather than linear [59]. Cyclic convolution can be performed in discrete-time systems only if the signals are of infinite length, or at least when one of the signals is periodic over the range of convolution. It is difficult to make an OFDM signal of infinite length. However, it can be made periodic by using a technique called cyclic prefix. In such a scheme, a portion of the samples at the end of an OFDM frame is copied at the front, as illustrated in Figure 2.21.

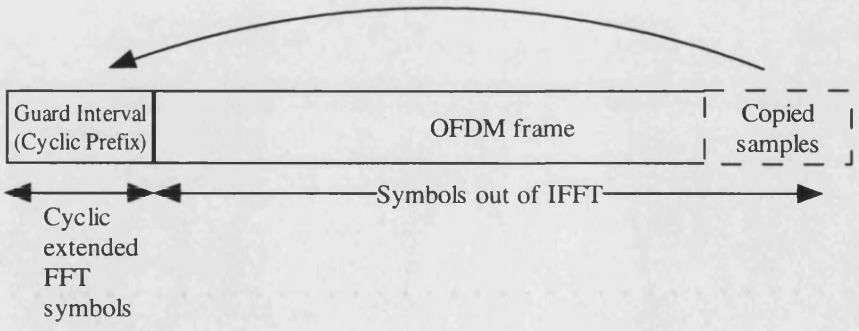

Figure 2.21 – Cyclic extended OFDM frame

The cyclic extended guard interval will ensure that the delayed replicas of the OFDM symbol to always have an integer number of cycles within the FFT interval, as

long as the delay is smaller than the guard time. The result is that the convolution of the OFDM symbol with the channel impulse response is transformed into multiplication of received data symbols with the channel coefficients. If the channel coefficients are known, then the effects of fading are removed by using a simple equaliser after the forward FFT. The disadvantage of using such a scheme is in the reduction of the bandwidth efficiency of the OFDM system since some of its bandwidth is allocated for the guard interval and not for carrying information.

2.7.4 Limitations of OFDM

OFDM has a number of limitations. It is vulnerable to frequency and timing errors (frequency offset, timing offset, sampling errors). However, techniques have been developed to overcome these problems. These techniques along with an explanation of the limitations of OFDM are studied in Chapter 3.

Another disadvantage is that OFDM exhibits a high peak-to-average ratio (PAR). An OFDM signal consists of a number of independently modulated subcarriers which are added coherently. When the subcarriers are added having the same phase, then the power generated is N times higher than the average value. The disadvantage is in the requirement of needing highly linear devices. When devices operate in their non-linear region harmonics are created in the OFDM signal which would result in spectral leakage between the subcarriers and thus ICI.

2.7.5 Multicarrier CDMA

The OFDM main advantages are the usage of simple equalisation techniques and good performance in frequency selective channels. On the other hand, CDMA (Code Division Multiple Access) has the advantage of having high processing gain and using diversity (rake) receivers. The combination of those systems was considered for high data rate cellular systems and they were termed as multicarrier CDMA systems.

Multicarrier CDMA schemes are subdivided in three categories. These are multicarrier MC-CDMA [60], multicarrier direct sequence MC-DS-CDMA [61] and multitone MT-CDMA [62] schemes. The difference between them is in the way in which the data is spread and modulated onto different subcarriers.

2.7.5.1 MC-CDMA

In the MC-CDMA scheme the user data is first spread (multiplied by the spreading code) and then modulated onto different subcarriers. The length of the spreading code is equal or less to the number of the OFDM (IFFT) subcarriers. The spreading sequence is applied before the IFFT and thus, in the frequency domain. If the spreading sequence length is equal to the number of the FFT subcarriers the data rate in each OFDM branch is equal to the rate of the user data as shown in **Figure 2.22**. Otherwise, the spreading sequence is applied to a set of subcarriers.

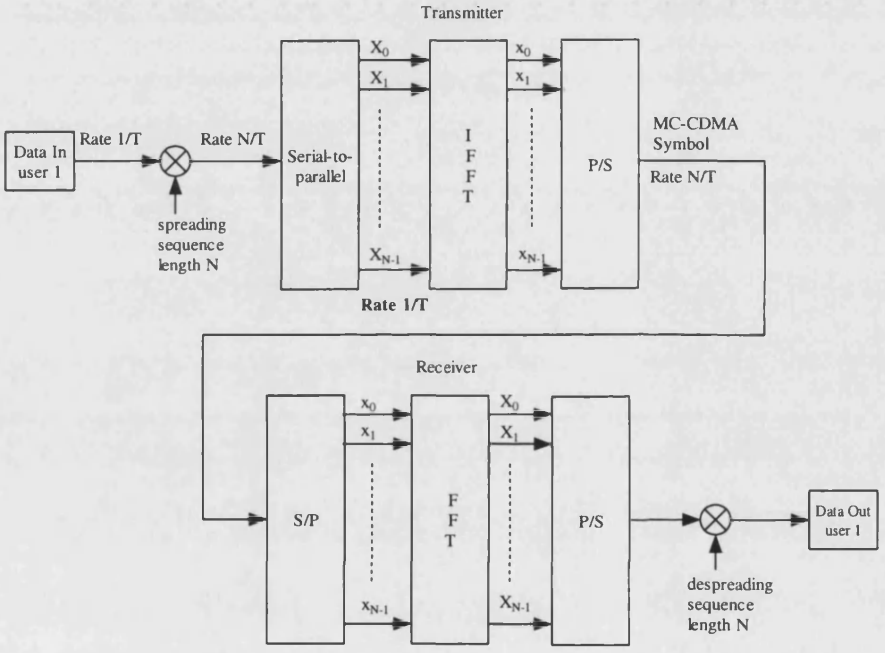

Figure 2.22 – FFT implementation of MC-CDMA

The subcarrier separation of MC-CDMA when the spreading sequence length is equal to the number of FFT carriers is equal to the user data rate, which is given by:

$$f_d = \frac{1}{T} \qquad \text{eq. (2.21)}$$

where, T is the duration of the user data.

The spreading sequences in MC-CDMA are used to separate the desired signal from the signals of other users, provided that their spreading sequences are orthogonal

to each other. Orthogonal codes have zero cross-correlation and therefore are suitable for such a scheme [63].

2.7.5.2 MC-DS-CDMA

If a higher processing gain is required then the MC-DS-CDMA scheme is used. In such a scheme the same spreading code is used in each subcarrier. Therefore, the chip rate of each branch is higher than the rate of the user data. The block diagram of this scheme is shown in Figure 2.23.

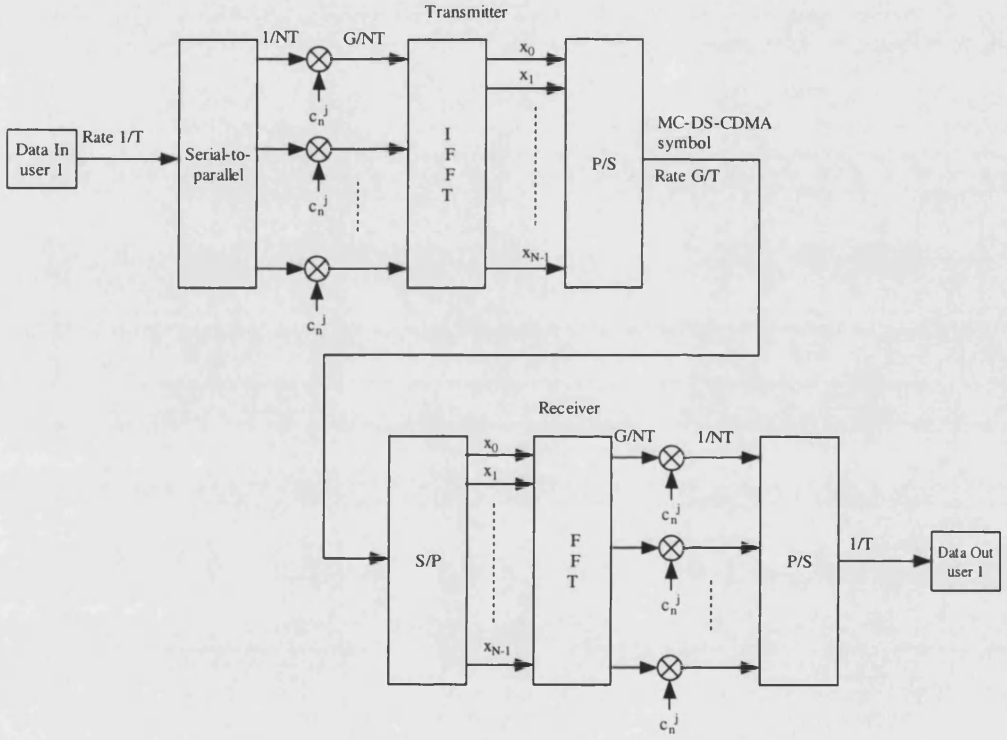

Figure 2.23 – FFT implementation of MC-DS-CDMA

The subcarrier separation of such scheme is given by:

$$f_d = \frac{G}{NT} \qquad \text{eq. (2.22)}$$

where, G is the processing gain of the system, T the duration of the user data symbol and N the number of subcarriers used. Therefore, in MC-DS-CDMA, each subcarrier has a wider bandwidth than the MC-CDMA scheme subcarrier bandwidth.

2.7.5.3 MT-CDMA

The subcarriers of both the previous CDMA techniques maintain their orthogonality. However, by applying the spreading sequence in time, the MT-CDMA subcarriers lose their orthogonality. The subcarriers regain their orthogonality at the receiver, when the received signal is multiplied by the receiver spreading sequence. The advantage of this scheme is the increase of the processing gain of the system within a given bandwidth. The block diagram of this scheme is shown in Figure 2.24.

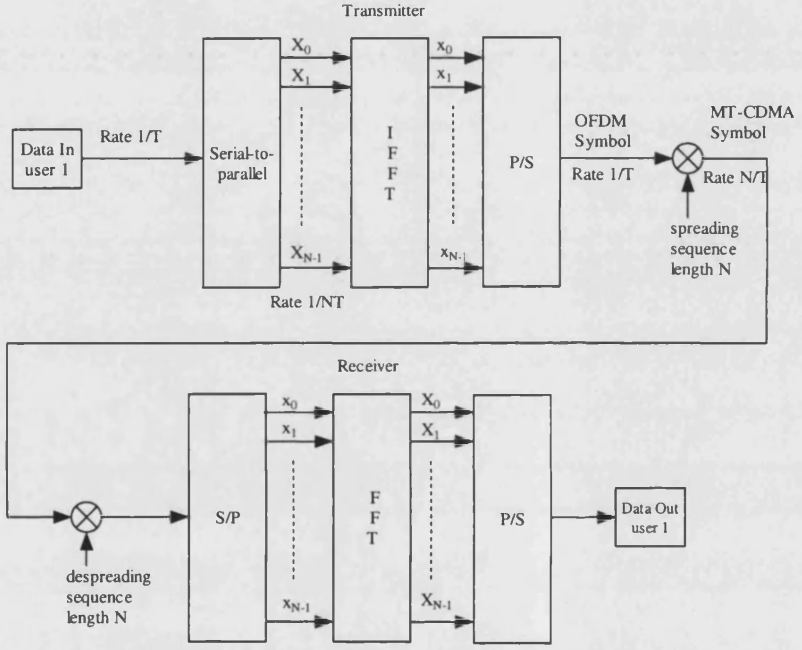

Figure 2.24 – FFT implementation of MT-CDMA

2.7.6 Wireless systems using OFDM

2.7.6.1 IEEE 802.11 Wireless LAN

The IEEE 802.11 standard was first introduced in 1997. It was intended for use in indoor environments and was only able to support data rates of up to 2 Mbps. The physical layer of this standard specified three different versions. The first one is Infra-Red (IR) support, operating at 850 to 950 nm band. The second one is Frequency Hopped Spread Spectrum (FH-SS) modulation operating at 2.4 GHz using 22 hop patterns. The third modulation scheme is Direct Sequence Spread Spectrum (DS-SS) modulation operating at the same band [64].

However, the IEEE 802.11 system was not adequate enough to support the data rates needed at the time. For this reason, IEEE expanded the original IEEE 802.11 standard in 1999 to create 802.11b [65] and 802.11a [66] standards. The 802.11b standard operates at the same frequency band (2.4 GHz) using DS-SS modulation. The introduction of new coding schemes enabled the support of data rates of up to 11 Mbps, comparable to fixed Ethernet. The advantage of such a scheme was its low cost and good performance over long ranges. Disadvantages were the support of a few simultaneous users and interference with home appliances (e.g. microwave oven). The 802.11a standard was intended for use in office environments. A new modulation scheme was proposed based on multicarrier modulation (OFDM) and a new frequency band (5 GHz). New coding schemes and adaptive modulation, offered data rates of up to 54 Mbps. Advantages of this scheme were the support of many simultaneous users and no interference from home appliances since it is operating in a regulated band. The disadvantages were that this system was not backward compatible to previous 802.11 standards, high cost and only operating at short ranges.

Recently, the IEEE standard introduced the version g of 802.11 combining the best of the a and b versions [67]. This version operates at 2.4 GHz, supporting both DS-SS and OFDM modulation and offering data rates of up to 54 Mbps. The major advantage of this scheme is backward compatibility to the 802.11b standard.

2.7.6.2 Digital video broadcast system

The Digital Video Broadcasting System (DVB) was developed by a European consortium of public and private sector organisations (ETSI). The DVB specification is part of a family of specifications which covers terrestrial (DVB-T) [68], satellite (DVB-S) [69] and cable (DVB-C) [70] operations. It allows digital video and audio distribution as well as transport of forthcoming multimedia services.

DVB-T operates within the existing UHF spectrum allocated for PAL and SECAM television transmissions. Although the system was developed for 8 MHz channels, it can be scaled to any channel bandwidth (8, 7 or 6 MHz) with corresponding scaling in the data capacity. The net bit rate in an 8 MHz channel varies between 4.98 and 31.67 Mbps. The variation depends on the choice of channel coding parameters, modulation types, and guard interval duration. The system is designed to be flexible and to adapt to all type of channels. It can withstand Gaussian channels as well as

Ricean and Rayleigh channels. It can withstand high-level long delay static and dynamic multipath distortion. It is also robust to interference from delayed signal, either from reflections from buildings, or signals from distant transmitters in a single frequency network (SFN).

DVB-T uses OFDM modulation to convey information. It has two operational modes, the "2k mode" which uses a 2k FFT and the "8k mode" which has an 8k FFT. In the 2k mode each symbol is constituted by a set of 1705 carriers whereas in the 8k mode each symbol is comprised of 6817 carriers. The 2k mode is designed for single transmitter operation and for small Single Frequency Networks (SFN) with limited distance between transmitters. The 8k mode can be used both for single transmitter operation and small and large SFN networks. In order to accommodate required data rates, different levels of QAM modulation and inner code rates exist. The main characteristics of the DVB-T system are shown in Table 2.6.

Table 2.6 – DVB-T specifications

Source Coding	
Video	Main profile syntax of ISO/IEC 13818-2 (MPEG-2 Video)
Audio	ISO/IEC 13818-2 (MPEG-2 Layer II audio) and Dolby AC-3
Transport Stream	ISO/IEC 13818-1 (MPEG-2 TS) transport stream
Transmission System	
Outer channel coding	R-S (204, 188, t 8)
Outer interleaver	12 R-S block interleaver
Inner coding	Punctured convolutional code: Rate: 1/2, 2/3, 3/4, 5/6, 7/8 Constraint length 7, Polynomials (octal) 171, 133
Inner interleaver	Bit-wise interleaving and frequency interleaving
Data randomisation	16-bit PRBS
Modulation	COFDM QPSK, 16QAM and 64QAM Hierarchical modulation: multi-resolution constellation (16QAM and 64QAM), Guard Interval: 1/32, 1/16, 1/8, 1/4 of OFDM symbol 2 model: 2k and 8k FFT

2.8 Summary

In this chapter, a general review of systems used for wireless communications, was carried out. The chapter started by providing a brief review of past and present cellular systems. Consequently, the physical layers and modulation techniques used in GSM and EDGE were described, respectively. In addition, considerations for 4G systems were stated. Furthermore, the technique that is most probable to be used in 4G systems, OFDM, was explained. The continuous- and discrete-time implementation of OFDM, as well as, cyclic prefix insertion was described in this section. Furthermore, variations of OFDM, using the CDMA principle, were depicted. Finally, this chapter concluded by providing a brief review of two prominent wireless systems using OFDM, WLAN and DVB.

Chapter 3

Design considerations for OFDM in a wireless system

3.1 Introduction

In the previous chapter, a review of past, current and future mobile communication technologies was carried out. In addition, the modulation techniques employed in those technologies were described. This chapter concentrates on OFDM which is the modulation that is mostly considered for fourth generation wireless technologies. What follows is a description of the method of designing an OFDM system and how it can be affected by the wireless channel and the receiver.

The first section starts with the design considerations for an OFDM transmitter. More specifically, the ways that the pilot symbols, guard interval and FFT size interact with each other will be analysed. In addition a simple design guide for an OFDM transmitter will be stated. The following section identifies the possible distortion factors that can affect an OFDM signal in a radio channel. These are additive noise and fading channels. Finally, the last section describes the effects of receiver imperfections on OFDM signals and the methods to recover such signals. More specifically, the effect of carrier synchronisation errors (frequency offset, phase noise) and symbol synchronisation errors (timing offset, sampling frequency) are analysed. Consequently, timing offset, frequency offset and channel estimation methods are described.

3.2 Transmitter design considerations

This section concentrates on the issues regarding the design of an OFDM transmitter. The most important factors affecting the design are: pilot symbol insertion, choice of FFT parameters and guard interval width.

3.2.1 Pilot symbol arrangement

Pilot symbols are used in an OFDM frame in order to mitigate the effects of fading. At the receiver the pilot symbols will be used to estimate the channel impulse response. Subsequently, the knowledge of the channel impulse response will help to correct the effects of the channel on the transmitted symbols. Channel estimation is described in more detail in a later section where receiver design issues are considered.

The choice of the number of pilot or training symbols is a trade-off between data rate and good channel estimation performance. In addition, the overall SNR of the signal is affected, since pilot symbols do not carry any useful information and are discarded at the receiver. Cavers [71], reported theoretical analysis on Pilot Symbol Assisted Modulation (PSAM) in single carrier systems. The author pointed out that it was appropriate that 10% of the sent symbols to be pilot information.

Pilot information can be arranged in an OFDM frame in many ways as illustrated in Figure 3.1, where two-dimensional positions of the pilot in frequency and in time (or subcarrier and OFDM frame) are shown. In Figure 3.1a, all the pilots are placed in one OFDM symbol. In Figure 3.1b, one pilot is inserted in every frame shifted one step in frequency. Figure 3.1c shows a pattern proposed by T. Mueller [72]. This pattern has scattered pilots which have equi-distant spacings in time and in frequency. Finally, Figure 3.1d shows a pattern presented by P. Hoeher [73]. Here, pilots are shifted one step in frequency in each pilot interval.

The pilot pattern is determined by the nature of the system. For example, in wireless systems where fast fading occurs it is better to have the pilot symbols scattered, in order to track continuously the changes of the impulse response of the channel. An example of this type of pilot pattern can be seen in DVB and DAB systems where pilot symbols are inserted in every frame, similar to the pattern shown in Figure 3.1c.

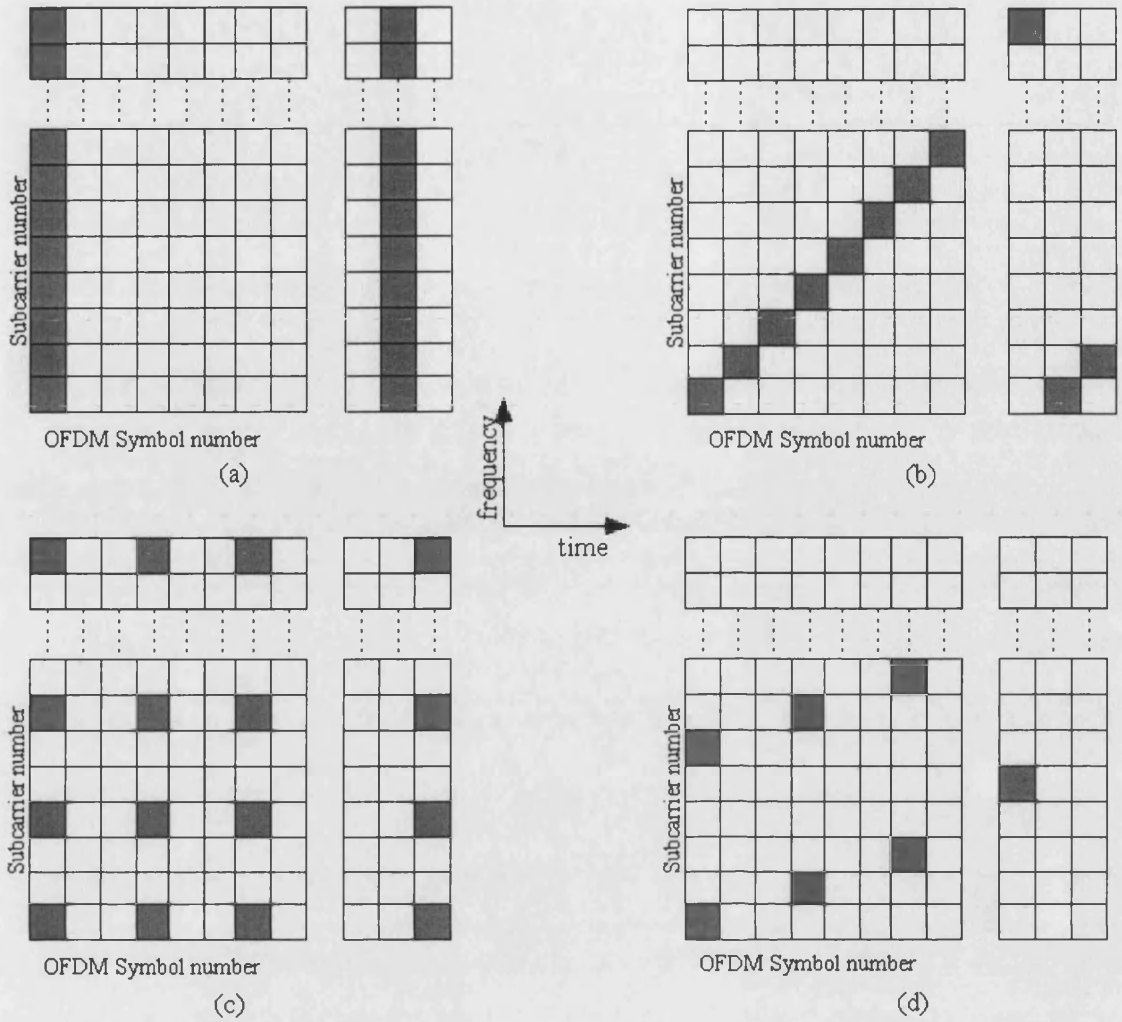

Figure 3.1 – Various pilot patterns

On the other hand, in slow fading environments where the impulse response of the channel remains constant there is no need to insert pilot information in every frame. In such cases a block type pilot pattern is used as shown in Figure 3.1a. This pilot configuration is also suitable for packet-type communication systems, such as WLAN [74]. In WLAN there is no need to estimate time fading since the packet length is short enough to assume a constant channel during the length of the packet. In addition, the scattering of the pilot symbols over several OFDM symbols introduces delays to the system that are not desirable in packet transmission [74]. The pilot pattern in the 802.11a WLAN system, that uses OFDM, is shown in Figure 3.2.

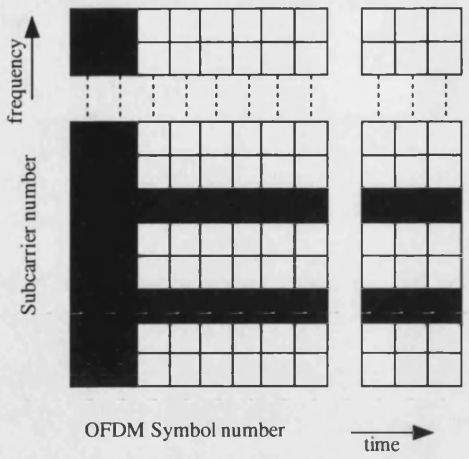

Figure 3.2 – WLAN IEEE 802.11a pilot symbol pattern

It is desirable to have a small number of pilot symbols compared to the useful data in order to have better error rate performance (higher SNR). Rearrangement of the pilot patterns enables a reduction in the number of needed pilot symbols [75]. Figure 3.3 shows a pattern derived from channel statistics and it is optimal in the sense that the total bit error rate is kept at a minimum in each symbol time.

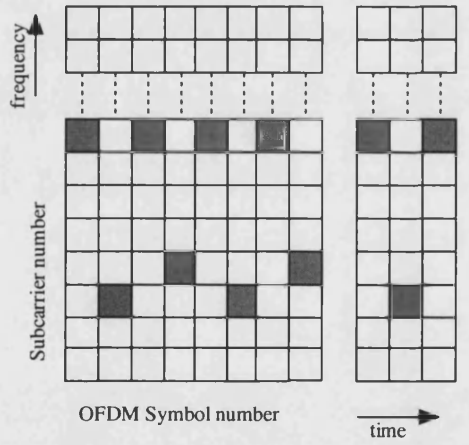

Figure 3.3 – Pilot pattern derived from channel statistics [75]

3.2.2 Choice of FFT parameters and guard interval

An OFDM system is defined in a wireless channel by its bandwidth, bit rate and delay spread tolerance. These parameters are often conflicting when the size of the FFT and the guard interval duration need to be defined. For example, the duration of the guard interval defines the maximum delay spread tolerance. However, large guard

interval duration dictates lower bandwidth for the system and consequently lower bit rate. Van Nee and Prasad [74], describe a method for designing a basic OFDM system for wireless systems. This method can be used as a general guideline to design such systems.

As a rule of thumb the guard time is chosen to be two to four times the rms delay spread. A larger value should be chosen for systems which are more sensitive to ICI or ISI, for example, in the case where the system implements higher order modulations. In addition, this value depends on the type of coding used.

The duration of the OFDM symbol should be much larger than the guard interval in order to minimise the SNR loss. A practical consideration is to make the OFDM symbol duration to be at least five times the guard interval, which implies a 1-dB SNR loss. On the other hand, careful consideration must be taken, because high symbol duration dictates smaller subcarrier spacing, which makes the system more sensitive to ICI, frequency offset and phase noise.

The number of subcarriers or size of the FFT is defined by the subcarrier spacing, which is the inverse of the OFDM symbol duration less the guard interval. Alternatively, the number of subcarriers may be defined by the required bit rate divided by the bit rate per subcarrier [74].

As an example, take the design of an OFDM system with the following requirements: Bit rate of 20 Mbps, delay spread tolerance of 200 ns and maximum bandwidth of 15 MHz. The guard interval is set at four times the delay spread or 800 ns. The OFDM symbol duration is set to be 6 times the guard time (4.8 μs). In this way the SNR loss is less than 1 dB. The subcarrier spacing is the inverse of the OFDM symbol duration minus the guard duration or 250 kHz. In order to decide the size of the FFT and what modulation to use, the number of bits per OFDM symbol must be determined. This is achieved by the following equation:

$$\text{Number of bits/OFDM symbol} = \text{Duration of symbol} * \text{Data rate} \qquad \text{eq. (3.1)}$$

For a bit rate of 20 Mbps each OFDM symbol must carry 96 bits of information. By using 16-QAM with ½-rate coding, two bits are assigned per subcarrier. Consequently,

48 subcarriers are needed per OFDM symbol. The bandwidth of the system is 48*250 kHz which is 12 MHz.

3.3 Channel modelling considerations

The modelling of the channel is an essential part in the design of an OFDM system for wireless communications. The main parameters that are defined in the channel are noise addition and fading. Other factors that can be defined are interference from other environments and non-linear elements from amplifiers. In this section the noise addition and fading channels will be described.

3.3.1 Definition of noise channel

In communication systems, noise analysis is based on an idealised form of noise called *white noise*. The term *white* is used in the sense that white light contains equal amounts of all frequencies within the visible band of electromagnetic radiation [3]. The power spectral density of white noise within a sample function, *w(t)*, is defined as:

$$S_W(f) = \frac{N_0}{2} \text{ W/Hz} \qquad \text{eq. (3.2)}$$

where, N_0 is the noise power spectral density.

The autocorrelation of white noise (inverse Fourier transform of power spectral density) gives:

$$R_W(t) = \begin{cases} \frac{N_0}{2}\delta(t), & \tau = 0 \\ 0, & \tau \neq 0 \end{cases} \qquad \text{eq. (3.3)}$$

In practice, white noise is not realisable, since it implies infinite energy and bandwidth. White noise is implemented in simulation systems with the bandwidth of the noise to be significantly larger than that of the system itself.

In practical systems, the most important factor of noise affecting the system is thermal noise. Thermal noise has a Gaussian probability density function given by:

$$f(x)=\frac{1}{\sqrt{2\pi N}}e^{\frac{x^2}{2N}} \qquad \text{eq. (3.4)}$$

where, N is the average noise power.

As a result, in communication systems, Additive White Gaussian Noise (AWGN) is added to realise noise in a system. The noise is measured in relation to the power transmitted in the system by the signal to noise ratio (SNR). White noise is added to the system as shown in Figure 3.4.

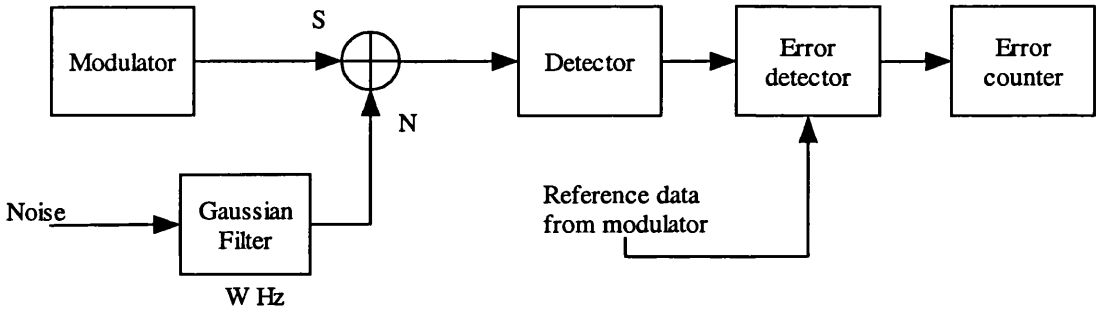

Figure 3.4 – Typical addition of white noise in a simulator

The signal-to-noise ratio (SNR) of the system is often expressed by the signal energy per binary data bit (E_b) to the noise power density (N_0). This ratio is given by:

$$\left.\begin{aligned} E_b &= ST_b \\ N_0 &= \frac{N}{W} \end{aligned}\right\} \Leftrightarrow \frac{E_b}{N_0}=\frac{S}{N}*WT_b \qquad \text{eq. (3.5)}$$

where, T_b is the bit duration and W is the noise bandwidth (Gaussian filter bandwidth).

3.3.2 Definition of fading channel

The mobile channel places fundamental limitations on the performance of wireless communication systems. The transmission path between the transmitter and

receiver may well be severely obstructed blocking the line-of-sight path. In fact, the received waves are a superposition of waves coming from all directions due to reflection, diffraction and scattering caused by buildings, trees and other obstacles. This effect is known as multipath propagation. Due to such propagation, the received signal consists of an infinite sum of attenuated, delayed and phase shifted replicas of the transmitted signal. Depending on the phase of each partial wave the effect can be either constructive, or destructive. Unlike wired channels that are stationary and predictable, radio channels are extremely random and difficult to analyse. Even the speed of motion impacts how rapidly the signal level fades as a mobile terminal moves in space. This is known as the Doppler effect, where it causes a frequency shift of each of the partial waves. Modelling the radio channel has been a difficult task. It is typically modelled in a statistical fashion based on measurements carried out in specific environments (rural, urban etc.) [4],[76].

Propagation models have traditionally focused on predicting the average received signal strength at a given distance from the transmitter, as well as the variability of the signal strength in close spatial proximity to a particular location. There are two main categories of propagation models. Firstly, there are large-scale propagation models that predict the mean signal strength over large distances from the transmitter which are useful to estimate the transmitter coverage area. Secondly, there are small-scale or fading models that characterise the rapid fluctuations of the received signal strength over very short travel distances [4].

3.3.2.1 Large-scale fading

Large-scale fading environments are characterised by the attenuation of the signal strength over large areas. The statistics of large-scale fading provide a way of computing an estimate of the path loss as a function of distance. This is described in terms of a mean path loss and a log-normal distribution of the variation about the mean [4].

Most of the models that are used to measure the path loss are derived using a combination of analytical and empirical methods. More specifically, the empirical approach is based on fitting curves or analytical expressions to recreate a set of measured data. However, such models are used only in the environments where the measurements were carried out. In order for such models to be viable in other

environments additional measurements must be taken. The propagation models are sub-categorised into outdoor and indoor propagation models. Outdoor propagation models are used to simulate environments such as rural and urban areas. The most known propagation model for urban environment is the Okumura-Hata model [4]. Indoor propagation models are dominated by the same mechanism as outdoor, i.e. reflection diffraction and scattering. However, conditions are much more variable, for example the signal levels vary greatly depending on whether interior doors are open or closed inside a building. In addition, the smaller propagation distances make it more difficult to insure far-field radiation for all receiver locations [4].

3.3.2.2 Small-scale fading

Small-scale fading is used to describe rapid fluctuations of the amplitude of a radio signal over a short period of time or travel distance. Large-scale fading effect may be ignored, since its effects will be negligible over short distances.

The main physical factors that influence fading are [4]:

- Multipath propagation, which may result in fluctuations of the signal strength
- The speed of the mobile, which may result in random frequency modulation due to different Doppler shifts in each of the multipath components
- The speed of the surrounding objects, which may induce a time-varying Doppler shift in multipath components
- The transmission bandwidth of the signal.

Therefore, fading affects a signal in two ways:

- Time-spreading due to multipath propagation
- Time-variant behaviour due to Doppler shifts

Time-spreading (multipath propagation) environment

In order to evaluate multipath environments, parameters which quantify the multipath channel are used. These are the mean excess delay, rms delay spread and

excess delay spread. These parameters are determined from a power delay profile. The power delay profile gives details of received signal strengths against time.

The mean excess delay is the first moment of the power delay profile and is defined to be [4]:

$$\bar{\tau} = \frac{\sum_k a_k^2 \tau_k}{\sum_k a_k^2} = \frac{\sum_k P(\tau_k)\tau_k}{\sum_k P(\tau_k)} \qquad \text{eq. (3.6)}$$

where, $P(\tau_k)$ is the power received at time τ_k and a_k is the amplitude

The rms delay spread is the square root of the second central moment of the power delay profile and is defined to be [4]:

$$\sigma_\tau = \sqrt{\overline{\tau^2} - (\bar{\tau})^2} \qquad \text{eq. (3.7)}$$

The maximum excess delay spread (X dB) of the delay profile is defined to be the time delay during which multipath energy falls to X dB below the maximum signal strength [4].

In addition to the above parameters the coherence bandwidth, B_c, which is the inverse of the rms delay spread is used to measure the bandwidth required for the system to be coherent. More specifically, the coherence bandwidth is a statistical measure of the range of frequencies over which the channel can be considered flat (a channel which passes all spectral components with approximately equal gain and linear phase). The coherence bandwidth can be approximated as the range of frequencies over which frequency correlation is higher than 0.5 [4]:

$$B_c \approx \frac{1}{5\sigma_\tau} \qquad \text{eq. (3.8)}$$

- **Flat fading**

When the coherence bandwidth of the channel is larger than the bandwidth of the signal, the signal undergoes flat fading. In this type of fading the spectral characteristics of the transmitted signal are preserved at the receiver. However, the

strength of the signal changes with time due to multipath propagation. Therefore, the signal is affected by a fixed delay at the receiver and undergoes amplitude variations. Flat fading channels, are also known as amplitude varying or narrowband channels.

- **Frequency selective fading**

When the coherence bandwidth of the channel is smaller than the bandwidth of the signal, it suffers from frequency selective fading. Under such conditions the channel impulse response has a multipath delay spread which is greater than the symbol period of the signal. The received signal is an accumulation of multiple delayed attenuated versions of the transmitted signal that distort it. Frequency selective fading is due to time dispersion of the transmitted symbols within the channel. Thus the channel induces intersymbol interference, ISI. Viewed in the frequency domain, certain frequency components in the received signal spectrum have greater gains than others [4]. Frequency selective fading channels are also known as wideband channels.

Time-varying (Doppler shift) environments

In time-varying environments, Doppler spread and coherence time are used to describe the time-varying nature of the channel.

Doppler spread, B_D, is a measure of the spectral broadening caused by the time rate change of the mobile radio channel and is defined as the range of frequencies over which the received Doppler spectrum is non-zero. When a pure sinusoidal tone of frequency f_c is transmitted, the received signal spectrum or Doppler spectrum will have components in the range $f_c - f_d$ and $f_c + f_d$, where f_d is the Doppler shift. The amount of spectral broadening depends on the Doppler shift, which is a function of the relative velocity of the mobile and the angle between the direction of motion of the mobile and the direction of arrival of the scattered waves [4].

Coherence time is the inverse of Doppler spread (time-domain representation of the Doppler shift). Coherence time is used for the same purpose as with coherence bandwidth in time-spreading environments. Coherence time is the time duration over which the channel impulse response is time-invariant (i.e. there is no Doppler shift). The coherence time can be approximated as the time over which the time correlation is above 0.5 [4]:

$$T_c \approx \frac{9}{16\pi f_m} \qquad \text{eq. (3.9)}$$

Where, f_m is the maximum Doppler shift.

- **Fast fading**

When the coherence time of the channel is smaller than the symbol period of the signal, then the signal undergoes fast fading. Under such conditions, the channel impulse response changes rapidly within the symbol duration. This causes frequency dispersion (or time-selective fading) due to Doppler spreading which distorts the signal.

- **Slow fading**

In slow fading environments, the coherence time of the channel is larger than the symbol period of the signal. In this case the channel may be assumed to be static over one or several symbol intervals [4].

It should be noted that when a channel specification is a fast or slow fading channel, it does not indicate whether the channel is flat or frequency selective fading. Therefore, combination of those channels is done to obtain a good overall definition of the radio channel.

Figure 3.5, shows all the types of fading that can occur in a small scale fading mobile radio channel.

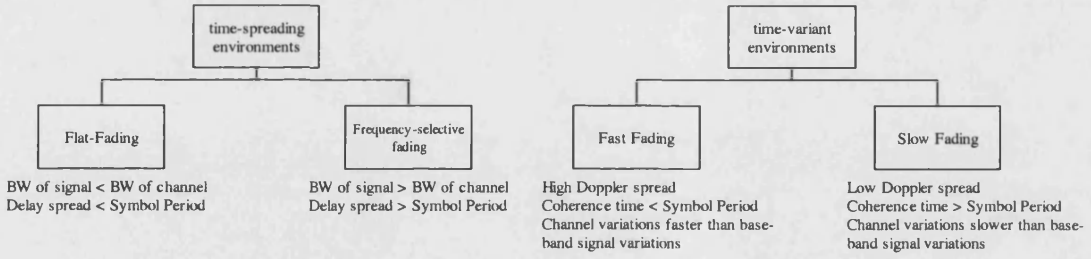

Figure 3.5 – Types of small scale fading [4]

Rayleigh and Ricean distribution

The Rayleigh distribution is used to describe the statistical time-varying nature of the received envelope of a flat fading signal, or the envelope of an individual multipath component. In addition, in Rayleigh distribution, the line-of-sight component is not taken into consideration. Therefore, this distribution is more suitable in

environments where obstacles exist that block line-of-sight communication, such as urban environments [4],[76].

The Rayleigh distribution, $|\mu(t)|$, is usually modelled as an addition of the envelope of two quadrature Gaussian random processes. Hence:

$$|\mu(t)| = |\mu_1(t)| + j|\mu_2(t)| \qquad \text{eq. (3.10)}$$

On the other hand, when there is a line-of-sight path, the small-scale fading distribution is Ricean. For this reason, Ricean distribution is a more suitable stochastic model for rural regions, where the line-of-sight component is dominant [4],[76].

The line-of-sight component of the received signal is described by a general time-variant part [76]:

$$m(t) = m_1(t) + jm_2(t) = \rho e^{j(2\pi f_\rho t + \theta_\rho)} \qquad \text{eq. (3.11)}$$

where, ρ, f_ρ and θ_ρ denote the amplitude, the Doppler frequency, and the phase of the line-of-sight component, respectively.

The Ricean distribution, $|\mu_\rho(t)|$ is formed from the superposition of the sum of the scattered components with the line-of-sight component. In other words, further complex Gaussian random processes are introduced which are added with the time-variant mean value *m(t)* [76]. Thus:

$$|\mu_\rho(t)| = |\mu_{\rho 1}(t)| + j|\mu_{\rho 2}(t)| = |\mu(t) + m(t)| \qquad \text{eq. (3.12)}$$

Usually, Rayleigh and Rice processes are preferred for modelling small-scale fading environments, whereas large-scaling fading environments are modelled using lognormal processes [76].

3.4 Receiver design considerations

The transmitter of a digital communication system contains a clock that indicates the timing instants at which the data symbols must be transmitted.

Furthermore, the transmitter contains a carrier oscillator, necessary for the upconversion of the data carrying baseband signal to the bandpass signal to be transmitted. At the receiver, the received bandpass signal is downconverted using a local carrier oscillator. The resulting signal is sampled at timing instants determined by the receiver clock. Based on the resulting samples, a decision is taken about the transmitted data symbols. Hence, the receiver must make an estimation of the frequencies and phases of the carrier oscillator and the clock used at the transmitter, based upon the received signal. This is why the design of the receiver is one of the most complex tasks in mobile communications. The effects of the channel on the transmitted signal introduce a number of distortions, for example, intersymbol or intercarrier interference due to fading environments. In addition, imperfections of the components used to implement the receiver introduce further distortion to the transmitted signal. In many instances the receiver may suffer from carrier and symbol synchronisation errors [77].

3.4.1 Effects of carrier synchronisation errors on OFDM receiver

Two types of carrier synchronisation errors may occur in a receiver. The first type of error is carrier frequency offset which is caused by inaccuracy (tolerance) in the local oscillator (LO) frequency [78]. The second problem is phase noise, which is caused by the random variation of the phase of the LO. Both types of errors can also be created by the time-variant behaviour of the radio channel.

Frequency offset

An OFDM signal is given by the following equation, as we have discussed in section 2.6.2.

$$x_k = \frac{1}{N}\sum_{n=0}^{N-1} X_n e^{j\frac{2\pi kn}{N}}, k = 0,\ldots,N-1 \qquad \text{eq. (3.13)}$$

where, X_n are the modulated data symbols, N is the number of the FFT samples, n=0,…,N-1, are the position of the subcarriers (input IFFT samples) and k=0,…,N-1 are the output FFT samples.

Assuming that the impulse response of the channel does not change much over the symbol interval (slow fading environment), a received OFDM signal with frequency

offset (before forward FFT is applied) and AWGN, will have the following equation [79].

$$y_k = \frac{1}{N}\sum_{n=0}^{N-1} X_n H_n e^{j2\pi k(n+\varepsilon)/N} + w_n \qquad \text{eq. (3.14)}$$

where, H_n is the channel impulse response, ε is the relative frequency offset of the channel (the ratio of the actual frequency offset to the intercarrier spacing) and w_n the complex envelope AWGN.

P. H. Moose [79] shows that when such signal is received through an FFT, it is comprised of three components as stated in the equation below.

$$Y_n = \sum_{k=0}^{N-1} y_k e^{-j2\pi k n/N} = X_n H_n \operatorname{sinc}(\pi\varepsilon) e^{j\pi\varepsilon(N-1)/N} + I_n + W_n \qquad \text{eq. (3.15)}$$

where,

$$I_n = \sum_{l=0}^{N-1} X_l H_l \left(\frac{\sin \pi\varepsilon}{N \sin(\pi(l-n+\varepsilon)/N)} \right) e^{j\pi\varepsilon(N-1)/N} e^{-j\pi(l-n)/N} \qquad \text{eq. (3.16)}$$

The above equations illustrate that the received OFDM symbol under frequency offset conditions, has amplitude variations and a common phase error (sinc term and $\pi\varepsilon$ phase term in the first component of eq. (3.15)). The second component of that equation, I_n, is the interference component caused by the frequency offset. This term shows that ICI occurs between the OFDM subcarriers. ICI exists because the orthogonality between the subcarriers is lost due to the non-integer frequency shift of the received sinc terms resulting in spectral leakage (subcarriers are not aligned) to adjacent subcarriers. The last term, W_n is the frequency spectrum of the AWGN [79],[80].

The frequency offset ε, is comprised of two parts, shown below:

$$\varepsilon = \varepsilon_o + n\omega_s \qquad \text{eq. (3.17)}$$

where, ε_o is called *fine* frequency error (magnitude of the error does not exceed one-half the subcarrier spacing) and $n\omega_s$ is called *coarse* frequency (integer number of carrier spacings), n is an integer number. These errors are illustrated in Figure 3.6.

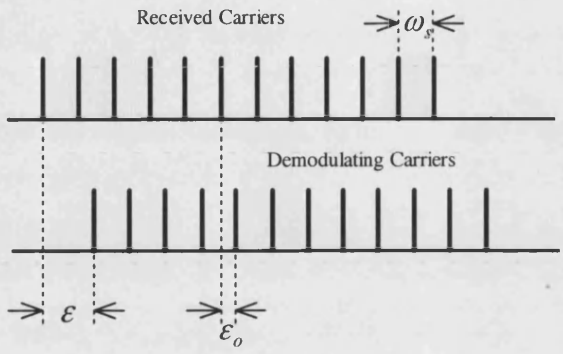

Figure 3.6 – Frequency offset illustration

When no fine frequency error exists, i.e. $\varepsilon_o = 0$, the orthogonality between the subcarriers is preserved even if a coarse frequency error exists as it represents an integer number of carrier spacing. However, the demodulated data comes out of the FFT at the wrong outputs which results in loss of data. On the other hand, when only fine frequency error exists, orthogonality of the subcarriers is lost, and there are N-1 cross-talk terms, introducing ICI and distorting the demodulated signal.

In [78], it has been shown that the subcarriers closer to the edge of the OFDM frame are less affected by ICI. The advantage is 3 dB in signal-to-interference ratio. Frequency offset will be more severe, if more subcarriers are used for a system in a given bandwidth, since the frequency separation between the subcarriers is reduced.

Phase noise

Phase noise occurs due to the random perturbation of the phase of the local oscillator frequency. The received OFDM signal affected by phase noise, will have similar expression as of an OFDM signal received with frequency offset. Therefore, its expression will resemble that of eq. (3.12) where it depicts a frequency offset condition. Thus, an OFDM signal affected by phase noise (before the FFT process) will have the following expression:

$$y_k = \frac{1}{N}\sum_{n=0}^{N-1} X_n H_n e^{j2\pi k(n+\theta(t))/N} + w_n \qquad \text{eq. (3.18)}$$

Again, H_k is the channel impulse response, and w_n the complex envelope AWGN.

The difference from the frequency offset case is that, the phase noise term $\theta(t)$, is not constant like the phase offset term ε, but varies with time. Usually, phase noise is modelled as a Wiener process [81],[82], where:

$$\theta(t) = 2\pi \int_0^t \mu(\tau) d\tau \qquad \text{eq. (3.19)}$$

where, $\mu(t)$ is a white Gaussian frequency noise. A carrier with $e^{j\theta(t)}$ will have a Lorenzian distribution [81],[83].

When such signal is received though the FFT process, its expression will be similar to that of equations (3.13) and (3.14) showing a demodulated subcarrier affected by frequency offset. Therefore, phase noise will introduce amplitude variations and a common phase error to the demodulated signal plus an interference term. However, the effects from phase noise are more difficult to be alleviated than those of frequency offset due to the fact that phase noise is random, whereas frequency offset is constant.

3.4.2 Effects of symbol synchronisation errors on OFDM receiver

Once more, there are two types of symbol synchronisation errors that affect the OFDM receiver. The first one, is a common timing offset error that occurs when an OFDM signal received is delayed. The second type of synchronisation error which is harsher on the receiver is a clock sampling error. In this case there is a time-varying offset.

Timing offset

A timing offset occurs, when each consecutive symbol is not sampled at the correct intervals. OFDM is relatively robust to timing offsets, due to the use of the guard interval. A timing offset may distort the OFDM signal in two ways, as shown in Figure 3.7.

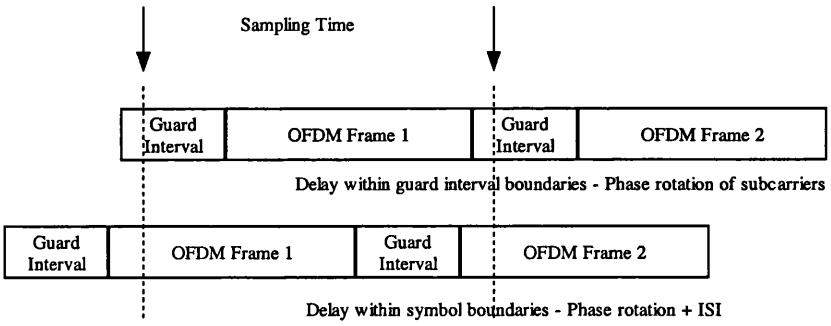

Figure 3.7 – Timing offset conditions

When the timing offset is large enough that the FFT interval extends over a symbol boundary, ICI and ISI occur and would result in severe signal distortions. On the other hand, when the FFT interval does not extend over the symbol interval, then each subcarrier suffers from a phase offset [74],[77],[80],[84]. The relation between the timing offset, τ and the phase variation of the subcarriers, φ_i is given below.

$$\varphi_i = 2\pi f_i \tau \qquad \text{eq. (3.20)}$$

where, f_i is the frequency of the i^{th} subcarrier.

For an OFDM system with N subcarriers and a subcarrier spacing of *1/T*, a timing delay of one sampling interval of *T/N*, causes a significant phase shift of $2\pi(1-1/N)$ rad between the first and last subcarrier [74]. Nonetheless, such phase shifts can be compensated using channel estimation techniques, which are going to be explained in a later section.

Clock synchronisation (sampling frequency) error

A sampling frequency error occurs when the receiver clock frequency is not aligned with that of the transmitter. This has the result, that the received OFDM symbol has a different sampling rate from the transmitted symbols (the demodulating carriers have the wrong spacing) [77],[78]. This phenomenon is effectively timing jitter [77].

A received OFDM symbol with sampling frequency error will have the following equation (before the FFT process) [80]:

$$y(t)=\sum_{n=0}^{N-1} X_n H_n e^{j2\pi nt/T_n} e^{j2\pi f_0 t} \qquad \text{eq. (3.21)}$$

where, f_0 is the RF carrier frequency and

$$T_n = \frac{N}{f_{s,rx}} = \frac{N}{f_{s,tx} + \delta f} \qquad \text{eq. (3.22)}$$

where, $f_{s,rx}$ is the sampling frequency of the receiver, $f_{s,tx}$ is the sampling frequency of the transmitter and δf is the sampling frequency error.

The l_{th} demodulated subcarrier, after downconversion and FFT process is given by [80]:

$$Y_l = X_n H_n \operatorname{sinc}\left(\pi n \frac{\delta f}{f_{s,tx}}\right) e^{j\pi n \frac{\delta f}{f_{s,tx}}} + i_l + w_l \qquad \text{eq. (3.23)}$$

where, i_l is the interference component (w_l the noise term) given by:

$$I_l = \sum_{n=0}^{N-1} (-1)^{1-l} X_n H_n e^{j\pi\left((1-l)+n\frac{\delta f}{f_{s,tx}}\right)} \times \frac{1}{1-l} \times \frac{\delta f}{f_{s,tx}} \qquad \text{eq. (3.24)}$$

The first component of eq. (3.23) indicates similar amplitude variations and phase errors to the subcarriers. However, the interference component shows that in a time variant offset error, the distortion depends on the subcarrier index, as it is illustrated in Figure 3.8. The figure is indicative of such systems behaviour and it is based on a typical OFDM system with 128 subcarriers. The middle subcarriers (subcarrier number 63) is the least affected by ICI when compared to other subcarriers especially those at frequency band edges (subcarrier number 0 and 128) [77],[78],[80],[85],[86].

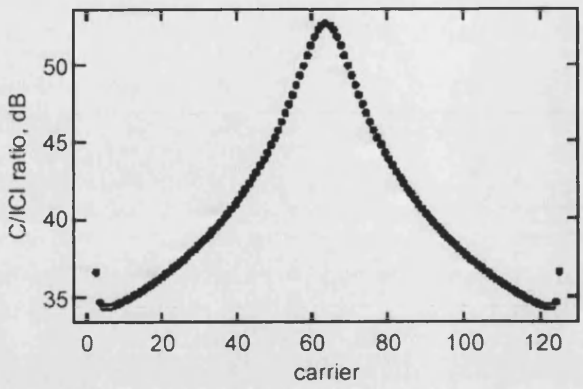

Figure 3.8 – Time variant offset effect on OFDM subcarriers (carrier-to-interference ratio (C/ICI) vs subcarrier number) [78]

3.4.3 Synchronisation methods

In sections 3.4.1 and 3.4.2 we have seen how the receiver is affected by frequency and timing errors, respectively. Therefore, carrier frequency and symbol timing synchronisation is an essential part in the design of an OFDM receiver. Many methods of synchronisation were proposed in the literature and are summarised below.

3.4.3.1 Frequency offset estimation techniques

The estimation techniques are either based in the time-domain region of the receiver (before the FFT process) and in the frequency domain region of the receiver to complement the time domain techniques and thus increase the range of estimation [87]. In addition, estimation techniques are performed in two steps; first the coarse frequency offset is estimated (Acquisition mode) and then the fine frequency offset is tuned (Tracking mode).

Time-domain techniques are mostly based on correlation techniques. Such techniques need training symbols to estimate frequency offsets. P. H. Moose [79] was one of the first researchers to propose a coarse frequency error estimation method by correlating two identical OFDM training blocks. Subsequent techniques [88]-[90] were developed to increase the range of estimation, i.e. estimate fine frequency offsets, using a single OFDM training block with repetitions.

In frequency domain techniques, estimation is performed after the receiver forward FFT. The advantage of this scheme is that the correlation of symbols in the

time domain is essentially a multiplication function in the frequency domain. Thus, the equalisers needed are less complex than the time domain ones. Some estimation schemes that use frequency equalisation are proposed in [91]-[94]. However, such schemes require the presence of pilot symbols that reduce the bandwidth efficiency of OFDM signals. In addition, another disadvantage is that the received OFDM symbol has to be fully demodulated before estimation to be achieved which introduces further delays and bottlenecks to the system.

A different approach to alleviate the effects of frequency offsets is proposed in [95]. In this approach a method to reduce the sensitivity of OFDM from ICI is proposed by using a self-ICI cancellation scheme. This scheme is based on analytical methods where an expression of the ICI effects from frequency offsets on an OFDM signal is determined. Based on that expression, the transmitted bits are re-arranged so that at the receiver the ICI created from the frequency offset is cancelled out. However, the self-ICI cancellation scheme also has the disadvantage of reduced bandwidth efficiency of the OFDM signal, due to the fact that the ICI affected symbols at the receiver are mapped to more subcarriers at the transmitter. An advantage of this method is frequency diversity gain in multipath fading channels [95]-[97]. Another method proposed to reduce the sensitivity of OFDM systems to ICI is by using pulse-shaping filters [98],[99] or time-domain windows [100],[101], at the transmitter. Once again, the disadvantage of such methods is that the bandwidth efficiency of OFDM is reduced. A different approach is to perform frequency offset estimation by using probability functions. More specifically, the estimation can be performed by maximising the average log-likelihood function [102].

Research has also been performed on estimating frequency offsets without the need for pilot symbols. Such estimation techniques are known as *blind* estimation techniques. In such schemes, the characteristics of the transmitted OFDM signal are exploited in order to achieve synchronisation. In [103]-[105] the authors took advantage of the presence of virtual carriers (null carriers from oversampling) in OFDM signalling and proposed blind estimation methods reminiscent of spectral analysis techniques in array processing, i.e. ESPRIT [105]. This method offers good bandwidth efficiency performance but has difficulties in implementation due to the high processing and complex circuitry requirements.

The estimation method that is used for DVB OFDM systems, involves the use of the cyclic prefix [106],[107]. The cyclic prefix reduces the bandwidth efficiency of

OFDM, but it is an essential part for systems operating in wireless channels. The estimation method is performed by correlating a received OFDM signal with a delayed version of itself. The estimated offset is fine tuned in conjunction with maximum likelihood estimation. This technique will be described in more detail in a later section.

3.4.3.2 Timing offset estimation techniques

Timing offset estimation techniques follow the same principles of operation as with frequency offset estimation techniques. There are estimation methods that are performed either in the time domain or the frequency domain as well as techniques involving pilot symbols or blind detection algorithms. As with frequency offset schemes the DVB OFDM frame is synchronised by correlation of the cyclic prefix in conjunction with maximum likelihood estimation [106]-[108]. The next section describes this method in more detail. In [109], a synchronisation burst is used which is correlated at the receiver with a locally generated one. However, the estimation is not optimal under high frequency offset conditions. In [88] a robust symbol synchronisation scheme is proposed where the training symbol is designed as such to be optimal in both burst and continuous time mode of operations. The authors of [110] propose a differential detection of the phase difference between adjacent tones. This scheme is applied for QPSK mapping, and the signal has to be first raised to its fourth power in order to remove the modulation and detect the timing offset. This has the disadvantage of increasing peak to average power ratio and noise. Finally, a basic cyclic prefix and pilot symbol estimation scheme is proposed in [111].

3.4.3.3 Synchronisation method used in DVB systems

In DVB systems maximum-likelihood estimation is used to synchronise the received signals [106]-[108].

A received OFDM symbol $r(k)$, with additive noise $n(k)$, frequency offset ε and timing offset θ will have the following equation:

$$r(k) = s(k-\theta)e^{j2\pi\varepsilon k/N} + n(k) \qquad \text{eq. (3.25)}$$

By correlating *r(k)* with a version of itself delayed by *m*, *r(k+m)* over an observation interval of $2N+L$ the following is observed:

$$E\{r(k)r^*(k+m)\} = \begin{cases} \sigma_s^2 + \sigma_n^2, & m = 0 \\ \sigma_s^2 e^{j2\pi\varepsilon}, & m = N \\ 0, & \text{otherwise} \end{cases} \qquad \text{eq. (3.26)}$$

where, σ_s^2 is the energy of the OFDM symbol and σ_n^2 is the energy of the additive noise.

The log-likelihood function for θ and ε is the logarithm of the probability density function of $2N+L$ observed samples in r given the arrival time θ and carrier frequency offset ε. The maximum likelihood function is the argument maximising this function. Under the assumption that r is a jointly Gaussian vector, the log-likelihood function is shown to be [108]:

$$\Lambda(\theta,\varepsilon) = 2|\gamma(\theta)|\cos\{2\pi\varepsilon + \angle\gamma(\theta)\} - \rho \mathrm{E}(\theta) \qquad \text{eq. (3.27)}$$

where, $\angle$ denotes the argument of a complex number,

$$\gamma(m) \equiv \sum_{k=m}^{m+L-1} r(k)r^*(k+N) \qquad \text{eq. (3.28)}$$

is the correlation term and

$$\mathrm{E}(m) \equiv \sum_{k=m}^{m+L-1} |r(k)|^2 + |r(k+N)|^2 \qquad \text{eq. (3.29)}$$

is the energy term, ρ is the correlation coefficient.

The simultaneous ML-estimation of θ and ε is:

$$\begin{aligned} \hat{\theta}_{ML} &= \arg\max_{\theta}\{2|\gamma(\theta)| - \rho \mathrm{E}(\theta)\} \\ \hat{\varepsilon}_{ML} &= -\frac{1}{2\pi}\angle\gamma\left(\hat{\theta}_{ML}\right) \end{aligned} \qquad \text{eq. (3.30)}$$

Van de Beek, Sandell and Borjesson [108] give an example of the operation of this estimator which is reproduced in Figure 3.9. In Figure 3.9a, the peaks from the correlation give the timing estimates, where at the same instants the phase of the argument of $\gamma(\theta)$ gives the frequency offset estimate.

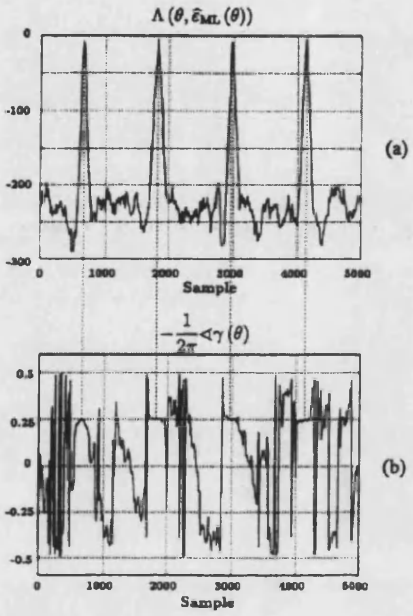

Figure 3.9 – Cyclic prefix ML estimation [108]

The block diagram of such ML estimator for OFDM is shown below:

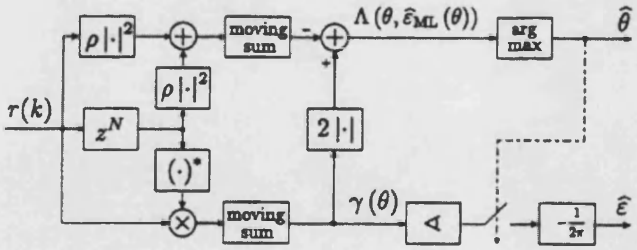

Figure 3.10 – Block diagram of ML estimator [108]

3.4.4 Channel estimation methods for OFDM

Coherent OFDM receivers rely mostly on pilot assisted modulation methods for estimating the channel impulse response. In section 3.2.1, the various ways of arranging the pilot symbols within the OFDM frame were discussed. In channels where

fast-fading occurs, the pilots have closer distance to each other within the OFDM frame, whereas in slow fading channels, the pilots are less frequent in the OFDM frame. Therefore, from the spacing of the pilot symbols the maximum Doppler component, f_{Dmax} and excess delay tolerance $\tau_{\max}$ of the OFDM system can be found [112]:

$$f_{D\max} = \frac{1}{2N_t T_s (1+\Delta)} \qquad \text{eq. (3.31)}$$

$$\tau_{\max} = \frac{T_s}{N_f} \qquad \text{eq. (3.32)}$$

where, N_t is the pilot spacing in the time-direction, N_f is the pilot spacing in the frequency-direction, T_s is the OFDM symbol interval and Δ is the guard interval ratio.

The pilot symbols will act as sampling instants of the channel response. Therefore, the received pilot tones will contain samples of that response, as shown in Figure 3.11. The rest of the channel is recovered by interpolating the received pilot stream. The simplest method is linear interpolation as shown in Figure 3.12. The disadvantage of this method is that if the pilot symbols have large separation, the interpolation and consequently channel estimation is not accurate.

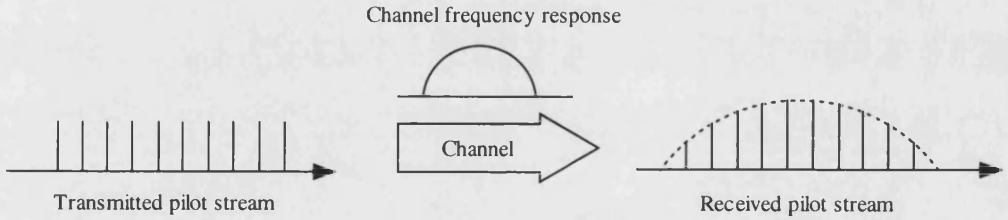

Figure 3.11 – Sampling the channel impulse response

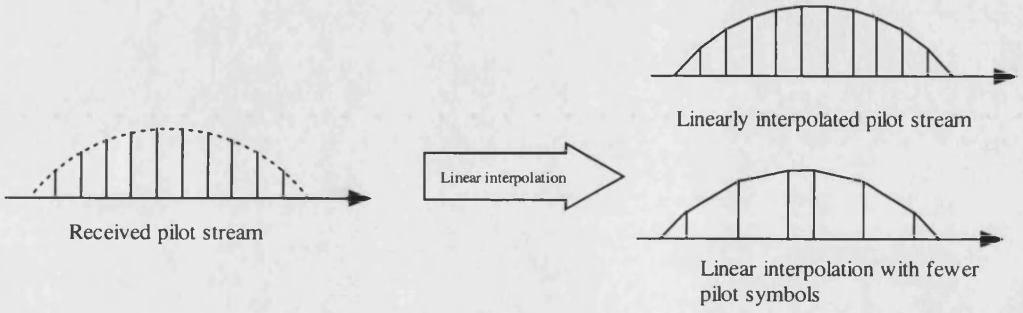

Figure 3.12 – Channel estimation by linear interpolation of pilot tones

The simplest form of recovering the received signal is by using the least-square (LS) estimation or zero-forcing method. The estimated signal X is then:

$$X = \hat{h}_{LS}^{-1} Y \qquad \text{eq. (3.33)}$$

where, $\hat{h}_{LS}$ is an array of the linear interpolated pilots and Y is the demodulated OFDM symbol.

This method of estimation is not very accurate due to potentially high mean-square errors. Most estimation techniques are based on using 2-dimensional (2D) estimators. Such estimators perform estimation in both time and frequency. For this reason the received pilot symbols are re-arranged in blocks or matrices. The channel is estimated using the property of correlation. More specifically, the two main methods of estimation are the least-square (LS) and the minimum mean square error (MMSE) methods [113],[114].

The minimum mean square estimate of the channel estimates $\hat{h}_{MMSE}$ from the channel values h using the pilot values $\hat{p}$, is given by [74]:

$$\hat{h}_{MMSE} = R_{h\hat{p}} R_{\hat{p}\hat{p}}^{-1} \hat{p} \qquad \text{eq. (3.34)}$$

where, $R_{h\hat{p}}$ is the cross-covariance matrix between h and the pilot values $\hat{p}$ and $R_{\hat{p}\hat{p}}$ is the auto-covariance matrix of the pilot values.

In order to produce more accurate estimation the issue of interpolation has been addressed. In [115] and [116] instead of linear interpolation a lowpass second order Gaussian filter has been used for interpolating the pilot estimates. The MMSE estimation method is even more accurate when using a Wiener filter for interpolation instead of the traditional linear interpolation [117]. However, the disadvantage of this scheme is the high computational complexity. For this reason, separable filters instead of 2D filters are used to reduce the computational complexity. In [73] estimation is first performed in the frequency direction using a 1D filter and consequently in the time direction using another 1D filter. Another approach is by using low rank approximations, which are either based on DFT estimators that perform modifications to the LS and MMSE estimators compromising performance and complexity [113], or

by optimal rank reduction schemes [118]. The latter method, suffers from an irreducible error floor.

3.5 Summary

This chapter reviewed aspects of OFDM modulation. In the first part details of how pilot symbol are arranged in an OFDM frame and simple guidelines to OFDM system design were given. The wireless channel and the fading channel and its effect on OFDM signals were outlined. Finally, receiver design considerations for OFDM modulation were discussed. Designing the receiver is a complicated task, since the receiver must be able to cope with its own limitations (synchronisation errors) and the effects of the fading channel. Aspects of the design guidelines and estimation techniques reviewed in this chapter are used in the following chapters when considering the design of different OFDM systems.

Chapter 4

A multimode GSM-EDGE-OFDM transceiver for mobile communications and its performance under adjacent- and co- channel interference

4.1 Introduction

Mobile communications had an explosive growth over the past 10 years. New technologies have emerged increasing the complexity in implementing the new systems onto existing mobile networks. An example of this is the introduction of GPRS, EDGE and UMTS systems onto the current GSM network. In order to reduce cost, the mobile industries have turned to multimode systems, where for example one base station could simultaneously transmit and receive GSM and EDGE signals. The interaction between those systems is measured in terms of Adjacent-Channel Interference (ACI), where the interferer is placed at the frequency of a channel adjacent to the wanted channel or Co-Channel Interference (CCI), where the interfering channel is at the same carrier frequency as the wanted channel. The European Telecommunication Standards Institute (ETSI) has defined the ACI and CCI levels at which GSM and EDGE systems can perform optimally [8].

Another emerging technology in wireless communications is Orthogonal Frequency Division Multiplexing. Its advantages to wireless transmission were discussed in section 2.7 and chapter 3. Some mobile manufacturers have recently shown interest in designing an OFDM system coexistent with the current GSM and

EDGE systems[2]. For such purpose it was decided to design an OFDM system supporting data rates of 1 Mbps with the same GSM bandwidth. The OFDM design will then be integrated within a multimode system supporting GSM and EDGE and the overall system will be evaluated in environments where multipath fading, ACI or CCI exist.

The chapter starts by providing a short review of the work done in this area. The next section describes the design of the OFDM system. The grounds for deciding the modulation, frame structure and number of FFT carriers for the proposed system are given in this section. Then, the construction of the simulated multimode model is described in the next section. The simulation platform used is Agilent Advanced Design System (ADS) [119]. Its Digital Signal Processing (DSP) simulation package is based on the Ptolemy platform, developed at the University of Berkeley and described in [120]. The final section of the chapter is concerned with the evaluation of the system. The system performance is tested in additive noise, GSM typical multipath environments, ACI and CCI.

4.2 Research in multimode mobile systems

The upcoming 2.5G and 3G systems have unlocked new unexplored sections in research areas involving multimode systems. The advantage of multimode systems is the reduced cost in terms of needing only a single base station to support all the technologies used. The disadvantage of such systems is the increased complexity and reduced performance compared to a single system supporting only one technology.

In [121] a multimode GSM/EDGE/WCDMA modulator is presented. The modulator is constructed as a single integrated circuit which meets the spectral, phase and Error Vector Magnitude (EVM) standards specified for each system by ETSI [8],[122],[123]. In [124], adaptive pre-distortion is introduced in a multimode transmitter to alleviate the non-linear effects of the power amplifier. In [125], a multimode receiver involving a high degree of digitisation is described. This receiver supports UMTS and GSM modes but can be modified to support cdma2000 as well. A key feature of this receiver is the use of direct conversion which takes the RF signal of the UMTS system to zero IF and to low IF for GSM. Software radio is then

[2] Private communications with the sponsor "Nokia Networks UK"

implemented to digitise the IF signal. Advantages of this scheme are reduction in cost, size and adaptability.

A multimode system implementing EDGE and Wideband OFDM (W-OFDM) for downlink transmissions has been proposed in [126]. W-OFDM is a variant of OFDM where the spacing of the carriers is chosen to be large enough so that any frequency errors between transmitter and receiver are only a small fraction of the spacing, and thus have a negligible effect on the performance of the system [127]. This article discussed the combination of EDGE and W-OFDM in an asymmetrical solution using Dynamic Packet Assigning techniques [44]. The W-OFDM system uses 624 subcarriers having a total bandwidth of 3.96 MHz. The subcarriers are re-arranged into 24 clusters of 26 subcarriers (165 kHz) and eight timeslots of 10.5 OFDM blocks each within a 20 ms frame of 100 blocks, in order to have same frame structure as that of EGDE. The W-OFDM system can achieve bit rates of 5 Mbps. The disadvantages of this scheme are that the W-OFDM system requires new spectrum (only for downlinks) and that the cost of integrating W-OFDM into the base stations is high, since new equipment are required. Furthermore, an OFDM system with a carrier frequency of 1900 MHz has been presented in [128]. This system has a bandwidth of 800 kHz (four 200 kHz GSM channels). It can achieve a data rate of 384 kbps using DQPSK modulation and ½-rate Reed-Solomon coding. Its performance is analysed in [129] over noise and multipath fading. It was deduced that at high speeds the system suffers from Doppler spread and therefore requires high SNR to operate optimally. Furthermore, no research has been reported about the interaction between this OFDM system and the GSM and EDGE systems. Hence, the proposed OFDM system performance in the presence of such systems is uncertain.

Research has been also carried out on the interaction between GSM and EDGE systems. These systems can co-exist provided that the standards specified by ETSI are met [8], [130].

4.3 Design aspects of the proposed OFDM system

4.3.1 Introduction

This section discusses the fundamentals of designing the proposed OFDM system. First, the design decisions concerning the format; modulation, number of FFT

carriers and guard interval duration are discussed. The choice of these parameters is based on the design guide of an OFDM system described in section 3.2.2. In addition, the frame structure of the OFDM signal will be discussed. The frame will be designed so as to have similar structure to a GSM frame. Secondly, the receiver design considerations are discussed. In this section the choice of synchronisation and channel estimation schemes are stated.

4.3.2 OFDM signal design

4.3.2.1 Symbol mapping

The system is designed to coexist with the GSM/EDGE core network. Hence, its bandwidth must be less than or equal to the 200 kHz bandwidth of those systems. The designed OFDM system will have a bit rate greater than 1 Mbps to cope with current user demand. A bandwidth of 200 kHz gives a maximum symbol rate of 200 ksymbols/s. Hence, in order to achieve a bit rate greater than 1 Mbps, efficient high order modulation, such as, QAM64 or higher must be used. For example, QAM64 will achieve a maximum data rate of 200 ksymbols/s*6=1.2 Mbps.

4.3.2.2 OFDM frame structure

The GSM TDMA frame is composed of eight timeslots (Figure 4.1), as described in section 2.3.5. Each timeslot has a period of 577 μs and effectively specifies 156.25 bit periods. In normal mode of operation the "Normal Burst" contains 148 bits (excluding 8.25 bits, used for guard interval for protection against ISI and delay spread). Of these 148 bits, 114 are used for data, 26 are pilot symbols, 2 used for control information, 6 are used for protection against ISI (Tail Bits) [7].

To minimise interference, the duration of the OFDM frame must be the same as the duration of the GSM/EDGE slot. Consequently, the GSM TDMA frame will have equal duration with an OFDM multiframe (8 OFDM frames). In this way, all the signals of each system received by a multimode receiver can be sampled simultaneously. It was decided to design the OFDM frame infrastructure as shown in Figure 4.2.

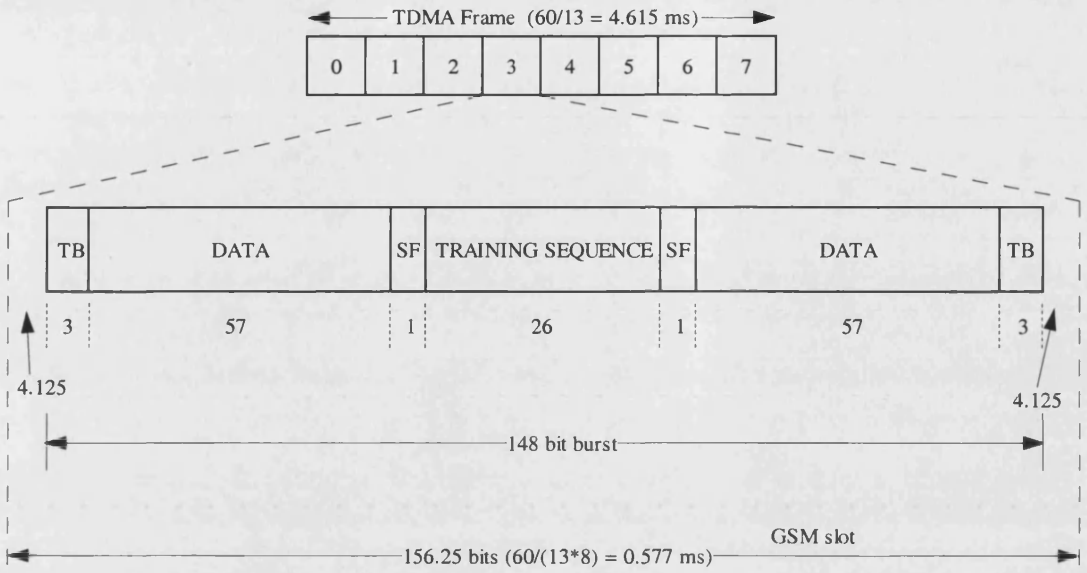

Figure 4.1 – GSM Normal Burst [7]

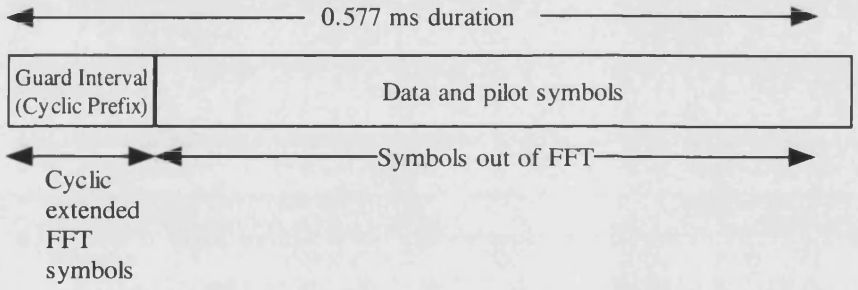

Figure 4.2 – OFDM frame infrastructure

Number of carriers in the FFT

In section 2.7.2, the advantages and the necessity of the IFFT/FFT to perform OFDM modulation are stated. An important issue is to set the number of carriers for each OFDM symbol. Choosing an appropriate number of carriers in conjunction with the correct symbol mapping, will set the required data rate and bandwidth. For this purpose, OFDM design guidelines, as described in section 3.2.2, are used to obtain the required values.

For a bit rate of 1 Mbps, each OFDM symbol/frame of period 577 μs, will carry:

$$\text{Number of bits/OFDM symbol} = \text{Duration of symbol} * \text{Data rate} = 577\ \mu s * 1\ \text{Mbps} = 577\ \text{bits} \qquad \text{eq. (4.1)}$$

A 64-point FFT assigns to each carrier approximately 9 bits and requires a symbol mapping of 2^9=512 constellation points. This type of symbol mapping is not suitable since it would be highly degraded in a noisy environment. On the other hand, a 128-point FFT will assign 4.5 bits per carrier and QAM64 modulation will be sufficient.

Zero-padding

QAM64 modulation assigns to each symbol/carrier 6 bits. This means that each OFDM frame will have 128*6=768 bits. Since a maximum of 577 bits are needed, the rest can be zero-padded. Zero-padding is the process in which zeros are appended to the original sequence. In effect, zero-padding oversamples the signal by increasing the length of the OFDM frame, which provides closely spaced samples of the Inverse FFT of the original sequence [131].

In the designed OFDM frame, 32 of the available 128 samples/carriers are zero padded. The remaining 96 are used for data and pilot symbols, leaving each frame to contain 576 bits.

Pilot symbol arrangement

In section 3.2.1, the different ways that pilot symbols are arranged in an OFDM frame were described. In all the designs of OFDM systems, 10% ratio of pilot symbols to data symbols is considered sufficient for operation in a fading environment [71],[74]. This action though gives 1 dB reduction in SNR as well as reduced data rates. In our design, a block type pilot symbol arrangement will be used with 8 pilot symbols (out of the 96) chosen as a good compromise between channel estimation ability and bandwidth efficiency. WLAN and DVB systems use the value 4/3 as pilot symbols [65]-[68]. Figure 4.3, shows the pilot symbol arrangement for our design.

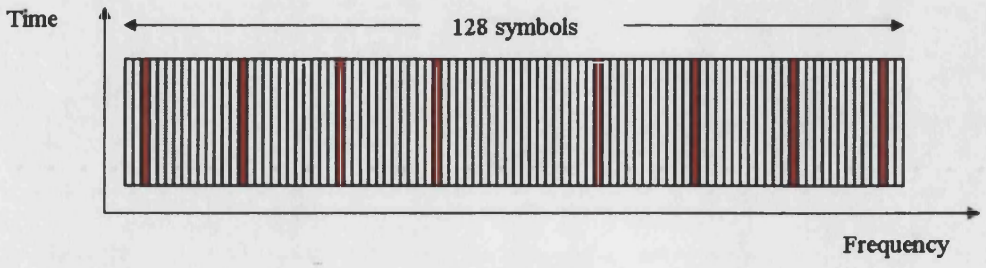

Figure 4.3 – Pilot symbol (red) arrangement in the OFDM frame

Delay spread and guard interval

In GSM the guard period is approximately $8.25*3.7\mu s = 30.525\,\mu s$. Therefore, each GSM frame can tolerate up to 30 μs of delay spread.

In OFDM the data symbols out of the IFFT are 128. Cyclically extending 20 symbols will make the OFDM frame to have 148 symbols which is identical to the frame structure of the GSM frame without the guard interval (see Figure 4.1). The cyclically extended OFDM frame must have the same period as the GSM frame which is 0.577 ms. Hence, the OFDM system must have a sampling time of $0.577\text{ms}/148 = 3.8986486\mu s$. The guard period of the OFDM system is then $20*3.8986486\mu s \cong 78\,\mu s$. Hence, the system will be able to tolerate delay spreads up to 78 μs, which is much better than the delay spread tolerance of GSM.

Figure 4.4 shows the OFDM frame structure and compares it to the GSM slot structure.

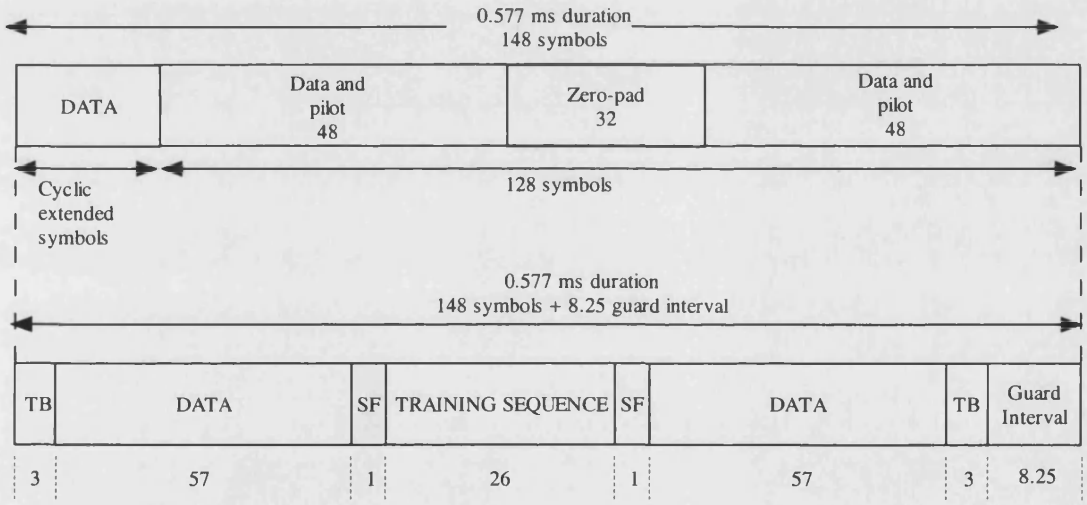

Figure 4.4 – OFDM frame structure compared to GSM slot structure

Pulse-shaping the OFDM signal

The shape of the spectrum at the output of the OFDM transmitter will be different from the shape of a GSM or EDGE spectrum as shown in Figure 4.5a. More specifically, the edges of the OFDM spectrum will create distortions in adjacent GSM or EDGE channels. To resolve this issue, the OFDM signal spectrum is shaped using a linearised Gaussian filter with a bandwidth bit duration product of 0.3. This filter is

chosen to be the same as that used in EDGE which is described in section 2.4.2. Figure 4.5b shows a linearised Gaussian filtered OFDM spectrum between adjacent GSM interferers. This filter will create ISI in the OFDM signal, but the ISI effects can be removed at the receiver using zero-forcing equalisers [4],[132]-[134].

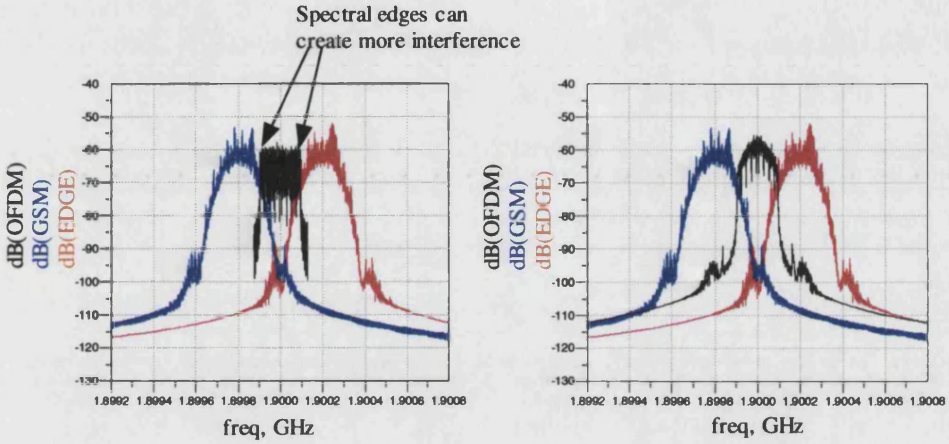

Figure 4.5 – OFDM spectrum (with two interferers GSM/EDGE); (a) normal OFDM spectrum, (b) linearised Gaussian filtered OFDM spectrum

4.3.3 Receiver design

4.3.3.1 Synchronisation issues

In section 3.4.3, a description of various synchronisation methods for OFDM was outlined. It was decided to adopt the method using the cyclic prefix in conjunction with ML estimation, since it is currently used in several OFDM systems such as DVB and DAB [68],[135]. Synchronisation using the cyclic prefix is based on correlating a delayed version of the OFDM signal with itself [106]-[108]. The principle is described in more detail in section 3.4.3.3.

4.3.3.2 Channel estimation method

Channel estimation techniques for OFDM systems have been reviewed in section 3.4.4. The best estimation technique involves the use of MMSE estimation and Wiener interpolation [117]. However, this technique, although reliable, suffers from

high computational complexity and is usually avoided. For our design it was decided to use a simple one-dimensional linear interpolated LS estimator. The choice of LS estimation as opposed to the MMSE technique is justified on the basis of the reduction in the simulation time and therefore, in practice implementation simplification. In addition, the OFDM system is designed to be simple in order to be used as a reference model. In this way the minimum requirements of the OFDM system when operating in the presence of GSM and EDGE systems can be found.

On the basis of the above design discussions the table below shows the main characteristics of the designed OFDM system:

Table 4.1 – Main OFDM parameters

Number of FFT subcarriers	128
Number of data subcarriers	88
Number of pilot subcarriers	8
Unused subcarriers	32
OFDM symbol duration	0.577 ms
OFDM cyclic prefix duration	78 μs
Subcarrier spacing	2 kHz
3 dB bandwidth	192 kHz
Modulation	QAM64
Sampling ratio (time/rate)	20 (0.19493 μs/5.13005 MHz)

4.4 Modelling and verification of the multimode system

4.4.1 Introduction

The previous section discussed the design aspects of the proposed OFDM system. In this section the proposed design along with GSM and EDGE are modelled in the simulation platform ADS. The constructed models will be used to verify the appropriateness of the proposed design and furthermore that the GSM and EDGE systems operate optimally. In addition, they will be used as a test bench for performance evaluation under various environments, such as fading or interfering channels.

The simulation platform ADS has a large database containing models for many systems, that includes GSM and EDGE. The user can build such systems by selecting the appropriate models. In addition, the user has the option to construct his own models by using the Ptolemy software which is integrated with ADS. In [136] modelling and performance assessment of OFDM and in general modelling of communication systems in ADS is described.

In our design, the GSM and EDGE systems were constructed using models from ADS library (referred as blocks). On the other hand, some of the models of the proposed OFDM system were constructed in the Ptolemy software. The next section as well as Appendix A.2 describe the design of the proposed OFDM system in ADS and give more details about this matter. The subsequent sections give a brief description of GSM and EDGE systems.

4.4.2 OFDM system

4.4.2.1 Transmitter design

The block diagram of the OFDM transmitter is shown in Figure 4.6

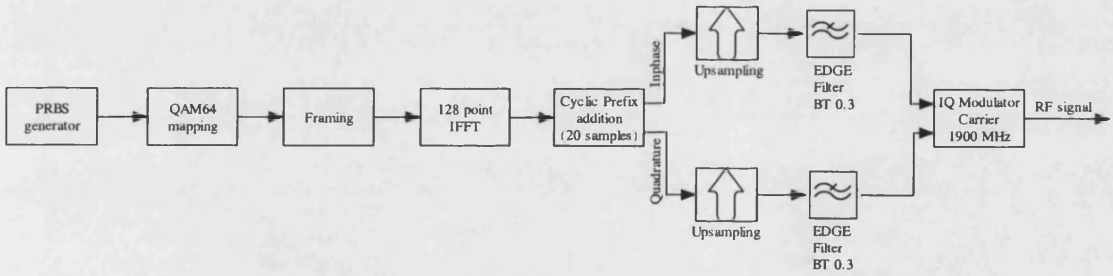

Figure 4.6 – OFDM transmitter block diagram

A pseudo-random binary sequence PRBS data is fed to a block that performs QAM64 mapping. The OFDM "burst" slot is then created through a block designed in Ptolemy which inserts the pilot symbols and arranges the data symbols as discussed in section 4.3.2 and shown in Figure 4.3. The "Framing" block is comprised of a number of sub-blocks that were designed using Ptolemy. Its contents can be found in Appendix A.2.1. The next two blocks perform the 128 point IFFT to create the OFDM symbol and insert the guard interval. The OFDM signal is then split into two branches containing the inphase (real) and quadrature (imaginary) components of the OFDM

symbol. The signal is upsampled by a factor of 20, which increase the sampling rate of the signal and is sufficient to meet the Nyquist sampling criterion [137]. ADS documentation specifies that the upsampling ratio must be higher than 10 in order to obtain the best possible results [119]. The next block pulse-shapes the OFDM signal by using the linearised Gaussian filter of EDGE. Finally, the pulse-shaped OFDM signal is upconverted using the IQ modulator at a carrier frequency of 1900 MHz[3]. The spectrum of the pulse-shaped OFDM signal is shown in Figure 4.7. This figure shows that the OFDM signal spectrum falls within the limits of the GSM spectrum mask.

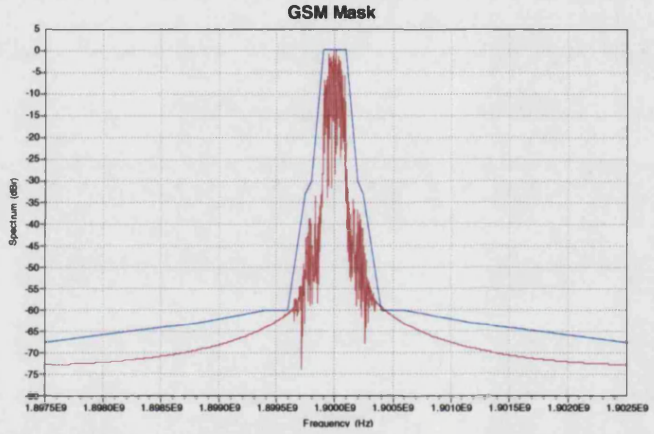

Figure 4.7 – Pulse-shaped OFDM spectrum in GSM spectrum mask

4.4.2.2 Receiver design

The receiver design block diagram is shown in Figure 4.8.

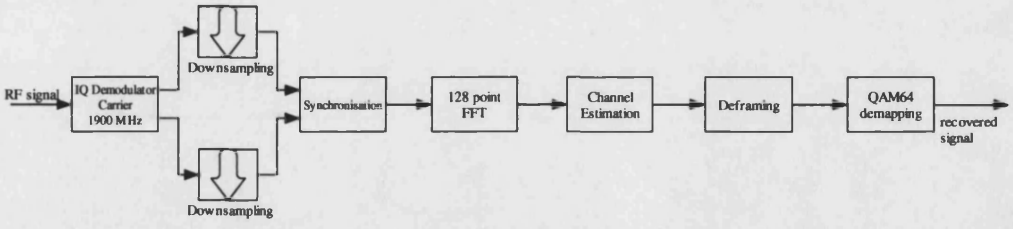

Figure 4.8 – OFDM receiver block diagram

[3] The 1900 MHz band is used for the purpose of the studies required in this work. Other GSM bands (900, 1800 MHz) can be used. The only variation will be in the fading model.

The OFDM RF signal is received through an IQ demodulator and then downsampled. The next block performs synchronisation using the method described in section 3.4.3.3. This block performs frequency and timing offset estimation by exploiting the correlation of the cyclic prefix of the OFDM signal in conjunction with ML estimation. The synchronised OFDM samples are demodulated by an FFT and then fed to the block that performs channel estimation. The channel estimation block, shown in Figure 4.9, was designed and implemented in Ptolemy. The Ptolemy codes for the different components are given in Appendix A.2.3.

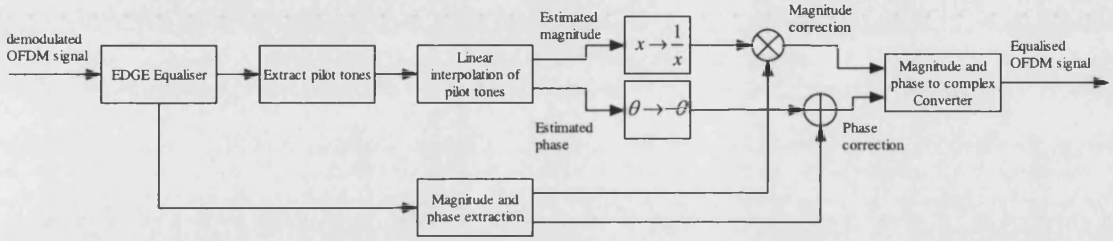

Figure 4.9 – Channel estimation for OFDM

The channel estimation model contains an equalising filter to remove the effects of the linearised Gaussian filter used in the transmitter. LS estimation is then performed using the extracted pilot symbols. The effects of the channel are removed by taking the reciprocal of the estimated channel magnitude response and multiplying it with the magnitude of the OFDM signal. In addition, the channel phase response is subtracted from the phase of the OFDM signal. The "Deframing" block removes the pilot symbols and zero-padding. The final block performs QAM64 decoding. The signal at the output of this model is the recovered transmitted signal.

4.4.3 GSM system

4.4.3.1 Transmitter design

The GSM transmitter block diagram is shown Figure 4.10. The pseudo-random binary sequence is fed to a block that creates the full rate traffic channel and then to a block that arranges the traffic channel in the normal burst mode of operation. The traffic channel and normal burst of GSM were described in sections 2.3.4 and 2.3.5, respectively. The Normal Burst slot is then differentially encoded and GMSK

modulated by the next two blocks. The GMSK signal is upsampled and then upconverted by an IQ modulator. The carrier frequency of the GSM model is set in the PCS1900 band at 1900 MHz.

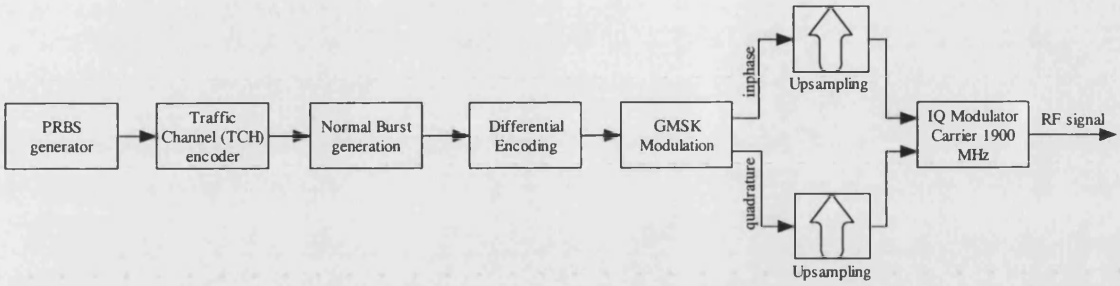

Figure 4.10 – GSM transmitter block diagram

4.4.3.2 Receiver design

The GSM receiver model block diagram is shown in Figure 4.11.

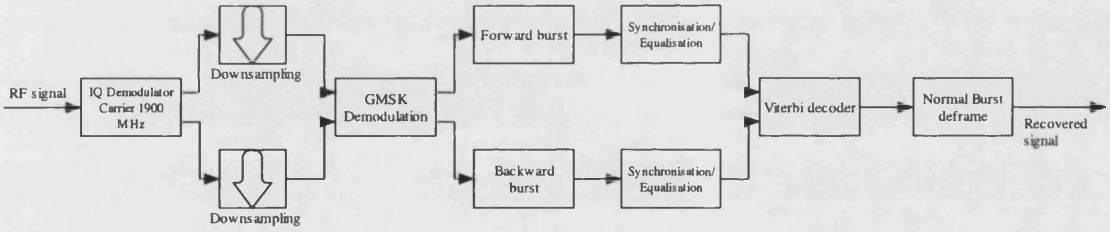

Figure 4.11 – GSM receiver block diagram

The transmitted GSM RF signal is downconverted to baseband by an IQ demodulator. The signal is then downsampled and then demodulated. The decoded normal burst frame is then split into two burst frames of 82 samples each, the forward and backward burst. The forward burst starts from the beginning of the training sequence and ends at the end of the normal burst. The backward burst starts at the end of the training sequence and ends at the beginning of the frame. This is illustrated in Figure 4.12. The backward and forward bursts are used to correct the effects of the channel on the first half and second half data symbols respectively. The newly formed burst frames are compared with the known training sequence in order to estimate the channel impulse response and then using this information the data symbols are equalised. The equalised data symbols are then inserted into a Viterbi decoder to obtain

the transmitted signal. The GSM system was designed using models obtained from the databases of ADS. The ADS schematics of this model are shown in Appendix A.3.

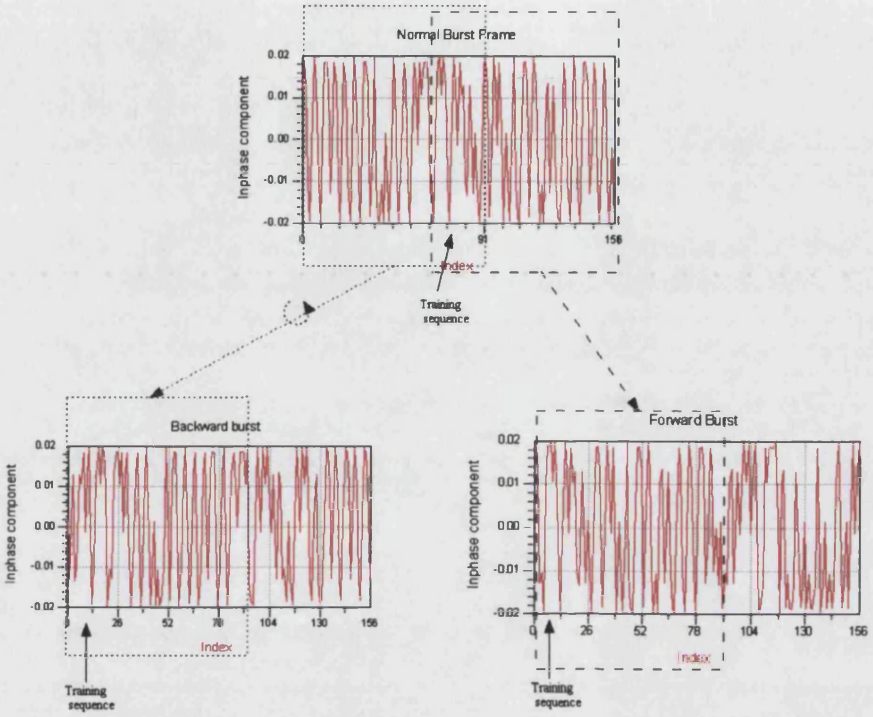

Figure 4.12 – Forward and backward burst frames used for equalisation

4.4.4 EDGE system

4.4.4.1 Transmitter design

The EDGE transmitter block diagram is shown in Figure 4.13.

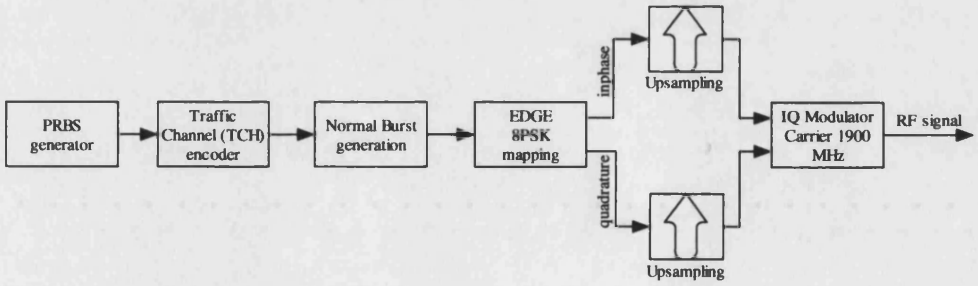

Figure 4.13 – EDGE transmitter block diagram

The EDGE normal burst slot is created in the same way as with the GSM normal burst. The normal burst frame is then $3\pi/8$ 8PSK encoded and pulse shaped using the linearised Gaussian filter with a BT product of 0.3 using the EDGE 8PSK mapping model. Finally, the EDGE signal is upconverted to RF using an IQ modulator. The trajectory diagram of the EDGE signal is shown in Figure 4.14.

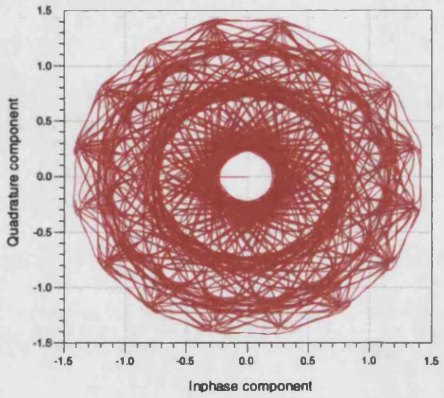

Figure 4.14 – $3\pi/8$ 8PSK trajectory diagram

4.4.4.2 Receiver design

The EDGE receiver block diagram is shown in Figure 4.15.

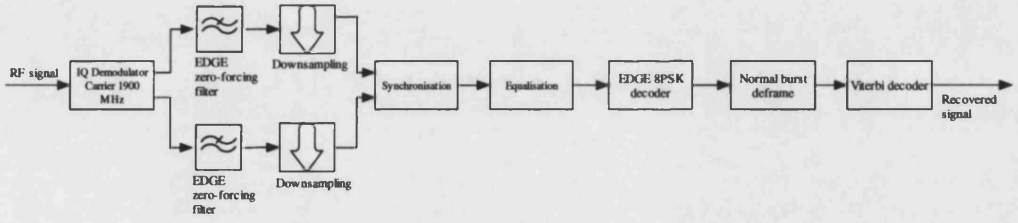

Figure 4.15 – EDGE receiver block diagram

The downconverted signal after the IQ demodulator is first fed to an EDGE zero-forcing filter that removes the ISI effects added to the signal due to the EDGE transmitter filter. The EDGE signal is then synchronised and equalised following a similar procedure to that of GSM. An EDGE 8PSK decoder in conjunction with a Viterbi decoder block are then used to obtain the Normal burst frame. The recovered signal is then obtained by using a block to remove the normal burst frame arrangement.

The EDGE system was constructed using models acquired from the database of ADS, shown in Appendix A.4.

4.5 Simulation system setup

4.5.1 Introduction

The previous section described the modelling of the multimode system in the simulation platform ADS. This section states the design of the simulation test benches needed to perform the performance evaluation of the multimode system under fading and interference environments.

The section starts by describing the simulation test benches. The multimode system will be evaluated using the same measurement methods approved by ETSI for evaluation of GSM and EDGE systems. First, the fading and Doppler spread environments that are used to test GSM and EDGE systems are described. The subsequent sections describe how adjacent- and co-channel interference for GSM or EDGE is measured.

4.5.2 Multipath fading and Doppler spread

GSM recommendation 05.05 specifies three multipath fading channel profiles for simulations with different radio propagation environments and vehicle speeds [8]. These are the Hilly Terrain (HT), Typical Urban (TU) and Rural Area (RA) models. Each of these models is simulated at specific vehicular speeds ranging from 3 km/h to 250 km/h. Hilly Terrain and Typical Urban environments use Rayleigh fading distribution, where the line-of-sight (LOS) component is negligible and therefore not taken into consideration to define their environments [76]. On the other hand, Rural Area environments use Ricean fading distribution where the LOS component is taken into consideration [76]. The fading channel was discussed in section 3.3.2. The Hilly Terrain model is a frequency selective model with small coherence bandwidth. It is usually used in conjunction with a vehicle speed of 100 km/h. The Typical Urban model is a frequency-selective model with a relatively large coherence bandwidth and typically used with vehicle speeds of 3 and 50 km/h. Finally, the Rural Area model is frequency non-selective (flat fading) and used in conjunction with vehicle speed of 250

km/h. The minimum coherence time of all the models is greater than the timeslot duration of the GSM-EDGE-OFDM systems (the coherence time of the RA channel at a vehicle speed of 250 km/h is 5 ms while the timeslot duration is 0.577 ms). Therefore, in all cases, the channels are defined as slow-fading [139].

The GSM/EDGE system is usually tested under the channel environments shown in Table 4.2 [8],[139]. The "x" term in the "HTx" model defines the vehicle speed. For example, HT100 is Hilly Terrain environment at a vehicle speed of 100 km/h.

Table 4.2 – Typical characteristics of GSM multipath channel models [139]

Model	Vehicle Speed (km/h)	Number of taps	Doppler spectrum	Multipath delay spread
HTx	100	6	Rayleigh	5.42T
TUx	3, 50	6	Rayleigh	1.36T
RAx	250	6	Ricean or Rayleigh	0.14T

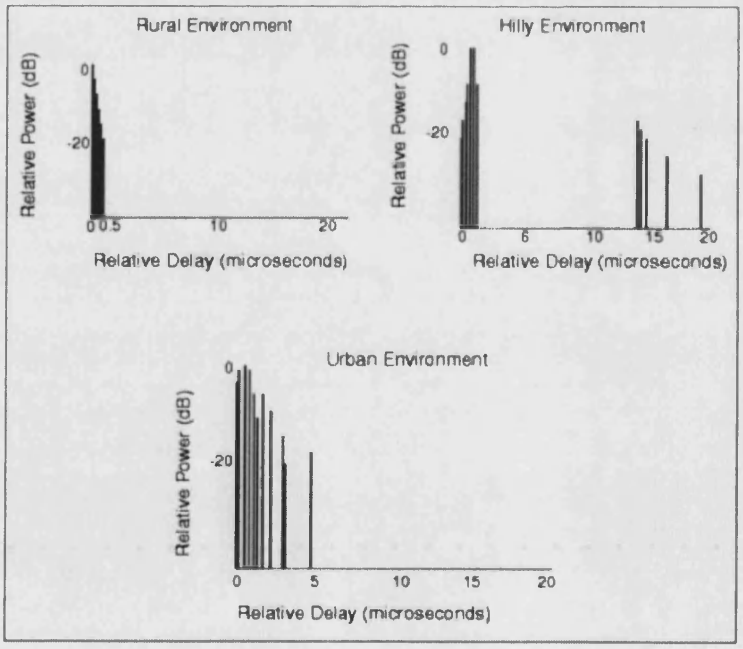

Figure 4.16 – Relative delay profiles of GSM multipath fading channels [119]

The GSM specifications define 10 different propagation profiles, two for rural area and four for each of the hilly terrain and urban area environments. Each profile can be characterised by 6-tap or 12-tap filters [8].

Figure 4.16 shows the average delay profiles of each environment characterised by 6-tap filters. The y-axis shows the average signal strength of each of the multipath components at the receiver while the x-axis shows the corresponding delay of each frame. The rms delay spread of each multipath environment is calculated by using the equations outlined in section 3.3.2.2.

4.5.3 Simulation of co-channel interference

For simulation of co-channel interference the GSM recommendations specify that the main and interfering signals are both to be subjected to the same propagation profile but independently generated for each signal [139], as illustrated in Figure 4.17.

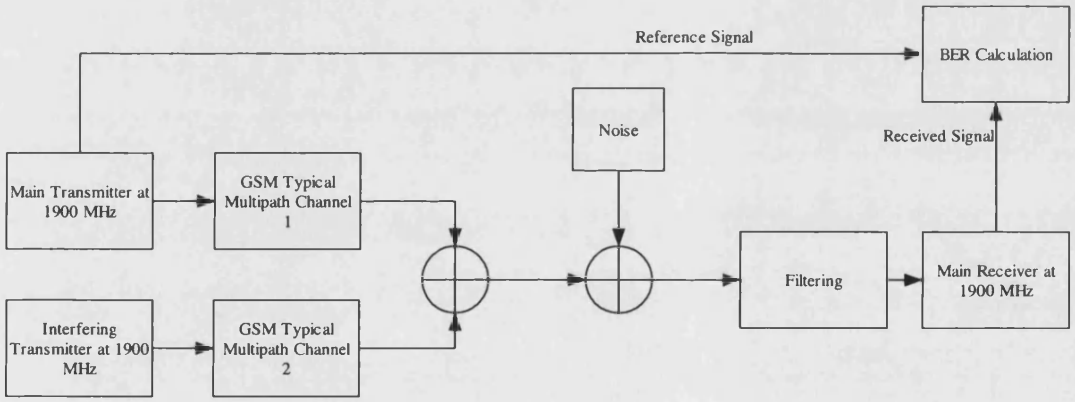

Figure 4.17 – Block diagram of co-channel interference simulation

In addition, the recommendations specify that under co-channel interference the minimum carrier-to-interference ratio (for the GSM system to work correctly) should be 9 dB. For EDGE, the reference interference increases to 14.5 dB [1],[8].

4.5.4 Simulation of adjacent-channel interference

For simulation of adjacent-channel interference the GSM recommendations specify that only the main signal is to be subjected to multipath fading environments, while the interferer can be a static GMSK signal with a given carrier frequency [139].

In our case, the interferer will be a static GMSK, 8PSK or an OFDM/QAM64 signal. The block diagram for adjacent-channel interference simulation is given in Figure 4.18.

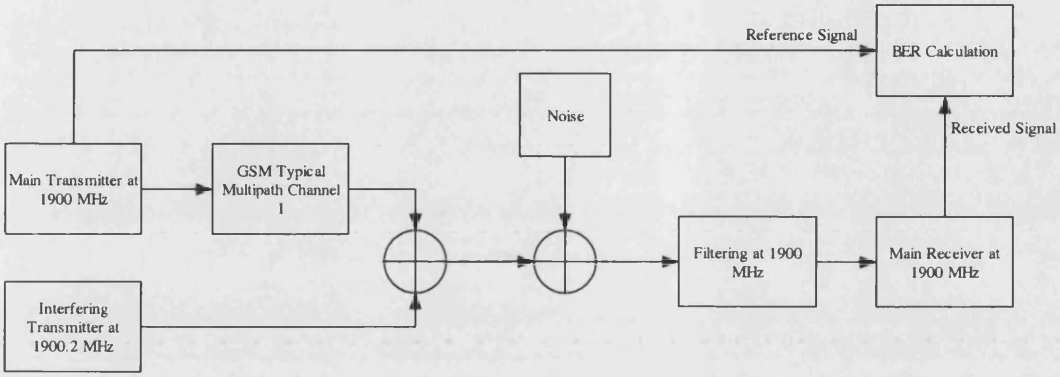

Figure 4.18 – Block diagram of adjacent-channel interference simulation

The minimum carrier-to-interference ratio, in a 200 kHz adjacent-channel condition is -9 dB for GSM. For EDGE, the ratio increases to -2 dB. Table 4.3, shows the minimum ratios required for adjacent channels of 400 and 600 kHz. The ADS schematics of the channel modelling can be found in Appendix A.2.2.

Table 4.3 – ETSI adjacent channel interference reference levels (** in brackets shown the reference levels when an adjacent 8PSK signal is present instead of a GMSK one)[8]

Adjacent channel frequency separation	**GMSK**	**8PSK**
200 kHz	-9 dB (-18 dB**)	-18 dB
400 kHz	-41 dB (-50 dB**)	-50 dB
600 kHz	-49 dB (-58 dB**)	-58 dB

4.6 Evaluation of multimode system

4.6.1 Introduction

This section displays the results obtained from simulations based on the measurement methods described in the previous section. First the performance of the multimode system is tested under additive noise environment. Consequently, the simulation results obtained when the system is present in fading environments are then

displayed. Finally, the simulation results obtained when the multimode system suffers from adjacent- or co- channel interference are displayed.

The performance of the multimode system will be analysed by comparing the BER results obtained. Most of the results displayed will take a reference error rate of 10^{-3}. The choice is reasonable since at this error rate the wireless system has optimal performance.

4.6.2 Performance in noise

This section investigates the performance of the multimode system in an environment where noise is the only interferer. The block diagram of the system employed in the simulations is shown in Figure 4.17, with the interfering and multipath fading channels inactive. Figure 4.19, shows the error rate versus E_b/N_0.

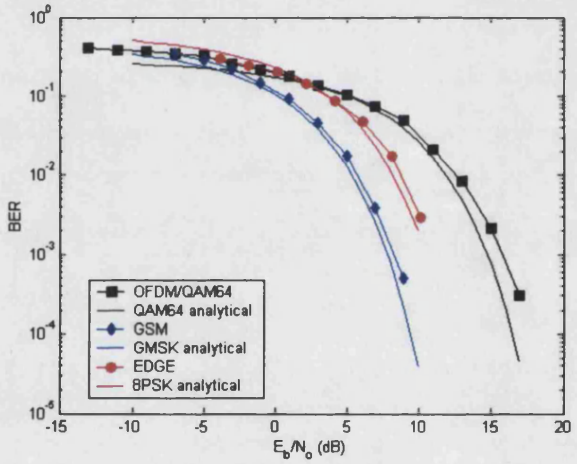

Figure 4.19 – Performance of multimode system under Gaussian noise

The figure shows that the error rates of the multimode system are similar to the error rates obtained from analytical expressions of GMSK, 8PSK and QAM64 modulations [137]. However, the OFDM/QAM64 has an approximately 2 dB degradation (at 10^{-3} error rate) compared to the analytical expression of QAM64, which is due to the cyclic prefix insertion and the use of filtering at the transmitter.

4.6.3 Performance in fading channels

4.6.3.1 GSM Typical Urban environment

In this section the system is evaluated in GSM Typical Urban environments[4]. In such environments, low to medium speeds are the most dominant. In our case the system will be tested at speeds of 3 and 50 km/h. Figure 4.20, shows the error rate versus E_b/N_0 .

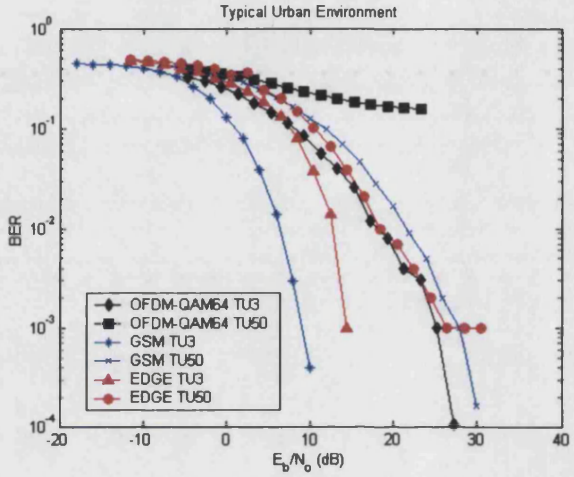

Figure 4.20 – Performance of multimode system in a GSM typical urban environment

The figure shows a large difference in the performance of GSM and EDGE systems compared to OFDM when the vehicle is moving at 3 km/h. The OFDM system in a TU3 environment, needs an E_b/N_0 ratio of approximately 19 dB to achieve 10^{-2} error rate whereas the GSM and EDGE systems achieve the same error rate performance, at the same environment, with approximately 6 dB and 12 dB ratios, respectively. A reason for such difference is due to the QAM64 modulation used by OFDM that is sensitive to noisy environments. When the mobile is moving at a speed of 50 km/h, OFDM/QAM64 performance is severely deteriorated, whereas the performance of the other two systems deteriorate at a lesser extent. It is important to note that for all our tests we used an OFDM system with *no coding*. This results in further deterioration of the OFDM system when compared to GSM/EDGE in all of the test environments. In practice, appropriate coding is expected to be implemented which

[4] GSM delay environments define 6-tap and 12-tap models. Both were used for the performance assessment of this system. The results obtained were consistent, thus, for simplicity we only report the results of one model (6-tap). This applies also for subsequent simulations.

will result in giving the OFDM system expected error rate improvements. Figure 4.21 shows the performance of the OFDM system in a TU50 environment under different mapping schemes. The following figure proves that as the complexity of the mapping scheme in OFDM is reduced the error rates obtained are improved and approach or even surpass the error rates of GSM and EDGE. However, the reduction of the order of the mapping scheme reduces the data rate of OFDM. With QAM16 mapping the achievable data rate is approximately 600 kbps whereas with QAM4 mapping the data rate reduces to approximately 300 kbps. Note that GSM has maximum data rate per user of 14 kbps and EDGE has maximum data rate per user of 473.6 kbps. Figure 4.21, also displays that at high E_b/N_o ratios the error rates of OFDM and EDGE stabilise. This is due to the Doppler spread of the multipath environment. This is justified by looking Figure 4.22 that shows error rates of the proposed OFDM system using QAM16 modulation in TU3, TU25 and TU50 environments.

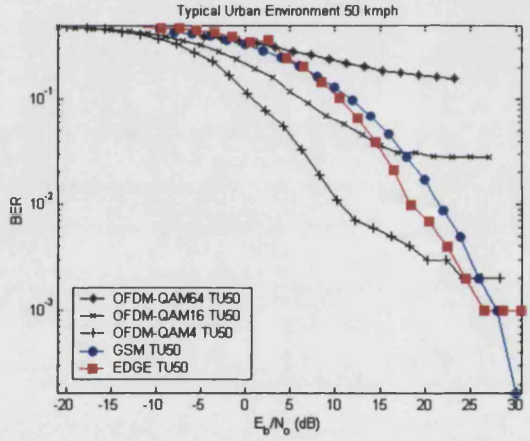

Figure 4.21 – Performance of multimode system in the TU50 multipath environment

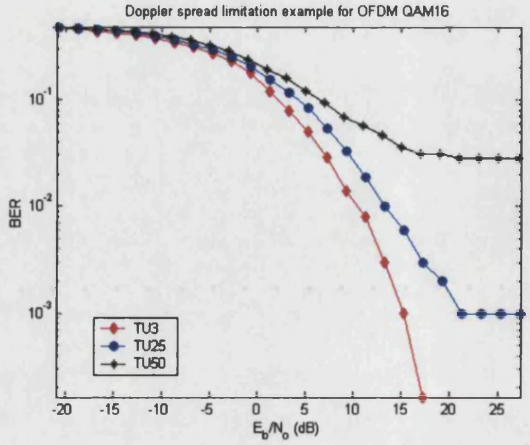

Figure 4.22 – Proposed OFDM system Doppler spread limitation example

The figure above shows that as the speed of the mobile device increases, the error rate of the system stabilise at a higher error value. For example, in the TU50 environment the error rate exhibits a floor at approximately $0.5 \cdot 10^{-1}$, whereas in the TU25 environment at 10^{-3}. This is also observed for GSM and EDGE systems, but at higher speeds as Figure 4.23 depicts.

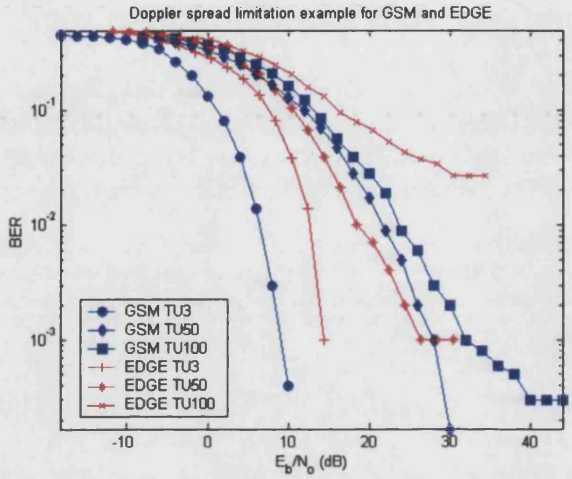

Figure 4.23 – Doppler spread limitation for GSM and EDGE

The figures above indicate that the proposed OFDM system suffers from higher sensitivity to Doppler effects than GSM or EDGE systems. In section 3.4.4 it was stated that the spacing of the pilot symbols is inversely proportional to the maximum Doppler spread tolerance. Therefore, a possible solution to resolve this issue would be to reduce the spacing of the pilot symbols. This can be achieved by increasing the number of pilot carriers within one OFDM symbol. However, this action reduces the effective data rate of the system.

4.6.3.2 GSM Typical Hilly Terrain environment

ETSI standards state that GSM/EDGE systems are tested in HT environments at speeds of 100 km/h. Therefore, the system will be susceptible to high Doppler spreads. The following figure shows the results obtained when the system is susceptible to such environments. Due to the high speed of the mobile, at high E_b/N_0 ratios the error rates obtained show high error floor behaviour. It can also be observed that the results are similar to the results obtained in the TU environment. At high speeds, OFDM using

QAM16 and QAM64, give highly erroneous results (the error rates obtained are higher than 10^{-1}). However, when the OFDM system uses QAM4 modulation its BER performance is better than that of EDGE. Such observations are valid for high E_b/N_0 ratios, where the multimode system is Doppler spread limited.

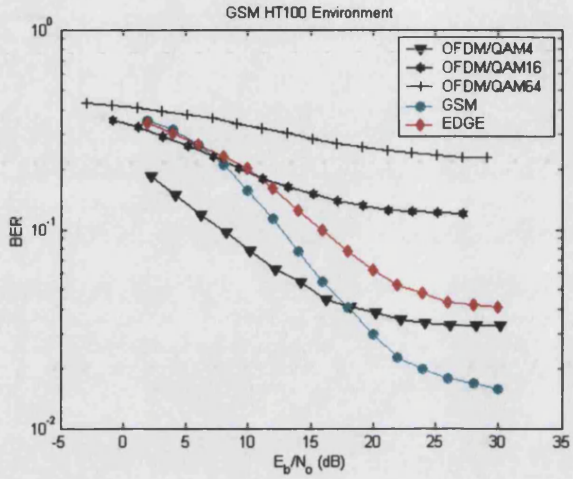

Figure 4.24 – Performance of multimode system in the HT100 GSM environment

4.6.3.3 GSM Rural Area environment

In Rural Area environments ETSI specifies testing with speeds of 250 km/h. This will result in obtaining highly erroneous results, which are shown in Figure 4.25.

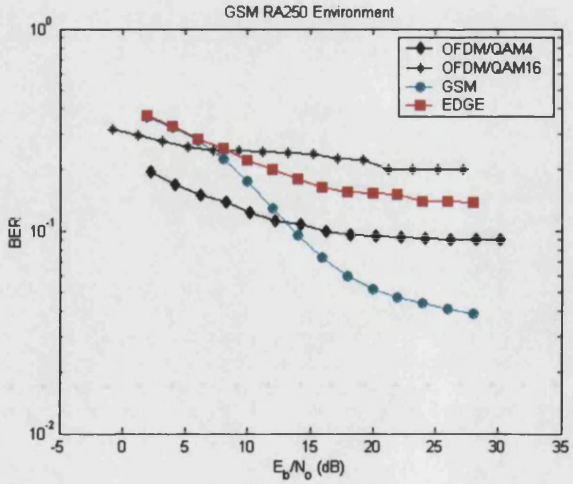

Figure 4.25 – Performance of multimode system in RA250 environment

The results obtained are similar to the results obtained in HT environments. The performance of OFDM/QAM16 shows very high error rates, whereas OFDM/QAM4 has better performance than EDGE. The high error rates observed are due to the high vehicular speeds that the systems are tested giving high Doppler frequency values.

4.6.3.4 Discussion of the results

The results obtained from the simulations indicate that at low speeds, for example in the TU3 environment, the performance of the OFDM/QAM64 system is comparable to the performance of EDGE and better by 3dB to the performance of GSM operating at TU50 environments. The performance of the OFDM/QAM64 system is only limited by its sensitivity to noisy environments due to its highly complex modulation scheme. As the mobile speed increases, for example in TU50, HT100 and RA250 environments, the performance of the OFDM/QAM64 deteriorates. However, switching to a less complex modulation (QAM16 or QAM4), the performance of the OFDM/QAM4 or OFDM/QAM16 approaches the performance of the other two systems, with the disadvantage of the reduction of the maximum achievable data rate. An adaptive modulation scheme [140] similar to the one used for WLAN [65]-[67], can provide a significant improvement in the performance of the OFDM system. It is also important to note that the OFDM system does not have any error coding scheme which will improve its performance [141],[142]. However, adding an error coding scheme, reduces the efficiency of OFDM which in turn reduces the maximum achievable data rate. This could be compensated by using a higher number of carriers. However, such action will shorten the separation of the OFDM subcarriers which could make the system more susceptible to adjacent- or co- channel interference. In addition, the results indicated that the OFDM system has a higher Doppler spread sensitivity than GSM and EDGE systems. A possible solution to this problem is to reduce the spacing of the pilot symbols by increasing their number within one OFDM symbol, which has the disadvantage of reducing the effective data rate.

4.6.4 BER performance with adjacent-channel interference

This section is concerned with the investigation of ACI effects on OFDM, on EDGE and on GSM systems. Initially, the ACI effects of EDGE on OFDM, GSM on OFDM and OFDM on OFDM are investigated. Subsequently, simulation results are

presented to investigate the effects of ACI on GSM and on EDGE. The OFDM system will use QAM64 modulation and has the characteristics given in Table 4.1.

In order to have a more detailed analysis of the performance of the system in ACI, the direct conversion receiver of the multimode system has been replaced by a double conversion one[5]. The new receiver adds to the system the noise and non-linear elements of real life systems. The block diagram of the simulation system is similar to Figure 4.18, with the AWGN block removed and replaced by a double conversion RF front-end model. All the interference simulations were made in a GSM Typical Urban environment with a vehicular speed of 3 km/h[6].

4.6.4.1 Adjacent-channel interference on OFDM

The BER results of ACI on OFDM are shown in Figure 4.26, using 200 kHz carrier frequency separation between the wanted and interfering signals for different levels of interfering power. On the x-axis of the figure, *Pdiff*, denotes the difference in power between the wanted and interfering signals.

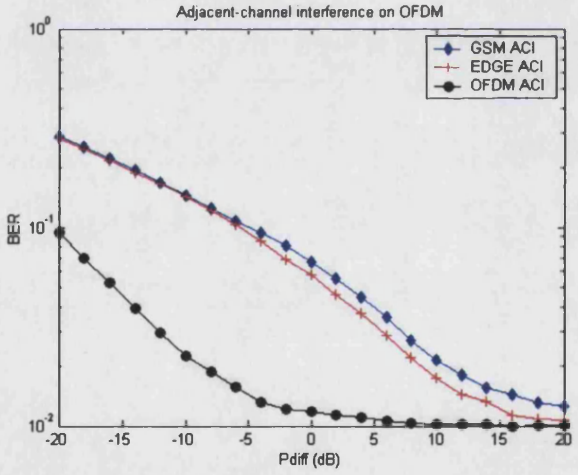

Figure 4.26 – BER versus P_{diff} for OFDM with ACI

The figure above shows that adjacent GSM and EDGE channels result in the same level of distortion on the OFDM system whereas the interference from an adjacent

[5] Detailed receiver RF front-end (amplifiers, mixers) was provided by Nokia Networks UK. The details of this receiver are not given due to commercial sensitivity. This should not result in any loss of generality of the results described or the conclusions drawn.

[6] Specifically requested in discussions with Nokia Networks UK. It is also a reasonable choice due to the consistency of the results under this environment.

OFDM channel produces less distortion from the other two systems. At low levels of interference, where the multimode system is noise limited the interference from every channel is approximately the same. The above figure also indicates that the double conversion receiver is noise limited at E_b/N_o ratios of 20 dB and above. This is due to the non-linear components of the double conversion receiver that worsens the performance of OFDM in noise. It must also be noted that the OFDM system has no coding scheme and that the simulation take place in a TU3 environment that further deteriorates the performance of the system.

In order to understand the reason that an adjacent OFDM system causes less distortion to the main OFDM system than adjacent GSM and EDGE systems, the spectral leakage of each system is measured. This is performed by measuring the power leakage of the main carrier to the adjacent one. The spectral leakage is measured using the block diagram shown in the figure below.

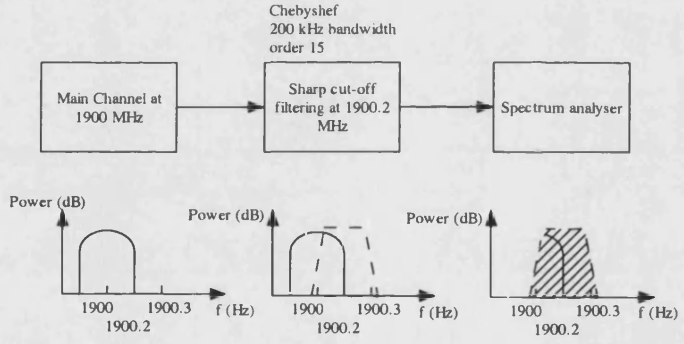

Figure 4.27 – Measurement of spectrum leakage onto adjacent-channel

The power leakage is measured by placing a sharp cut-off filter (10^{th} order Chebyshev filter, 200 kHz bandwidth) at the adjacent channel frequency of 1900.2 MHz and then using a spectrum analyser to observe the section of the main channel spectrum that leaks onto the adjacent channel. Figure 4.28, shows adjacent channel spectral leakage of; an OFDM channel with a linearised Gaussian filter, an OFDM channel with no interpolation filter, an EDGE and finally a GSM channel.

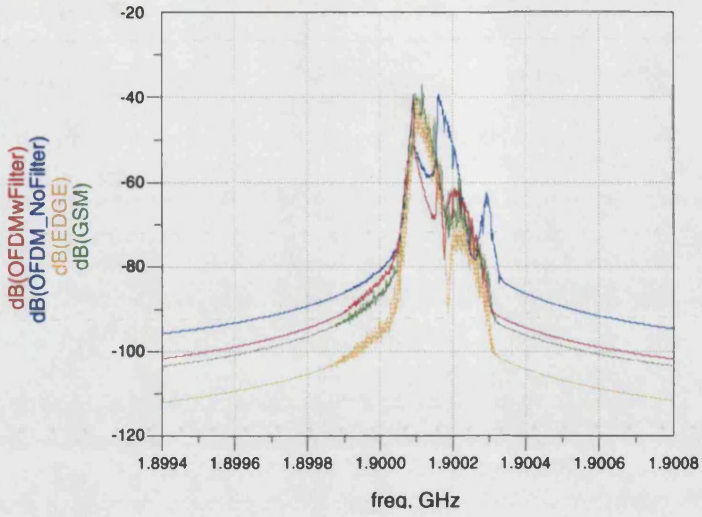

Figure 4.28 – Adjacent spectrum leakage of multimode system

The OFDM channel with the EDGE filter (shown in red) has less spectral leakage than both the GSM and EDGE channels. This explains the fact that OFDM on OFDM interference results in less distortion to OFDM rather than adjacent interference from EDGE and GSM channels. In addition, the spectral leakage of an OFDM channel with no filter (shown in blue) has more leakage than any other channel which is in accordance with Figure 4.5, where it was stated that a non-filtered OFDM spectrum could cause more interference to the adjacent channels.

4.6.4.2 Adjacent-channel interference on GSM

The BER results of ACI on GSM are shown in Figure 4.29.

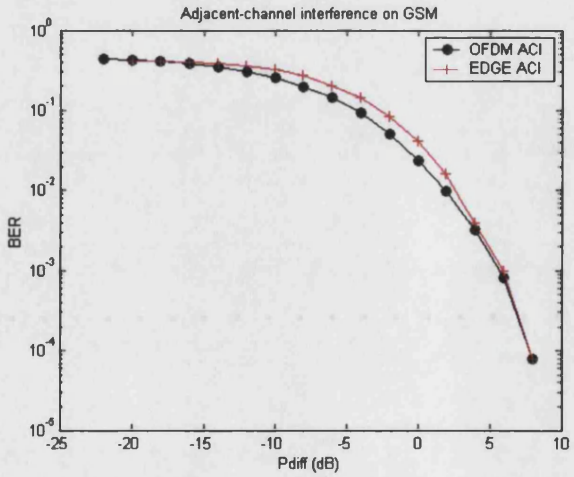

Figure 4.29 – BER versus P_{diff} for GSM with ACI

The above figure shows that at mid-level P_{diff} values, for example for 10^{-1} error rate there is an approximately 2 dB difference in the level of distortion between an OFDM and an EDGE interfering channel. On the other hand, at 10^{-4} error rates where adjacent channel interference influence is less (noise is more significant), the same level of distortion to the GSM channel irrespective of the source of interference is observed, although the OFDM channel has lower spectrum leakage than EDGE.

4.6.4.3 Adjacent-channel interference on EDGE

The BER results of ACI on EDGE are shown in Figure 4.30.

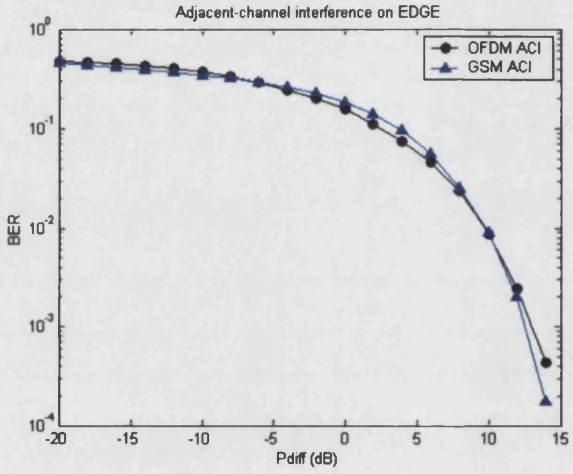

Figure 4.30 – BER versus P_{diff} for EDGE with ACI

Figure 4.30 shows that at 10^{-3} error rates, the same level of distortion is achieved by either an adjacent OFDM or an adjacent GSM channel on the EDGE channel. At mid-level P_{diff} values (10^{-1} error rate) the level of distortion of GSM is 1 dB higher than OFDM, in contrast with the error rates shown in Figure 4.29.

4.6.4.4 Discussion of the results

The simulation results show that the interference effects between each system are comparable at low error rates (approximately 10^{-3}). Therefore, it is expected that the performance of each system will be similarly degraded from ACI, without needing to know the nature of the interfering channels. Hence the introduction of OFDM into the existing GSM/EDGE network will not result into different level of degradation

depending on the source of ACI. Consequently, the same frequency planning schemes can be used for the OFDM signals.

4.6.5 BER performance with co-channel interference

The multimode system is tested under the same conditions as carried out in the previous section with the interfering channel carrier frequency being the same as the carrier frequency of the wanted channel. The simulation block diagram is the same as that shown in Figure 4.17.

4.6.5.1 Co-channel interference on OFDM

The BER results are shown in Figure 4.31.

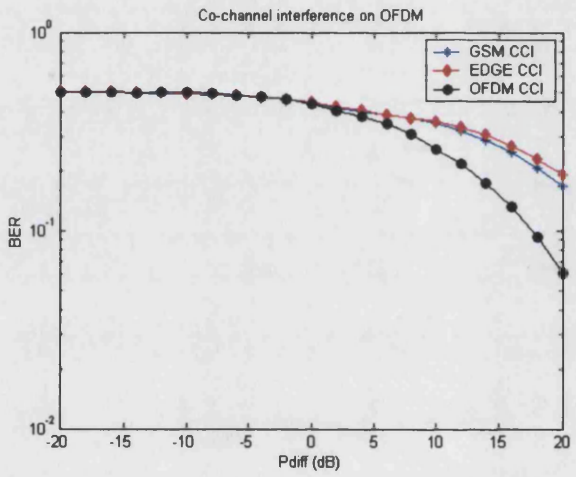

Figure 4.31 – BER versus P_{diff} for OFDM with CCI

Figure 4.31 shows that the distortions from a co-channel OFDM interferer will result in fewer distortions to OFDM than either a co-channel GSM or EDGE system.

4.6.5.2 Co-channel interference on GSM

The BER results are shown in Figure 4.32.

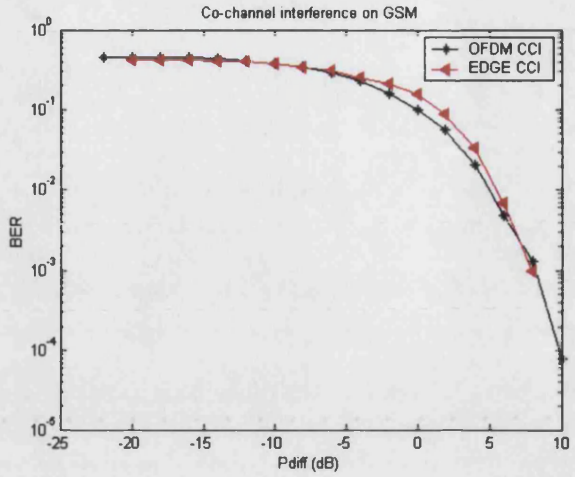

Figure 4.32 – BER versus P_{diff} for GSM with CCI

Figure 4.32 shows similarities with Figure 4.29. For example, at 10^{-1} error rates the distortions of EDGE are 2 dB higher than the distortions of OFDM. On the other hand, at low error rate values (10^{-3}), the same level of distortion is observed by each system

4.6.5.3 Co-channel interference on EDGE

The BER results are shown in Figure 4.33.

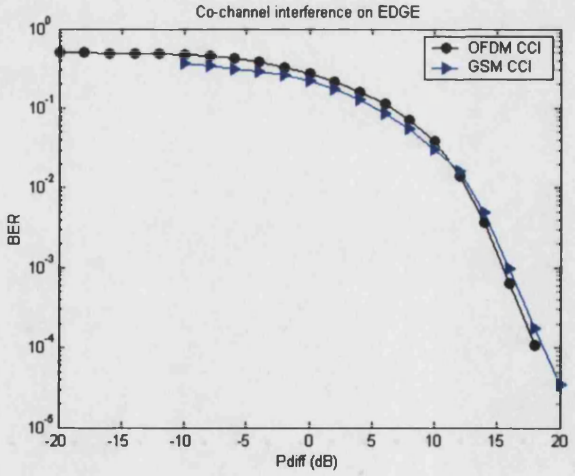

Figure 4.33 – BER versus P_{diff} for EDGE with CCI

The above figure shows that co-channel interference on EDGE produces the same level of distortion independently of the source of CCI which is similar with Figure 4.30, showing ACI on EDGE.

4.6.5.4 Discussion of the results

Under co-channel interference, it is observed that at 10^{-3} error rates the interference level from each system causes the same level of distortion to GSM and EDGE. In addition, the interference to OFDM shows higher error rates (10^{-1} and higher). However, it is expected that with the use of coding and adaptive modulation, the OFDM system performance will be significantly improved.

4.7 Summary

This chapter has analysed the performance of a multimode system implementing OFDM, GSM and EDGE, in the presence of AWGN, multipath fading and adjacent- and co-channel interference. The performance of the system was evaluated using models developed in the simulation software ADS.

Evaluation of the multimode system in noise showed that the error rates of GSM and EDGE systems match the analytical error rates of GMSK and 8PSK modulations. However, the error rate of OFDM system implementing QAM64 modulation had an approximately 2 dB difference (at an error rate of 10^{-3}) compared to the analytical error rate of QAM64 modulation. A predictive reason was that the OFDM system was limited by the linearised Gaussian filter placed at the OFDM transmitter and the cyclic prefix and the lack of coding.

Evaluation of the multimode system in GSM typical environments indicated that at low vehicular speeds the performance of OFDM/QAM64 is comparable to the performance of GSM and EDGE systems at mid-vehicular speeds. At high vehicular speeds, for example in TU50, HT100 and RA250 environments, the performance of OFDM/QAM64 deteriorates. This disadvantage can be avoided by using an adaptive modulation scheme similar to the scheme used in WLAN. The drawback of this method is that at high speeds the available data rate of the OFDM system is reduced.

Finally the evaluation of the multimode system in a TU3 environment under ACI or CCI, indicated that the performance of the system is similarly degraded independently of the source of ACI or CCI. We can also conclude the same effects will

be observed when simulating ACI/CCI in various multipath environments since such environments are linear. Consequently, we can safely conclude that the OFDM system will not infer any problems when introduced with GSM/EDGE systems.

Chapter 5

Fast-OFDM: A bandwidth efficient OFDM scheme

5.1 Introduction

In this chapter a new modulation technique will be investigated, which is a variation of the OFDM. Fast-OFDM (FOFDM) was developed by M.R.D. Rodrigues and Izzat Darwazeh at University College London in 2002 [143]. The basic feature of FOFDM is its bandwidth efficiency when compared to OFDM. This feature applies only for single dimensional modulation schemes like BPSK or M-ASK. More specifically, an FOFDM system with BPSK modulation will require half the bandwidth of an OFDM system using the same modulation to transmit the same data rate.

The objective of this chapter is to design an FOFDM system and compare its performance with a similar OFDM system. Both systems will be tested in environments of I/Q imbalance, synchronisation error, frequency offset, phase noise and frequency selective fading. The next section is concerned with describing the basic principles of Fast-OFDM stating its advantages and disadvantages. A brief description of the research done in this area will be carried out next. Subsequently, the modelling of an FOFDM/BPSK and OFDM/BPSK system and their implementation in the simulation software ADS, will be described. Finally, the performance of both systems will be compared in the environments stated previously.

5.2 Principles of FOFDM

5.2.1 Introduction

Fast-OFDM is based on the OFDM principle with the advantage of having twice the bandwidth efficiency of OFDM. Fast-OFDM has similar principles with MSK, where the peak frequency deviation is equal to 1/4 the bit rate, which effectively makes the two MSK frequencies to be separated by half the bit rate. Since the basic principle of MSK is to achieve the minimum frequency separation that allows orthogonal detection [4], this means that orthogonality is still preserved when two frequencies are separated by half the bit rate. This idea is utilised by FOFDM, where the frequency separation of its subcarriers is $(1/2T)$ Hz, where T is the duration of the signalling interval. MSK is sometimes referred to as *fast* FSK [144], thus the term *Fast*-OFDM.

5.2.2 Continuous-time implementation

In section 2.7.1, the continuous-time (oscillator based) implementation of an OFDM scheme was described. According to this chapter the complex envelope representation of an OFDM signal $S_{tx,OFDM}(t)$, with cyclic prefix is given by:

$$S_{tx,OFDM}(t) = \sum_{k=-\infty}^{\infty} \sum_{n=0}^{N-1} a_{n,k} g_n(t-kT) \qquad \text{eq. (5.1)}$$

$$g_{n,OFDM}(t) = \begin{cases} \dfrac{1}{\sqrt{T-T_{CP}}} e^{j\frac{2\pi nt}{T-T_{CP}}}, t \in [0,T] \\ 0, \qquad\qquad t \notin [0,T] \end{cases} \qquad \text{eq. (5.2)}$$

where, T is the duration of the signalling interval, $a_{n,k}$ is the complex symbol transmitted on the n^{th} subcarrier at the k^{th} signalling interval, N is the number of OFDM subcarriers, $g_{n,OFDM}(t-kT)$ represents the complex subcarrier used to convey the complex data in the same timeslot and subchannel and T_{CP} is the duration of the cyclic prefix.

An FOFDM signal will have its subcarriers separated by a frequency which is the inverse of half the signalling interval. Thus, the complex envelope representation of an FOFDM signal $S_{tx,FOFDM}(t)$, is [143]:

$$S_{tx,FOFDM}(t) = \sum_{k=-\infty}^{\infty} \sum_{n=0}^{N-1} a_{n,k} g_{n,FOFDM}(t - kT) \qquad \text{eq. (5.3)}$$

$$g_{n,FOFDM}(t) = \begin{cases} \dfrac{1}{\sqrt{T - T_{CP}}} e^{j\frac{2\pi nt}{2(T-T_{CP})}}, t \in [0,T] \\ 0, \qquad\qquad t \notin [0,T] \end{cases} \qquad \text{eq. (5.4)}$$

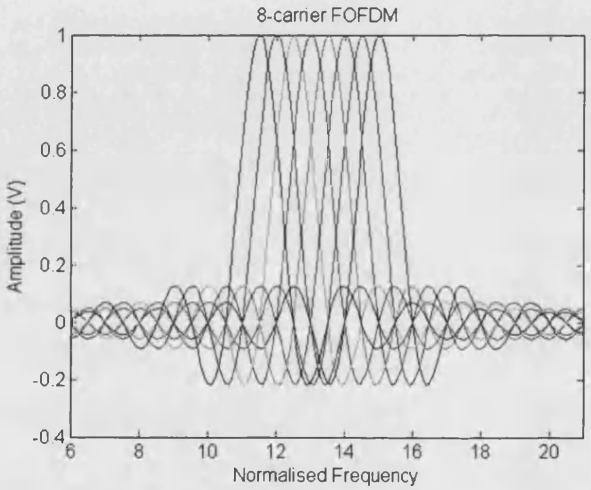

(a)

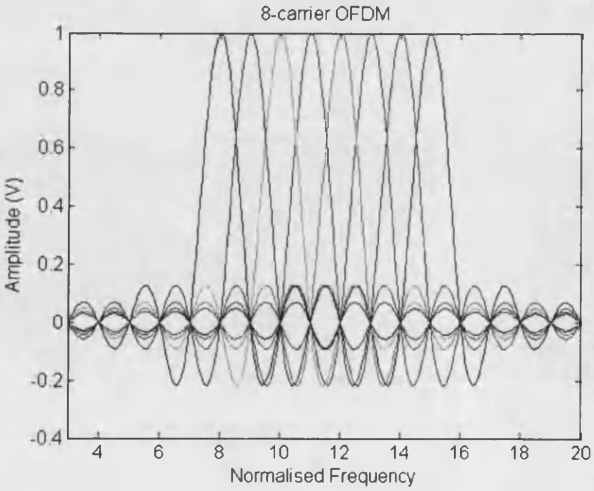

(b)

Figure 5.1 – Spectrum of; (a) 8-carrier FOFDM and (b) 8-carrier OFDM

Comparing eq. (5.3) and eq. (5.4) with eq. (5.1) and eq. (5.2), it can be observed that the FOFDM subcarriers will be separated by half the frequency separation of the OFDM subcarriers. This gives an important advantage of FOFDM, which is that an FOFDM system will achieve the same data rate as an OFDM one, whilst using half of the bandwidth. The bandwidth efficiency of FOFDM compared to OFDM is clarified by considering Figure 5.1, where an 8 carrier FOFDM (Figure 5.1a) is compared to an 8 carrier OFDM (Figure 5.1b).

The block diagram of an oscillator based FOFDM baseband transceiver, ignoring the cyclic prefix, is given in Figure 5.2.

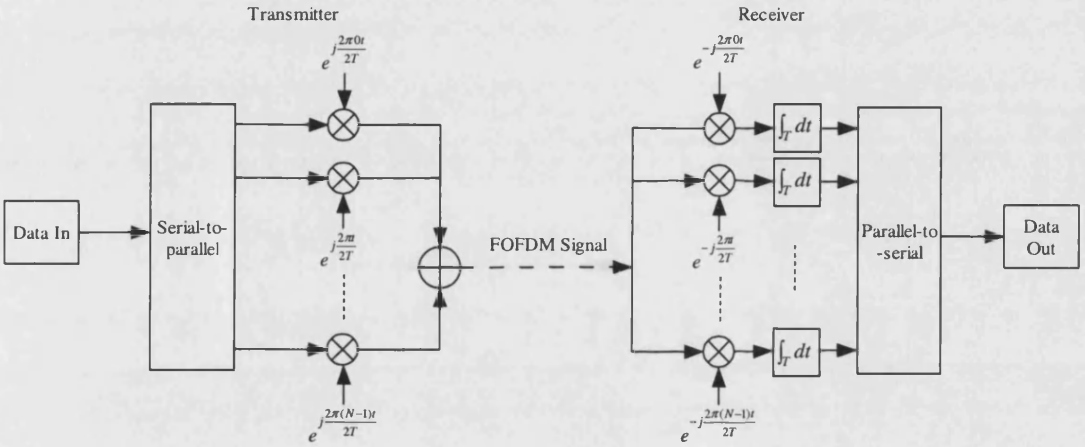

Figure 5.2 – Baseband block diagram of oscillator based FOFDM transceiver

5.2.3 Discrete-time implementation

In section 2.7.2, OFDM signal generation using Fourier transforms, was described. The scaled samples, $x_k = \sqrt{T/N}\,x(kT/N)$, where k is 0 to N-1, of an OFDM symbol can be generated by taking the IFFT of the complex modulation symbols, as shown in the following equation. Thus:

$$x_{k,OFDM} = \frac{1}{N}\sum_{n=0}^{N-1} X_n e^{j\frac{2\pi kn}{N}}, k = 0,\ldots,N-1 \qquad \text{eq. (5.5)}$$

where, X_n are the modulated data symbols, N is the number of the FFT samples, n=0,...N-1, are the position of the subcarriers (input IFFT samples) and k=0,...,N-1 are the output FFT samples.

A discrete-time FOFDM symbol (ignoring the cyclic prefix), is given by:

$$\begin{aligned} x_{k,FOFDM} &= \sqrt{\frac{T}{N}} s_{tx,FOFDM}\left(\frac{kT}{N}\right) \\ &= \sqrt{\frac{T}{N}}\sqrt{\frac{1}{T}}\sum_{n=0}^{N-1} X_n e^{j\frac{\pi n}{T}\frac{kT}{N}} \\ &= \sqrt{\frac{1}{N}}\sum_{n=0}^{N-1} X_n e^{j\frac{\pi nk}{N}} \end{aligned} \qquad \text{eq. (5.6)}$$

However, the latter equation cannot be realised using the Fourier transform. J. Oh and M. Lim have observed in [145] that a partial symmetry in the IFFT samples exists when real symbols, (X_0, X_1,...,X_{N-1}) input into an IFFT. Such symbols can be obtained when data has only real values as in one dimensional modulation schemes such as BPSK or M-ASK. This is illustrated in Figure 5.3.

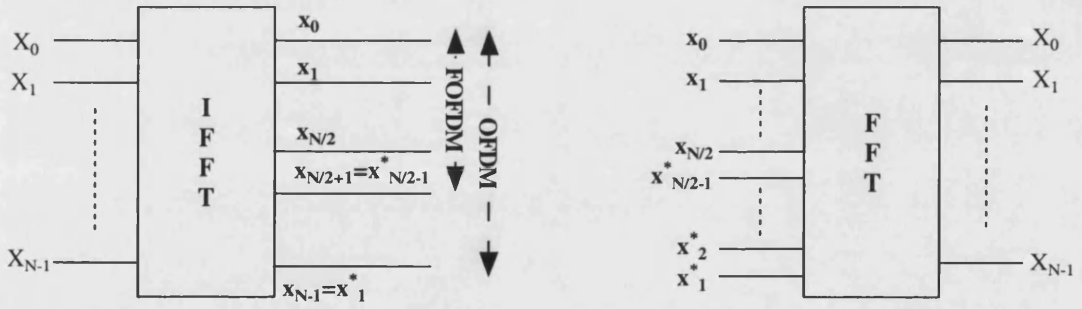

Figure 5.3 – Partial symmetry of FFT samples

It was observed that the output IFFT samples are such that $x_{N-k} = x_k^*$ for k=1,...,N-1. By transmitting the first $(N/2)+1$ IFFT samples and discarding the rest, i.e. $x_{k',FOFDM} = x_{k,OFDM}$, $k = 0,...,(N/2+1)$, eq. (5.6) is realised effectively generating an FOFDM signal using the IFFT. At the receiver the discarded samples are recovered by taking the complex conjugates of the received values, as shown in Figure 5.3, which makes the recovery of the transmitted bit stream achievable. The authors have used this symmetry to develop a bandwidth efficient MC-CDMA system. The disadvantage of

this scheme is visibly apparent as the partial symmetry of the IFFT samples will not hold when complex values are processed by the IFFT. More details will be available in the next section where the limitations of FOFDM will be described.

The FOFDM scheme can also be implemented using an IFFT without needing to reconstruct the discarded samples at the transmitter as described in [146]-[148]. In this method zeros are inserted at the receiver forward FFT instead of complex conjugates of the received samples. In this way the complexity of the system is reduced. A block diagram of an FFT-based FOFDM system is shown in the following figure.

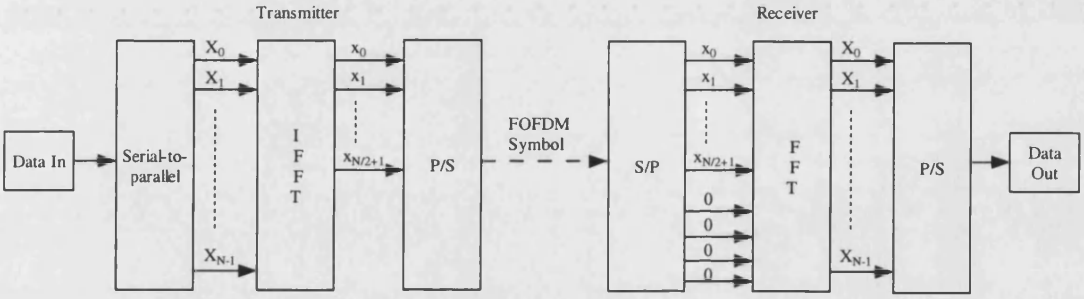

Figure 5.4 – Block diagram of an FFT-based FOFDM system

5.2.4 Limitations of FOFDM

5.2.4.1 Continuous-time FOFDM

In the above discussion it was stated that the major disadvantage of FOFDM is that it can only handle one-dimensional modulation schemes like BPSK or M-ASK. To justify this statement we consider two signals $s_1(t) = e^{j2\pi f_1 t}$ and $s_2(t) = e^{j2\pi f_2 t}$, both having duration T. Their correlation coefficient ρ, is:

$$\rho = \frac{1}{T}\int_0^T s_1(t)s_2^*(t)dt = \frac{1}{T}\int_0^T e^{j2\pi f_1 t}e^{-j2\pi f_2 t}dt = \mathrm{sinc}[\pi(f_1 - f_2)T]e^{j\pi(f_1 - f_2)T} \qquad \text{eq. (5.7)}$$

where $\mathrm{sinc}(x) = \dfrac{\sin x}{x}$

This defines two components, real ρ_r and imaginary ρ_i given in [137]:

$$\rho_r \equiv Re(\rho) = \text{sinc}[\pi(f_1 - f_2)T] \cdot \cos(\pi(f_1 - f_2)T) = \frac{\sin(2\pi(f_1 - f_2)T)}{2\pi(f_1 - f_2)T}$$

and eq. (5.8)

$$\rho_i \equiv Im(\rho) = \text{sinc}[\pi(f_1 - f_2)T] \cdot \sin(\pi(f_1 - f_2)T) = \frac{\sin^2(\pi(f_1 - f_2)T)}{\pi(f_1 - f_2)T}$$

Figure 5.5, shows plots of the real and imaginary part of the correlation coefficient versus normalised frequency difference $(f_1 - f_2)T$.

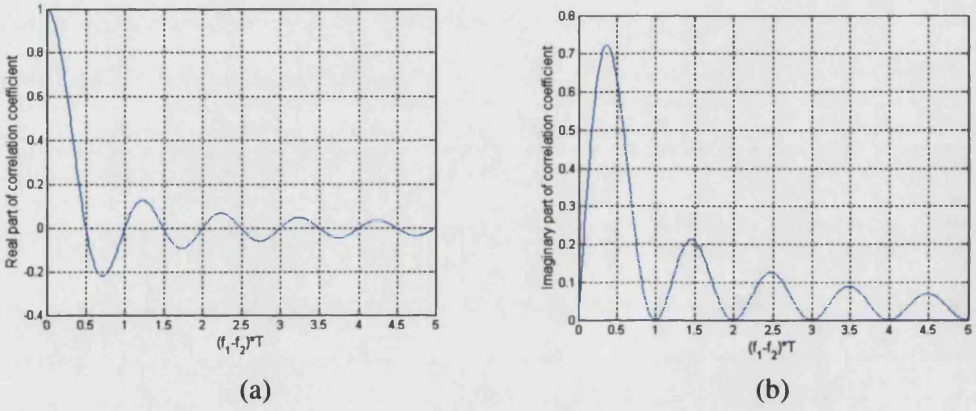

(a) (b)

Figure 5.5 – Plots of ρ versus normalised frequency difference: (a) real and (b) imaginary part

The above figure shows that ρ_r is zero when the frequency difference between the two signals is an integer multiple of $1/2T$. Therefore, the real parts of the two signals are orthogonal when their minimum frequency separation is $1/2T$. On the other hand, ρ_i is zero when the frequency difference between the two signals is an integer multiple of $1/T$. In the OFDM case, where the separation of the subcarriers is $1/T$, orthogonality is preserved in both the real and imaginary part of the OFDM signal. On the other hand, in the FOFDM case, where the subcarrier separation is $1/2T$, orthogonality between the subcarriers is preserved only for the real part of the FOFDM signal, thereby limiting the use of FOFDM to real signals.

Hence, assuming a lossless channel, we consider the reception of an FOFDM signal, which is characterised by eq. (5.3) and eq. (5.4). For a received signal

$r(t) = S'_{tx,FOFDM}(t)$, the recovered symbol $y_{n,k}$, assuming that the cyclic prefix is discarded, is:

$$\begin{aligned} y_{n,k} &= \int_{kT}^{(k+1)T} r(t) \cdot g^*_{n,FOFDM}(t-kT)dt \\ &= \int_{kT}^{(k+1)T} S'_{tx,FOFDM}(t) \cdot g^*_{n,FOFDM}(t-kT)dt \\ &= \int_{kT}^{(k+1)T} \sum_{k'=-\infty}^{\infty} \sum_{n'=0}^{N-1} a_{n',k'} g_{n',FOFDM}(t-k'T) \cdot g^*_{n,FOFDM}(t-kT)dt \qquad \text{eq. (5.9)} \\ &= \frac{1}{T} \int_0^T \sum_{n'=0}^{N-1} a_{n',k} e^{j\frac{\pi n' t}{T}} \cdot e^{-j\frac{\pi n t}{T}} dt \\ &= \frac{1}{T} \int_0^T \sum_{n'=0}^{N-1} a_{n',k} e^{j\frac{\pi (n'-n) t}{T}} dt \end{aligned}$$

In a similar derivation to eq. (5.7), eq. (5.9) can be expressed as:

$$y_{n,k} = \sum_{n'=0}^{N-1} a_{n',k} \text{sinc}\left(\pi\left(\frac{n'-n}{2}\right)\right) e^{j\frac{\pi(n'-n)}{2}} = \sum_{n'=0}^{N-1} a_{n',k} \cdot j^{(n'-n)} \cdot \text{sinc}\left(\pi\left(\frac{n'-n}{2}\right)\right) \qquad \text{eq. (5.10)}$$

The above equation indicates that the received symbol is multiplied by the complex term $j^{(n'-n)} \cdot \text{sinc}\left(\pi\left(\frac{n'-n}{2}\right)\right)$. If the received data symbol $a_{n',k}$ is real, for example when using BPSK or M-ASK modulation, only the imaginary part of the recovered symbol will be distorted, as illustrated in Figure 5.6, where constellation diagrams of transmitted and received FOFDM/BPSK signals are shown. The symbol can be recovered with no ICI by taking its real part, since the information is carried only in the real part of the symbols. For this reason, no degradation in BER is expected.

On the other hand, when $a_{n',k}$ contains complex numbers, for example, when using QAM4 modulation, the multiplication with the complex term of eq. (5.10) will distort both the real and imaginary parts of that symbol. This is depicted in Figure 5.7, showing transmitted and received FOFDM/QAM4 constellation diagrams. Thus demodulation of complex signals in FOFDM modulation is not possible.

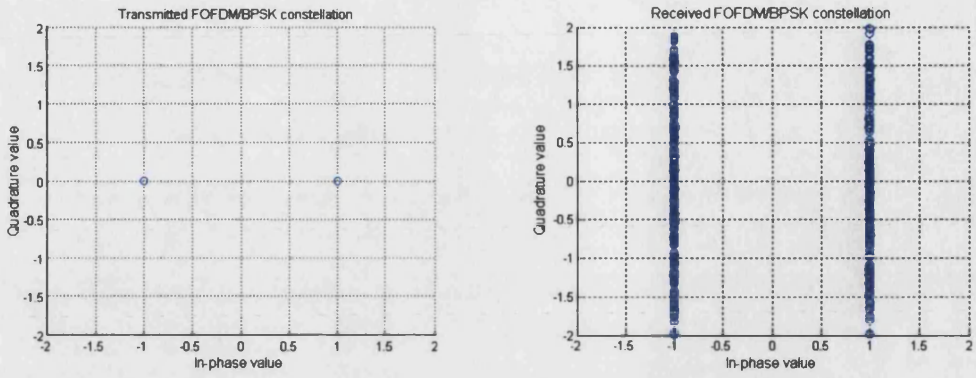

(a) (b)

Figure 5.6 – (a) Transmitted and (b) received FOFDM/BPSK constellation diagrams

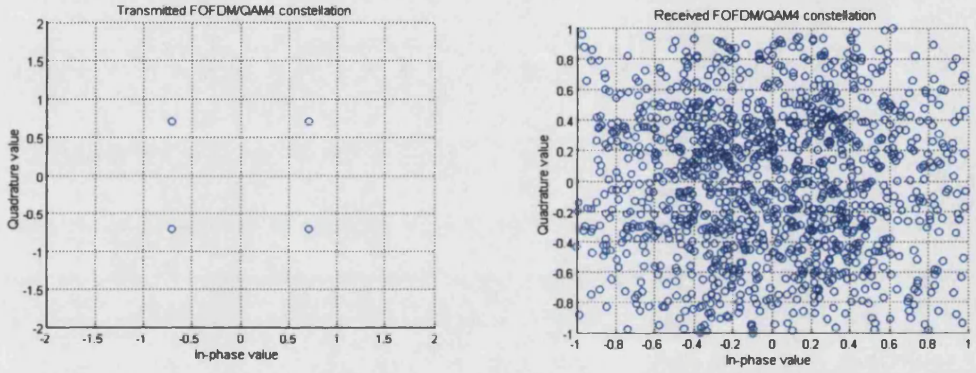

(a) (b)

Figure 5.7 – (a) Transmitted and (b) received FOFDM/QAM4 constellation diagrams

5.2.4.2 Discrete-time FOFDM

In section 5.2.3 a description of the methods of implementing a Fast-OFDM system using the FFT was carried out. An FOFDM symbol is realised by discarding samples at the FOFDM transmitter which are replaced by complex conjugates of the received samples at the receiver in order to recover the signal [145]. Again, this is only achievable when real modulation is used, since only then there is a partial symmetry between the IFFT samples. Alternatively, when complex modulation is used, since no partial symmetry exists, the recovered symbols resemble the constellation diagram of Figure 5.7b. In [146]-[148], the discarded samples are not reconstructed at the receiver and are replaced by zeros. The block diagram of a "zero-insertion" FOFDM receiver

was shown in Figure 5.4. The latter method has different properties from the "complex-conjugate" FOFDM receiver scheme, discussed previously. The following figure shows received FOFDM/BPSK constellation diagrams for different number of FOFDM subcarriers.

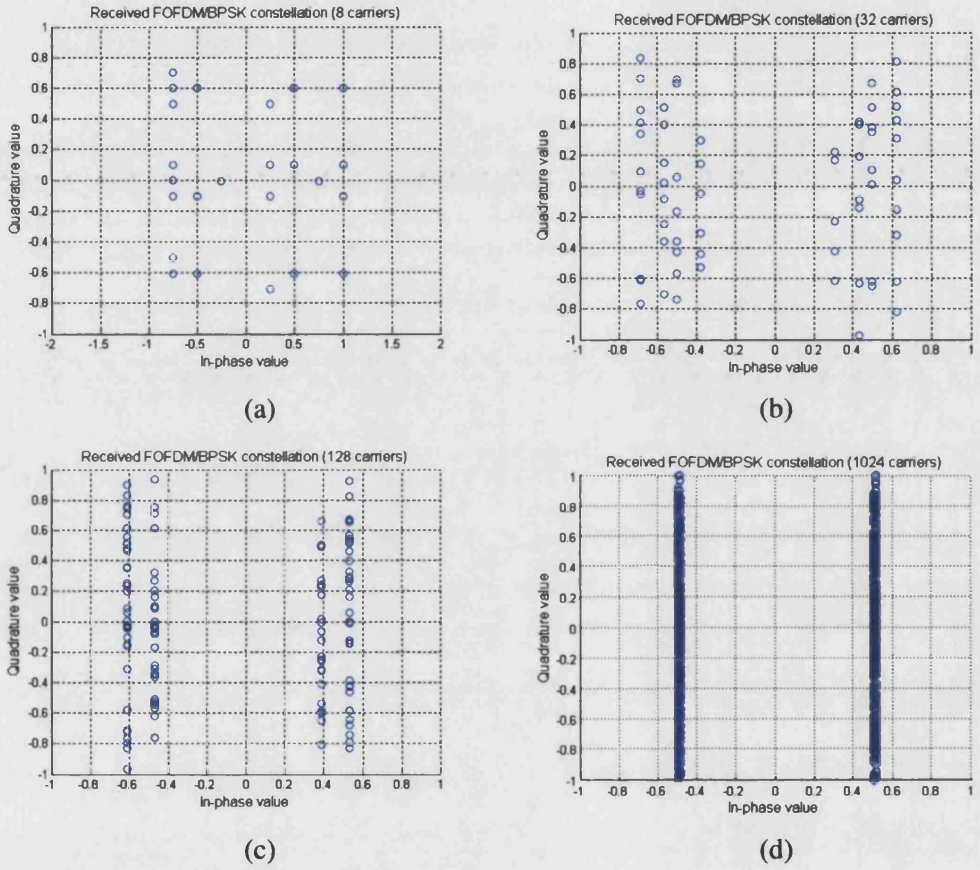

Figure 5.8 – Received FOFDM/BPSK constellation diagrams with (a) 8 carriers (b) 32 carrier (c) 128 carriers and (d) 1024 carriers

Figure 5.8 illustrates that as the number of FFT carriers increase, the "zero-insertion" FOFDM method approaches the oscillator-based FOFDM scheme. The above figure shows that when a low number of FFT carriers is used, the constellation points are spread (Figure 5.8a), however the signal is still recoverable. As the number of FFT carriers increases, there is more information to reconstruct the signal (the number of FFT samples transmitted approximates to $N/2$). The received BPSK constellation points concentrate on +/- 0.5 on the x-axis (instead of +/- 1) as Figure 5.8d illustrates, since only half of the samples are used to recover the signal. It is worthwhile

noting that if the receiver used the "complex conjugate" method, the received constellation will be that of an ideal BPSK.

5.3 Research performed in this area

Fast-OFDM was first proposed by M.R.D. Rodrigues and Izzat Darwazeh in [143]. An alternative FOFDM scheme, implemented for FFT and aimed at MC-CDMA schemes was proposed by Oh and Lim in [145]. FOFDM is a new concept and not much research has been performed in this field. However, some research has been carried out in finding ways to increase the bandwidth efficiency of OFDM systems. Bandwidth efficiency is termed as the useful data rate of the OFDM signal over its total bandwidth.

Some studies focus on the reduction of the guard interval while still retaining the properties of OFDM in a frequency selective channel. In [149] an equaliser is proposed to shorten the overall delay of an effective channel. In [118] the cyclic prefix is avoided and channel estimation is performed using the properties of singular value decomposition. However, the disadvantage of such schemes is the increased complexity in the receiver architecture.

Other studies propose ICI and ISI tolerant OFDM systems. An example is in [150] where an OFDM symbol is transmitted having both ICI and ISI. Sufficient statistics and a one-tap decision feedback equaliser are then used to recover the signal at the receiver.

5.4 Modelling an OFDM/Fast-OFDM system in ADS

5.4.1 Design considerations for the OFDM/FOFDM system

In order to assess the capabilities and limitations of the FOFDM technique, an FOFDM system was designed and studied. The studies compare the performance metrics of the FOFDM system to those of a similar OFDM one. As a design guide for both systems we will follow the design procedures discussed in section 3.2.2 and based on [74]. In addition, a description of modelling OFDM systems in ADS can be found in [136].

OFDM system

First the OFDM system will be designed. The FOFDM system will be then designed to have similar specifications. The specifications of the OFDM system are; bit rate of 10 Mbps, delay spread tolerance of 100 ns and bandwidth of less than 15 MHz. A delay spread of 100 ns is found in many macrocellular and picocellular environments [74].

The guard interval of the OFDM system is set at 4 times the maximum delay spread tolerance, which is 400 ns. The OFDM symbol period will then be 6 times the duration of the guard interval, thus, the OFDM symbol period is 2.4 μs. The subcarrier spacing is then: $\frac{1}{(2.4-0.4)\mu s} = 500\,\text{kHz}$. For a bit rate of 10 Mbps, each OFDM symbol should carry:

$$\begin{aligned}\text{Number of bits/OFDM symbol} &= \text{Duration of symbol} * \text{Data rate} \\ &= 2.4\,\mu s * 10\,\text{Mbps} = 24\,\text{bits}\end{aligned} \qquad \text{eq. (5.11)}$$

Both systems will use BPSK modulation, assigning 1 bit per OFDM subcarrier, or 24 subcarriers for each OFDM symbol. A 32 sample FFT with 8 zero-padded bits for oversampling will be adequate for this model. The bandwidth of the OFDM symbol will be $24 * 500\,\text{kHz} = 12\,\text{MHz}$.

FOFDM system

The FOFDM system will achieve the same data rate, using half the bandwidth of OFDM, since the subcarrier spacing will be halved from 500 kHz to 250 kHz. The FOFDM symbol duration will be equal to the symbol duration of the OFDM one. Hence, its symbol period is 2.4 μs.

5.4.2 Implementation of OFDM/FOFDM design in ADS

The main issue in implementing the two systems in ADS is in translating the designs discussed in the previous section into the discrete sampled world of the ADS simulation platform. As both systems are defined to have the same data rate, the simulation time step must be set in such a way so that both systems have 2.4 μs symbol duration.

5.4.2.1 OFDM system

After the IFFT process there are 32 FFT samples per OFDM symbol. The OFDM symbol (discarding the cyclic prefix) has duration of 2 μs. Setting the simulation time step to $2\mu s/32 = 62.5ns$, should give the desired symbol duration. However, the time step is set after the addition of the guard interval, hence, we need first to determine the number of samples needed for the guard interval. Using the rule of proportionality, since 32 samples have duration 2 μs, 38.4 samples will have duration 2.4 μs. Thus, the number of guard interval samples required is 6.4. Setting the guard interval to 7 samples, the total number of samples of the OFDM symbol is 39. The simulation time step is set to $2.4\mu s/39$ or approximately 61.5 ns[7]. The block diagram of the OFDM system is shown in Figure 5.9.

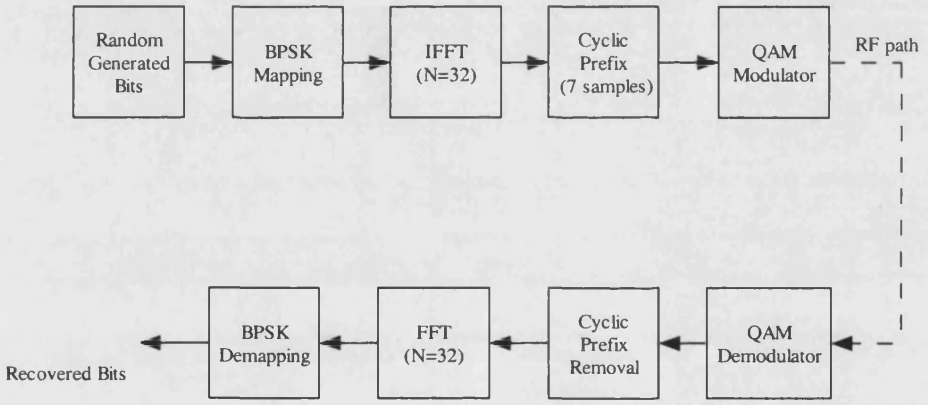

Figure 5.9 – Block diagram of 32 carrier OFDM/BPSK system

5.4.2.2 FOFDM system

The FOFDM symbol, discarding the unwanted samples, will be comprised of 17 samples. The FOFDM symbol is of equal duration to the OFDM symbol which is 2 μs. Hence, like in the OFDM case, by using the rule of proportionality, the number of samples required for the guard interval is 3.4. Four samples are cyclic extended in the FOFDM symbol which sets the simulation time step to $2.4\,\mu s/(17+4)$ or approximately 114.3 ns. The block diagram of the FOFDM system is shown in Figure 5.10. The ADS schematics of the FOFDM system can be found in Appendix B.

[7] Since the simulation modelling is IFFT/FFT based, the design values proposed here should also be appropriate for physical DSP implementation and for setting the clocking and conversion rates of such.

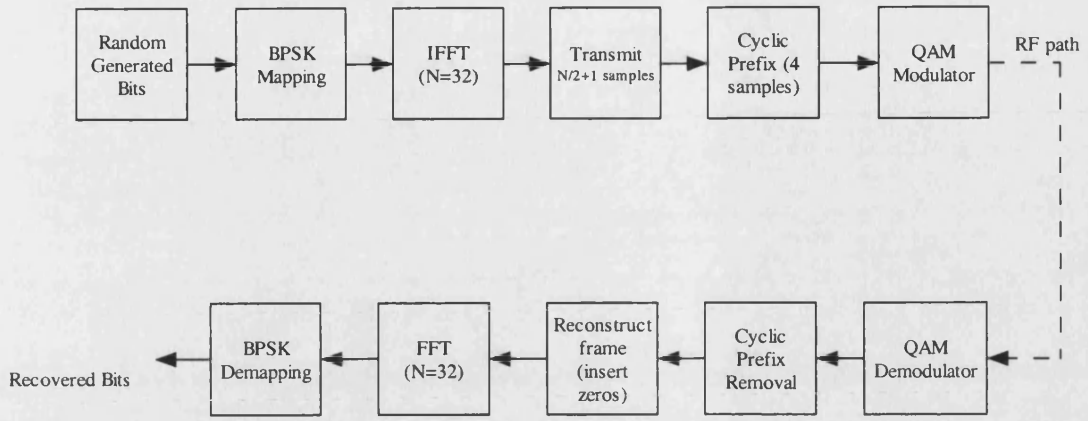

Figure 5.10 – Block diagram of 32 carrier FOFDM/BPSK system

5.5 Performance comparison of FOFDM/OFDM systems

In this section the performance of this model will be compared to an OFDM/BPSK one. Both systems will be tested under additive noise, receiver front-end non-idealities and fading environments. The performance comparison will start by comparing the systems under additive noise. The subsequent section will test the systems under conditions such as I/Q imbalance, frequency offset, synchronisation errors and phase noise. Finally, both systems will be tested under GSM fading environments.

5.5.1 Performance in additive Gaussian noise

Both systems are simulated in an environment where only Gaussian noise is present. Figure 5.11 shows bit error rates versus E_b/N_0. The results show, that there is no performance degradation of FOFDM in respect to OFDM. In addition, it can also be concluded that an FOFDM signal will have higher SNR ratios at the receiver than an OFDM signal, since FOFDM occupies less bandwidth.

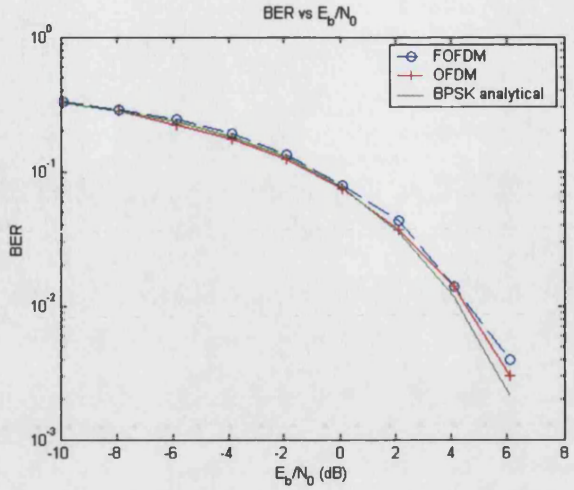

Figure 5.11 – OFDM/BPSK versus FOFDM/BPSK in noise

5.5.2 Performance under receiver front-end non-idealities

5.5.2.1 I/Q imbalance

I/Q imbalance arises in the front-end component when there is either power imbalance between the inphase and quadrature branch (amplitude imbalance) of the modulator or when the orthogonality between these branches is not maintained (phase imbalance) [78],[151]. A QAM demodulator with amplitude imbalance a in dB, where $\varepsilon = \frac{10^{a/20}-1}{10^{a/20}+1}$, and phase imbalance $\Delta\varphi$, is depicted in Figure 5.12.

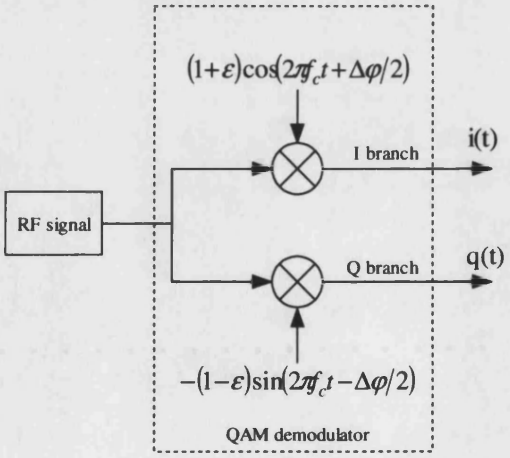

Figure 5.12 – Imbalanced I/Q demodulator

When an RF signal is received through an imbalanced IQ demodulator (ignoring noise), the downconverted signals $i(t)$ and $q(t)$ at the I and Q branches respectively become [152],[153]:

$$i(t)=(1+\varepsilon)[\mathrm{Re}\{x(t)\}\cos(\Delta\varphi/2)-\mathrm{Im}\{x(t)\}\sin(\Delta\varphi/2)] \quad \text{eq. (5.12)}$$

$$q(t)=-(1-\varepsilon)[\mathrm{Im}\{x(t)\}\cos(\Delta\varphi/2)-\mathrm{Re}\{x(t)\}\sin(\Delta\varphi/2)] \quad \text{eq. (5.13)}$$

The downconverted complex signal $y(t)=i(t)+jq(t)$ is then:

$$\begin{aligned} y(t)&=[\varepsilon\cos(\Delta\varphi/2)+j\sin(\Delta\varphi/2)]x(t)+[\cos(\Delta\varphi/2)-j\varepsilon\sin(\Delta\varphi/2)]x^*(t) \\ &=ax(t)+bx^*(t) \end{aligned} \quad \text{eq. (5.14)}$$

where, $a=\varepsilon\cos(\Delta\varphi/2)+j\sin(\Delta\varphi/2)$ and $b=\cos(\Delta\varphi/2)-j\varepsilon\sin(\Delta\varphi/2)$.

Therefore, an I/Q imbalance in the demodulator will result in a distorted signal which will be an addition of a scaled version of the desired signal $x(t)$ with a scaled version of its complex conjugate image signal $x^*(t)$ [154].

If $x(t)$ is an OFDM symbol, i.e. $x(t)=\frac{1}{N}\sum_{k=0}^{N-1}d_k e^{j\frac{2\pi k}{T}t}$, where N is the number of OFDM subcarriers, k=0,…,N-1 and d_k is the modulated signal, eq. (5.14) becomes:

$$\begin{aligned} y(t)=ax(t)+bx^*(t)&=a\frac{1}{N}\sum_{k=0}^{N-1}d_k e^{j\frac{2\pi k}{T}t}+b\frac{1}{N}\sum_{k=0}^{N-1}d^*_{-k}e^{j\frac{2\pi k}{T}t} \\ &=\frac{1}{N}\sum_{k=0}^{N-1}\left(ad_k+bd^*_{-k}\right)e^{j\frac{2\pi k}{T}t} \end{aligned} \quad \text{eq. (5.15)}$$

After the FFT, and from eq. (5.14), the demodulated signal, $\hat{d}_k$ becomes:

$$\hat{d}_k=\left(\varepsilon d_k+d^*_{-k}\right)\cos(\Delta\varphi/2)+j\left(d_k-\varepsilon d^*_{-k}\right)\sin(\Delta\varphi/2) \quad \text{eq. (5.16)}$$

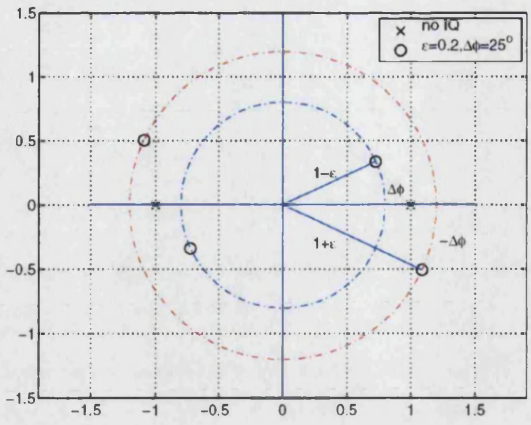

Figure 5.13 – Effect of IQ imbalance on BPSK/OFDM constellation [152]

Therefore, an RF OFDM signal downconverted by an imbalanced demodulator will result in interference between its subcarriers. The constellation diagram of a received OFDM/BPSK signal is illustrated in Figure 5.13. The constellation points will shift by $1-\varepsilon$ and $1+\varepsilon$ due to amplitude imbalance and by $\pm\Delta\varphi$ due to phase imbalance.

I/Q demodulator amplitude imbalance effect on OFDM/FOFDM

In a pure I/Q amplitude imbalance condition, i.e. $\Delta\varphi = 0$, the demodulated OFDM/FOFDM signal of eq. (5.16) becomes:

$$\hat{d}_k = \varepsilon d_k + d_{-k}^* \qquad \text{eq. (5.17)}$$

The above equation states that in the case of a pure amplitude imbalance the real part (or imaginary) of the subcarrier *k* interferes with the real part (or imaginary) of its image subcarrier *–k*. In case of the demodulated signal being an OFDM/BPSK signal the effect of pure amplitude imbalance will be the spreading of the demodulated BPSK constellation points in the x-axis as Figure 5.14a shows. In the case where the demodulated signal is an FOFDM/BPSK signal, amplitude imbalance will result in distorting only the real part of this signal. Therefore, since the imaginary components of this signal are not distorted in the FFT demodulation process, the demodulated BPSK constellation points will be also spread in the x-axis as Figure 5.14b shows. Therefore, no performance degradation is expected for the FOFDM/BPSK system when compared

with the OFDM/BPSK one. This is verified by studies of error rates for different amplitude imbalance values and illustrated in Figure 5.15.

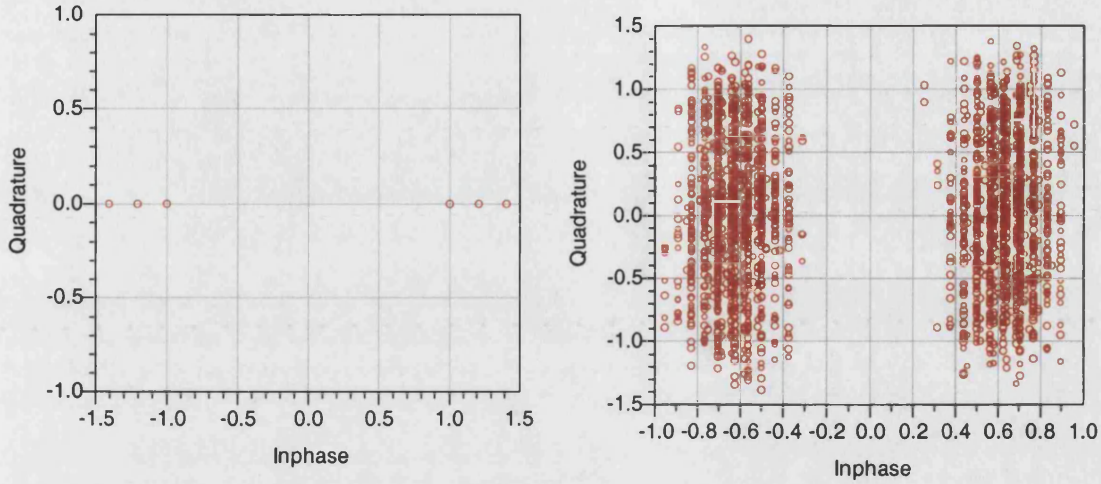

(a) (b)

Figure 5.14 – Received (a) OFDM/BPSK and (b) FOFDM/BPSK constellation diagrams under pure amplitude imbalance ($\varepsilon = 3dB$)

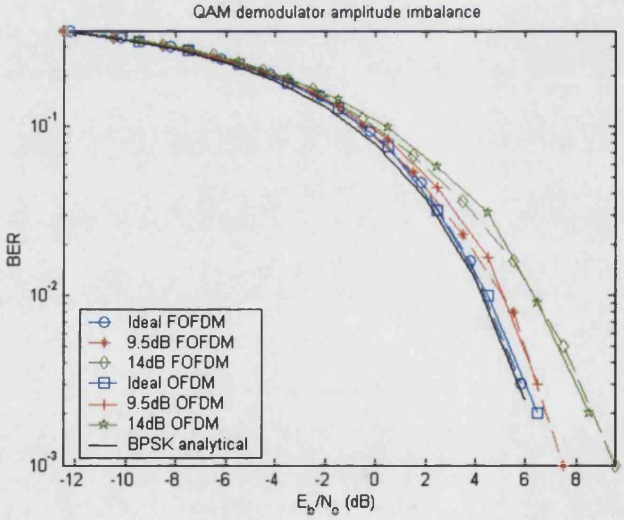

Figure 5.15 – Performance under amplitude imbalance

I/Q demodulator phase imbalance effects on OFDM/FOFDM

In a pure phase imbalance condition, eq. (5.16) becomes:

$$\hat{d}_k = d^*_{-k}\cos(\Delta\varphi/2) + jd_k\sin(\Delta\varphi/2) \qquad \text{eq. (5.18)}$$

Therefore, the imaginary part (or real) of the subchannel k will interfere with the real part (or imaginary) of the image subchannel $-k$. This will result in rotating and spreading of the received OFDM/BPSK constellation points, as Figure 5.16a depicts. On the other hand, in an FOFDM/BPSK system, after the demodulation through the FFT process, the resulted signal will be complex. Therefore, it will be multiplied with the complex term of eq. (5.10), resulting in distortion of the constellation points of the demodulated BPSK/FOFDM signal. Figure 5.16b, shows the received FOFDM/BPSK constellation in a phase imbalance condition.

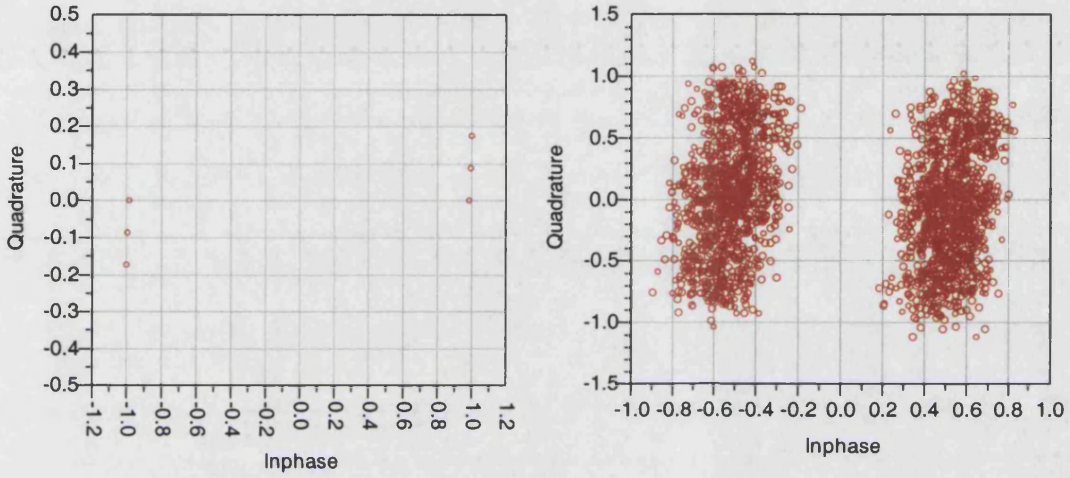

(a) (b)

Figure 5.16 – Received (a) OFDM/BPSK and (b) FOFDM/BPSK constellation diagrams under pure phase imbalance ($\Delta\varphi = 10^o$)

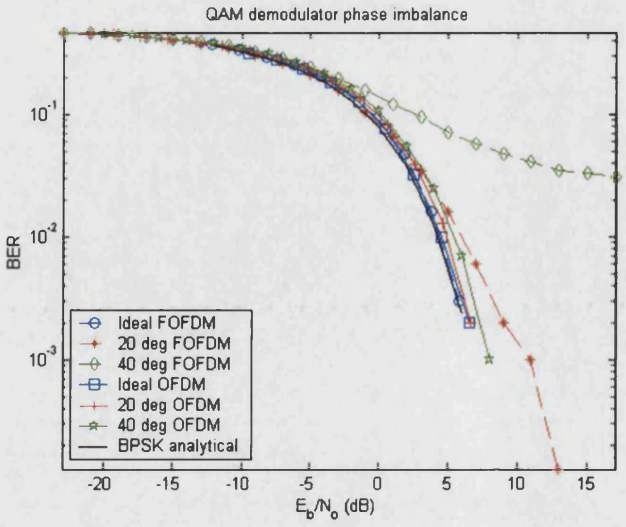

Figure 5.17 – Performance under phase imbalance

In Figure 5.17, the error rates obtained of an OFDM and FOFDM system under different phase imbalance values are displayed. An important fact can be observed in this figure. For small phase imbalance values the performance of the FOFDM system is comparable to the OFDM one. As the phase imbalance increases the FOFDM system deteriorates faster than OFDM. It is noteworthy here to state that the imbalance levels chosen for the simulation are much higher than those encountered in practical systems. Hence, a 40 degree phase imbalance is rarely encountered in practice. Thus, it can be safely stated that under practical phase imbalance conditions there is minor degradation in the performance of FOFDM compared to OFDM.

5.5.2.2 Frequency offset

In section 3.4.1, the effects of frequency offset on OFDM were discussed. The frequency offset is subdivided into two categories: coarse (an integer number of subcarrier spacing) and fine frequency offset (magnitude does not exceed one-half the carrier spacing). The effects of a frequency offset on OFDM are twofold: first, after the FFT process, the demodulated OFDM symbol contains amplitude variations and a common phase error; secondly, it introduces interference due to the loss of orthogonality between the subcarriers.

The loss of orthogonality between the subcarriers will be more severe when an FOFDM symbol is demodulated since the FOFDM subcarriers must be almost perfectly aligned for demodulation to occur. The demodulation of the symbol $y_{n,k}$, when an FOFDM signal $r(t)=S'_{tx,FOFDM}(t)$, is received though an I/Q demodulator with frequency offset $\lambda=\lambda_o+r\omega_s$, where, λ_o represents a "fine" frequency error, ω_s the FOFDM carrier spacing and $r\omega_s$ a coarse frequency error (r integer number of carrier spacing), will have the following equation after the FFT process:

$$y_{n,k} = \int_{kT}^{(k+1)T} r(t)\cdot g^*_{n,FOFDM}(t-kT)dt$$
$$= \int_{kT}^{(k+1)T} S'_{tx,FOFDM}(t)\cdot g^*_{n,FOFDM}(t-kT)dt$$

$$= \int_{kT}^{(k+1)T} \sum_{k'=-\infty}^{\infty} \sum_{n'=0}^{N-1} a_{n',k'} g_{n',FOFDM}(t-k'T) \cdot g^{*}_{n,FOFDM}(t-kT)dt$$

$$= \int_{0}^{T} \sum_{n'=0}^{N-1} a_{n',k} e^{j\frac{\pi n' t}{T}} \cdot e^{-j\left(\frac{\pi n t}{T}+\lambda t\right)} dt$$

$$= \int_{0}^{T} \sum_{n'=0}^{N-1} a_{n',k} e^{j\frac{\pi n' t}{T}} \cdot e^{-j\left(\frac{\pi(n+r)}{T}+\lambda_o\right)t} dt$$

$$= \int_{0}^{T} \sum_{n'=0}^{N-1} a_{n',k} e^{j\left(\frac{\pi(n'-n-r)}{T}-\lambda_o\right)t} dt$$

$$= \sum_{n'=0}^{N-1} a_{n',k} e^{j\left(\frac{\pi(n'-n-r)}{T}-\lambda_o\right)*T/2} \cdot \mathrm{sinc}\left(\left(\frac{\pi(n'-n-r)}{T}-\lambda_o\right)\cdot\frac{T}{2}\right)$$

$$= \left(\sum_{n'=0}^{N-1} a_{n',k} e^{j\left(\frac{\pi(n'-n-r)}{2}\right)} \cdot \mathrm{sinc}\left(\frac{\pi(n'-n-r)}{2}-\lambda_o\cdot\frac{T}{2}\right)\right)\cdot e^{-j\lambda_o * T/2}$$

Hence, the demodulated symbol $y_{n,k}$ is:

$$y_{n,k} = \left(\sum_{n'=0}^{N-1} a_{n',k}(j)^{(n'-n-r)} \cdot \mathrm{sinc}\left(\frac{\pi(n'-n-r)}{2}-\lambda_o\cdot\frac{T}{2}\right)\right)\cdot e^{-j\lambda_o\cdot T/2} \qquad \text{eq. (5.19)}$$

$y_{n,k}$ can be expressed by its real and imaginary parts, where:

$$\mathrm{Re}\{y_{n,k}\} = \left(\sum_{n'=0}^{N-1} a_{n',k} \cdot \cos\left(\frac{\pi(n'-n-r)}{2}\right)\cdot \mathrm{sinc}\left(\frac{\pi(n'-n-r)}{2}-\lambda_o\cdot\frac{T}{2}\right)\right)\cdot e^{-j\lambda_o\cdot T/2} \qquad \text{eq. (5.20)}$$

$$\mathrm{Im}\{y_{n,k}\} = \left(\sum_{n'=0}^{N-1} a_{n',k} \cdot \sin\left(\frac{\pi(n'-n-r)}{2}\right)\cdot \mathrm{sinc}\left(\frac{\pi(n'-n-r)}{2}-\lambda_o\cdot\frac{T}{2}\right)\right)\cdot e^{-j\lambda_o\cdot T/2} \qquad \text{eq. (5.21)}$$

The above equations indicate three distortion factors. Firstly, there are amplitude variations due to the sinc term. Secondly, the addition of the frequency offset ratio r will result in ISI, since $\mathrm{Re}\{y_{n,k}\} \neq a_{n',k}$ when $n' = n$. Finally, the last distortion factor is a common phase rotation of the subcarriers dependent from λ_o (due to $e^{-j\lambda_o * T/2}$). This phase rotation will add another complex term in the above equations which will be multiplied with $(j)^{(n'-n-r)}$. This complex multiplication will distort the

signal which is identical with the case of Figure 5.7, when a complex symbol is demodulated by an FOFDM receiver.

Figure 5.18, shows received constellation diagrams of OFDM/BPSK and FOFDM/BPSK under 1% normalised frequency offset ratio (normalised to symbol duration).

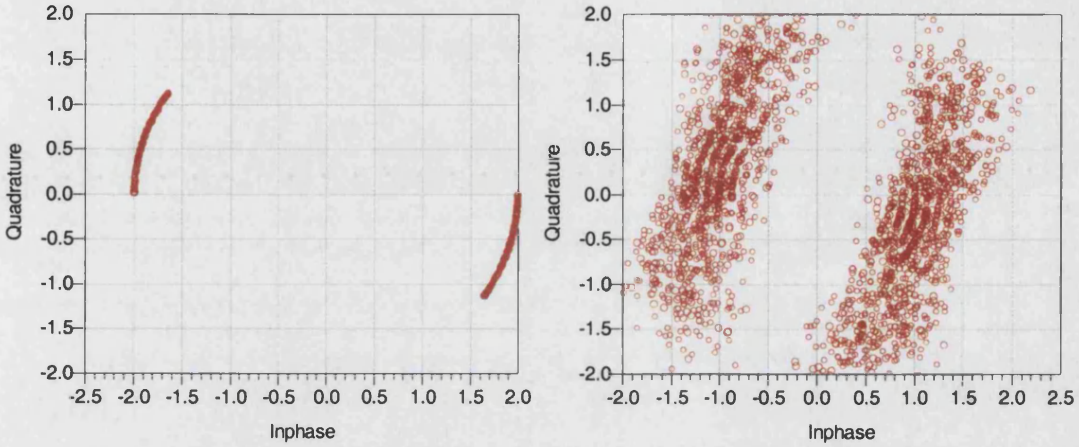

(a) (b)

Figure 5.18 – Received (a) OFDM/BPSK and (b) FOFDM/BPSK constellation diagrams under normalised frequency offset of 1%

Figure 5.19, shows the error rates obtained for various normalised frequency offset ratios. The frequency offset is normalised to the subcarrier separation of each system.

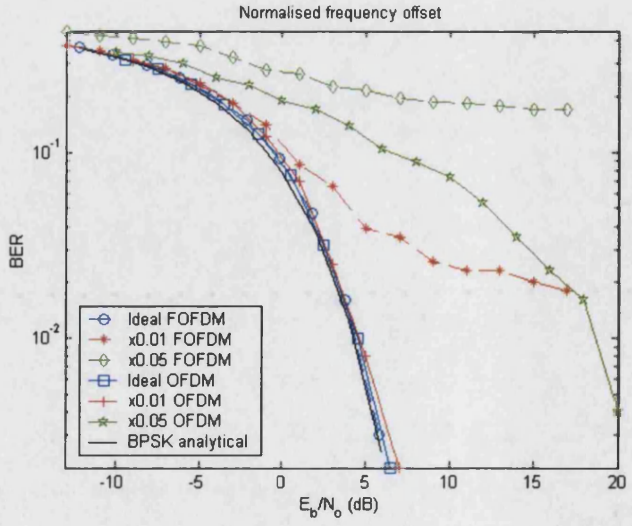

Figure 5.19 – Performance under frequency offset

The above figure shows the vulnerability of FOFDM to frequency offsets. The phase rotation of the subcarriers, results in complex multiplication to the demodulation process that deteriorates much faster the performance of the FOFDM/BPSK system compared to OFDM.

5.5.2.3 Synchronisation errors

Section 3.4.2 covered the effect of symbol synchronisation errors on OFDM. OFDM is highly robust to such offsets due to the use of guard intervals. In an OFDM system the timing errors do not produce necessarily any interference terms as it was the case with carrier and sampling clock errors, but a phase offset. The relation between the phase offset φ_n, and the timing offset τ when the synchronisation error is within the guard interval duration, is $\varphi_n = 2\pi f_n \tau$, where, $f_n = n/T$ is the frequency of the nth complex subcarrier [84].

The demodulated symbol $y_{n,k}$ of a received FOFDM signal $r(t) = S'_{tx,FOFDM}(t)$, received by an FOFDM receiver having synchronisation errors will have the following equation:

$$
\begin{aligned}
y_{n,k} &= \int_{kT}^{(k+1)T} S'_{tx,FOFDM}(t) \cdot g^{*}_{n,FOFDM}(t-kT)dt \\
&= \int_{kT}^{(k+1)T} \sum_{k'=-\infty}^{\infty} \sum_{n'=0}^{N-1} a_{n',k'} g_{n',FOFDM}(t-\tau_{n'}-k'T) \cdot g^{*}_{n,FOFDM}(t-kT)dt \\
&= \int_{0}^{T} \sum_{n'=0}^{N-1} a_{n',k} e^{j\frac{\pi n' t}{T}} \cdot e^{-j\left(\frac{\pi n' \tau_{n'}}{T}\right)} \cdot e^{-j\left(\frac{\pi n t}{T}\right)} dt \\
&= \left(\int_{0}^{T} \sum_{n'=0}^{N-1} a_{n',k} e^{j\frac{\pi n' t}{T}} \cdot e^{-j\frac{\pi n t}{T}} dt \right) \cdot e^{-j\left(\frac{\pi n' \tau_{n'}}{T}\right)} \\
&= \left(\int_{0}^{T} \sum_{n'=0}^{N-1} a_{n',k} e^{j\frac{\pi (n'-n) t}{T}} dt \right) \cdot e^{-j\left(\frac{\pi n' \tau_{n'}}{T}\right)} \cdot \\
&= \left(\sum_{n'=0}^{N-1} a_{n',k} \operatorname{sinc}\left(\frac{\pi (n'-n)}{2}\right) e^{j\frac{\pi (n'-n)}{2}} \right) \cdot e^{-j\frac{\pi n' \tau_{n'}}{T}}
\end{aligned}
\qquad \text{eq. (5.22)}
$$

where, $\tau_{n'}$ is the random delay of each OFDM sample.

Hence, the demodulated symbol after the FFT process becomes:

$$y_{n,k} = \left(\sum_{n'=0}^{N-1} a_{n',k} \cdot j^{(n'-n)} \cdot \mathrm{sinc}\left(\frac{\pi(n'-n)}{2} \right) \right) \cdot e^{-j\frac{\pi n' \tau_{n'}}{T}} \qquad \text{eq. (5.23)}$$

According to the above equation, in the demodulation the subcarriers will have phase errors related to the normalised timing offset ratio $\tau_{n'}/T$. The difference to frequency offset conditions is that the phase error is not constant on every subcarrier but depends on the index of the subcarrier itself. For example, the first FOFDM subcarrier will have a phase rotation of $e^{-j\frac{\pi\tau_{n'}}{T}}$, whereas the last one will have a higher phase rotation of $e^{-j\frac{32\pi\tau_{n'}}{T}}$. In the discrete OFDM system case, timing offsets, within the guard interval duration, result in phase rotation of the received constellation due to the FFT cyclic shift property, as discussed in section 3.4.2. On the other hand in the discrete FOFDM system case the effect of timing offset does not result in phase rotation of the received constellation.

In the "complex-conjugate" FOFDM case, the effect of timing offset results in ICI, because the complex conjugate reconstructed FOFDM signal, before the FFT process, contains complex conjugate versions of the guard interval since the FOFDM signal will arrive delayed at the reconstruction process. In the "zero-insertion" FOFDM case, no phase rotation is observed since the signal before the FFT process is not repetitive (contains zeros) and the cyclic shift property does not hold (as discussed in section 2.7.3).

In the simulation DSP platform ADS, the synchronisation error is modelled as a variable delay that has Gaussian distribution according to [155]. The range of the delay is set to vary between 0-100 ns and 0-250 ns, i.e. has maximum normalised timing offset ratio (normalised to the symbol duration) of approximately 4% and 10% respectively. The ADS schematics of timing offset modelling can be found in Appendix B.2.2.

Figure 5.20 shows the constellation diagrams of received "complex-conjugate" and "zero-insertion" FOFDM/BPSK signals under 4% normalised timing offset ratio.

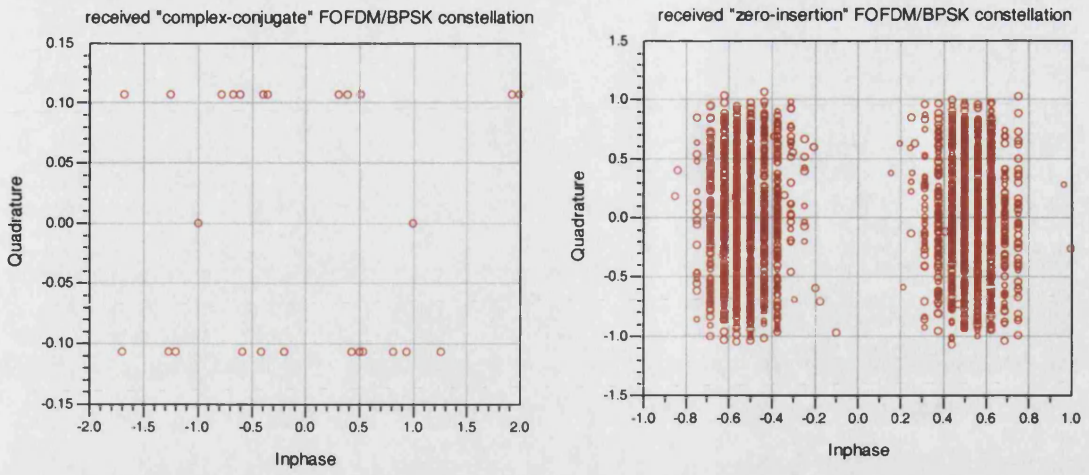

(a) (b)

Figure 5.20 – Received (a) "complex-conjugate" and (b) "zero-insertion" FOFDM/BPSK constellation diagrams under 4% normalised timing offset ratio

The above figure shows that in the "complex-conjugate" case ICI exists in the received constellation diagram (Figure 5.20a), whereas in the "zero-insertion" case the constellation diagram appears blurred (Figure 5.20b).

Figure 5.21, shows the error rates obtained under 4% and 10% normalised timing offset ratios.

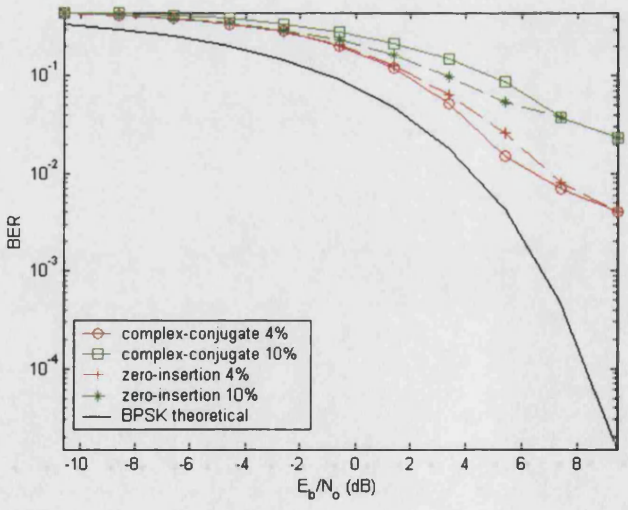

Figure 5.21 – FOFDM performance under synchronisation errors

The results show, that both FOFDM methods have similar performance under timing offset conditions. The OFDM system will have better performance than

FOFDM, since timing offsets create phase rotations to the received OFDM constellation that can be easily recovered through the use of a channel estimator. It is also important to note that in FOFDM systems channel estimation cannot be achieved using conventional OFDM estimators since in FOFDM timing offsets lead to ICI.

5.5.2.4 Phase noise

An explanation of phase noise and its distortion effects on OFDM systems is carried out in 3.4.1. Phase noise can be interpreted as a parasitic phase modulation in the oscillator signal [156]. Usually, it is modelled as a phase modulation of the carrier. A system having phase noise will have similar distortion effects as those of a system having frequency offset conditions. More specifically, the demodulated symbol will contain a common phase error (to all subcarriers), as well as, interference between the OFDM subcarriers. In the FOFDM case, such distortion will misalign the demodulating FOFDM subcarriers (similar to the frequency offset case) which will distort the demodulating signal.

- Implementation of phase noise in ADS

Phase noise can be expressed by its bandwidth (Δf_{φ}) or duration (T_{φ}) [156]. So, supposing that a signal has symbol interval T of 10 ns, then a phase noise of duration, T_{φ}, 1 ms, will have a phase noise bandwidth of $\Delta f_{\varphi} = 1/T_{\varphi} = 1\,\text{kHz}$. Therefore phase noise will appear 1 kHz above and below the centre carrier frequency.

Phase noise is simulated in ADS by frequency modulating a carrier with random white noise using an FM modulator. In this case:

$$\Delta f_{\varphi} = k_f * V_B \qquad \text{eq. (5.24)}$$

where, k_f is a normalisation variable and V_B the amplitude of the noise. Frequency modulating V_B:

$$V_{tx} = A\cos\left(2\pi f_c t + 2\pi \int_0^t V_B(a)da\right) \qquad \text{eq. (5.25)}$$

As the amplitude of V_B increases the phase variation increases which consequently increases the magnitude of phase noise.

Both systems are tested under normalised phase noise ratios. We chose to normalise the phase noise to the duration of the symbol interval, i.e. $T_\varphi / T_{OFDM,FOFDM}$. Figure 5.22, show the error rates obtained for various normalised phase noise ratios.

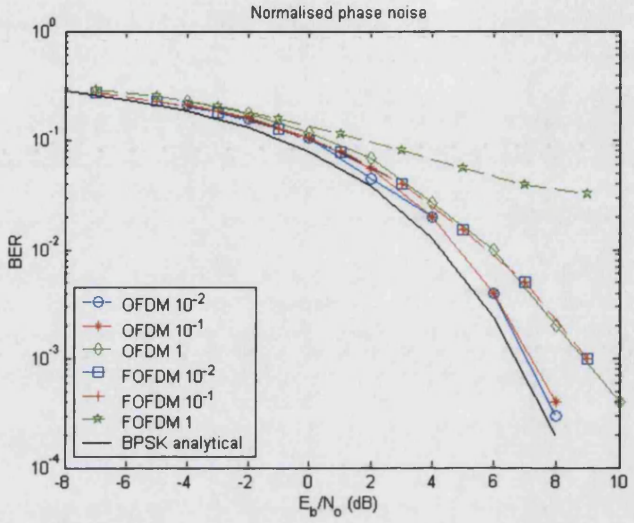

Figure 5.22 – Performance under phase noise

The above figure indicates that the FOFDM/BPSK system matches the performance of OFDM/BPSK when the latter system has a normalised phase noise ratio of 1 and the FOFDM system has a ratio 10^{-1}. The OFDM system with normalised ratios of 10^{-1} and 10^{-2} has a 2 dB advantage compared to the FOFDM system (at 10^{-3} error rate) with the same phase noise ratios. Again it is observed that under heavy distortions the FOFDM system deteriorates faster than the OFDM one. More specifically, when the phase noise bandwidth equals the subcarrier spacing of both systems (phase noise ratio of 1), the FOFDM system has 5 dB degradation in performance with respect to the OFDM system (at $0.5 \cdot 10^{-1}$ error rate) compared to 2 dB degradation under lower phase noise ratios.

5.5.3 Performance in multipath fading environments

Both systems are tested under GSM typical multipath environments [8]. A brief outline of such environments can be found in section 4.5.1. The reason for choosing

such environments to evaluate the performance of FOFDM systems is mainly because such environments are a good representation of multipath environments found in wireless channels. Models based on delay lines for these environments are found in ADS. In section 4.5.2, we stated that there are 6-tap and 12-tap delay models that characterise rural area, hilly terrain and urban area environments. In addition, in section 4.6.3, only the 6-tap delay model was used to test the GSM/EDGE/OFDM system in fading environments, since the results taken with this delay model were similar with those of the 12-tap model. For, the same reason the results displayed in this section will use only the 6-tap delay model.

5.5.3.1 Simulation system set-up

The specifications for both systems must change in order to accommodate the GSM typical multipath environment block of ADS. This block is designed for use in GSM and EDGE systems. Hence, it is designed for systems having bandwidth of 200 kHz and delay spread tolerances of GSM/EDGE systems. Consequently, the method of designing an OFDM system to coexist with the GSM/EDGE systems, (section 4.3) was followed. It is important to note that synchronisation and equalisation was not taken into consideration for the systems designed in this section since we want to evaluate the performance of both systems in their simplest form.

Both systems were designed to have 64 carriers with delay spread tolerances of 160 μs. The bandwidth of the OFDM system is 200 kHz, whereas the bandwidth of the FOFDM system is 100 kHz. The effective data rate of both systems is approximately 200 kbps.

5.5.3.2 Typical Urban environment

Figure 5.23, shows errors rates obtained with the 6-tap model using different delay profiles, *"mode 1"* and *"mode 2"*. The difference between those profiles can be found in [8]. It is important also to note that Doppler spread is not taken into consideration. Thus, both systems are assumed to be static. This is necessary because the introduction of Doppler spread would severely distort both systems, since neither implements any synchronisation or channel estimation techniques.

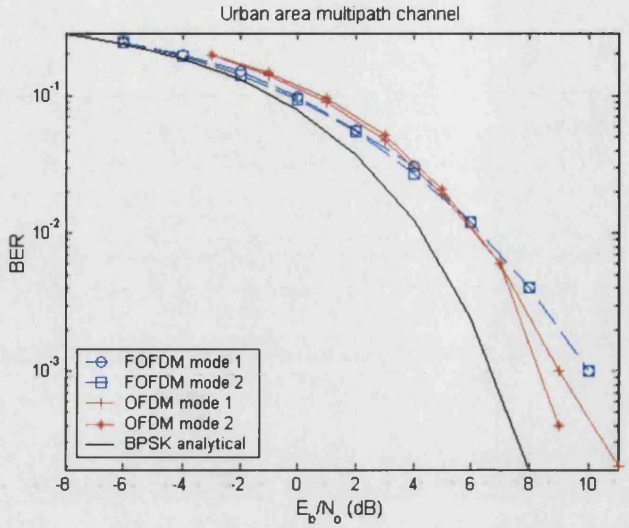

Figure 5.23 – Performance in GSM typical urban environments

The above figure indicates a comparable performance between the two systems up to 10^{-2} error rate. At 10^{-3} error rate there is a minor 1dB degradation of performance of FOFDM compared to OFDM.

5.5.3.3 Hilly Terrain environment

The Hilly Terrain environments are also characterised by 6-tap and 12-tap models with two modes respectively, as indicated by GSM recommendations [8]. Figure 5.24, illustrates the error rates obtained of both systems when present in the environment stated.

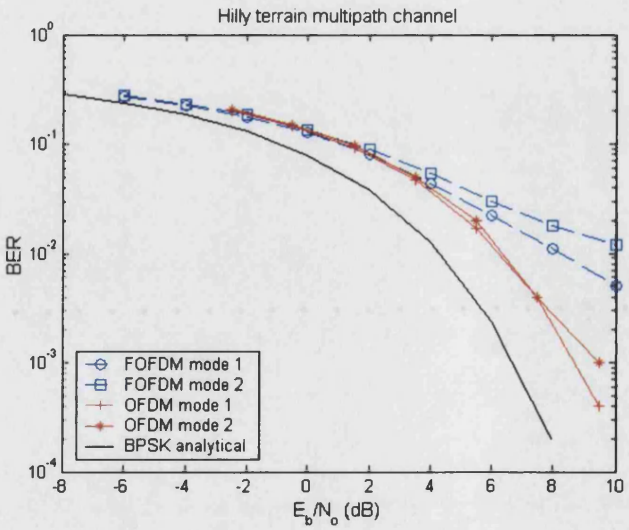

Figure 5.24 – Performance in GSM hilly terrain environments

This figure indicates that at 10^{-2} error rate there is an approximately 3-4 dB degradation of the FOFDM performance compared to the performance of OFDM. This is due to the high relative delays of Hilly Terrain environments which distort easier the imaginary components of FOFDM (timing offset condition).

5.5.3.4 Rural Area environment

Rural Area environments are characterised by small rms delay spreads (maximum relative delay is 0.6 μs). There are two GSM typical Rural Area environment modes. The first type has a 6-tap delay channel whereas the second one has a 4-tap delay channel. Figure 5.25 shows the results obtained.

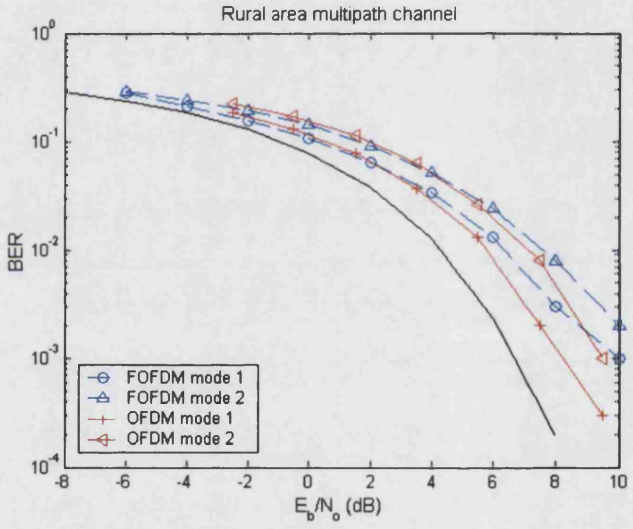

Figure 5.25 – Performance in GSM rural area environments

In the above figure we can observe a minor performance advantage of the OFDM system compared to OFDM at 10^{-3} error rate.

5.5.3.5 Analysis of the results obtained

The results show that for high relative delays, as in Hilly Terrain environments, the FOFDM system is more susceptible to errors due to its sensitivity to timing offsets. On the other hand, when small-to-medium relative delays are considered, as in Urban Area environments, the performance of both systems is identical. Hence, once more it is observed that under low distortions the performance of the FOFDM system is

comparable to that of OFDM. In contrast, as the magnitude of the distortion increases the FOFDM system performance deteriorates more rapidly.

5.6 Summary

This chapter carried out an investigation onto a new modulation technique which was developed by M.R.D. Rodrigues and Izzat Darwazeh at University College London [143]. Fast-OFDM, or FOFDM for short, achieves the same data rate of OFDM by using only half the bandwidth. The disadvantage of such scheme is that it can only handle real signals (BPSK, M-ASK). Hence, such system is bandwidth efficient to OFDM only when considering real signals. In this chapter several simulation based studies were carried out to compare the performance of FOFDM/BPSK to the performance of OFDM/BPSK under a number of different environments. Both systems were tested under environments of front-end non-idealities, like I/Q imbalance, frequency offset, timing offset and phase noise as well as in fading channels using a number of GSM typical multipath environments. The results showed that overall OFDM performs better than FOFDM under such environments. However, it was observed that at small distortions the performance of FOFDM is comparable to OFDM. On the other hand, under heavy distortion conditions the performance of FOFDM deteriorates faster than OFDM. In our studies neither synchronisation nor channel estimation techniques were discussed for FOFDM since we wanted to test a basic FOFDM system. However, in [146] a channel estimation technique for FOFDM was proposed. More specifically, a pre-distortion method is proposed; Pre-distorting the transmitted data will make the signal orthogonal (and thus have aligned subcarriers) at the receiver. The disadvantage of this technique is that the channel response must be known a-priori. This might make the technique very useful in a "wired" transmission environment where the channel characteristics are known.

It is important to note the FOFDM advantage of using half the spectral allocation of OFDM. In the future such scheme might be necessary to save bandwidth, for example, since real signals are used for pilot information, FOFDM could be used for pilot symbol transmission.

Chapter 6

Issues of filtering for OFDM systems in noise and interference limited environments

6.1 Introduction

In general a filter is defined as a device that converts an input signal into an output signal while retaining some desirable features and suppressing the rest. The filter is designed to separate, pass or suppress a group of signals from a mixture of desired and undesired signals [157],[158].

Filters are classified into analogue (when the filter processes analogue or time continuous signals) or digital (used for discrete-time signals). Additionally, filters are classified according to their frequency selective behaviour (lowpass, bandpass, highpass, bandstop and allpass) [157]-[160].

Interpolation filters are important elements in communication systems, since they provide the means to convert the signal from discrete (sampled) to continuous. There are five main analogue filters types characterised by their frequency response. These are the Butterworth, Chebyshev, Inverse Chebyshev, Gaussian, Elliptic and Bessel filter types [157]-[159].

In [130], a study has been performed into pre-detection filtering for the mobile communication systems GSM and EDGE. The author looked at how bandpass filtering affects the performance of such systems in noise and ACI conditions. It was concluded that a pre-distortion filter that gives the best performance in noise is not necessary the best filter when ACI is present. This study motivated us to consider

how interpolation filters affect the performance of a system implementing OFDM modulation. The effects of filtering on OFDM will be tested using the same conditions that were imposed on the GSM and EDGE systems in [130].

The following section provides a brief explanation of the types of filters that will be evaluated in conjunction with OFDM modulation. In addition, a description of interpolation and decimation techniques in communication systems will be carried out. The next section discusses the design of the modelling and simulation environments used to evaluate the interpolation filters. The simulation results are presented in the subsequent section. The final section discusses the results obtained.

6.2 Filter characteristics

6.2.1 Introduction

In this section the properties of the analogue filters that are going to be used in our design, namely the Chebyshev, Butterworth and Bessel filters are described. The following sections concentrate on defining the use of such filters in radio communication systems.

6.2.2 Analogue filters characteristics

Butterworth filter

Butterworth filters, also known as maximally-flat passband response filters, are typically used when a compromise between good selectivity (a measure of magnitude response) and good group delay flatness (a measure of phase response) is desired. Figure 6.1, shows magnitude and corresponding group delay responses of Butterworth filters for various orders. It can be observed that as the order of such filters increases their response edges become sharper.

Filters are often compared using their bandwidth-duration (or BT) product, where B is the 3 dB bandwidth of the filter and T is the bit duration. In other words, the 3 dB bandwidth of the filter is normalised by the bit duration of the system. Note that the definition of BT varies, since in some publications T is selected to be the symbol period instead of the bit duration.

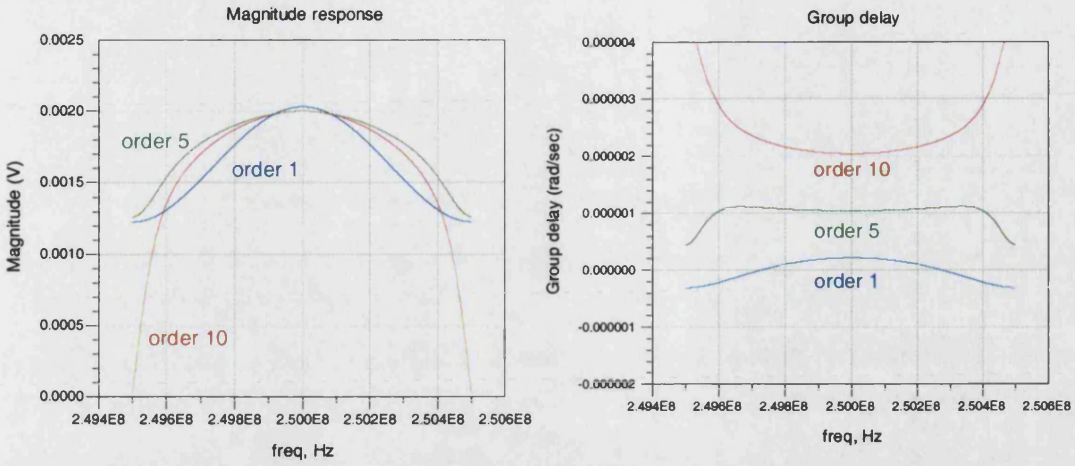

Figure 6.1 – Butterworth bandpass filter magnitude and group delay responses

Bessel filter

Bessel filters have better group delay flatness than Butterworth filters at the expense of less sharp cut-off response. Figure 6.2, shows magnitude and corresponding group delay responses of Bessel filters for various orders. Bessel filters offer the least amount of pulse distortion when compared to other filter categories.

Figure 6.2 – Bessel bandpass filter magnitude and group delay responses

Chebyshev filter

Chebyshev filters have the sharpest cut-off responses of all filters, with increased sharpness as the order of the filter increases. However, the phase linearity of

this filter worsens as its order increases. Figure 6.3, shows the corresponding magnitude and group delay responses of such filters.

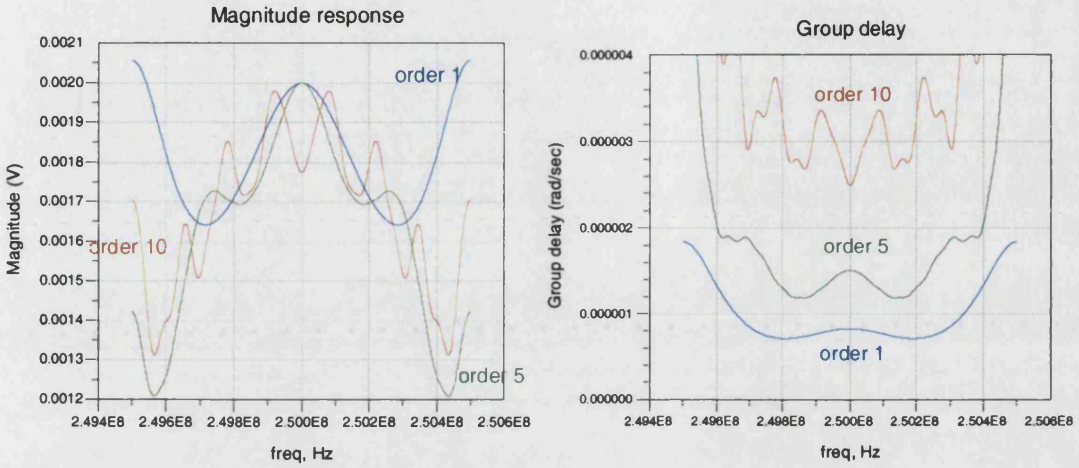

Figure 6.3 – Chebyshev bandpass filter magnitude and group delay responses

The following figure compares the magnitude and group delay responses of 10^{th} order Butterworth, Bessel and Chebyshev filters respectively.

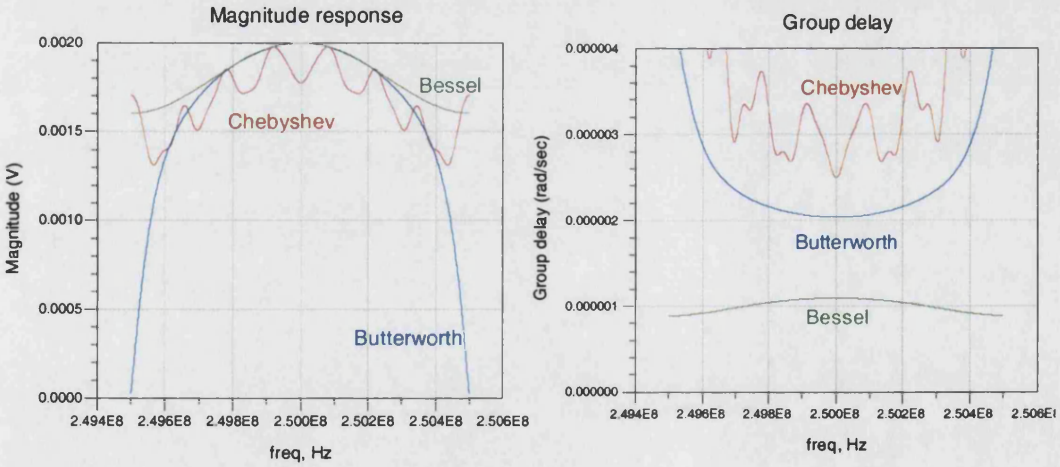

Figure 6.4 – Comparison of magnitude and group delay responses for various filters

6.2.3 Interpolation and decimation

In modern communication systems the transmitted signal is generated in the digital domain using DSP techniques. In order for the signal to be transmitted over the radio path, it is necessary to move the signal from the discrete-time environment into

the analogue environment. This can be performed using interpolation techniques. At the receiver the signal is moved back to the digital domain using decimation techniques. Figure 6.5, shows a block diagram of such operation.

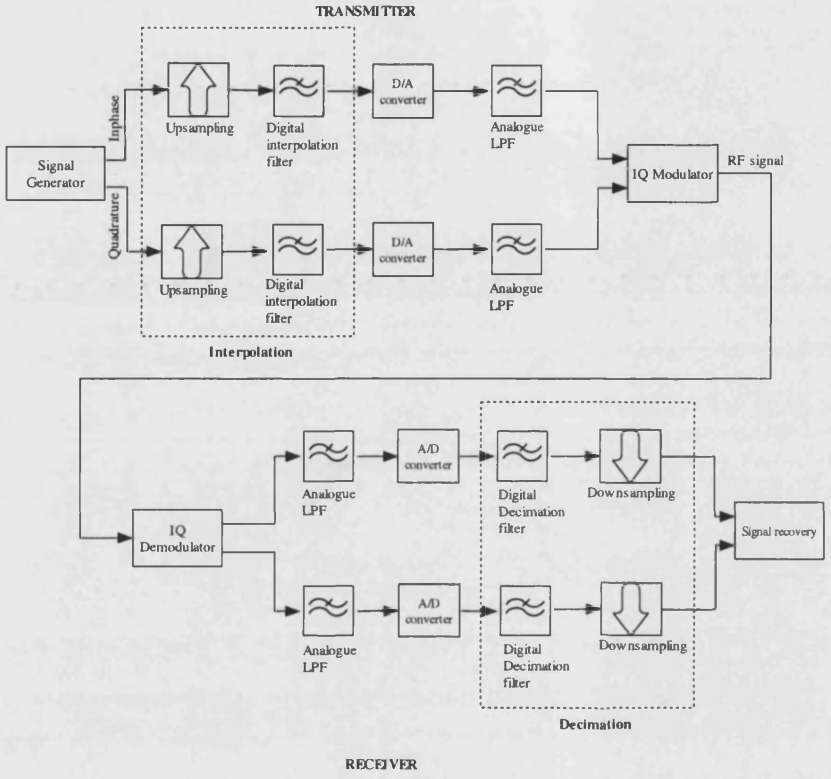

Figure 6.5 – Interpolation and decimation in communication systems

In our simulation model, before interpolation, the signal is upsampled using zero-insertion interpolation, i.e. zeros are inserted between successive samples. Filtering is required because by upsampling, images and/or aliases will be created in the frequency domain representation of the digital signal. An appropriate digital filter will remove such images as shown in Figure 6.6. The analogue filter is then used to reconstruct the signal in the continuous-time domain. At the receiver the lowpass filter is needed to remove any further interference, such as noise. A digital decimation filter is then used to reconstruct the baseband signal.

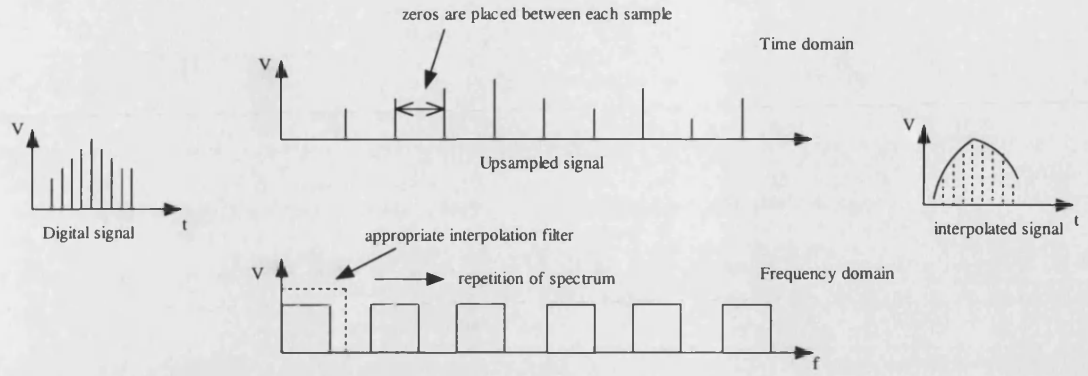

Figure 6.6 – Effect of interpolation on transmitted signal

6.3 Research involving interpolation filters

Interpolation and decimation filters are important parts in the design of communication systems. In general, filters in OFDM systems are used for many purposes. For example in [161] and [162] special filters are used at the receiver to combat the effects of intercarrier interference. More specifically, in [161] a non-linear adaptive restoration filter is placed at the receiver to suppress the ICI effects created by frequency offset or Doppler spread. In [162], an adaptive decision feedback filter is placed at the receiver to minimise orthogonality loss between the OFDM subcarriers due to both windowing and ICI.

Filters are also used at the transmitter in order to shape the spectrum of the OFDM signal and reduce the out-of-band radiation which could give ISI and ICI. Examples of such schemes can be observed in [163] and [164]. In [163], polyphase filtering techniques are used to increase the performance of the OFDM system in fading environments. The polyphase filter reduces the sidelobes of the OFDM spectrum, and concurrently increases the duration of the signal, thus making the system more robust to fading environments. This combined process exhibits known ACI and ISI which is easily removed at the receiver. In [164], an improved root raised-cosine filter is used to increase the spectral efficiency of OFDM systems which could make the system more immune to ACI. However, the author does not take into consideration modem impairments and channel distortions when evaluating this filter.

Another form of protection from ICI is achieved when filters are placed before the IFFT. Such filters are termed as pulse-shaping filters since they shape the waveform of the modulated signal. An example of this scheme can be observed in [98], where an

OFDM system which uses M-OQAM mapping with pulses of finite duration with minimised excess bandwidth is compared with an M-QAM OFDM scheme. Simulations in that paper showed that OFDM/OQAM when used in conjunction with equalisation has better resistance in frequency offsets compared to an OFDM/QAM system with no equalisation.

The effect of filtering on OFDM systems has been addressed in [165] and [166]. In [165] the effect of front-end filters on the performance of WLAN-OFDM systems is evaluated. The author evaluates the performance of OFDM implementing superheterodyne receiver architecture, using different IF channel select filters. The evaluation is performed using a model presented by the author that analyses the amount of ISI/ICI interference in relation to synchronisation. The simulation results showed that an OFDM system with Chebyshev channel select filter has good performance in non-dispersive channels, whereas Butterworth channel select filters are better to be used instead of Chebyshev filters in dispersive channels. In [166], the effect of interpolation filters on OFDM is investigated. The author states, that the interpolation filter smears the transmitted waveform leading to ISI. The BT duration of the filters determines the required cyclic prefix extension. The tighter the filter the longer the cyclic extension is required. The author also states that the ISI can be removed at the receiver by delaying the signal prior the FFT process. However, there is no analytical expression to determine the optimum delay amount which is determined by trial and error simulations. The author concludes that OFDM systems using Chebyshev interpolation filters require less guard band than other filters, which increase the spectral efficiency of the system.

Finally, in [130], the evaluation of pre-distortion filters on the overall performance of GSM and EDGE systems in the presence of AWGN and ACI is performed. The author investigates the effects of Gaussian, Butterworth and Chebyshev bandpass filters in the presence of AWGN only, ACI only and both AWGN and ACI. It was deduced that the filters with the best performance in noise are not the best filters when ACI is present. Therefore, the design of pre-detection filters should take into consideration the effects of ACI. The work reported in this chapter considers the interpolation filter effects in OFDM systems. To the author best knowledge, this is the first time such studies are carried out.

6.4 System modelling

This section describes the design of the OFDM system that will be tested under different interpolation filters and the simulation system set-up. The DSP simulation package ADS will be once more used to evaluate this system. The OFDM model is designed to be simple in order to observe the effects of the filters on the modulation itself with no other interference present[8]. The next section briefly describes the OFDM model whereas the final section gives an explanation of the simulation system set-up.

6.4.1 OFDM model

The design procedure followed is based on the OFDM design considerations given by Prasad [74], which were used to design the OFDM systems in the previous chapters and explained in Chapter 3. The OFDM model implements BPSK modulation, 32-point FFT, guard interval, and 10 Mbps data rate. The block diagram of the OFDM transmitter is shown in Figure 6.7.

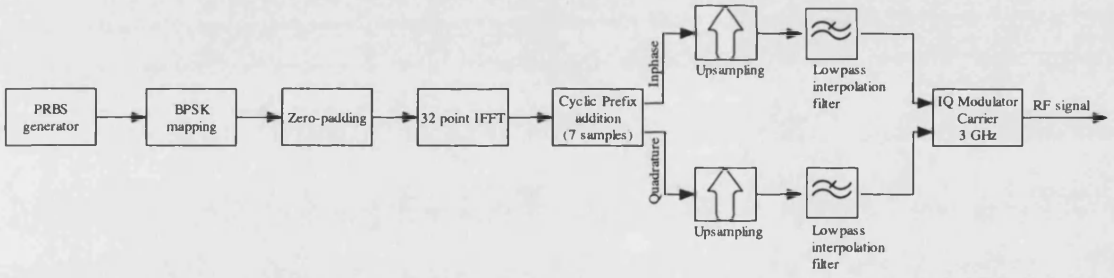

Figure 6.7 – OFDM transmitter using interpolation filters

It was decided to use a guard interval since it is employed in all practical wireless OFDM systems (WLAN, DVB). The OFDM signal is upsampled by a ratio of 100 using zero-insertion interpolation. Figure 6.8, shows the spectrum of an OFDM signal when such upsampling scheme is implemented. The figure illustrates that images are created whose separation depends on the sampling time of the simulator.

[8] A similar procedure was followed in [130], where the effect of bandpass filters on GSM and EDGE systems is evaluated. The GSM and EDGE systems were replaced by GMSK and 8PSK signals, respectively.

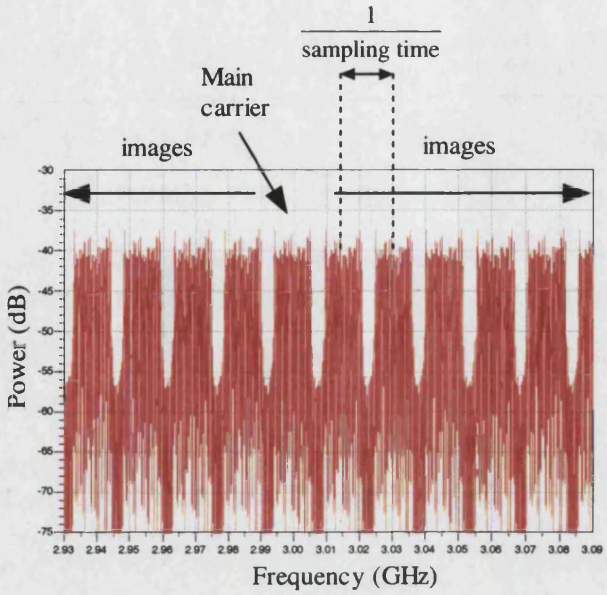

Figure 6.8 – Effect of zero-insertion interpolation on OFDM spectrum

Bessel, Butterworth and Chebyshev family of filters will be used for interpolation in this work. The simulation package ADS already contains models for such filters, hence it was not necessary to design them. Figure 6.9, shows the effect of each interpolation filter on the shape of the transmitted OFDM signal spectrum.

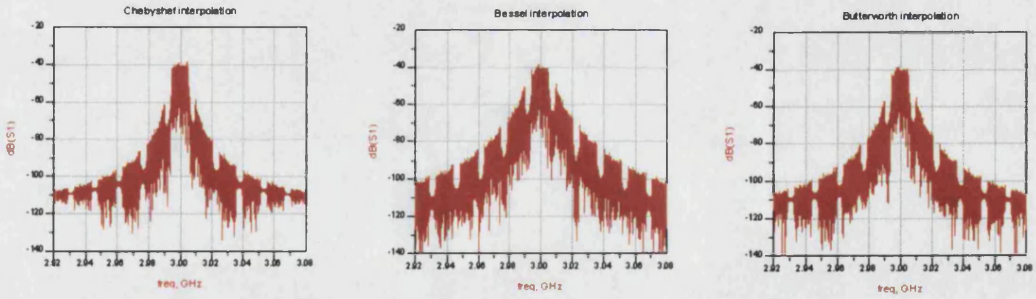

Figure 6.9 – Effect of interpolation on the shape of the OFDM spectrum

The above figure illustrates that the shape of the spectrum is dictated by the type of the interpolation filter. The shape of the spectrum is similar to the frequency response of each filter. Information about the OFDM modelling in ADS can be found in Appendix C.

The OFDM receiver can use two lowpass filters at the inphase and quadrature branches of the receiver (named channel select filters), to filter out noise and any

adjacent channel interference. It is not necessary to place such filters in the modelling of the OFDM receiver, since direct conversion IQ demodulation is used, as it is explained in the next section. The OFDM receiver block diagram, using lowpass filters, is shown in Figure 6.10.

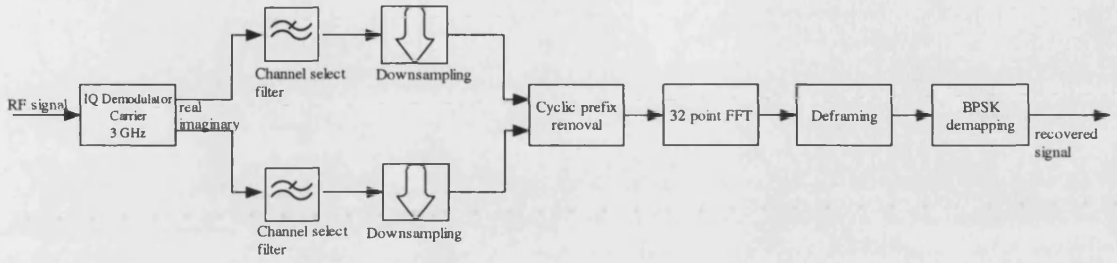

Figure 6.10 – OFDM receiver using decimation filters

6.4.2 Noise and interference models

This section describes the arrangement of the simulation models in order to simulate noise limited, ACI limited or noise and ACI environments.

Noise limited environments

The block diagram for simulating the designed OFDM system in noise limited environments is shown in Figure 6.11. The figure shows that the channel select filter can either be placed before or after the I/Q demodulator. Simulations showed that the error rates obtained are the same in any of the two locations that this filter can be placed. In ADS decimation can be performed without any filters by using a specific block taken from ADS libraries. In addition, decimation filtering is not into the scope of the work reported here.

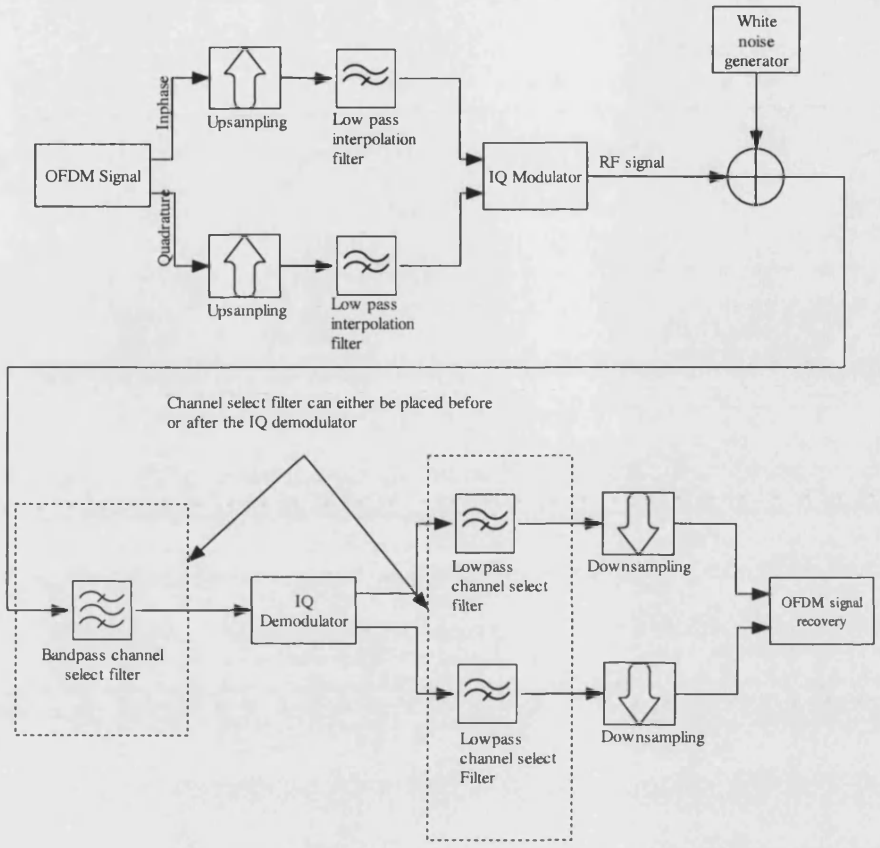

Figure 6.11 – Noise limited simulation environment

ACI limited environments

The block diagram for simulating under this environment is shown in Figure 6.12. Once more placing the channel select filter before or after the I/Q demodulator had no effect on the error rates obtained. A question arises on deciding the frequency of the interfering OFDM channel. It was decided to use the IEEE 802.11 specifications for adjacent channel interference, since the designed OFDM model has similar specifications to the WLAN system. In the WLAN standards [65], it is specified that the interfering channel can either be placed at 5 MHz or 10 MHz away from the required channel. Note that the interfering OFDM system will use the same interpolation filters of the main OFDM channel.

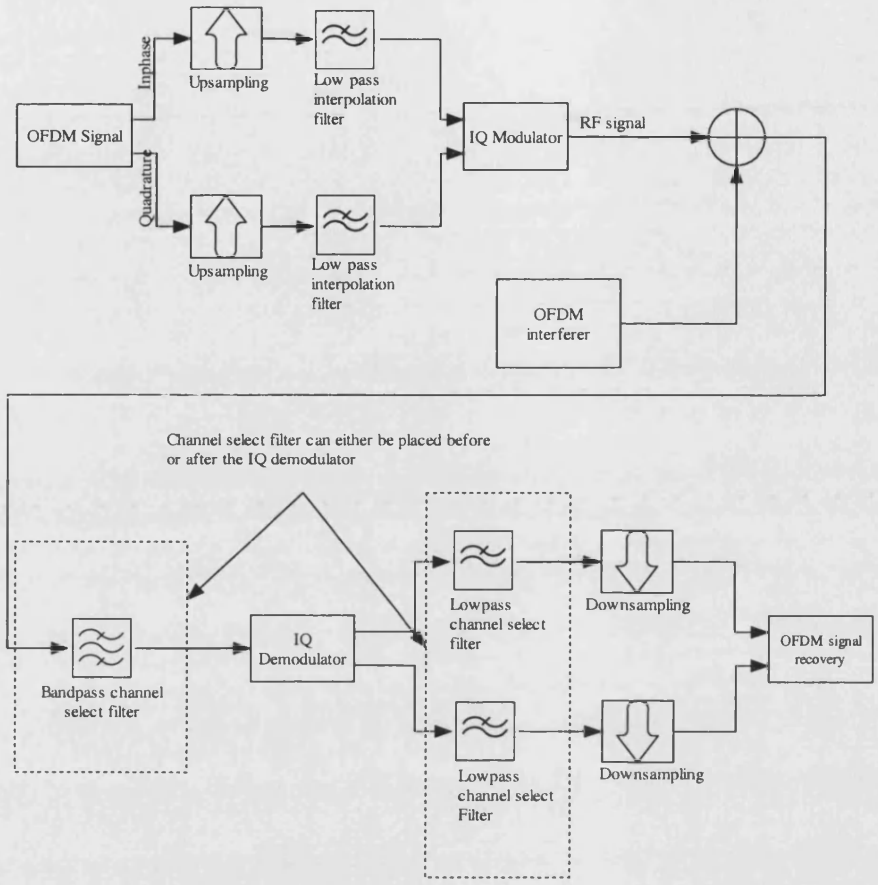

Figure 6.12 – ACI limited simulation environment

Simulation environment with noise and ACI

The block diagram for simulation under both noise and ACI conditions is shown in Figure 6.13. Noise is placed after the addition of the interfering channel in order to obtain the correct signal-to-noise ratio.

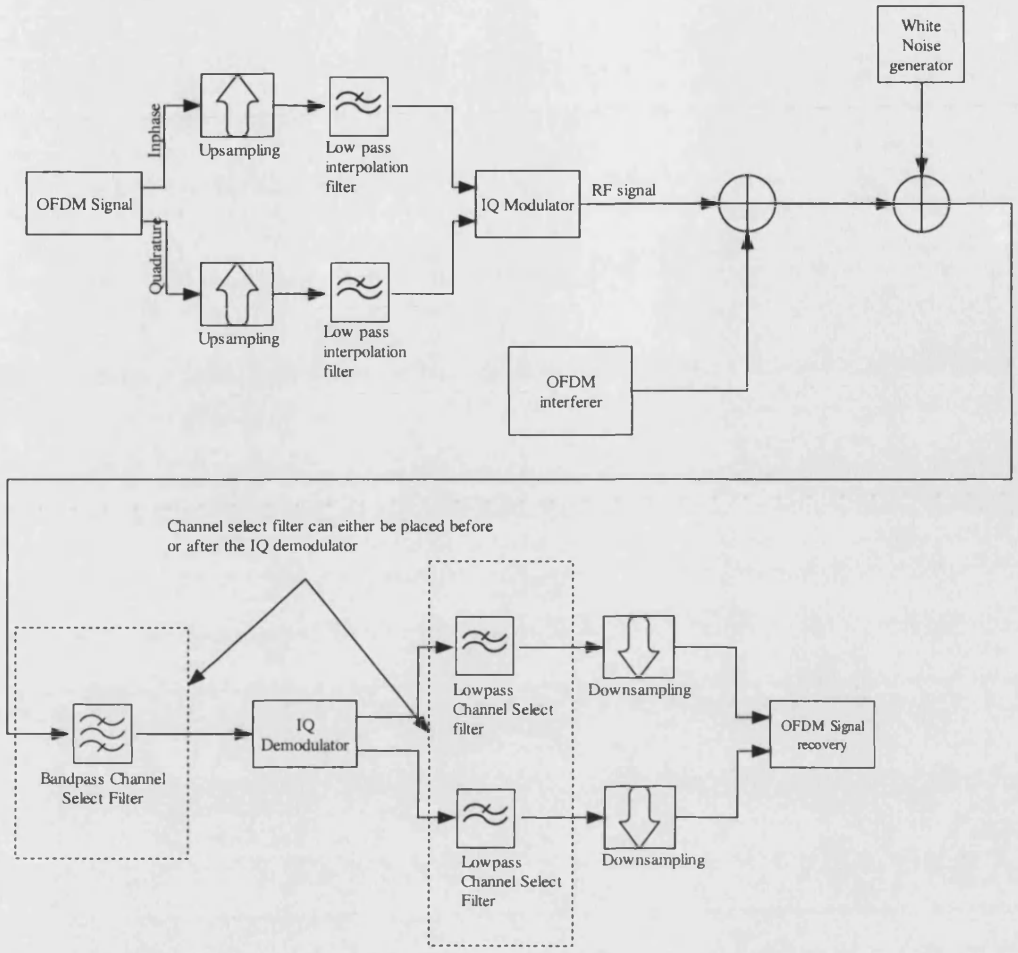

Figure 6.13 – Simulation under both noise and ACI conditions

6.5 Simulation results

6.5.1 Introduction

This section displays the results obtained from the simulation of the models described above. The results displayed in the next section will show how the interpolation filters affect the OFDM system in an environment where noise is the only interference. Subsequently, the next section will show results when the system is under ACI interference only. Finally, simulation results when the OFDM system is placed under noise and ACI interference are reported. The results will help to identify the best interpolation filter combination (BT and order) for the OFDM system in noise and interference limited environments. The simulation results should show a similar behaviour that was observed in [130]. In all simulations no decimation filters are used, as explained in the previous section.

6.5.2 Performance in noise

Simulations of the system for different interpolation filters over a range of different BT and order values were carried out in order to identify suitable filters in the presence of AWGN. The simulation system block diagram is shown in Figure 6.11. A first order Chebyshev filter with BT 1.5 used as a bandpass channel select filter was adopted for all the simulations. This was necessary in order to obtain comparable results amongst simulations of different interpolation filters. For reasons of simplicity the interpolation filters that give the OFDM system optimal performance in noise only conditions are termed as "Noise Filters".

Figure 6.14 shows the variation of the bit error rates obtained in an OFDM system using (a) Chebyshev (b) Butterworth and (c) Bessel interpolation filters for different BT and order combinations. The SNR at the input of the receiver was maintained at -12 dB.

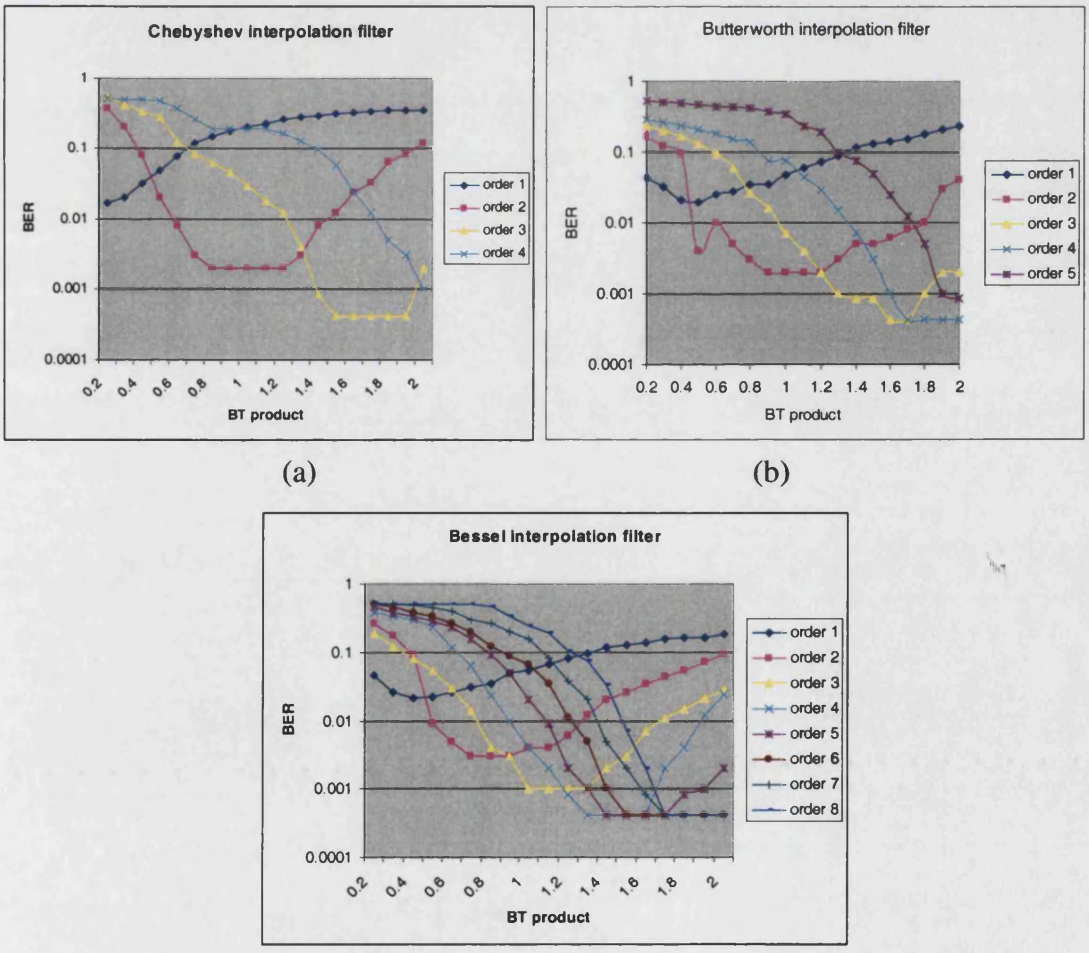

Figure 6.14 – Performance of interpolation filters in noise

From these figures the characteristics of each filter can be observed. The Bessel filter due to its wide frequency response can achieve good performance in noise over a wide filter order range. In contrast, the Chebyshev filter that has the sharpest cut-off frequency response can achieve good error rate performance for higher orders (third order Chebyshev in Figure 6.14a). The Butterworth filter with the best intermediate shape has good performance in noise over a higher filter order number than Chebyshev. In conclusion, this figure indicates that each filter can be used in an OFDM system to obtain good performance in AWGN conditions at specific BT/order combinations.

The next figure shows error rates versus E_b/N_o for a range of interpolation filters with specific filter orders that have the best performance in noise. This figure shows that the simulation results differ by approximately 2 dB from the ideal BPSK curve. In addition, this figure also shows that filters from different families achieved the same performance for different BT/order combinations. The reason for this 2 dB difference is due to the choice of the same bandpass channel select filter and the use of the cyclic prefix (reduces the SNR by 1 dB). Simulations showed that by using different combinations of interpolation and channel select filters of other filter families can result in improvement of the performance of the system.

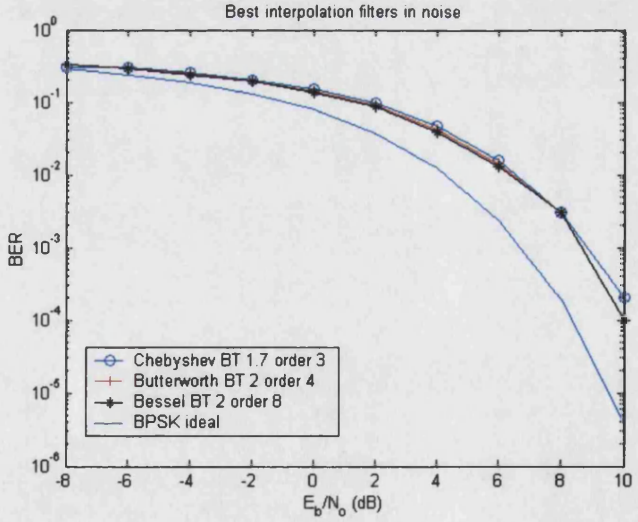

Figure 6.15 – OFDM system performance in noise using various interpolation filters

6.5.3 Performance in ACI

The performance of the system in the presence of ACI as the only interference is investigated in this section. The block diagram of Figure 6.12 is used as a basis for

simulation under ACI conditions. For the reasons mentioned in the previous section the same channel select filter (first order Chebyshev BT 1.5) is used.

Figure 6.16 shows the bit error rates obtained from simulating an OFDM system using (a) Chebyshev, (b) Butterworth and (c) Bessel interpolation filters for different BT/order combinations under 0 dB ACI, where the interferer is transmitting at a carrier frequency 5 MHz away from the main carrier. Due to the high number of simulations the plots only indicate low error rates (less than 0.1 BER), in order to make the figures more comprehensible.

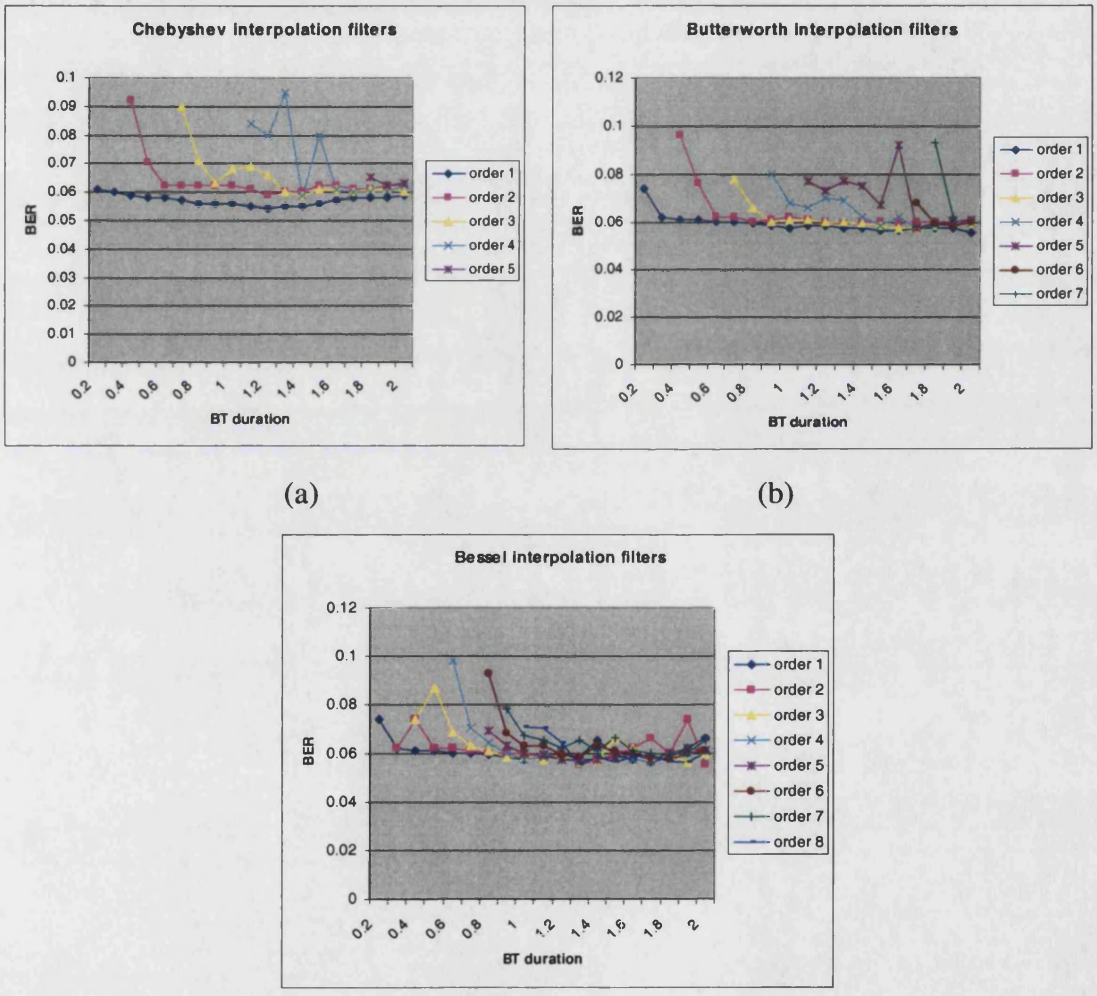

Figure 6.16 – Performance of interpolation filters in ACI

This figure indicates that there are similarities in the way the filters perform in ACI only and noise only conditions. The Bessel interpolation filter has a wide range of

filter orders that give low error rates. In contrast, Chebyshev filters have a narrow filter order range that give low error rates. In addition, the above figures indicate that there is no significant performance advantage by using a specific filter since the error rates obtained by each filter tend to stabilise in the 0.06 error rate area. However, by carefully examining these error rates it can be observed that the first order Chebyshev BT 1.2, first order Butterworth BT 1.5 and first order Bessel BT 1 filters have the best performance in ACI only conditions. For simplicity the interpolation filters that give the OFDM system optimal performance in ACI only conditions are termed as "ACI filters".

Furthermore, the performance of the "Noise filters" have approximately a 2 dB degradation in ACI only conditions (at 10^{-4} error rate) compared to the performance of the "ACI filters", as depicted in Figure 6.17.

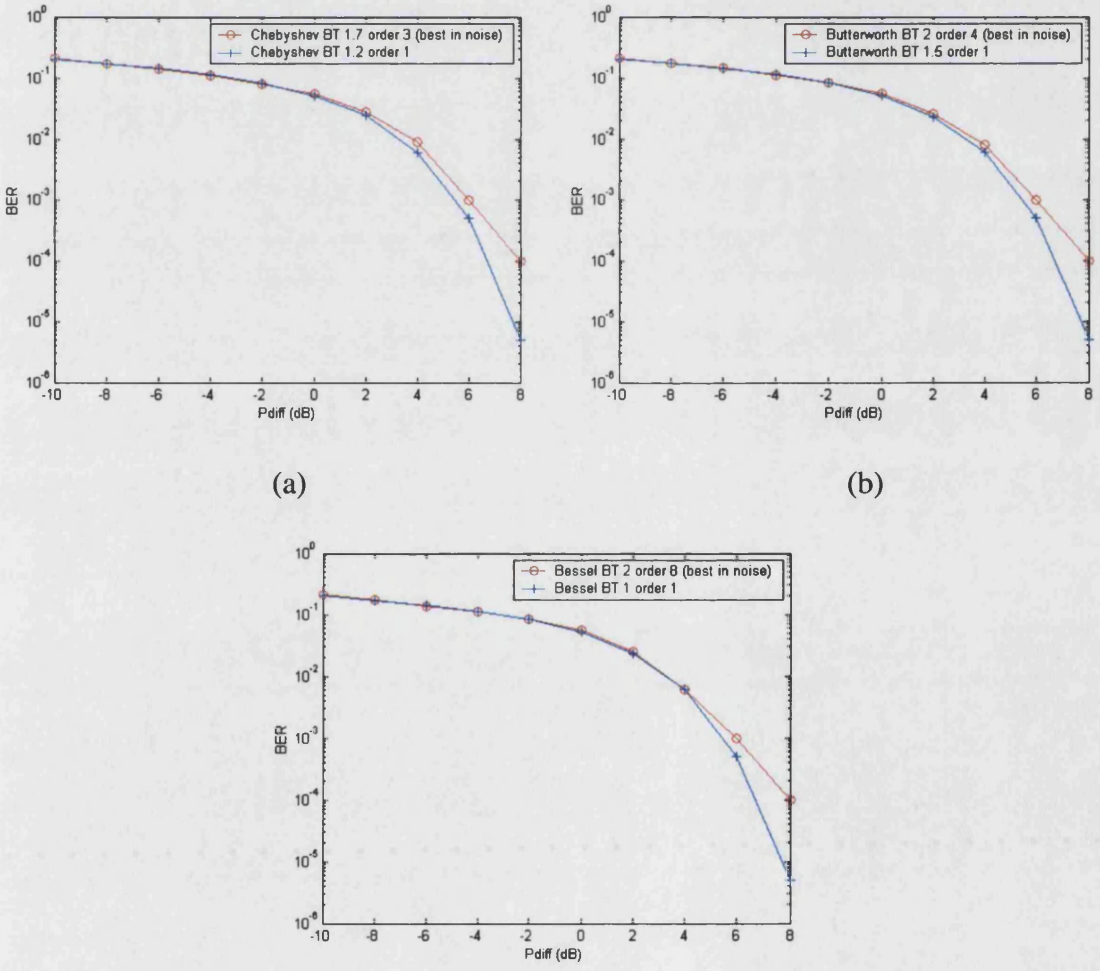

Figure 6.17 – Performance of "noise filters" in ACI only conditions: (a) Chebyshev (b) Butterworth and (c) Bessel filters

Figure 6.17 depicts that the filters that were found most suitable for noise environments do not result in the best performance of the OFDM system in interference only environments. This is justified by the received eye diagrams of Figure 6.18 for "Noise filters" and "ACI filters" in ACI only conditions at a P_{diff} of 20 dB. The "Noise filter" eye diagram has more distortions than the "ACI filter" eye diagram.

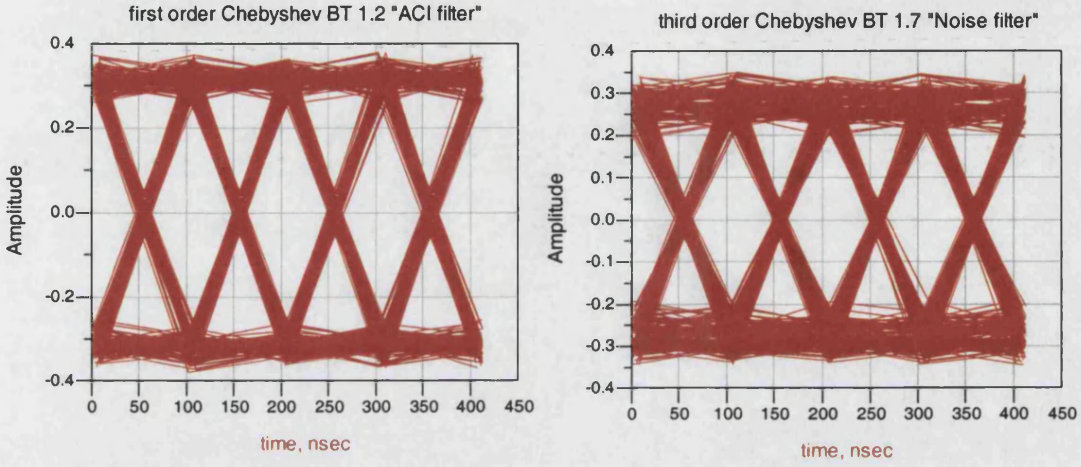

(a) (b)

Figure 6.18 – Received eye diagrams of (a) "ACI filters" and (b) "noise filters" in ACI only conditions

Figure 6.19, shows BER versus E_b/N_o under noise only conditions using ACI and noise filters. The figure below shows a major performance degradation of the "ACI filters" in noise only conditions. It is justified by observing the received eye diagrams shown in Figure 6.20.

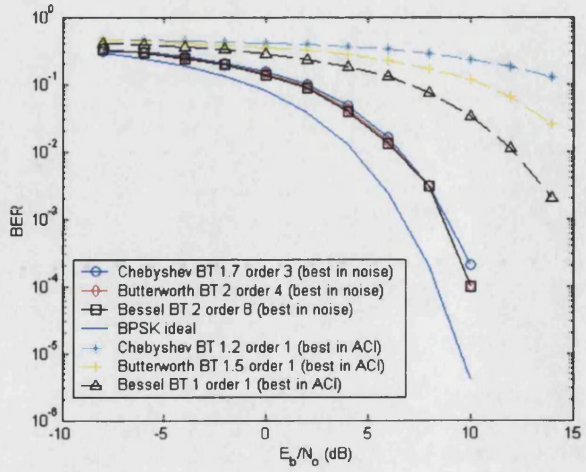

Figure 6.19 – Comparison of "ACI filters" and "noise filters" in noise only conditions

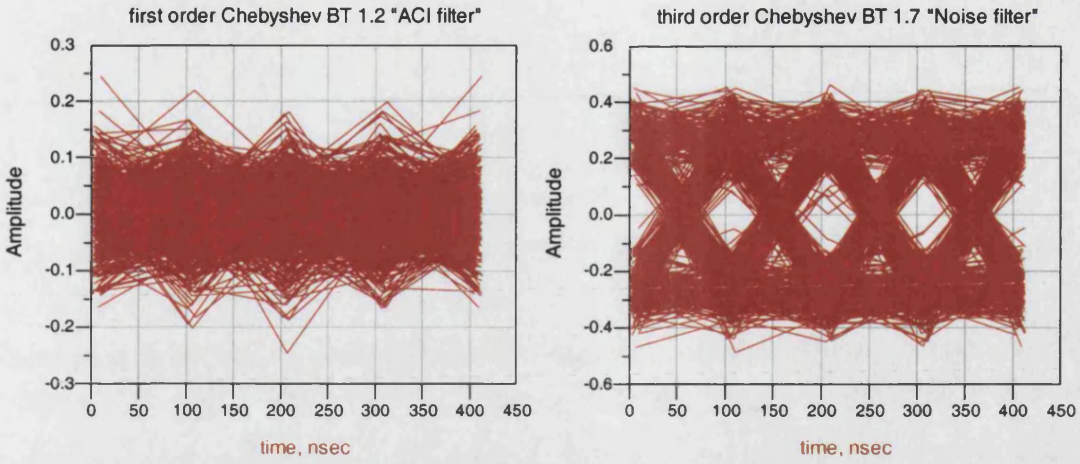

(a) (b)

Figure 6.20 – Received eye diagrams of (a) "ACI filters" and (b) "Noise filters" in noise only conditions

The received eye diagram of the "ACI filters" is completely distorted whereas the received eye diagram of the "Noise filters" is less distorted[9]. More conclusions can be drawn by considering the behaviour of the above filters under both noise and interference conditions, i.e. in an environment more likely to be found in practical wireless communication systems.

6.5.4 Performance in noise and ACI

The previous two sections discussed the performance of interpolation filters in noise only and interference only environments. The simulations indicated that, for optimum performance, the interpolation filters have to be configured accordingly for each environment, since the "Noise filters" do not give good performance in ACI and the "ACI filters" have the worst performance in noise. This final section tests the performance of OFDM in an environment where additive noise and adjacent channel interference are present. The block diagram of Figure 6.13 is used as a basis for simulation under these conditions.

The simulations are carried out, by varying the noise whilst keeping constant the interference ratio (measured as P_{diff}, the difference in power between the wanted and the

[9] The simulation in noise only conditions is carried out using an SNR of 20 dB. No channel select filters are placed, when measuring eye diagrams, in order to observe only the effect of the interpolation filters on OFDM.

interference signal). Figure 6.21, shows the error rates obtained for P_{diff} of 6 dB, 4 dB and 0 dB versus SNR. Two different areas of interference are observed, one for low SNR values where noise is the most dominant interferer and the other for high SNR values where ACI is the dominant interferer.

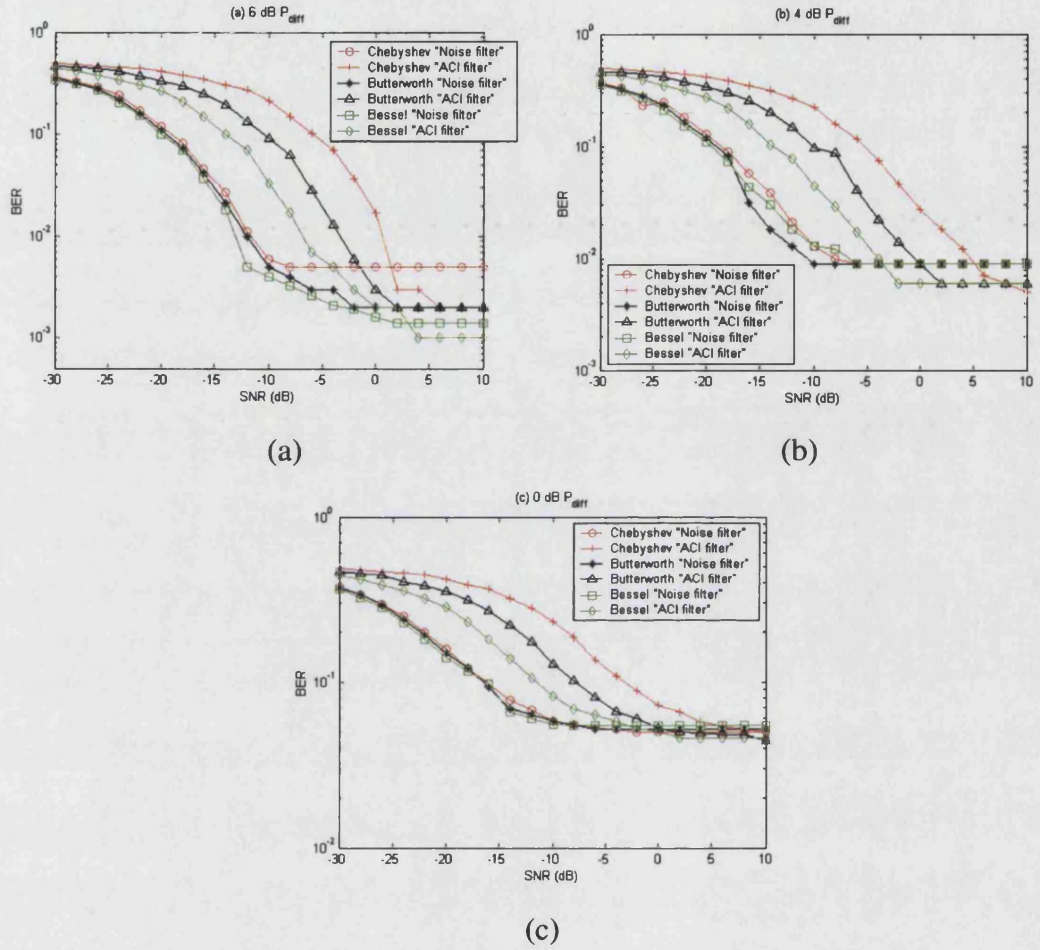

Figure 6.21 – Performance of filters under noise and interference conditions; (a) 6 dB P_{diff}, (b) 4 dB P_{diff}, (c) 0 dB P_{diff}

The results confirm the sensitivity of the "ACI filters" in noise, as pointed out by Figure 6.19. Due to this fact, the "ACI filters" perform better than their counterparts only at high SNR ratios (0 dB and beyond). For example, in Figure 6.21a, where there is a 6 dB difference between the wanted and the interference channel, the "Noise filters" have a 10 dB performance advantage against the "ACI filters" at 10^{-2} error rate. However, at 10^{-3} error rate, where ACI is more dominant, the "ACI filters" achieve lower error rate than their counterparts. Therefore, the performance advantage of the "ACI filters" compared to the "Noise filters" can be observed only at high SNR ratios.

Furthermore, the results indicate that filters with sharpest cut-off do not necessarily give the best performance. More specifically, the results pointed out that low order filters from each filter (order 1) family gave the best performance in ACI, whereas the best filters in noise have a wide range of orders, with the Bessel filter having the highest (order 8) due to its slow frequency decay. In addition, the results indicated that in ACI conditions the bandwidth of the interpolation filters needs to be relatively low whereas in noise conditions the bandwidth must be wide. This is justified by the fact that in both tests the noise bandwidth was mainly determined by the channel select filter, which was kept unchanged. In ACI and noise conditions a compromise between frequency separation and filter order must be made in order to achieve best overall performance. This might not be easily achievable in practice and a sub-optimum solution has to be undertaken.

6.6 Summary

This chapter studied the effect of interpolation filters on the performance of an OFDM system under noise and/or ACI conditions. The OFDM system was designed to have 10 MHz bandwidth and 10 Mbps data rate, which are similar to specifications of the WLAN system. It was decided to study the use of Chebyshev, Butterworth and Bessel filters for interpolation. The first part of this work was to identify suitable interpolation filters to give the best performance in noise only conditions. Simulations indicated that third order Chebyshev BT 1.7, fourth order Butterworth BT 2 and eighth order Bessel BT 2 gave optimal performance under noise only interference. Subsequently, these filters were tested under ACI. Simulations showed that the "Noise filters" are not optimal under ACI only conditions. The filters that give the best performance in ACI are the first order Chebyshev BT 1.2, Butterworth BT 1.5 Bessel BT 1 filters. However, these filters have worse performance than their counterparts when the interference is noise only. The behaviour of these filters was verified by studying their performance under noise and ACI conditions. Simulations were carried out using constant ACI ratio (constant P_{diff}, the difference in transmitting power between the main and the interfering channel) and varying the noise. The results indicated that "ACI filters" are much more sensitive to noise than the "Noise filters" to ACI. The "ACI filters" performed better than their counterparts only at high E_b/N_o ratios. In addition, the results indicated that the interpolation filters need to have narrow

bandwidth and low order so as to give good performance in ACI, whereas good performance in noise is achieved by the interpolation filters having wide bandwidth and relatively high orders. To conclude, this work indicated that the effects of ACI must be taken into consideration when designing an OFDM system. Since the interpolation filters are digital in nature they can be easily reconfigured. Therefore, such a scheme could be easily implemented in Software Radio systems (with a closed feedback loop) to give up to 2 dB advantage over systems that use fixed interpolation filters.

Chapter 7

Concluding remarks and future recommendations

The work carried out in this thesis covered a range of research areas relating to wireless communications. The first part of the research was concerned with the design, modelling and performance assessment of a multimode system implementing OFDM, GSM and EDGE systems. The second part of the research was concerned with studies of Fast-OFDM modulation, which is a variation of OFDM, offering twice the bandwidth efficiency of OFDM but at the expense of handling only one dimensional modulation schemes. The performance of FOFDM was evaluated for several operating conditions, receiver imperfections and channel distortions. FOFDM performance was compared to that of an OFDM system having similar specifications. The final part of this research was concerned with studying the effects of interpolation filtering on the performance of a wireless OFDM system in noise limited and interference limited environments.

An overview of past, present and future cellular networks was first carried out. More specifically, the evolution of cellular networks from first generation (1G) to 3rd generation (3G) cellular systems was described. In addition, the main parameters of GSM and EDGE systems, namely, modulation and air interface structure and the proposals made for future generation mobile systems, namely the fourth generation system (4G) were specified. One of the modulations considered for 4G systems is OFDM. The advantages and disadvantages of this modulation and the routes to OFDM implementation were outlined. The ability of OFDM to work well in fading channels introduced new modulations that use this scheme, such as multicarrier CDMA which was described. Finally, applications that use OFDM, such as WLAN and DVB systems were outlined.

Furthermore, other aspects of OFDM were addressed. More specifically, a design guide for an OFDM transmitter, describing the interaction between modulation, pilot symbol addition, guard interval and FFT size. In addition, an OFDM receiver design guide, showing the effect of carrier/symbol synchronisation and methods to alleviate such effects were explained. Finally, the elements that define a wireless channel (noise, fading channels) were outlined.

The first part of research work reported here addressed the design, implementation and performance assessment of a multimode system implementing OFDM, GSM and EDGE systems. The design considerations of a system using OFDM integrated with GSM and EDGE systems were detailed and a discussion of the choice of data rate, modulation, FFT size, pilot symbol addition, guard interval addition, synchronisation and estimation methods was carried out. Subsequently, the modelling and verification of the multimode system using the simulation software ADS, showed that all models performed correctly. The multimode system was first evaluated in an environment where noise is the only interference. The results indicated that the error rates obtained from the GSM and EDGE models, matched the analytical error rates of GMSK and 8PSK modulations. However, the obtained error rates from the OFDM/QAM64 model showed 1-2 dB penalty when compared to the analytical error rate of QAM64. A predicted reason was that the OFDM system was limited by the OFDM filtering process and the LS channel estimator at the OFDM receiver. The ETSI models for fading environments were used with the models developed to assess the multimode system performance in "Typical Urban", "Hilly Terrain" and "Rural Area" environments. The simulation results indicated that at low mobile vehicular speeds the performance of OFDM/QAM64 is comparable to the performance of GSM and EDGE systems at mid-vehicular speeds. It was concluded that an adaptive modulation scheme is necessary for the OFDM system to provide better performance at higher speeds. The drawback is that at such speeds the data rate of the OFDM system drops since lower order modulation needs to be used to alleviate this problem. In addition, the results indicated that the OFDM system has higher Doppler spread sensitivity than GSM and EDGE systems. A possible solution to this problem is to reduce the spacing of the pilot symbols by increasing their number within one OFDM symbol, which has the disadvantage of reducing the effective data rate. Another solution is to use more accurate channel estimation methods, for example MMSE. Following the evaluation in fading channels, the multimode system was tested in an environment with ACI or CCI.

The ETSI specifications were used to define models for such environments. The interference studies showed that the lowest interference into an OFDM system resulted from another OFDM signal, whilst interference by GSM and EDGE system resulted in the same levels of distortion. This was attributed to the spectral structure of the filtered OFDM where it has less spectral leakage than both GSM and EDGE systems. Furthermore, the simulations showed that, at high P_{diff} values, the interference into a GSM system results in the same level of distortion irrespective of the source of interference. At mid-level P_{diff} values there is an approximately 3 dB difference in the level of distortion caused by an OFDM and an EDGE interferer. This was not observed when studying the interference into an EDGE system. Simulations indicated that the levels of distortion are approximately the same irrespective of the source of interferer. In addition, the results indicated that an OFDM interferer would create more errors on EDGE than GSM which is reasonable due to the higher order modulation of EDGE (8PSK) compared to GSM (GMSK). Overall, the simulation results indicated that the OFDM system needs to be modified so as to improve its performance in fading channels. On the other hand, the interference simulations showed that the OFDM system can be perfectly integrated with the other two systems when operating in the same frequency range. The advantage is that the same frequency planning schemes specified by ETSI can be used also for the OFDM system.

The second element of research involved the investigation of a new modulation technique, Fast-OFDM, which is a variation of OFDM. FOFDM achieves twice the bandwidth efficiency of OFDM by halving the carrier separation of the FOFDM symbol when compared to the separation of the OFDM subcarriers. The basic principles of FOFDM, its continuous-time and discrete-time implementations and its differences from OFDM were discussed, together with its limitations. We showed that by correlating two FOFDM signals, the correlation factor of the imaginary part is not zero at the sampling instants. Analysing the reception of an OFDM signal it was observed that at the demodulation process, the demodulated symbol is multiplied by a complex term. Therefore, a major limitation of FOFDM is that it can only handle single-dimensional (effectively real) modulation schemes (BPSK, M-ASK), where the imaginary part of the signal is zero. Furthermore, it was also observed that any distortion to the imaginary part of the FOFDM symbol will have serious consequences at the receiver due to the existence of the complex term at the demodulation process (due to complex multiplication). In order to investigate the performance of FOFDM,

two systems, an OFDM and an FOFDM with equal data rates, were designed and implemented in ADS. The comparison was made in terms of noise, receiver front-end non-idealities and fading channels conditions. The first simulation results showed that both systems have identical performance in noise. In addition, simulations under I/Q amplitude imbalance indicated that both OFDM and FOFDM systems have similar performance. On the other hand, simulations under I/Q phase imbalance indicated that the FOFDM system deteriorates faster than OFDM. This deterioration is due to the phase rotation of the received FOFDM symbol. The same behaviour is observed when simulating both systems under frequency offset conditions. Analysing the reception of an FOFDM symbol by a receiver having frequency offset, it was observed that a common phase error exist that will affect the imaginary components of the FOFDM symbol, thus making demodulation more difficult. The simulation results also verified this observation showing a faster deterioration of the performance of FOFDM compared to OFDM. The same behaviour was also observed when simulating both systems under timing offset and phase noise conditions. However, it is important to note that at small distortion factors the performance of FOFDM is comparable to OFDM. As the distortion factor increases the performance of FOFDM deteriorates faster. Finally, the FOFDM system was tested in fading environments comparing its performance with OFDM. This was necessary in order to have a complete picture of the appropriateness of FOFDM for wireless systems. The simulation results indicated that FOFDM has a comparable performance to OFDM. Overall, a system using OFDM modulation is more robust to errors compared to a system using FOFDM.

The last part of this research studied the effect of interpolation filtering on the performance of OFDM systems in noise limited or ACI limited environments. Simulations in environments where noise was the only interference concluded that the third order Chebyshev BT 1.7, fourth order Butterworth BT 2 and eighth order Bessel BT 2 filters gave best performance in the OFDM system. For reason of simplicity, these filters were termed as "Noise Filters". Simulations where ACI was the only interference pointed out that the first order Chebyshev BT 1.2, Butterworth BT 1.5 and Bessel BT 1 filters gave best performance in the OFDM system. For reason of simplicity these filters were termed as "ACI filters". The simulation results indicated that the "ACI Filters" have an approximately 2 dB better error rate performance than "Noise Filters" in ACI only conditions. On the other hand, the performance of systems employing "ACI filters" deteriorate in noise only conditions. It was necessary to test

these filters in an environment with noise and ACI. The results indicated the sensitivity of "ACI Filters" to noise. The "ACI Filters" performed better than their counterparts only at high E_b/N_o ratios. In addition, the results indicated that the interpolation filters need to have narrow bandwidth and low order in order to give good performance in ACI. Optimal performance in noise is achieved when the interpolation filters have wide bandwidth and relatively high orders. To conclude, this work indicated that the effects of ACI must be taken into consideration when designing an OFDM system. Since the interpolation filters are digital in nature they can be easily reconfigured. Therefore, such a scheme could be implemented in Software Radio systems and can result in a 2 dB performance advantage if filters are chosen appropriately.

7.1 Recommendations for future research

Based on the experience and knowledge acquired during the research, areas of research that are worthy of future investigations can be suggested. These are:

Multimode system (Chapter 4)

- Minor modifications are needed for the proposed OFDM system to be implemented with GSM and EDGE systems. The simulation results suggested that more pilot symbols are needed as well as adaptive modulation. In addition, a coding scheme, (for example RS codes) will improve the performance of OFDM. The modification can be implemented in the proposed OFDM frame structure without altering the FFT size. The zero-padding of that frame can be reduced.
- Comparison of the simulated multimode system with a practical GSM/EDGE multimode base station transceiver developed by Nokia Networks UK. The comparison can be performed using a spectrum analyser able to communicate with ADS software. This study will assist to further analyse the interference relationship between each system.

Fast-OFDM (Chapter 5)

- An investigation of the effect of non-linearities and PAR on the performance of FOFDM. This study would further help understand the properties of

FOFDM and its suitability for wireless systems. Through this study the amplifier specifications for an FOFDM system can be identified.

- Studies in finding appropriate channel estimation methods for FOFDM, for example, pre-equalisation. Such investigation can result in improved performance of FOFDM in radio channels
- Performance assessment of pre-equalised FOFDM and OFDM using equalisation techniques in fading channels.
- An investigation into "wired" Fast-OFDM transmission by modelling an FOFDM system for optical communications. Studies of the potential distortion effects of such transmission method to FOFDM.

Interpolation filtering (Chapter 6)

- Performance comparison of OFDM systems employing practical interpolation filters used in current wireless systems (e.g. WLAN) with the interpolation filters used in this work.
- In this study the interferering system used the same interpolation filters as the main system. A further study is to evaluate the performance of the interpolation filters when the interferer uses different interpolaton filters. This can be achieved by modelling an OFDM system with reconfigurable interpolation filters.

Overall, this thesis reported novel developments in OFDM systems. The developments reported have the potential to result in new OFDM systems and system architectures. It is hoped that the research reported would lead to further studies in this interesting research area.

APPENDIX A

Description of ADS simulation models for the multimode GSM-EDGE-OFDM system

A.1. Introduction

In this appendix, the modelling of the multimode system in the simulation platform ADS is described. The figures, showing the block diagrams of various components of the system, are screenshots taken from the ADS schematics. Appendix A starts by describing the modelling of the proposed OFDM system. Figures showing the main components of the OFDM system, as well as its contents will be depicted. The appendix continues by explaining the modelling of the wireless channel. Finally, the modelling of GSM and EDGE systems is described.

In ADS there are two types of simulation methods, "numeric" and "timed". The difference between the two is that in "timed" simulation the duration of each pulse and consequently the period and frequency of the signal are known. "Numeric" simulation is usually used to model baseband systems, whereas, "timed" simulation is more suitable for RF systems. It is important to note that ADS can perform both "timed" and "numeric" simulation at the same time. In ADS a system is comprised of various models called "blocks". Colour coding is used, in order to distinguish between "timed" and "numeric" simulation. A "timed" block has a black arrow, whereas a "numeric" block has yellow arrow (indicating binary input/output numbers), green arrow (indicating complex input/output numbers), blue arrow (indicating floating point input/output numbers) or red arrows (any input/output). This will become more apparent later on by looking the block diagrams of the simulation models.

A.2. Proposed OFDM system design

A.2.1 OFDM transmitter modelling

The OFDM transmitter is shown in Figure A.1. The first block is the random bit generator followed by the QAM64 mapping block. The next block performs the framing of the OFDM signal, as described in section 4.3.2. The contents of the framing block are shown in Figure A.2. In the first part of this block the bits are arranged in such a way so as to match the framing arrangement discussed in section 4.3.2. The "OFDM_Frame" block, whose contents are shown in Figure A.3, and the "pilot_mux" block, whose contents are shown in Figure A.4, perform this task. The second part of the framing block performs zero-padding which was discussed in section 4.3.2. Subsequently, the "FFT_Cx" block creates the OFDM signal. The guard interval is inserted using the "InsertGuard" block. The signal is then split into its real and imaginary parts in order to add the EDGE filtering and the timing information. First the signal is upsampled by a ration of 20 using the "Upsample" block. The OFDM signal is filtered using the "EDGE_PulseShapingFltr" block that contains a linearised Gaussian filter of BT 0.3 as discussed in section 2.4.2. Timing information is added to the signal using the "FloatToTimed" block. The importance of this block is that it converts the signal from "numeric" to "timed" simulation. The real and imaginary branches are fed into the "QAM_Mod" block that performs IQ modulation.

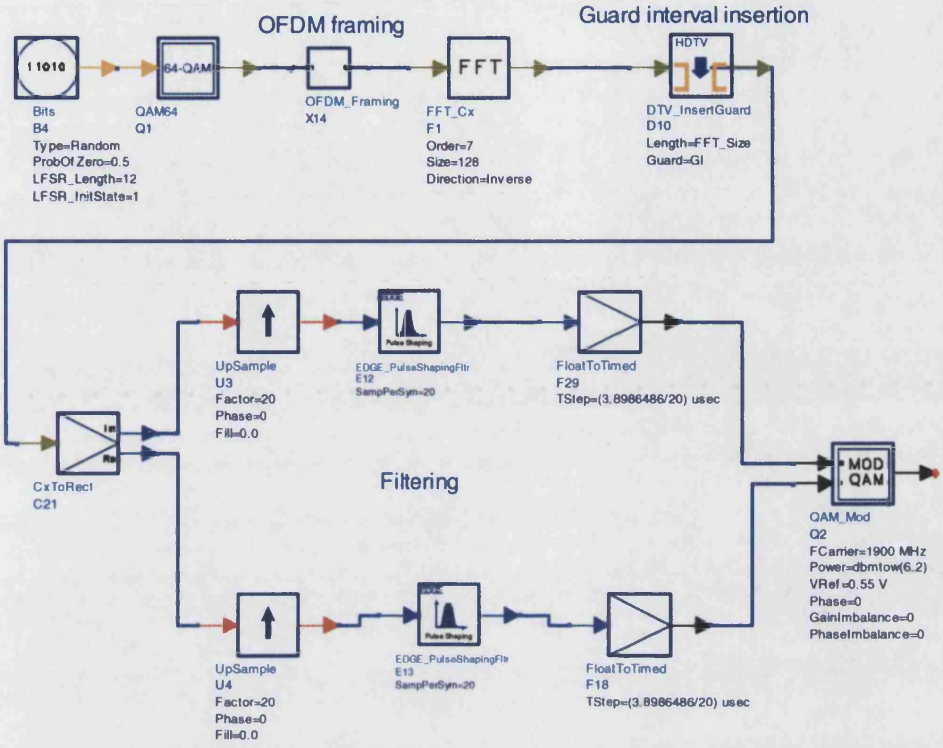

Figure A.1 – Block diagram of proposed OFDM transmitter in ADS

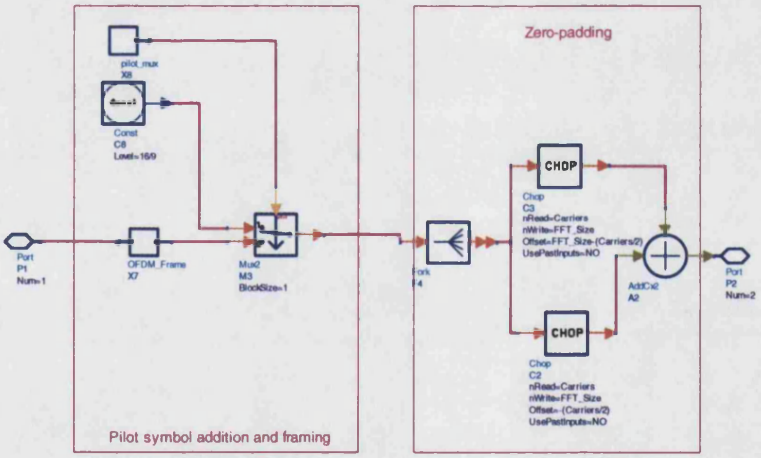

Figure A.2 – Framing block

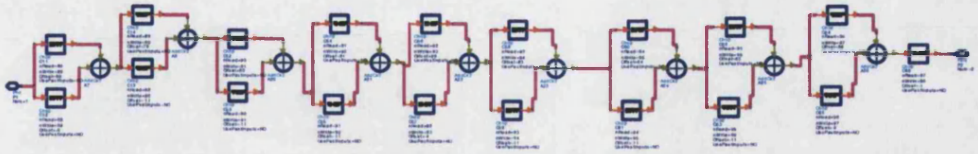

Figure A.3 – Frame arrangement (contents of "OFDM_Frame" block)

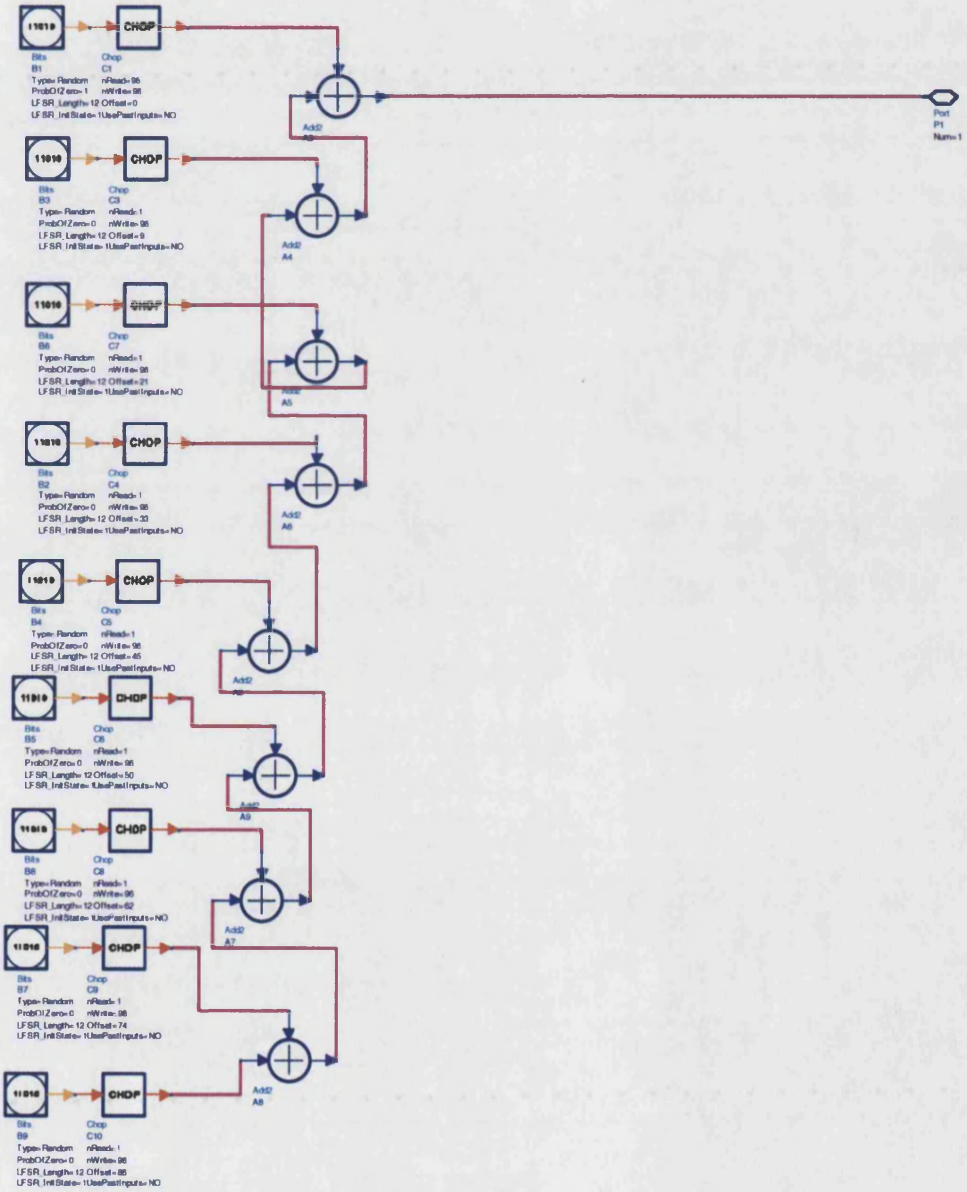

Figure A.4 – Pilot symbol arrangement (contents of "pilot_mux" block)

A.2.2 Channel modelling

The RF channel modelling is shown in Figure A.5. Any adjacent or co-channel interference is added through the "Summer_RF" block. The channel model is used for simulation of ACI, CCI and multipath fading as discussed is section 4.5.3 and 4.5.4. The "EDGE_MultipathDown" block is the model that contains the typical multipath environments defined by ETSI. Any noise can be added later by using the "AWGN_Addition" block, whose contents are shown in Figure A.6. The "BPF_ButterworthTimed" block is used as a channel select filter. The "DBL_CNV_OFDM_Rx" block contains the mixer and amplifier specifications for a practical EDGE receiver provided by Nokia. Details of this block cannot be discussed due to commercial confidentiality.

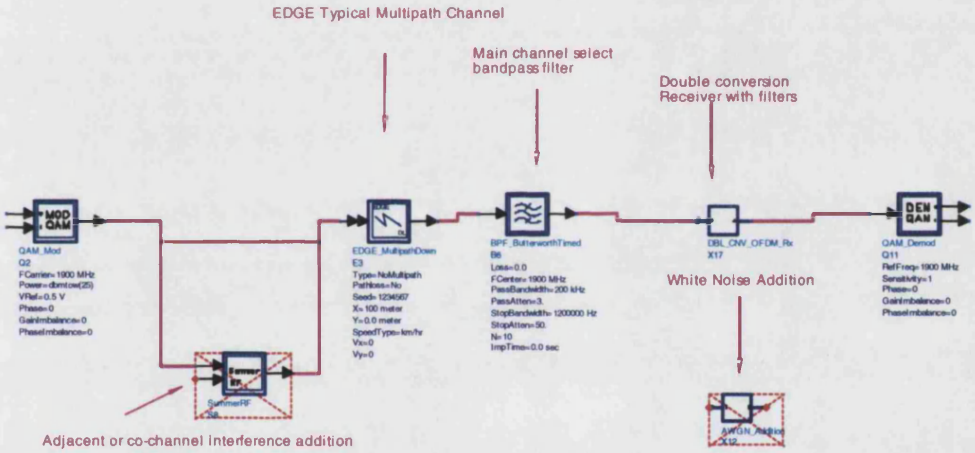

Figure A.5 – RF channel modelling

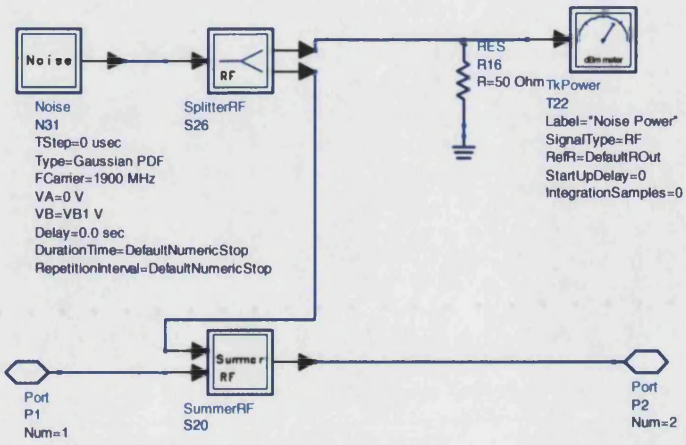

Figure A.6 – Noise addition (contents of "AWGN_Addition" block)

A.2.3 OFDM receiver modelling

The modelling of the OFDM receiver is shown in Figure A.7.

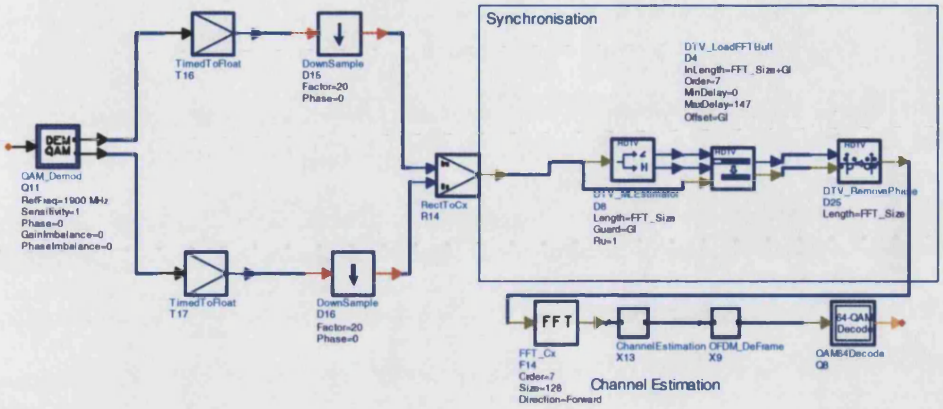

Figure A.7 – Block diagram of proposed OFDM receiver in ADS

The "QAM_Demod" block performs I/Q demodulation and the "TimedToFloat" block converts the signal from "timed" to "numeric" simulation. The "Downsample" block removes the sampling of the signal which was carried out in the transmitter by the "Upsample" block. The next three blocks perform synchronisation using the cyclic prefix and maximum likelihood estimation as discussed in section 3.4.3.3. The blocks used were taken from the DVB library of ADS. After the forward FFT, channel estimation is performed to the signal using the "ChannelEstimation" block that uses the LS estimation method. The contents of this block are shown in Figure A.8. A description of the LS channel estimator for the proposed OFDM system is carried out in section 4.4.2.2. The "EDGE_Rx" block which is the EDGE equalising filter and the "Equaliser_Cx" block which performs the main equalisation were designed in Ptolemy. The Ptolemy code for these blocks is shown on the next page.

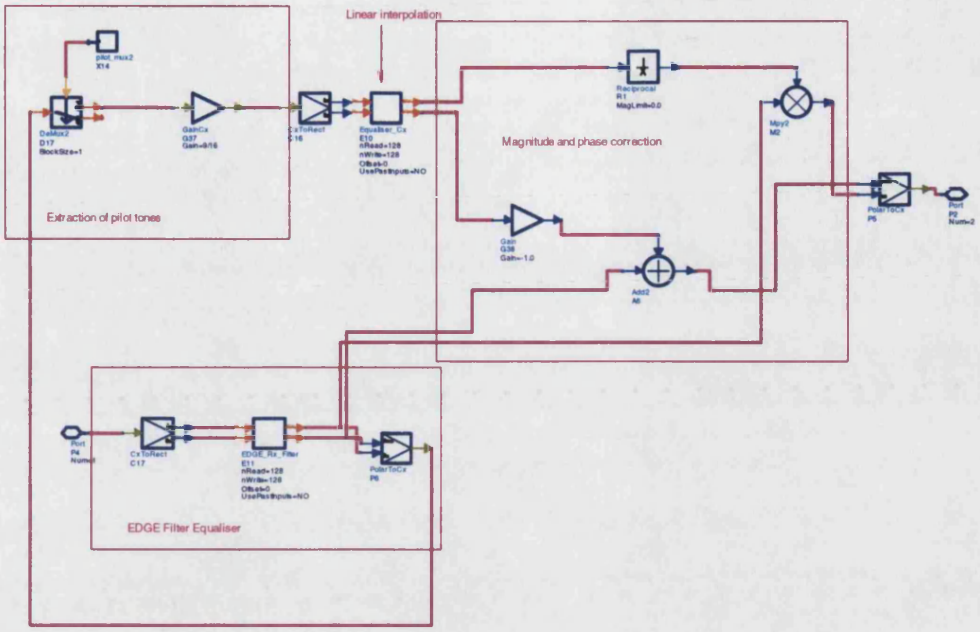

Figure A.8 – Channel estimator (contents of "ChannelEstimator" block)

"EDGE_Rx_Filter" Ptolemy code:

```
defstar {
        name {EDGE_Rx_Filter}
        domain {SDF}
        desc { EDGE Receive Filter for OFDM }

        location { My Stars }

        input {
                name{TxI}
                type{ANYTYPE}
        }

        input {
                name{TxQ}
                type{ANYTYPE}
        }
```

```
output {
        name{EqPhase}
        type{=TxI}
}

output {
        name{EqMag}
        type{=TxI}
}

defstate {
        name {nRead}
        type {int}
        default {128}
        desc { number of data items read }
}
defstate {
        name {nWrite}
        type {int}
        default {128}
        desc { number of data items written }
}
defstate {
        name {Offset}
        type {int}
        default {0}
        desc { start of output block relative to start of input block }
}
defstate {
        name {UsePastInputs}
        type { enum }
        default { "NO" }
   enumlist { NO, YES }
        desc { use previously read inputs }
```

```
    }
    protected {
        int hiLim, inidx, loLim;
    }
  method {
    name { computeRange }
    type { "void" }
    arglist { "()" }
    access { protected }
    code {
        // Compute the range of output indexes that come from inputs
        // This method is called in the setup() method for the Chop
        // star, and in the go method for ChopVarOffset because
        // it resets the offset parameter
        hiLim = int(nWrite) - int(Offset) - 1;
        if (hiLim >= int(nWrite)) hiLim = int(nWrite) - 1;
        else if (int(UsePastInputs)) hiLim = int(nWrite) - 1;

        loLim = int(nWrite) - int(nRead) - int(Offset);
        if (loLim < 0) loLim = 0;

        inidx = int(nRead) - int(nWrite) + int(Offset);
        if (inidx < 0) inidx = 0;
    }
  }
  setup {
        if (int(nRead) <= 0) {
          Error::abortRun(*this, "The number of samples to read ",
                        "must be positive");
          return;
        }
        if (int(nWrite) <= 0) {
          Error::abortRun(*this, "The number of samples to write ",
                        "must be positive");
```

```
            return;
        }

        if (int(UsePastInputs)){
            TxI.setSDFParams(int(nRead),int(nRead)+int(Offset)-1);
                TxQ.setSDFParams(int(nRead),int(nRead)+int(Offset)-1);
                }
        else
            {
                TxI.setSDFParams(int(nRead),int(nRead)-1);
                TxQ.setSDFParams(int(nRead),int(nRead)-1);
                }
        EqMag.setSDFParams(int(nWrite),int(nWrite)-1);
        EqPhase.setSDFParams(int(nWrite),int(nWrite)-1);


        computeRange();
}
go {
    double r[128];
        double q[128];
        double phase[128];
        double mag[128];
        double reshape[128];
        double estmag[128];
    double z[128];
        double h[128];

        int inputIndex = 0;//inidx;
        for (int i = 0; i < int(nWrite); i++) {
                                r[inputIndex] = (TxI%inputIndex);
                                q[inputIndex] = (TxQ%inputIndex);
                                inputIndex++;
            }
```

```
        for (i=0;i<128;i++){
        phase[i] =atan2(q[i],r[i]);
                        }

        for (i=0;i<128;i++){
        mag[i] =  sqrt(r[i]*r[i]+q[i]*q[i]);
                        }

h[0]=73.2503041172595280;
h[1]=68.7701494496612930;
h[2]=64.2900163143798140;
h[3]=59.8099254682923310;
h[4]=55.3298961064088070;
h[5]=50.8499450533169650;
h[6]=46.3700859210528190;
h[7]=41.8903282214814520;
h[8]=37.4106764206295050;
h[9]=32.9311289215798110;
h[10]=28.4516769614980360;
h[11]=23.9723034070866970;
h[12]=19.4929814312166520;
h[13]=15.0136730516349410;
h[14]=10.5343275104316890;
h[15]=6.05487947031173410;
h[16]=1.57524700057196010;
h[17]=-2.90467067805904830;
h[18]=-7.38499572503461100;
h[19]=-11.8658745287186070;
h[20]=-16.3474809193089370;
h[21]=-20.8300198007585950;
h[22]=-25.3137312658293910;
h[23]=-29.7988952697331830;
h[24]=-34.2858369516063370;
h[25]=-38.7749327099368820;
```

h[26]=-43.2666171588079160;
h[27]=-47.7613911174409900;
h[28]=-52.2598308173284480;
h[29]=-56.7625985509225380;
h[30]=-61.2704550356175930;
h[31]=-65.7842738295231300;
h[32]=-70.3050582151228820;
h[33]=-74.8339610684630150;
h[34]=-79.3723083618514910;
h[35]=-83.9216271164300130;
h[36]=-88.4836788399521980;
h[37]=-93.0604997718771190;
h[38]=-97.6544496362365240;
h[39]=-102.268271105756850;
h[40]=-106.905162854945710;
h[41]=-111.568869991244050;
h[42]=-116.263796896319540;
h[43]=-120.995149220516280;
h[44]=-125.769114151292480;
h[45]=-130.593091413920170;
h[46]=-135.475992194468490;
h[47]=-140.428629951538110;

h[80]=-68.0351548821218180;
h[81]=-73.0707618139428130;
h[82]=-78.0233995710124620;
h[83]=-82.9063003515608090;
h[84]=-87.7302776141884880;
h[85]=-92.5042425449646540;
h[86]=-97.2355948691614100;
h[87]=-101.930521774236920;
h[88]=-106.594228910535270;
h[89]=-111.231120659724110;
h[90]=-115.844942129244450;

h[91]=-120.438891993603820;

h[92]=-125.015712925528780;

h[93]=-129.577764649050950;

h[94]=-134.127083403629530;

h[95]=-138.665430697017910;

h[96]=-143.194333550358070;

h[97]=-147.715117935957860;

h[98]=-152.228936729863400;

h[99]=-156.736793214558470;

h[100]=-161.239560948152550;

h[101]=-165.738000648039960;

h[102]=-170.232774606673120;

h[103]=-174.724459055544120;

h[104]=-179.213554813874730;

h[105]=176.299503504252230;

h[106]=171.814339500348370;

h[107]=167.330628035277630;

h[108]=162.848089153827890;

h[109]=158.366482763237610;

h[110]=153.885603959553570;

h[111]=149.405278912578070;

h[112]=144.925361233947040;

h[113]=140.445728764207310;

h[114]=135.966280724087340;

h[115]=131.486935182884100;

h[116]=127.007626803302350;

h[117]=122.528304827432380;

h[118]=118.048931273020980;

h[119]=113.569479312939240;

h[120]=109.089931813889480;

h[121]=104.610280013037560;

h[122]=100.130522313466220;

h[123]=95.6506631812020740;

h[124]=91.1707121281102320;

h[125]=86.6906827662267430;

h[126]=82.2105919201392150;

h[127]=77.7304587848577720;

z[0]=117.759021772592650;

z[1]=117.711066218752760;

z[2]=209.008528259313580*9*0.0625;

z[3]=117.328006910708770;

z[4]=116.993681412984740;

z[5]=116.564998060183680;

z[6]=116.042822932980490;

z[7]=115.428207165596540;

z[8]=114.722382559628540;

z[9]=113.926756453760690;

z[10]=113.042905875608900;

z[11]=112.072571005655110;

z[12]=111.017647986806440;

z[13]=109.880181116547200;

z[14]=193.177519043426640*9*0.0625;

z[15]=107.366482940746310;

z[16]=105.995002915236870;

z[17]=104.550462347330010;

z[18]=103.035510567193580;

z[19]=101.452887709185150;

z[20]=99.8054138716634400;

z[21]=98.0959780592727880;

z[22]=96.3275269683830620;

z[23]=94.5030536783652760;

z[24]=92.6255863133573950;

z[25]=90.6981767411838470;

z[26]=157.731358894605190*9*0.0625;

z[27]=86.7057901712908750;

z[28]=84.6469358304998210;

z[29]=82.5503633898032160;

z[30]=80.4190801763846430;

z[31]=78.2560542745294900;

z[32]=76.0642055761336170;

z[33]=73.8463975181136510;

z[34]=71.6054296177203310;

z[35]=69.3440309309296230;

z[36]=67.0648545779544050;

z[37]=64.7704735051762450;

z[38]=111.046004776561680*9*0.0625;

z[39]=60.1459730157796720;

z[40]=57.8205821960699850;

z[41]=55.4894480357409670;

z[42]=53.1547396594898650;

z[43]=50.8185623281244410;

z[44]=48.4829717899265590;

z[45]=46.1499944288779760;

z[46]=43.8216549664747120;

z[47]=41.5000141942798880;

z[80]=39.1872202840200630;

z[81]=41.5000141942800390;

z[82]=43.8216549664748010;

z[83]=46.1499944288780560;

z[84]=48.4829717899265590;

z[85]=50.8185623281245390;

z[86]=53.1547396594899450;

z[87]=55.4894480357410740;

z[88]=57.8205821960700210;

z[89]=106.926174250275220*9*0.0625;

z[90]=62.4633776868159260;

z[91]=64.7704735051763160;

z[92]=67.0648545779544670;

z[93]=69.3440309309298360;

z[94]=71.6054296177204200;

z[95]=73.8463975181137580;

z[96]=76.0642055761335280;

z[97]=78.2560542745295610;

z[98]=80.4190801763847140;

z[99]=82.5503633898033410;

z[100]=84.6469358304998210;

z[101]=154.143626971184160*9*0.0625;

z[102]=88.723889378215315;

z[103]=90.6981767411839180;

z[104]=92.6255863133574310;

z[105]=94.5030536783653300;

z[106]=96.3275269683831330;

z[107]=98.0959780592729300;

z[108]=99.8054138716635460;

z[109]=101.452887709185300;

z[110]=103.035510567193760;

z[111]=104.550462347330210;

z[112]=105.995002915236960;

z[113]=190.873747450216100*9*0.0625;

z[114]=108.662354461927470;

z[115]=109.880181116547340;

z[116]=111.017647986806530;

z[117]=112.072571005655200;

z[118]=113.042905875608990;

z[119]=113.926756453760820;

z[120]=114.722382559628660;

z[121]=115.428207165596630;

z[122]=116.042822932980670;

z[123]=116.564998060183860;

z[124]=116.993681412984830;

z[125]=208.583123396815930*9*0.0625;

z[126]=117.567297145863800;

z[127]=117.711066218752820;

```
for (i=48; i<80; i++)
{
 h[i]=0;
 z[i]=0;
}

for (i=0; i<128; i++)
{
 phase[i]=phase[i]-(h[127-i]*PI*0.005555556);
 estmag[i]=mag[i]*pow(z[127-i],-1);
}

                inputIndex =0;//inidx;
                for (i = 0; i < int(nWrite); i++) {
                        (EqPhase%i) << phase[inputIndex];
                        (EqMag%i) <<  estmag[inputIndex];
                        inputIndex++;
                   }
                }
        }
```

End of "EDGE_Rx" Ptolemy code

"Equaliser_Cx" Ptolemy code:

```
defstar {
        name {Equaliser_Cx}
        domain {SDF}
        desc { Linear Equalisation }

        location { My Stars }

        input {
                name{TxI}
                type{ANYTYPE}
```

```
}

input {
        name{TxQ}
        type{ANYTYPE}
}
output {
        name{EqPhase}
        type{=TxI}
}

output {
        name{EqMag}
        type{=TxI}
}

defstate {
        name {nRead}
        type {int}
        default {128}
        desc { number of data items read }
}
defstate {
        name {nWrite}
        type {int}
        default {128}
        desc { number of data items written }
}
defstate {
        name {Offset}
        type {int}
        default {0}
        desc { start of output block relative to start of input block }
}
```

```
    defstate {
        name {UsePastInputs}
        type { enum }
        default { "NO" }
      enumlist { NO, YES }
        desc { use previously read inputs }
    }
    protected {
        int hiLim, inidx, loLim;
    }
  method {
      name { computeRange }
      type { "void" }
      arglist { "()" }
      access { protected }
      code {
        hiLim = int(nWrite) - int(Offset) - 1;
        if (hiLim >= int(nWrite)) hiLim = int(nWrite) - 1;
        else if (int(UsePastInputs)) hiLim = int(nWrite) - 1;

        loLim = int(nWrite) - int(nRead) - int(Offset);
        if (loLim < 0) loLim = 0;

        inidx = int(nRead) - int(nWrite) + int(Offset);
        if (inidx < 0) inidx = 0;
      }
    }
    setup {
        if (int(nRead) <= 0) {
          Error::abortRun(*this, "The number of samples to read ",
                          "must be positive");
          return;
        }
```

```
        if (int(nWrite) <= 0) {
          Error::abortRun(*this, "The number of samples to write ",
                          "must be positive");
          return;
        }

        if (int(UsePastInputs)){
          TxI.setSDFParams(int(nRead),int(nRead)+int(Offset)-1);
              TxQ.setSDFParams(int(nRead),int(nRead)+int(Offset)-1);
              }
        else
          {
              TxI.setSDFParams(int(nRead),int(nRead)-1);
              TxQ.setSDFParams(int(nRead),int(nRead)-1);
              }
        EqMag.setSDFParams(int(nWrite),int(nWrite)-1);
        EqPhase.setSDFParams(int(nWrite),int(nWrite)-1);


        computeRange();
}
go {
  double r[128];
        double q[128];
        double phase[128];
        double mag[128];
        double reshape[128];
        double estmag[128];
  double pilots[128];
        int rotate=1;
        double a;
        double a2;
        double a3;
        double ac;
```

```
int inputIndex = 0;;
for (int i = 0; i < int(nWrite); i++) {
                        r[inputIndex] = (TxI%inputIndex);
                        q[inputIndex] = (TxQ%inputIndex);
                        inputIndex++;
   }
for (i=0;i<128;i++){
        phase[i] =atan2(q[i],r[i]);
        reshape[i]=0;
        pilots[i]=0;
        }

        pilots[125]=phase[125];
        pilots[113]=phase[113];
        pilots[101]=phase[101];
        pilots[89]=phase[89];
        pilots[38]=phase[38];
        pilots[26]=phase[26];
        pilots[14]=phase[14];
        pilots[2]=phase[2];

for (i=0;i<128;i++){
        mag[i] =  sqrt(r[i]*r[i]+q[i]*q[i]);
        }

        reshape[125]=phase[125];

        if (floor(phase[125]*180)<0 && floor(phase[113]*180)>0){
        reshape[113]=phase[113]-2*rotate*PI;
        rotate++;
        }
        else reshape[113]=phase[113];

        if (floor(phase[113]*180)<0 && floor(phase[101]*180)>0){
```

```
                reshape[101]=phase[101]-2*rotate*PI;
                rotate++;
                }
                else reshape[101]=phase[101];

                if (floor(phase[101]*180)<0 && floor(phase[89]*180)>0){
                reshape[89]=phase[89]-rotate*PI*2;
                rotate++;
                }
                else reshape[89]=phase[89];

reshape[38]=phase[38];

                if (floor(phase[38]*180)<0 && floor(phase[26]*180)>0){
                reshape[26]=phase[26]-rotate*2*PI;
                rotate++;
                }
                else reshape[26]=phase[26];

                if (floor(phase[26]*180)<0 && floor(phase[14]*180)>0){
                reshape[14]=phase[14]-2*rotate*PI;
                rotate++;
                }
                else reshape[14]=phase[14];

                if (floor(phase[14]*180)<0 && floor(phase[2]*180)>0){
                reshape[2]=phase[2]-2*rotate*PI;
                rotate++;
                }
                else reshape[2]=phase[2];

        for (i=0; i<128; i++)
        phase[i]=0;
        int counter=0;
```

```
        for (i=127; i>=113; i--) {
                a=(14-counter)*0.0833333;
                ac=(1-cos((14-counter)*0.0833333*PI))*0.5;
                phase[i]=a*reshape[125]+(1-a)*reshape[113];
                if (ceil(phase[i]*100)<-314){
        phase[i]=phase[i]+2*PI;
                                }
          estmag[i]=ac*mag[125]+(1-ac)*mag[113];
          counter++;
          }

        if (floor(pilots[125]*180)<0 && floor(pilots[113]*180)>0){
                        reshape[113]=pilots[113];
                        phase[113]=pilots[113];
                        }
counter=15;
        for (i=112; i>=101; i--) {
        a=(26-counter)*0.0833333;
        ac=(1-cos((26-counter)*0.0833333*PI))*0.5;
        phase[i]=a*reshape[113]+(1-a)*reshape[101];
         if (ceil(phase[i]*100)<-314)
       {
        phase[i]=phase[i]+2*PI;
       }
          estmag[i]=a*mag[113]+(1-a)*mag[101];
          counter++;
          }

        if (floor(pilots[113]*180)<0 && floor(pilots[101]*180)>0){
                        reshape[101]=pilots[101];
                        phase[101]=pilots[101];
                        }
        counter=27;
```

```
for (i=100; i>=89; i--) {
a=(38-counter)*0.0833333;
ac=(1-cos((38-counter)*0.0833333*PI))*0.5;
phase[i]=a*reshape[101]+(1-a)*reshape[89];
if (ceil(phase[i]*100)<-314)
{
phase[i]=phase[i]+2*PI;
}
  estmag[i]=a*mag[101]+(1-a)*mag[89];
  counter++;
  }

if (floor(pilots[101]*180)<0 && floor(pilots[89]*180)>0){
                reshape[89]=pilots[89];
                phase[89]=pilots[89];
                }

counter=39;

for (i=88; i>38; i--) {
        a=(89-counter)*0.019607843;
        a2=(38-counter)*0.0833333;
        a3=(101-counter)*0.0833333;
        phase[i]=a2*reshape[101]+(1-a2)*reshape[89];
        estmag[i]=a2*mag[101]+(1-a2)*mag[89];
if (counter>60)
{estmag[i]=a3*mag[38]+(1-a3)*mag[26];
  phase[i]=a3*reshape[38]+(1-a3)*reshape[26];}
  counter++;
  }
if (floor(pilots[89]*180)<0 && floor(pilots[38]*180)>0){
                reshape[38]=pilots[38];
                phase[38]=pilots[38];
```

```
                }
counter=90;

for (i=37; i>=26; i--) {
        a=(101-counter)*0.0833333;
        ac=(1-cos((101-counter)*0.0833333*PI))*0.5;
        phase[i]=a*reshape[38]+(1-a)*reshape[26];
        if (ceil(phase[i]*100)<-314)
        {
                phase[i]=phase[i]+2*PI;
        }
        estmag[i]=a*mag[38]+(1-a)*mag[26];
        counter++;
        }

if (floor(pilots[38]*180)<0 && floor(pilots[26]*180)>0){
                reshape[26]=pilots[26];
                phase[26]=pilots[26];
                }


counter=102;
for (i=25; i>=14; i--) {
        a=(113-counter)*0.0833333;
        ac=(1-cos((113-counter)*0.0833333*PI))*0.5;
        phase[i]=a*reshape[26]+(1-a)*reshape[14];
        if (ceil(phase[i]*100)<-314)
        {
                phase[i]=phase[i]+2*PI;
        }
        estmag[i]=a*mag[26]+(1-a)*mag[14];
        counter++;
}
if (floor(pilots[26]*180)<0 && floor(pilots[14]*180)>0){
```

```
                reshape[14]=pilots[14];
                phase[14]=pilots[14];
                }

        counter=114;
        for (i=14; i>=0; i--) {
                a=(125-counter)*0.0833333;
                ac=(1-cos((125-counter)*0.0833333*PI))*0.5;
                phase[i]=a*reshape[14]+(1-a)*reshape[2];
                if (ceil(phase[i]*100)<-314)
                {
                        phase[i]=phase[i]+2*PI;
                }
                estmag[i]=ac*mag[14]+(1-ac)*mag[2];
                counter++;


        for (i=48; i<80; i++)
        {
                phase[i]=0;
                estmag[i]=0;
        }

estmag[2]=1;
estmag[14]=1;
estmag[26]=1;
estmag[38]=1;
estmag[89]=1;
estmag[101]=1;
estmag[113]=1;
estmag[125]=1;

                inputIndex =0;
                for (i = 0; i < int(nWrite); i++) {
```

```
                    (EqPhase%i) << phase[inputIndex];
                    (EqMag%i) << estmag[inputIndex];
                    inputIndex++;
                }
            }
        }
```

End of "Equaliser_Cx" Ptolemy code

Finally, the transmitted signal is recovered by removing the framing imposed in the transmitter using the "OFDM_DeFrame" block (shown in Figure A.9) and demapping it by using the "QAM64Decode" block.

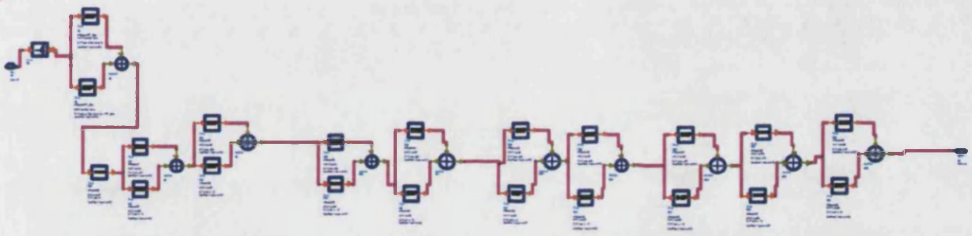

Figure A.9 – Deframing (contents of OFDM_DeFrame block)

A.3 GSM modelling

The block diagram of the GSM transmitter is shown in Figure A.10.

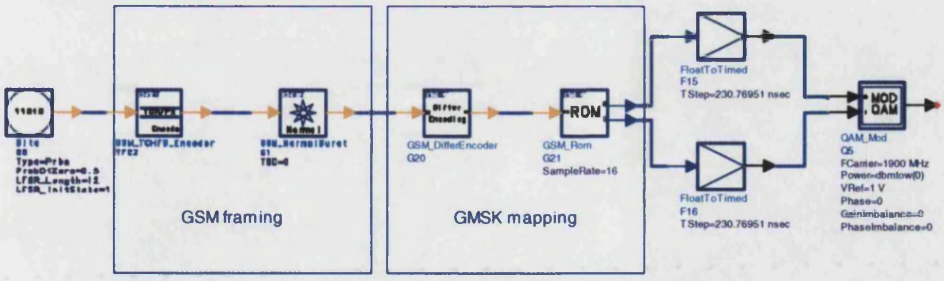

Figure A.10 – GSM transmitter model

All the blocks were taken from the GSM library of ADS. After pseudo-random bit generation, the next two blocks perform coding and framing of the bits in the "Normal Burst" configuration as discussed in section 2.3.4 and 2.3.5. The two subsequent blocks perform GMSK modulation. The signal is upconverted to RF using the IQ modulator block. The GSM transmitter design was discussed in section 4.4.3.1.

The block diagram of the GSM receiver is shown in Figure A.11. The RF signal is IQ demodulated and downsampled and then fed to the "GSM_Receiver" block that performs synchronisation, equalisation and demapping. The signal out of this block is the recovered MSK signal. The GSM receiver design was discussed in section 4.4.3.2.

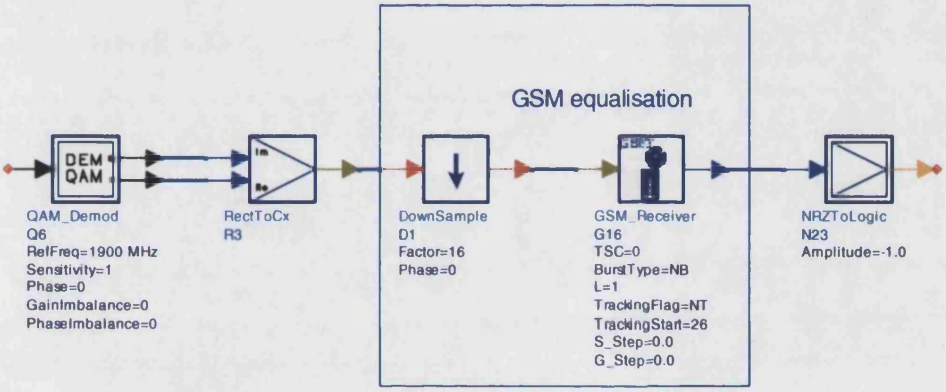

Figure A.11 – GSM receiver model

A.4. EDGE modelling

The block diagram of the EDGE transmitter is shown in Figure A.12.

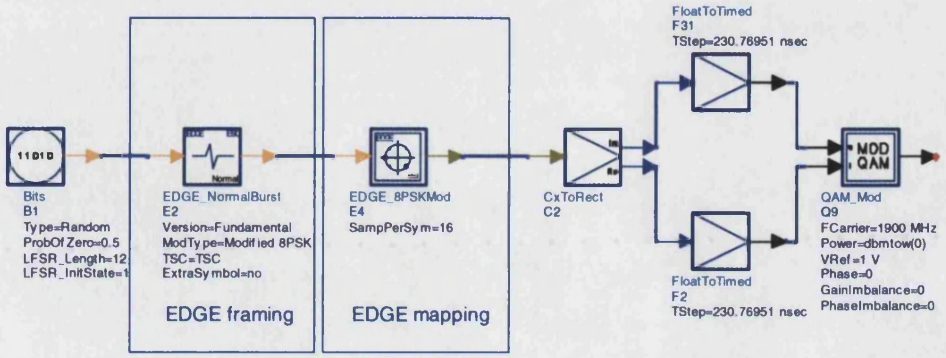

Figure A.12 – EDGE transmitter model

The "EDGE_NormalBurst" block, as its name implies, creates a "Normal Burst" frame. The "EDGE_8PSKMod" block performs the rotated 8PSK mapping and linearised Gaussian filtering as discussed in section 2.4.2. Timing information is inserted to the signal and then upconverted to RF using an IQ modulator block.

The EDGE receiver block diagram is shown in Figure A.13.

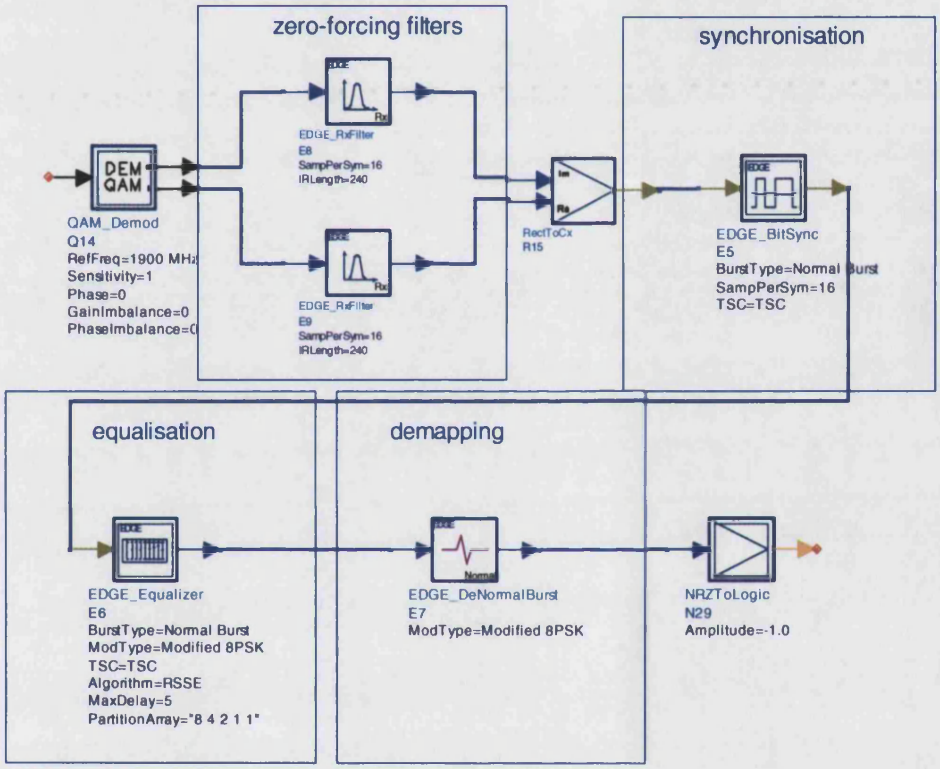

Figure A.13 – EDGE receiver model

The RF signal is downconverted to baseband through an IQ demodulator and then received through two zero forcing filters ("EDGE_RxFilter" blocks) that remove the ISI due to the linearised Gaussian filtering at the transmitter. The two subsequent blocks ("EDGE_BitSync" and "EDGE_Equaliser") perform the necessary synchronisation and channel estimation. Finally the "EDGE_DeNormalBurst" block removes the framing and 8PSK modulation. The output of this block is the recovered transmitted bit stream.

A.4. Summary

In this appendix screenshots of the ADS schematics that were used to simulate the GSM/EDGE/OFDM multimode system and its testing environments were shown. The next appendix shows screenshots of the ADS schematics that were used to model a Fast-OFDM system.

Appendix B

Description of ADS simulation models for the Fast-OFDM system

B.1 Introduction

In this appendix screenshots are displayed, of the ADS schematics that were used to model the Fast-OFDM system discussed in chapter 5. The ADS schematics of the OFDM system are not displayed since the design process is similar. The appendix starts by showing the block diagram of the FOFDM transmitter and then the receiver. In addition, the "zero-insertion" and "complex-conjugate" reconstruction methods at the receiver will be explained.

B.2 Design of FOFDM system

B.2.1 FOFDM transmitter model

The block diagram of the FOFDM transmitter is shown in Figure B.1. This schematic is similar to the block diagram of the proposed OFDM transmitter shown in Appendix A.2.1 and Figure A.1. The difference between the two is that in the current model the signal is only zero-padded (shown in Figure A.2). After the Inverse FFT block, the FOFDM signal is created by using the "Chop" block. This block discards the last N/2-1 samples transmitting the remaining, as discussed in section 5.4. Timing information is then inserted to the signal through the "FloatToTimed" blocks. The simulation time step is set to 114.3 ns as discussed in section 5.4.2.2. The "USampleRF" block samples the signal by a ratio of 100 and then the signal is upconverted to RF through an I/Q modulator.

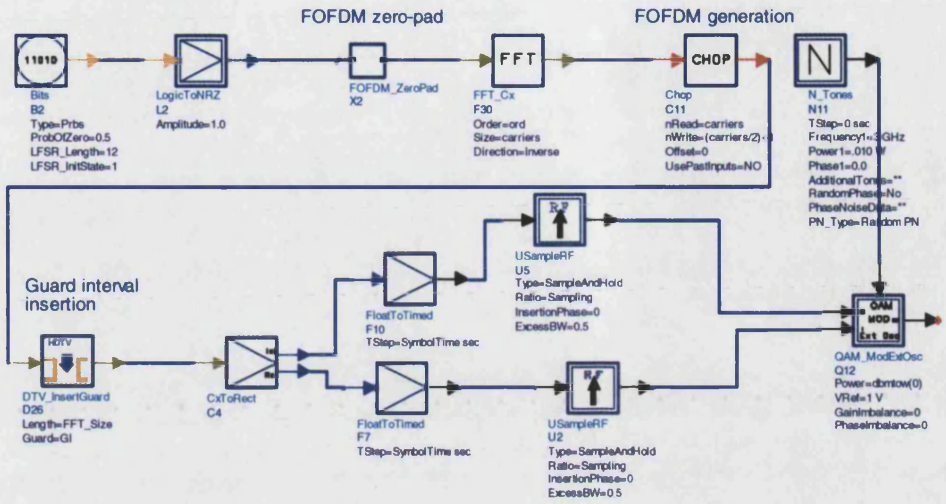

Figure B.1 – FOFDM transmitter model

B.2.2 FOFDM receiver model

The FOFDM receiver block diagram is shown in Figure B.2.

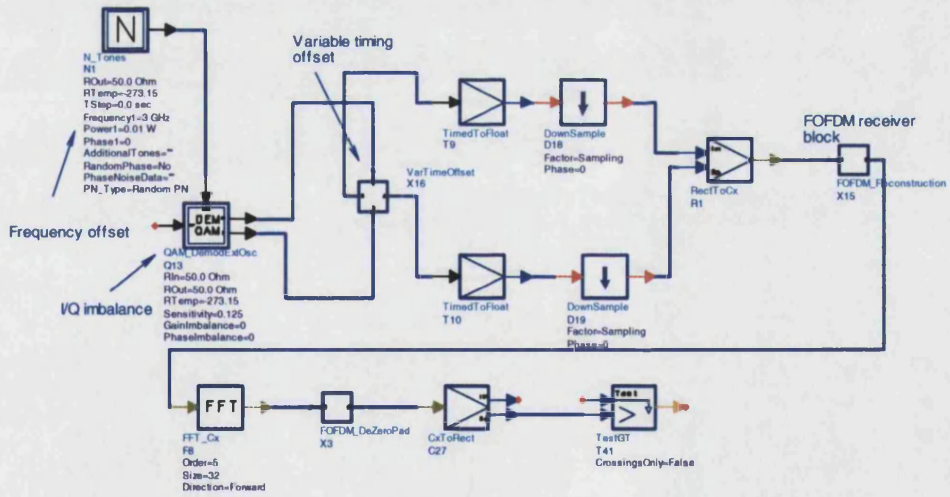

Figure B.2 – FOFDM receiver model

The signal is downconverted by an I/Q demodulator block. This block is also used to simulate environments of I/Q imbalance and frequency offsets that were discussed in section 5.5.2. The "VarTimeOffset" block is used to simulate conditions of

time offset as discussed in section 5.5.2.3. The contents of this block are shown in Figure B.3.

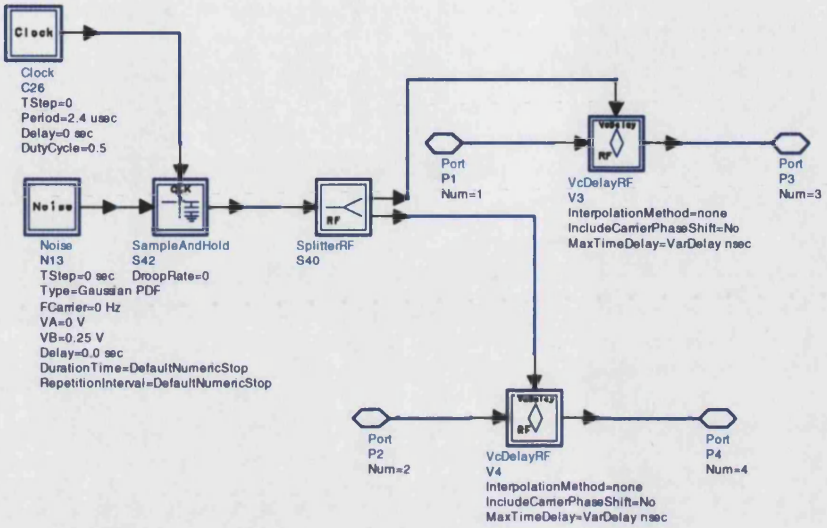

Figure B.3 – Contents of "VarTimeOffset" block

The variable timing offset is applied to the signal through the "VcDelayRF" block. The variance of the delay is obtained from an external source. In our case the variance of the delay is defined from the amplitude of the noise source ("Noise" block). The noise is fed through a sample&hold block in order to maintain the same delay for one FOFDM signal period (2.4 μs).

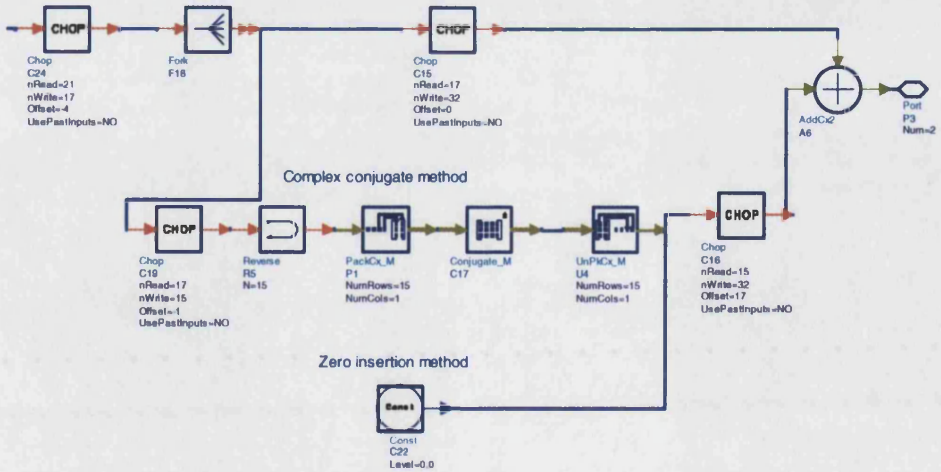

Figure B.4 – Contents of "FOFDM_Reconstruction" block

The "FOFDM_Reconstruction" block is used to recover the FOFDM signal using the "complex-conjugate" or "zero-insertion" method as discussed in sections 5.2.3 and 5.2.4.2. Its contents are shown in Figure B.4. Without this block the receiver can be used to receive OFDM signals. The "reconstructed" FOFDM signal is then fed into a forward FFT and then the zero-padding is removed through the "FOFDM_DeZeroPad" block. The signal out of the latter block is the recovered bit stream.

B.3 Summary

In this appendix the modelling of the Fast-OFDM system in ADS, discussed in chapter 5 was described. In addition, block diagrams of models used to simulate receiver front-end distortions were depicted. In Appendix C, a description of the modelling in ADS of interpolation filtering in OFDM will be carried out.

Appendix C

Description of ADS simulation models for the effect of interpolation filtering on OFDM

C.1 Introduction

The design of the necessary models in ADS in order to study the effects of interpolation filtering on OFDM systems is described in this appendix. Schematics of of an OFDM transmitter with a Chebyshev interpolation filter will be shown. Modelling of OFDM systems with other interpolation filters (Bessel and Butterworth) follow the same principle, hence there is no need to display them. In addition, only the transmitter part will be described, since the receiver design is similar to the OFDM receiver design of Appendix A and Appendix B (without the FOFDM reconstruction block).

C.2 OFDM transmitter modelling

The block diagram of an OFDM transmitter using Chebyshev interpolation is shown in Figure C.1. Interpolation is performed by first sampling the signal using the "USampleRF" block. This block is configured as such in order to insert zeros between each sampling interval. Filtering is then applied using the "LPF_ChebyshevTimed" block, which is the lowpass Chebyshev filter. The user can configure the latter block to have specific order and BT values. The modelling of the OFDM system was discussed in section 6.4.1.

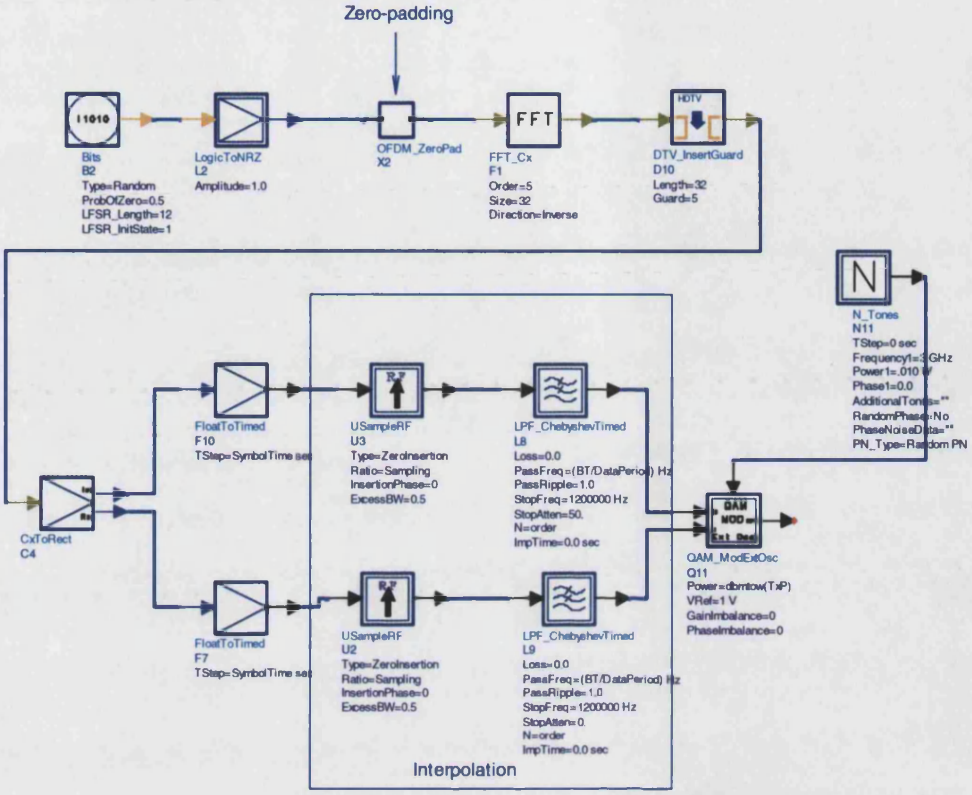

Figure C.1 – OFDM with Chebyshev interpolation filter

C.3 Summary

In this appendix the modelling of an OFDM system using Chebyshev interpolation filtering was discussed. Modelling of OFDM system using other interpolation filters follows the same principle.

References:

[1] João Lima Pinto, Dimitrios Karampatsis and Izzat Darwazeh, "GSM Evolution towards 3rd Generation – 2.5 Generation", International Symposium on Telecommunications, pp. 239-243, Sept 2001, Tehran, Iran

[2] Special Issue on IMT-2000: Standards Efforts of the ITU, IEEE Personal Commun., vol. 4, no.4, pp. 8-40, 1997

[3] S. Haykin, "Communication Systems,", 3rd edition, New York, John Wileys & Sons, 1994

[4] Theodore S. Rappaport, "Wireless Communications: Principles & Practice,", New Jersey, Prentice-Hall Inc., 1996

[5] S. Pasupathy, "Minimum Shift Keying: A Spectrally Efficient Modulation,", IEEE Comm. Magazine, vol. 17, issue 4, pp. 14-22, July 1979

[6] K. Murota, K. Hirade, "GMSK Modulation for Digital Mobile Radio Telephony,", IEEE Trans. on Comm., vol. COM-29, no. 7, pp. 1044-1050, July 1981

[7] Dunlop J., Smith D.G., "Telecommunication Engineering,", 3rd Edition, Chapman & Hall, 1994

[8] GSM Recommendation 05.05, "Radio Transmission and Reception,", ETSI, Dec. 1999

[9] M. Mouly, M.B. Pautet, "The GSM System for Mobile Communications,", CELL & SYS, 1992

[10] Vary, P., et al., "Speech Codec for the Pan-European Mobile Radio System,", Proceedings of ICASSP, pp. 227-230, 1988

[11] A. Furuskar, S. Mazur, F. Muller, H. Olofsson, "EDGE: Enhanced Data Rates for GSM and TDMA/136 Evolution", IEEE Personal Communications, vol. 6, no.3, pp. 56-66, June 1999

[12] Dimitrios Karampatsis, João Lima Pinto and Izzat Darwazeh, "Transmitter Modelling and EVM Estimation for the GSM Evolution - EDGE," Proc. of the International Conference on Telecommunications (ICT 2001), vol. 3, pp. 511-515, Bucharest, Romania, June 2001

[13] ETSI. Digital cellular telecommunications system (phase 2+); modulation (GSM 05.04 version 8.1.0 release 1999), Draft ETSI EN 300 959 V8.1.0 2000

[14] Data on 3G, An Introduction to the Third Generation, www.mobile3G.com

[15] R. Prasad, T. Ojanpera, "An Overview of CDMA Evolution Toward Wideband CDMA,", IEEE Comm. Surveys, vol. 1, no. 1, pp. 2-27, 1998

[16] B. G. Evans, K. Baughan "Visions of 4G,", Electronics & Communication Engineering Journal, vol. 12, no.6, pp. 293-303, December 2000

[17] Li Zhen, et al., "Consideration and research issues for the future generation of mobile communication,", Proc. of the 2002 IEEE Canadian Conference on Electrical and Electronic Engineering, pp. 1276-1281, 2002

[18] UMTS Forum, "The UMTS Third Generation Market Study Update,", Report no. 17 from the UMTS, August 2001

[19] M. Zeng, A. Annamalasi, and V. Bhargava, "Recent advances in cellular wireless communications", IEEE Commun. Mag., vol. 37, no.9, pp. 128-138, 1999

[20] N. Nakajima, Y. Yamao, "Development for 4th generation mobile communications", Wireless Communications and mobile computing, vol. 1 ,pp. 3-12, Jan. 2001

[21] R.C. Qiu, W. Zhu, Ya-Qin Zhang, "Third-Generation and Beyond (3.5G) Wireless Networks and Its Applications,", IEEE International Symposium on Circuits and Systems ISCAS 2002, vol.1, pp. I-41 – I-44, 2002

[22] Theodore Zahariadis, "Trends in the Path to 4G,", Communications Engineer magazine, pp. 12-15, February 2003

[23] Ha Jeounglak, Sung H. Kim and Dae-Sik Kim, "A phased approach to 4G network system,", 10th International Conference on Telecommunications ICT 2003, vol.2, pp. 1318-1322, 2003

[24] S. Ohmori, Y. Yamao, N. Nakajima, "The Future Generations of Mobile Communications Based on Broadband Access Technologies,", IEEE Communications Magazine, vol.38, no. 12, pp. 134-142, December 2000

[25] Ying Li, et al., "Path toward Next Generation Wireless Internet – Cellular mobile 4G, WLAN/WPAN and IPv6 backbone,", Proc. of the IEEE TENCON'02, pp. 1146-1149, 2002

[26] Y. Yamao, H. Suda, N. Umeda, and N. Nakajima, "Radio Access Network Design Concept for the Fourth Generation Mobile Communication System,", IEEE Vehicular Technology Conference, vol. 3, pp. 2285-2289, 2000

[27] Masaharu Hata, "Fourth Generation Mobile Communication Systems beyond IMT-2000,", Fourth Optoelectronics and Communications Conference , vol. 1, pp. 765-767, 1999

[28] G. Tsoulos, M. Beach, and J. MaGeehan, "Wireless Personal Communications for the 21st Century: European Technology Advances in Adaptive Antennas,", IEEE Commun. Magazine, vol. 35, no. 9, pp. 102-109, Sept. 1997

[29] H. Harada, Y. Kamio and M. Fujise, "Multimode Software Radio System by Parameter Controlled and Telecommunication Component Block Embedded Digital Signal Processing Hardware,", IEICE Trans. Commun., vol. E-83-B, no. 6, pp. 1217-1228, Aug. 2000

[30] M. Fujise, K. Sato and H. Harada, "New Road-Vehicle Communication Systems based on Radio on Fibre technologies for future Intelligent Transport Systems (ITS),", Proc. 1st Int'l. Symp. Wireless Pers. Multimedia Commun. , pp. 139-144, Nov. 1998

[31] Gunnar Wetzker, Martin Dukek, Harald Ernst. Friedrich Jondral, "Multi-Carrier Modulation Schemes for Frequency-Selective Fading Channels,", IEEE 1998 International Conference on Universal Personal Communications, vol. 2, pp. 939-943, 1998

[32] Michael Chrysochoos, Junghwan Kim, "Performance Analysis of an MC-CDMA Broadcasting System under High Power Amplifier Non-Linearities, Part I: System Proposal", IEEE Trans. on Broad., vol. 46, no. 4, pp. 256-262, December 2000

[33] Li Ping, "A Combined OFDM-CsDMA Approach to Cellular Mobile Communications", IEEE Trans. on Commun., vol. 47, no.7, pp. 979-982, July 1999

[34] F. Adachi, M. Sawahashi, and H. Suda, "Wideband DS-CDMA for Next Generation Mobile Communications Systems", IEEE. Commun. Magazine, vol. 36, no. 9, pp. 56-59, Sept. 1998

[35] Ertan Ozturk, G. E. Atkin, "Multiscale DS-CDMA for 4G Wireless Systems,", IEEE Global Telecommunication Conference GLOBECOM 2001, vol. 6, pp. 3353-3357, Nov. 2001

[36] Wuyang Zhou, Xiaowen Lu, Jinkang Zhu, "M-ary MC-CDMA System for 4G,", IEEE Vehicular Technology Conference VTC 2001, vol. 4, pp. 2234-2238, 2001

[37] Dimitrios Karampatsis and Izzat Darwazeh, "OFDM: A Possible Technology for 4th Generation Mobile Systems?,", International Symposium on Telecommunications IST, pp. 650-653, Sept. 2001, Tehran, IRAN

[38] Steven J. Vaughan-Nichols, "OFDM: Back to the Wireless Future,", Computer, vol. 35, issue: 12, pp. 19-21, December 2002

[39] M. Alard and R. Lassalle, 'Principles of modulation and channel coding for digital broadcasting for mobile receivers', EBU Review, vol. 224, pp. 47-69, Aug. 1987

[40] B. Le Floch, R. Halbert-Lassalle and D. Castelain, ' Digital Sound Broadcasting to mobile receivers', IEEE Trans. Consum. Electr., vol. 35, no. 3, pp. 493-503, Aug. 1989

[41] T. de Couasnon, R. Monnier and J. B. Rault, "OFDM for digital TV broadcasting", Signal Processing, vol. 39, no. 1-2, pp. 1-32, Sept. 1994

[42] ETSI, "Broadband radio access networks (BRAN); Hiperlan type 2; Physical (PHY) layer,", European Telecommunications Standard, TS 101-475, April 2000

[43] Wireless Medium Access Control and Physical Layer WG, IEEE Draft Standard P802.11, "Wireless LAN", IEEE Stds. Dept., D3, Jan. 1996

[44] Justin Chuang and Nelson Sollenberg, "Beyond 3G: Wideband Wireless Data Access Based on OFDM and Dynamic Packet Assignment", IEEE Commun. Magazine, vol. 38, no. 7, pp. 78-87, July 2000

[45] J. C-I. Chuang, "An OFDM-Based System with Dynamic Packet Assignment and Interference Suppression for Advanced Cellular Internet Service", Wireless Personal Communications, vol. 13, pp. 167-183, 2000

[46] Dakshi Agrawal, Vahid Tarokh Ayman Naguib and Nambi Seshadri, "Space-Time Coded OFDM for High Data-Rate Wireless Communication over Wideband Channels", IEEE Vehicular Technology Conference, vol. 3, pp. 2232-2236, 1998

[47] Ralf Bohnke, Mitsuhiro Suzuki, Kazuyki Sakoda, "Spectral Efficient Modulation Schemes in a SFH-TDMA Orthogonal Frequency Division Multiplexing (OFDM) Wireless Communication System to support Advanced Services", IEEE Vehicular Technology Conference, vol. 3, pp. 2202-2206, 1998

[48] Doelz M.L., Helad E.T., Martin D.L., "Binary Data Transmission Techniques for Linear Systems,", Proceedings of the IRE, vol. 45, pp. 656-661, May 1957

[49] Mosier R.R., Clabaugh R.G., "Kineplex, A bandwidth-Efficient Binary Transmission System,", AIEE Transactions (Part I: Communications and Electronics), vol. 76, pp. 723-728, January 1958

[50] Porter G.C., "Error-Distribution and Diversity Performance of a Frequency-Differential PSJ HF Modem,", IEEE Trans. on Communication Technology, vol. 16, pp. 567-575, August 1968

[51] Zimmerman M.S., Kirsch A. L., "The AN/GSC-10 (KATHRYN) Variable Data Rate Modem for HF Radio,", IEEE Trans. on Communication Technology, vol. 15, pp. 197-205, April 1967

[52] Bello P.A., "Selective Fading Limitations of the Kathryn Modem and some System Design Considerations,", IEEE Trans. on Comm. Tech., vol. 13, pp. 320-333, September 1965

[53] Chang R.W., "Orthogonal Frequency Division Multiplexing,", U.S. Patent 3,488,445, Filed November 14, 1966, Issued January 6, 1970

[54] Chang R.W., "Synthesis of Band-Limited Orthogonal Signals for Multicarrier Data Transmission,", Bell Systems Technical Journal, vol. 45, pp. 1775-1796, December 1966

[55] Saktzberg B.R., "Multiply Orthogonal System for Transmitting Data Signals through Frequency Overlapping Channels,", U.S. Patent 3,511,936, Filed May 26, 1967, Issued May 12, 1970

[56] Saltzberg B.R., "Performance of an Efficient Parallel Data Transmission System,", IEEE Trans. on Comm., vol. 15, pp. 805-811, December 1967

[57] Weinstein S.B., Ebert P.M., "Data Transmission by Frequency-Division Multiplexing using the Discrete Fourier Transform,", IEEE Transcations on Comm. Tech., vol. 19, pp. 628-634, October 1971

[58] Cimini L.J. Jr, "Analysis and Simulation of a Digital Mobile Channel Using Orthogonal Frequency Division Multiplexing,", IEEE Trans. on Comm., vol. COM-33, no. 7, pp. 665-675, July 1985

[59] Morrison R., Cimini L.J. Jr, Wilson S.K., "On the Use of a Cyclic Extension in OFDM,", IEEE Vehic. Tech. Conf. VTC2001 Fall, vol. 2, pp. 664-668, Oct. 2001

[60] N. Yee, J-P Linnartz and G. Fettweis, "Multi-carrier CDMA in Indoor Wireless Radio Networks,", Proc. IEEE PIMRC' 93, pp. 109-113, Yokohama, Japan, September 1993

[61] V. M. Da Silva, E. S. Sousa, "Performance of Orthogonal CDMA Codes for Quassi-Synchronous Communication Systems,", Proc. IEEE ICUPC'93, pp. 995-999, Ottawa, Canada, Oct. 1993

[62] L. Vandendorpe, "Multitone Direct Sequence CDMA System in an Indoor Wireless Environment,", Proc. of the IEEE First Symposium of Comm. and Vehicular Tech., pp. 4.1.1-4.1.8, Delft, Holland, Oct. 1993

[63] L. Hanzo, M. Munster, B.J. Choi, T. Keller, "OFDM and MC-CDMA for Broadband Multi-user Communications, WLANs and Broadcasting,", Chichester, Wiley, 2003

[64] B.P. Crow, I. Widjaja, J.G. Kim, P. T. Sakai, "IEEE 802.11 Wireless Local Area Networks,", IEEE Comm. Magazine, pp. 116-126, Sept. 1997

[65] IEEE, "Supplement to Standard for Telecommunications and Information Exchange Between Systems – LAN/MAN Specific Requirements – Part 11: Wireless LAN Medium Access Control (MAC) and Physical Layer (PHY) Specifications: High Speed Physical Layer in the 2.4 GHz Band,", IEEE 802.11b, 1999

[66] IEEE, "Supplement to Standard for Telecommunications and Information Echange Btween Systems – LAN/MAN Specific Requirements – Part 11: Wireless LAN Medium Access Control (MAC) and Physical Layer (PHY) Specifications: High Speed Physical Layer in the 5 GHz Band,", IEEE 802.11a, 1999

[67] IEEE, "Further High-speed Physical Layer Extension in the 2.4 GHz Band,", IEEE 802.11g, January 2000

[68] ETSI, "Digital Video Broadcasting (DVB); Framing Structure, Channel Coding, and Modulation for Digital Terrestrial Television,", European Telecommunications Standard, ETSI EN 300-744 V1.4.1, Jan. 2001

[69] ETSI, "Digital Video Broadcasting (DVB); Framing Structure, Channel Coding and Modulation for 11/12 GHz Satellite Services,", European Telecommunications Standard, EN 300 421 V1.1.2, Aug. 1997

[70] ETSI, "Digital Video Broadcasting (DVB); Framing Structure, Channel Coding and Modulation for Cable Systems,", European Telecommunications Standard, EN 300 429 V1.2.1, Apr. 1998

[71] James K. Cavers, "An Analysis of Pilot Symbol Assisted Modulation for Rayleigh Fading Channels,", IEEE Trans. on Vehic. Tech., vol. 40, no. 4, pp. 686-693, Nov. 1991

[72] T. Mueller, K. Brueninghaus and H. Rohling, "Performance of Coherent OFDM-CDMA for Broadband Mobile Communications,", Wireless Personal Comms. Vol. 2, pp. 295-305, Kluwer Academic Publishes, Netherlands, 1996

[73] P. Hoeher, "TCM on Frequency-Selective Land-Mobile Fading Channels,", Proc. of 4th Tirrenia Int. Workshop in Dig. Comms., vol. 1, pp. 376-381, Tirrenia, Italy, Sept. 1991

[74] R. van Nee, R. Prasad, "OFDM for Wireless Multimedia Communications,", Artech House, 2000

[75] Frederik Tufvesson and Torleiv Maseng, "Pilot Assisted Channel Estimation for OFDM in Mobile Cellular Systems,", Vehicular Tech. Conf., vol. 3, pp. 1639-1643, 1997

[76] Matthias Patzold, "Mobile Fading Channels,", Wiley & Sons, 2002

[77] H. Steendam, M. Moeneclaey, "Sensitivity of Multicarrier Systems to Synchronization Errors,", International Symposium on Signals, Systems and Electronics ISSSE '01, Tokyo, (invited paper), pp. 66-69, July, 2001

[78] J. H. Scott, "The Effects of Frequency Errors in OFDM,", Research and Development Report, BBC, http://www.bbc.co.uk/rd/pubs/reports /1995_15.html

[79] P. H. Moose, "A Technique for Orthogonal Frequency Division Multiplexing Frequency Offset Correction,", IEEE Trans. on Comm., vol. 42, pp. 2908-2914, Oct. 1994

[80] M.S. El-Tanany, Yiyan Wu, "OFDM Uplink for Interactive Broadband Wireless: Analysis and Simulation in the Presence of Carrier, Clock and Timing Errors,", IEEE Trans. on Broadcasting, vol. 47, no.1, pp. 3-19, March 2001

[81] Elena Costa, Silva Pupolin, "M-QAM-OFDM System Performance in the Presence of a Nonlinear Amplifier and Phase Noise,", IEEE Trans. on Comm., vol. 50, no. 3, pp. 462-472, March 2002

[82] T. Pollet, M. Van Bladel and M. Moeneclaey, "BER Sensitivity of OFDM Systems to Carrier Frequency Offset and Wiener Phase Noise,", IEEE Trans. on. Comm., vol. 43, no. 2/3/4, pp. 191-193, Feb/Mar/Apr 1995

[83] D. Kress, O. Ziemann and R. Dietzel, "Electronic Simulation of Phase Noise,", Eur. Trans. Telecommun., vol. 6, pp. 671-674, Nov/Dec 1995

[84] Zogakis, T.N. and J.M. Cioffi, "The Effect of Timing Jitter on the Performance of a Discrete Multitone System,", IEEE Trans. on Comm., vol. 44, no. 7, pp. 253-257, Nov. 1994

[85] T. Pollet, P. Spruyt and M. Moeneclaey, "The BER Performance of OFDM Systems using Non-Synchronized Sampling,", IEEE Global Telecommunications Conference, GLOBECOM '94, Communications: The Global Bridge, vol. 1, pp. 253-257, Dec. 1994

[86] B. Stanchev and G. Fettweis, "Time-Variant Distortions in OFDM,", IEEE Comm. Letters, vol. 4(4), pp. 312-314, 2000

[87] S. Patel, L.J. Cimini Jr., Bruce McNair, "Comparison of Frequency Offset Estimation Techniques for Burst OFDM,", Proc. of VTC Spring 2002, vol. 2, pp. 772-776, May 2002

[88] T. M. Schmidl, D.C. Cox, "Robust Frequency and Timing Synchronization for OFDM,", IEEE Trans. Comm., pp. 1613-1621, Dec. 1997

[89] H.K. Song, Y.-H. You, J.H. Paikand, Y.S. Cho, "Frequency-Offset Synchronisation and Channel Estimation for OFDM-based Transmission," IEEE Commun. Letters, pp. 95-97, March 2000

[90] M. Morelli, U. Mengali, "An Improved Frequency Offset Estimator for OFDM Applications," IEEE. Commun. Letters, pp. 75-77, March 1999

[91] F. Classen, H. Meyr , "Frequency Synchronisation Algorithms for OFDM Systems Suitable for Communications over Frequency Selective Fading Channels,", Proc. of VTC'94, pp. 1655-1659, 1994, Stockholm

[92] Y. S. Lim and J.H. Lee, "An Efficient Carrier Frequency Offset Estimation Technique for an OFDM System", Proc. of VTC '00, vol. 5, pp. 2453-2457, 2000

[93] Dong-Seog Han, Jae-Hyun Seo and Jung-Jin Kim, "Fast Carrier Frequency Offset Compensation in OFDM Systems,", IEEE Trans. on Consumer Electr., vol. 47, no. 3, pp. 364-369, August 2001

[94] M. Sliskovic, "Carrier and Sampling Frequency Offset Estimation and Correction in Multicarrier Systems,", Proc. of GLOBECOM'01, vol. 1, pp. 285-289, Nov. 2001

[95] Y. Zhao and S. G. Haggman, "Sensitivity to Doppler Shift and Carrier Frequency Errors in OFDM Systems-The Consequences and Solutions,", IEEE Conference Proceedings VTC 1996, pp. 2474-2478, 1996

[96] J. Armstrong, "Analysis of New and Existing Methods of Intercarrier Interference due to Carrier Frequency Offset in OFDM,", IEEE Trans. on Commun., vol. 47, no. 3m pp. 365-369, Mar. 1999

[97] K. Sathananthan, R.M.A.P. Rajathera, "Analysis of OFDM in the Presence of Frequency Offset and a Method to Reduce Performance Degradation,", Proc. of GLOBECOM'00, vol. 1, pp. 72-76, Dec. 2000

[98] P.K. Remvik and N. Holte, "Carrier Frequency Offset Robustness for OFDM Systems with Different Pulse Shaping Filters,", Proc. of GLOBECOM'97, vol. 1, pp. 11-15, 1997

[99] H. Nikookar and B.G. Negash, "Frequency Offset Sensitivity Reduction of Multicarrier Transmission by Waveshaping,", Proc. of Personal Wireless Comm. Conference 2000, pp. 444-448, 2000

[100] R. Li and G. Stette, "Time-Limited Orthogonal Multicarrier Modulation Schemes,", IEEE Trans. Commun., vol. 43, pp. 1269-1272, Feb./Mar./Apr. 1995

[101] C. Muschalik, "Improving an OFDM Reception Using an Adaptive Nyquist Windowing," IEEE Trans. Consumer Electron., vol. 42, pp. 259-269, Aug. 1996

[102] F. Daffara and Ottavio Adami, "Maximum Likelihood Frequency Detectors for Orthogonal Multicarrier Systems,", Proc. Int. Conf. on Comm., pp. 766-771, May 1993

[103] H. Liu, U. Tureli, "A High-Efficiency Carrier Estimator for OFDM Communications,", IEEE Commun. Letters, vol. 2, pp. 104-106, Apr. 1998

[104] U. Tureli, H. Lie, "Software Radio Implementation of Carrier Offset Estimation for OFDM Communications,", Proc. on Conf. 32nd Signals Systems & Computers, vol. 1, pp. 60-64, 1998

[105] U. Tureli, H. Liu and M. Zoltowski, "OFDM Blind Carrier Offset Estimation: ESPRIT,", IEEE Trans. on Commun., vol. 48, pp. 1459-1461, Sept. 2000

[106] M. Sandell, J.J. van de Beek P.O. Borjesson, "Timing and Frequency Synchronisation in OFDM Systems Using the Cyclic Prefix,", Proc. of International Symposium on Synchronisation, pp. 16-19, Essen, Germany, Dec. 1995

[107] J.J. van de Beek, M. Sandell and P.O. Borjesson, "ML Estimation of Time and Frequency Offset in OFDM Systems,", IEEE Trans. on Signal Proc., vol. 45, no. 7, pp. 1800-1805, July 1997

[108] J.J. van de Beek, M. Sandell and P.O. Borjesson, "On Synchronization in OFDM Systems Using the Cyclic Prefix,", Proc. of *Radio Vetenskaplig Konferens* (REVK'96), pp. 663-667, Lulea, Sweden, June 1996

[109] L. Hazy and M. El-Tanany, "Synchronization of OFDM Systems over Frequency Selective Fading Channels,", Proc. Vehic. Tech. Conf., pp. 2094-2098, Phoenix, Arizona, USA, May 1997

[110] B. McNair, L.J. Cimini Jr. and N. Sollenberg, "A Robust Timing and Frequency Offset Estimation Scheme for Orthogonal Frequency Division Multiplexing (OFDM) systems,", Proc. Vehic. Tech. Conf., pp. 690-694, Houston, Texas, May 1999

[111] D. Landstorm, S.K. Wilson, J.J. van de Beek, O. Odling and P.O. Borjesson, "Symbol Time Offset Estimation in Coherent OFDM Systems,", Proc. Intr. Conf. on Comm., vol. 50, issue. 4, pp. 500-505, Vancouver, June 1999

[112] A.A. Hutter, R. Hasholzner, J.S. Hammerschmidt, "Channel Estimation for Mobile OFDM Systems,", Vehicular Technology Conference VTC 1999 - Fall, vol. 1 , pp. 305-309, 19-22 Sept

[113] J.J. van de Beek, O. Edfors, M. Sandell, S.K. Wilson, P.O. Borjesson, "On Channel Estimation in OFDM Systems,", Vehicular Technology Conference VTC '95, vol. 2 , pp. 815-819, 25-28 July 1995

[114] J.J. van de Beek, O. Edfors, P.O. Borjesson, M. Wahlqvist and C. Ostberg, "Channel Estimation in the Uplink of an OFDM System,", NRS Symposium, pp. 32-35, Lund, Sweden, August 1996

[115] J.H. Lodge and M. L. Moher, "TCMP – A Modulation and Coding Strategy for Rician Fading Channels,", IEEE Journal on Selec. Areas Commun., vol. 7, pp. 1347-1355, Dec. 1989

[116] S. Sampei, T. Sunaga, "Rayleigh Fading Compensation Method for 16QAM in Digital Land Mobile Radio Channels,", Proc. IEEE Vehic. Tech. Conf., pp. 640-646, San Francisco, USA, May 1989

[117] P. Hoeher, S. Kaiser, P. Robertson, "Two-Dimensional Pilot-Symbol-Aided Channel Estimation by Wiener Filtering,", Proc. IEEE ICASSP'97, pp. 1845-1848, Munich, Apr. 1997

[118] O. Edfors, et. al., "OFDM Channel Estimation by Singular Value Decomposition,", IEEE Trans. on Comm., vol. 46, no. 7, pp. 931-939, July 1998

[119] Agilent ADS Website, http://eesof.tm.agilent.com/products/adsoview.html

[120] University of Berkeley, "Ptolemy Project,", http://ptolemy.eecs.berkeley.edu/

[121] J. Vankka, et. al., "A GSM/EDGE/WCDMA Modulator With On-Chip D/A Converter for Base Stations", IEEE Trans. on Circuits and Systems-II: Analog and Digital Signal Processing, vol. 49, no. 10, pp. 645-655, Oct. 2002

[122] 3rd Generation Partnership Project; Technical Specification Group Radio Access Networks; UTRA (BS) TDD, "Radio Transmission and Reception,", 3G TS 25/105, V3.3.0, June 2000

[123] 3rd Generation Partnership Project; Technical Specification Group Radio Access Networks; UTRA (BS) FDD, "Radio Transmission and Reception,", 3G TS 25/104, V3.3.0, June 2000

[124] L. Robinson, P. Aggarwal , R.R. Surendran, "Direct Modulation Multi-mode Transmitter,", 3G Mobile Communication Technologies, Conference Publication no. 489, pp. 206-210, May 2002

[125] B.J. Minnis, P.A. Moore, "A Highly Digitized Multimode Receiver Architecture for 3G Mobiles,", IEEE Trans. on Vehicular Tech., vol. 42, no. 3, pp. 637-653, May 2000

[126] J. Chuang, L.J. Cimini, G. Ye Li, B. McNair, N. Sollenberger, "High-Speed Wireless Data Access Based on Combining EDGE with Wideband OFDM,", IEEE Comm. Magazine, pp. 92-98, November 1999

[127] WiLan, "Wideband Orthogonal Frequency Division Multiplexing,", Wi-Lan White Paper, http://www.wi-lan.com/

[128] B. McNair, L.J. Cimini Jr., N. Sollenberger, "Implementation of an Experimental 384 kb/s Radio Link for High-Speed Internet Access,", IEEE Vehicular Tech. Conf. VTC 2000 Fall, vol. 1, pp. 323-330, Sept. 2000

[129] B. McNair, L.J. Cimini Jr., N. Sollenberger, "Performance of an Experimental 384 kb/s 1900 MHz OFDM Radio Link In a Wide-Area High-Mobility Environment,", IEEE Vehicular Tech. Conf. VTC 2000 Fall, vol.3, pp. 1397-1404, Sept. 2000

[130] Joao Lima Pinto, "Studies of Predetection Filters and Error Vector Magnitude in GSM and EDGE Mobile Communication Systems,", University of Manchester Institute of Science and Technology (UMIST), Nov. 2001

[131] X. Li, L. J. Cimini Jr., "Effects of Clipping and Filtering on the Performance of OFDM,", IEEE Vehic. Tech. Conf., vol. 3, pp. 1634-1638, May 1997

[132] Jerry D. Gibson, "The Mobile Communication Handbook,", CRC Press, 2nd Edition, 1999

[133] K.S. Marvin, M.S. Himedi and W.C. Lindsey, "Digital Communication Techniques, Signal Design and Detection,", PTR Prentice Hall, 1995

[134] Kamilo Feher, "Advanced Digital Communications: Systems and Signal Processing Techniques,", Prentice Hall, 1997

[135] ETSI, "Digital Audio Broadcasting (DAB); DAB to Mobile, Portable and Fixed Receivers,", European Telecommunications Standard, ETS 300-401, February 1995

[136] D. Karampatsis and I. Darwazeh, "Modelling and Performance Assessment of OFDM Systems by Simulation,", Proc. of the International Conference on Telecommunications (ICT 2002), vol. 2, pp.420-424, Beijing, China, June 2002

[137] John G. Proakis, "Digital Communications,", 4th edition, McGraw-Hill International Edition, 2000

[138] R. Steele, "Mobile Radio Communications,", London: Pentech Press, 1992

[139] B.A. Bjerke, et. al., "A Comparison of GSM Receivers for Fading Multipath Chanels with Adjacent- and Co-Channel Interference,", IEEE Journal on selected comm., nol. 18, no. 11, pp. 2211-2219, Nov. 2000

[140] Rainer Grunheid and Hermann Rohling, "Adaptive Modulation and Multiple Access for the OFDM Transmission Technique,", Wireless Personal Communications, vol. 13, pp. 5-13, 2000

[141] F. Poegel, S. Zeisberg and A. Finger, "Comparison of Different Coding Schemes for High Bit Rate OFDM in a 60 GHz Environment,", Spread Spectrum Techniques and Applications Proceedings, Vol. 1 , pp. 122-125, 22-25 Sept. 1996

[142] Chi-Hsiao Yih, E. Geraniotis, "Analysis of Co-channel Interference in Multi-Cell OFDM Networks,", Ninth IEEE International Symposium on Personal, Indoor and Mobile Radio Communications, vol.2, pp. 544-548, Sep. 1998

[143] M.R.D. Rodrigues, I. Darwazeh, "Fast OFDM: A Proposal For Doubling the Data Rate of OFDM Schemes,", Proceedings of the International Conference on Telecommunications, Beijing, China, vol. 3, pp. 484-487, June 2002 (invited paper)

[144] F. Xiong, "Modern Techniques in Satellite Communications,", IEE Comm. Magazine, pp. 84-97, August 1994

[145] J. Oh and M. Lim, "The Bandwidth Efficiency Increasing Method of Multi-Carrier CDMA and its Performance Evaluation in Comparison with DS-CDMA with RAKE Receivers,", Proc. of the IEEE Vehic. Tech. Conf., vol. 1, pp. 561-565, May 1999

[146] D. Karampatsis, M.R.D. Rodrigues and I. Darwazeh, "Implications of Linear Phase Dispersion on OFDM and Fast-OFDM Systems,", Proc. of the London Communications Symposium-UCL, pp. 117-120, London, UK, Sept. 2002

[147] D. Karampatsis, M.R.D. Rodrigues and I. Darwazeh, "Performance Comparison of OFDM and FOFDM Communication Systems: Effects of Frequency Selective Fading, Frequency and Timing Offsets and I/Q QAM Modulator/Demodulator Imbalance,", 7th World Multiconference on Systemics, Cybernetics and Informatics (SCI 2003), pp. 396-400, Orlando, USA, July 2003 (invited paper)

[148] D. Karampatsis and I. Darwazeh, "Performance Comparison of OFDM and FOFDM Communication Systems in Typical GSM Multipath Environments,", Proc.

of the London Communication Symposium-UCL, pp. 369-372, London, UK, Sept. 2003

[149] J. Chow, et. al., "Equalizer Training Algorithms for Multicarrier Modulation Systems,", Proc. IEEE International Conference Commun., pp. 761-765, Switzerland, May 1993

[150] Yi Sun, "Bandwidth-Efficient Wireless OFDM,", IEEE Journal on Selec. Areas in Comm., vol. 19, no. 11, pp. 2267-2278, Nov. 2001

[151] Bob Cutler, "Effects of Physical Layer Impairements on OFDM Systems,", rfdesign magazine, pp. 36-44, May 2002

[152] J. Tubbax, B. Come, L. Van der Perre, L. Deneire, S. Donnay, M. Engels, "Compensation of IQ Imbalance in OFDM Systems,", IEEE International Conference on Communications ICC' 2003, vol. 5, pp. 3403-3407, 2003

[153] Chia-Liang Liu, "Impacts of I/Q Imbalance on QPSK-OFDM-QAM Detection", IEEE Trans. on Cons. Elect., vol. 44, no. 3, pp. 984-989, August 1998

[154] Martin Buchholz, et. al., "Effects of Tuner IQ Imbalance on Multicarrier-Modulation Systems,", Proc. of the 3rd IEEE Conf. on Devices, Circuits and Systems, pp. T65/1-T65/6, March 200

[155] C.R.N. Athaudage, "BER Sensitivity of OFDM Systems to Time Synchronisation Error,", International Conf. on Comm. Systems ICCS 2002, vol. 1, pp. 42-46, Nov. 2002

[156] A.G. Armada and M. Calvo, "Phase Noise and Sub-Carrier Spacing Effects on the Performance of an OFDM Communication System,", IEEE Comm. Letters, vol. 2, no. 1, pp. 11-13, Jan. 1998

[157] Harry Y.-F. Lam, "Analog and Digital Filters: Design and Realization,", Prentice Hall, 1979

[158] Wai-Kai Chen, "Passive and Active Filters: Theory and Implementations,", John Wiley and Sons, 1967

[159] Anatol Zverev, "Handbook of Filter Synthesis,", John Wiley and Sons, 1967

[160] Herman Blinchikoff and A. Zverev, "Filtering in the Time and Frequency Domains,", John Wiley and Sons, 1976

[161] S. Chang, E. J. Powers, "Cancellation of Inter-Carrier Interference in OFDM Systems Using a Nonlinear Adaptive Filter,", International Conference on Comm., vol. 2, pp. 1039-1043, June 2000

[162] P. Huang, Y. Lee, "Adaptive Decision Feedback Orthogonality Restoration Filter for Windowed OFDM,", Proc. of the IEEE Vehicular Tech. Conf. VTC 2001, vol. 2, pp. 1106-1110, Oct. 2001

[163] R.W. Lowdermilk, F. Harris, "Design and Performance of Fading Insensitive Orthogonal Frequency Division Multiplexing (OFDM) using Polyphase Filtering Techniques,", Conference Record of the Thirtieth Asilomar Conference on Signals, Systems and Computers, vol. 1, pp. 674-678, 1996

[164] N. Izuka, Y. Daido, S. Mizuno, Y. Yamakita, "Spectrum-shaping Method to Improve Spectral Efficiency of OFDM Systems,", 8th International Conference on Communication Systems ICCS 2002, vol. 1, pp. 234-238, Nov. 2002

[165] B. Debaillie, B. Come, et. Al., "Impact of Front-End Filters on Bit Error Rate Performances in WLAN-OFDM Transceivers,", IEEE Radio and Wireless Conf., RAWCON 2001, pp. 193-196, Aug. 2001

[166] M. Faulkner, "The Effect of Filtering on the Performance of OFDM Systems,", IEEE Trans. on Vehic. Tech. ,vol. 49, no. 5, pp. 1877-1884, Sep. 2000